AD NUMBER

AD480108

NEW LIMITATION CHANGE

TO

Approved for public release, distribution
unlimited

FROM

Distribution authorized to U.S. Gov't.
agencies and their contractors;
Administrative/Operational Use; JAN 1966.
Other requests shall be referred to Air
Force Aero P{ropulsion laboratory,
Wright-Patterson AFB, OH 45433.

AUTHORITY

AFAPL ltr, 12 Apr 1972

AFAPL-TR-66-12

UNCLASSIFIED

CENTRIFUGAL PUMP (HIGH PRESSURE) FOR POWER TRANSMISSIONS

480108

Paul Hildebrand
Tony Vodopia
Joseph Sanders
Lorant Nagyszalanczy

AIRESEARCH TECHNICAL REPORT NO. AFAPL-TR-66-12

January 1966

UNCLASSIFIED

NOTICES

When Government drawings, specifications, or other data are used for any purpose other than in connection with a definitely related Government procurement operation, the United States Government thereby incurs no responsibility nor any obligation whatsoever; and the fact that the Government may have formulated, furnished, or in any way supplied the said drawings, specifications, or other data, is not to be regarded by implication or otherwise as in any manner licensing the holder or any other person or corporation, or conveying any rights or permission to manufacture, use, or sell any patented invention that may in any way be related thereto.

CENTRIFUGAL PUMP (HIGH PRESSURE)
FOR POWER TRANSMISSIONS

Paul Hildebrand
Tony Vodopia
Joe Sanders
Lorant Nagyszalanczy

FOREWORD

This report is the culmination of a High Pressure, High Temperature Centrifugal Pump Program conducted by AiResearch Manufacturing Company, a division of The Garrett Corporation, Los Angeles, California, under Research and Technology Division Contract No. AF 33(657)-10151. The program was designated Task No. 8128-07 under Project No. 8128, and covered the period from 16 January 1963 through 15 December 1965.

The project was administered for the Research and Technology Division, Wright-Patterson Air Force Base, Ohio, by the Air Force Aero Propulsion Laboratory. At AiResearch, this project was under the administrative control of R. L. Schinnerer, Chief of Environmental Control. J. C. Riple, Project Engineer was responsible for overall guidance and coordination under the direct supervision of L. R. Woodworth, Senior Project Engineer. Major AiResearch contributors were N. Van Le, Chief of Aerodynamics, L. T. Sladek, Project Engineer, Turbomachinery Project, and J. W. Meermans, Supervisor of Design, Turbomachinery Project. This report was submitted January 22, 1966.

The AiResearch Document Number for this Program Report is 660095.

Publication of this report does not constitute Air Force approval of the report's findings or conclusions. It is published only for the exchange and stimulation of ideas.

Paul W. Montgomery, Major, USAF
Chief, Propulsion and Power Branch
Aerospace Power Division
Wright-Patterson Air Force Base, Ohio

ABSTRACT

This report describes the analytical study, design, and experimental investigation of a four-stage centrifugal pump capable of 30 gpm flow at a pressure of 4000 psi when pumping hydraulic fluid at an inlet temperature of 600°F.

The hydrodynamic analysis includes the computer program format predicting performance of elements of different pump configurations. Test results of 62 percent efficiency, including all mechanical losses, confirmed the validity of the analysis and pump design. A dynamic floating carbon bushing inter-stage seal element was developed and is described.

TABLE OF CONTENTS

ii

TABLE OF CONTENTS (Continued)

LIST OF TABLES

LIST OF ILLUSTRATIONS

LIST OF ILLUSTRATIONS (Continued)

LIST OF ILLUSTRATIONS (Continued)

LIST OF ILLUSTRATIONS (Continued)

SECTION I

PROBLEM STATEMENT

OBJECTIVES

The primary objective of the research and development program was to advance the state of the art of small, low capacity, high pressure (low specific speed) centrifugal pump technology. Specific requirements were to:

a. Theoretically derive an impeller and diffuser configuration applicable to a pump operating at 45,000 rpm delivering 30 gpm of MLO 8200 hydraulic fluid or equivalent at 4000 psi with a minimum overall efficiency of 65 percent. The fluid inlet conditions are a maximum of 100 psi and 600°F.

b. Investigate pump characteristics, configurations, and problem areas.

c. Fabricate a breadboard pump and conduct an experimental investigation on the behavior of the pump under various influences.

SECTION 2

SUMMARY

ACCOMPLISHMENTS

This report presents the results of a theoretical and experimental investigation into the use of a centrifugal pump in a low flow, high pressure, high temperature hydraulic system.

Hydrodynamic Design

The hydrodynamic design studies led ·to the selection of a four-stage centrifugal pump with 60-degree backward curved blades. The pump is designed to deliver a flow rate of 30 gpm at a pressure of 4000 psi when pumping MLO 8200 hydraulic fluid at a fluid inlet temperature of 600°F. The pump operates at a speed of 45,000 rpm.

The analytical design solution was based on the calculation results of a high speed computer program used to predict the performance of various pump configurations and elements over a complete range of speeds. The calculation procedures and computer program format are included in this report.

Mechanical Design and Experimental Performance

Centrifugal pump hydrodynamic elements were designed in accordance with the results of the analytical studies. A single-stage test rig was fabricated to confirm the hydrodynamic design. Results of the calibration of the 60-degree backward curved impeller indicated an impeller efficiency of approximately 80 percent with an overall stage efficiency, including mechanical losses, of 65 percent.

An interstage seal suitable for stage pressures of 1000 psi and fluid temperatures of 600°F to 700°F was successfully developed.

A four-stage pump was designed and fab. cated. The pump operated for a period of over twenty hours, of which six hours and 30 minutes were at a temperature of 600°F fluid inlet temperature. The design provided for self lubrication of all bearings. Performance tests of the four-stage pump indicated an overall efficiency of approximately 62 percent which includes all losses attributable to shaft seals, interstage seals, and pump bearings.

CONCLUSIONS AND RECCMENDATIONS

Experimental resuits of the pump have confirmed the validity of the design and of the computer program predictions. The tests confirm the capabilities of high-speed centrifugal pumps as hydraulic components in airborne systems.

The experimental investigation indicates that the further development is necessary to produce mechanical components capable of operating for extended time periods in MLO 8200 fluid at fluid temperatures of 600°F and higher. Further testing of the pump is recommended in order to establish its mechanical integrity and to develop mechanical components with low parasitic losses.

SECTION 3

HYDRODYNAMIC DESIGN

FEASIBILITY STUDY

At the initiation of the high temperature hydraulic pump development program, a feasibility study was conducted. Hydrodynamic calculations were coupled with centrifugal pump design and test experience in an effort to assure accurate comprehensive results. The procedure for this initial study was as follows.

The centrifugal pump to be investigated was characterized by a low specific speed, a small size, and a requirement for high performance. In compliance with the specification, this pump was to be designed for operation with MLO 8200 hydraulic fluid, delivering a flow of 30 gpm at 4000 psi. Maximum allowable inlet pressure was 100 psia and the temperature could be as high as 600°F. Operating speed was also to be taken at 45,000 rpm.

This feasibility study was based on a recent AiResearch investigation on a high performance small capacity pump. It was also conducted with the AiResearch background of proven high performance, small capacity centrifugal compressors. Latest advancements in the state of the art of these compressors has recently been translated for application to centrifugal pumps, which are indeed old in theory and in application.

Efficiency Versus Number of Stages

In order to carry out this parametric study, pump performance data were gathered, based on actual tests of a large number of pumps. This data is presented in Figure 1. The attainable efficiency of these pumps is shown as a function of the specific speed for a Reynolds Number larger than 10^7. To account for the operation of smaller pumps in a viscous oil presently considered, a correction was introduced using the data of Reference 17. By this method, the attainable optimum performance of pumps operating under various Reynolds Numbers is presented in Figure 2.

Since the pump involved in this study was small, scaling effects must be considered.

One approach to arriving at a required pump characteristic is to use the similarity or scaling law of turbo-machines. Derivation of the performance of pumps of a given size can be made starting from a proper prototype.
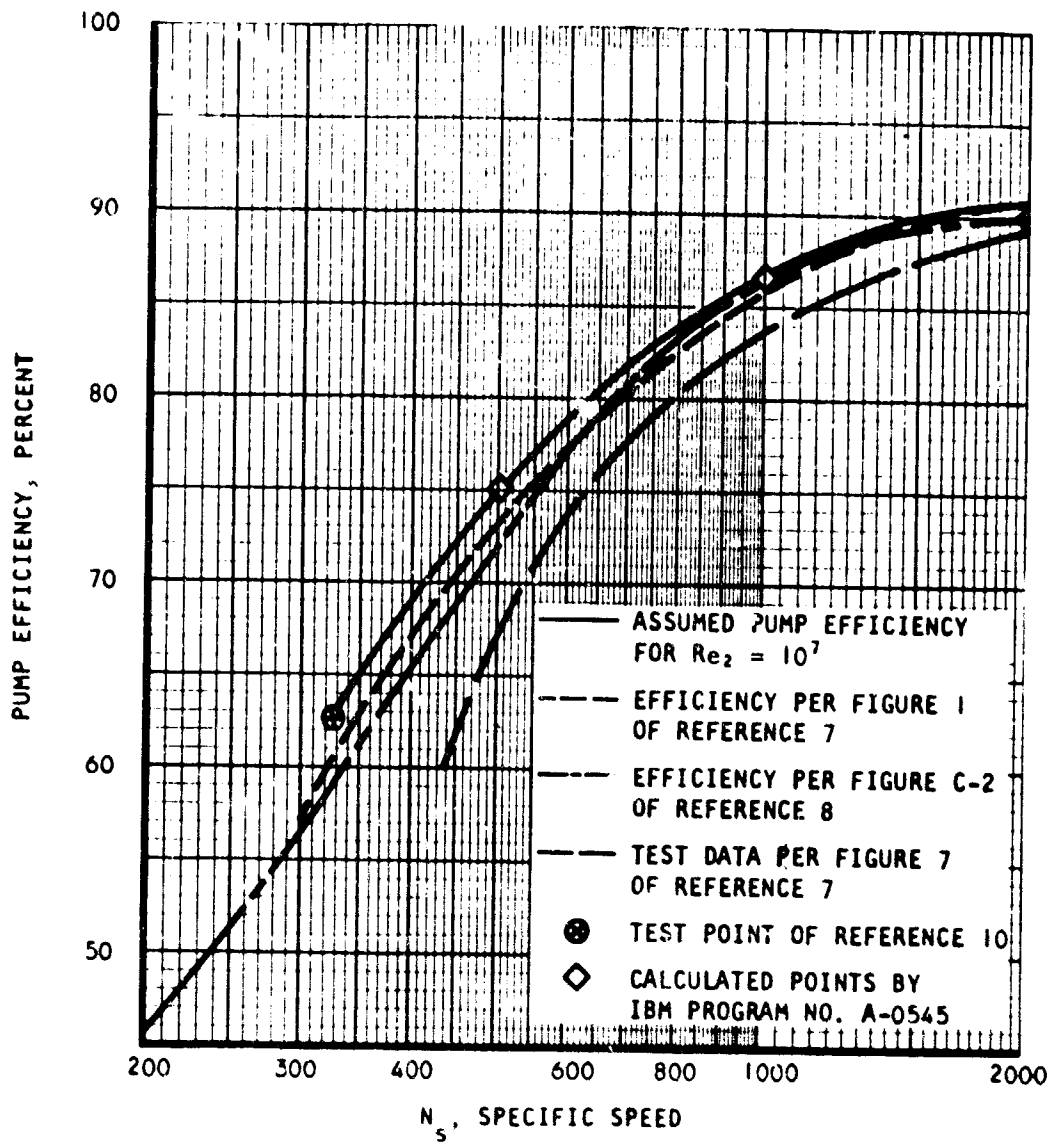
Figure 1. Efficiency Comparison with Published Data

A-6974
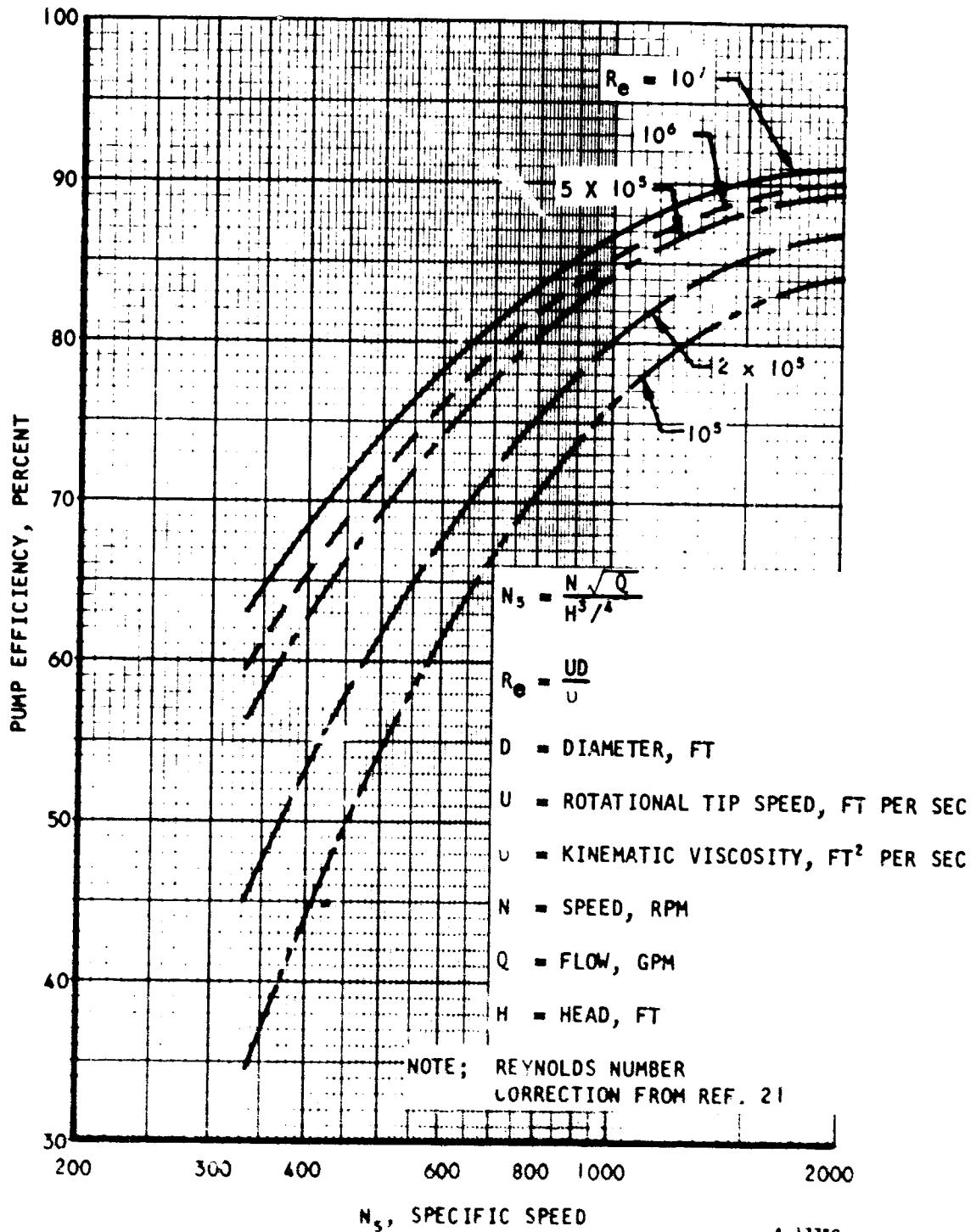
Figure 2. Estimated Pump Efficiency Versus Specific
Speed for Various Reynolds Numbers

Chart labels:

PUMP EFFICIENCY, PERCENT (y-axis, 30 to 100)

$R_e = 10^7$

10^6

5×10^5

2×10^5

10^5

$$N_s = \frac{N\sqrt{Q}}{H^{3/4}}$$

$$R_e = \frac{UD}{\upsilon}$$

D = DIAMETER, FT

U = ROTATIONAL TIP SPEED, FT PER SEC

υ = KINEMATIC VISCOSITY, FT^2 PER SEC

N = SPEED, RPM

Q = FLOW, GPM

H = HEAD, FT

NOTE: REYNOLDS NUMBER
CORRECTION FROM REF. 21

N_s, SPECIFIC SPEED

A-17750

In scaling from a model pump to a new requirement, the flow, speed, and diameter are given by similar laws as follows:

$$\frac{Q}{ND^3} = \left(\frac{Q}{ND^3}\right)_m$$

$$\frac{H}{N^2D^2} = \left(\frac{H}{N^2D^2}\right)_m$$

Pumps of various sizes, designed with the same hydrodynamic features and same performance parameters will have the same performance, provided the mechanical design features and manufacturing tolerances can be maintained within the same proportion. For instance, a seal clearance of 0.002 inches on a 10-inch wheel must be maintained at 0.001 inch to achieve good performance with a 5-inch wheel.

If a 5-in. impeller has the same Reynolds number, say 10^6, as a 10-inch impeller manufactured with a surface finish of RMS 32 (root mean square of 32 microinches), the small impeller must be made with a finish of RMS 16 to duplicate the performance of the large pump.

Typical penalty in performance is presented in Figure 3. This curve has been established as a result of comparing actual test data with theoretical performance for many different impellers.

The pump must perform at a wide range of density and viscosity conditions because of the wide operational temperature spectrum. It will operate with a low Reynolds number (200,000) at low temperature and still should deliver a larger head with lower density fluid at 600°F operation. Because of these considerations, the feasibility study was conducted with the design point viscosity at 80°F but the density at 600°F.

On this basis, the performance of this pump was computed while operating at 45,000 rpm utilizing different numbers of stages. Results are presented in Figure 4, indicating that the pump should have at least 3 stages to produce the desired performance. To have a safety margin, a 4-stage design is preferable.

Influence of the Operating Speed

Although the problem statement specifies a speed of 45,000 rpm, a short investigation was performed to determine performance at different operating speeds. The inlet and discharge diameters were also calculated. Figure 5 shows the change of the inlet diameter at different operational speeds. The inlet diameter is not a function of the number of stages, but it does depend on the inlet vane angle which must be chosen to meet the suction specific speed requirements to assure a cavitation free operation.
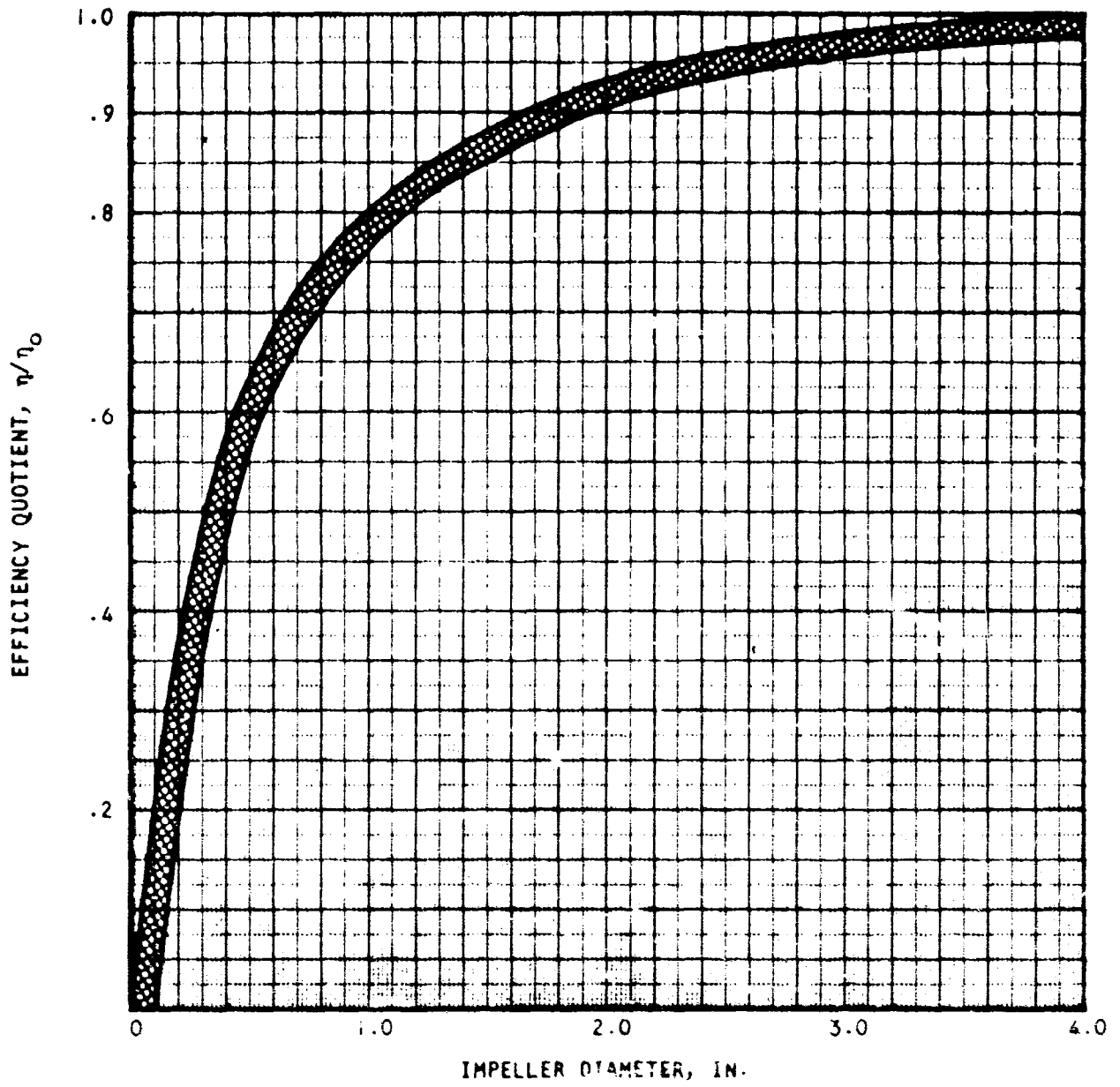
Figure 3. Effect of Impeller Size on Pump Efficiency

A-3396

8
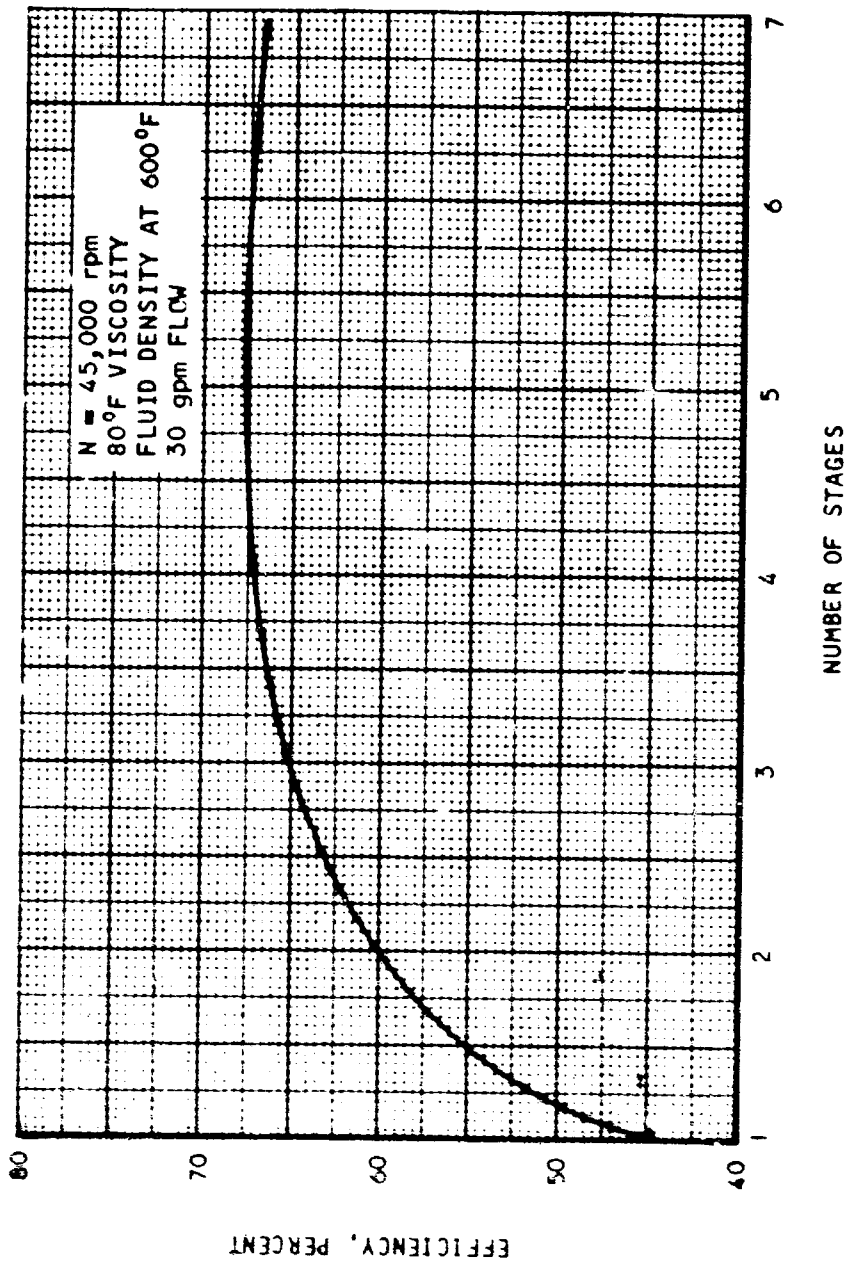
Figure 6. Efficiency as a Function of Number of Stages
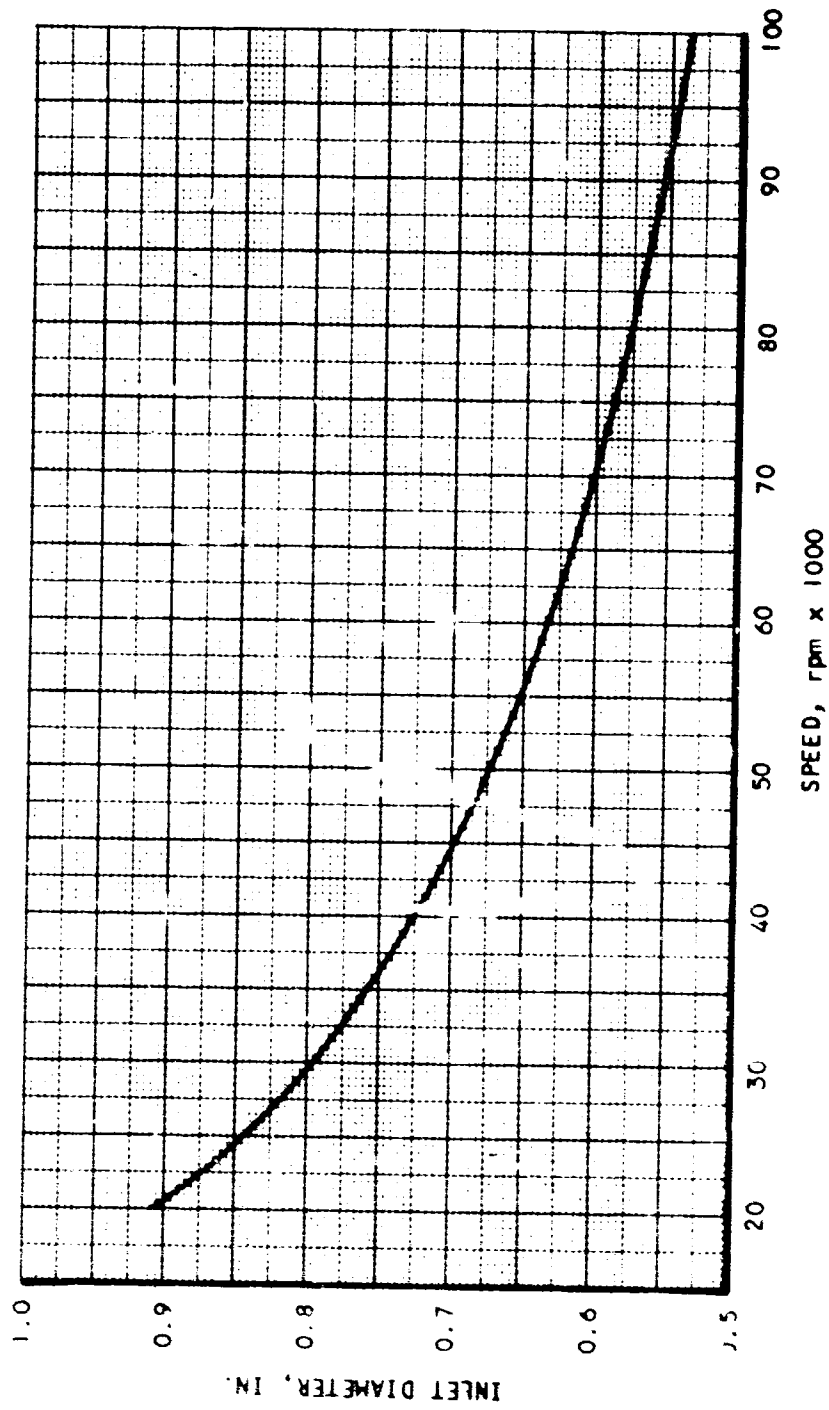
A-17751

Figure 5. Inlet Diameter as a Function of Rotational Speed

A-17758

10

In Figure 6, the impeller tip diameters are presented at different number of stages as a function of the speed.

The calculated efficiencies are shown in Figure 7 for different numbers of stages. It can be seen that the best performance is near the specified 45,000 rpm at a higher number of stages.

Effect of Blade Angle on Performance

The performance of the low specific speed machines is generally lower than that of the higher specific speed ones. This is due to the increased friction of the impeller. At such low Reynolds number operation like the contemplated design, an additional problem arises, namely the decreasing efficiency of the diffuser because of the increasing boundary layer and increasing friction factor and separation effect. To be able to choose the highest performance design for this application, a one-dimensional investigation was made by varying the discharge vane angle of the impeller. A 4-stage unit was chosen for this investigation with an operating speed of 45,000 rpm at an inlet temperature of 80^{0}F. The inlet diameter was kept constant; the tip diameter changed with the slip factor. The slip factor was calculated according to B. Eck's equation (Reference 5) which is a modified form of Stodola's formula. It is in good correlation with Buseman's and Weinig's investigations. Furthermore, it allows the investigation of the forward curved vaned impellers in general. Figures 8 through 10 show the calculated head coefficient change with the vane angle at different number of vanes and at different flow factors as parameters.

These curves show in general that the head factor (and the head) increases going to lower flows below 90^{0} vanes but decreases at bigger angles (forward blades). This means that the shutoff head is higher using lower vane angles, so the operating characteristics become more stable. The curves also show a definite increase in the head factor using a greater number of vanes. This one-dimensional calculation did not include an internal loss investigation inside the impeller, so at the time, it was not known what the numerical effect of the increasing number of vanes would be in percentage of the total efficiency. However, the higher number of vanes give little improvement in efficiency even when the same impeller loss factor was used in every case (see Figure 11). The most promising design was approximately 8 vanes for smaller than 90^{0} vane angles and 16 (8 blades and 8 splitter vanes) for bigger angles. Recent small pump experience shows that an 8-vaned 90^{0} vane angle impeller had no measurable efficiency decrease due to the increased number of vanes.

Figure 12 presents the calculated efficiencies of an 8-vaned impeller versus vane angle and the flow factor as a parameter. Obviously, the efficiency of the pump does not change too much at relatively low flow factors. The calculated best performance is with a 0.05 flow factor, but operation at such a low flow requires very small flow angles when entering the diffuser, which results in a long flow path and fast boundary layer growth in the diffuser (Figure 13). This effect was not included in the present one-dimensional calculations, but it was later investigated during the actual three-dimensional computer design calculations. The difference in efficiencies between 0.05 and 0.10 flow factors is only about 5 percent.

11
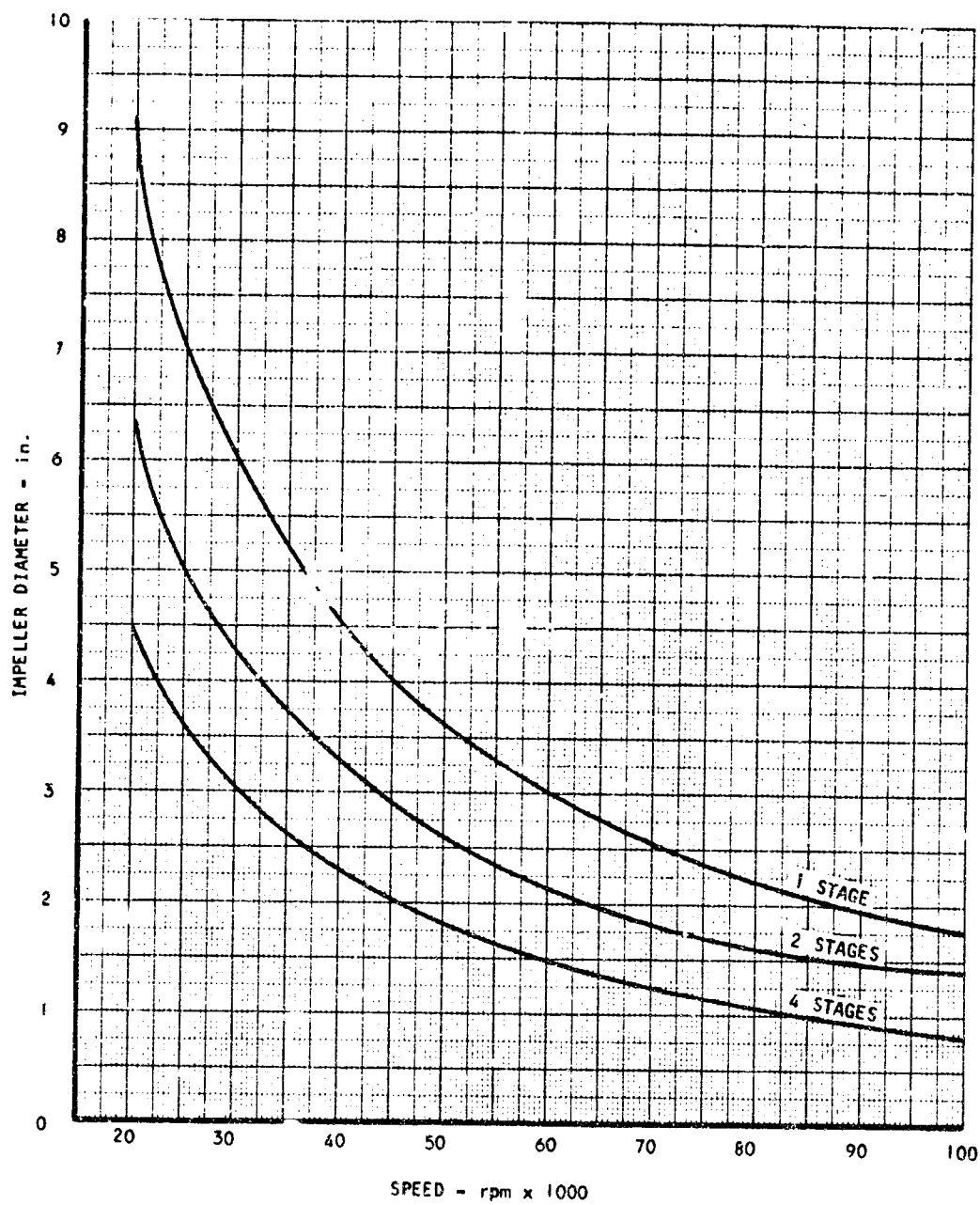
Figure 6. Discharge Diameter Versus
Speed and Number of Stages

A-17753

12

EFFICIENCY, PERCENT

SPEED, THOUSANDS OF rpm
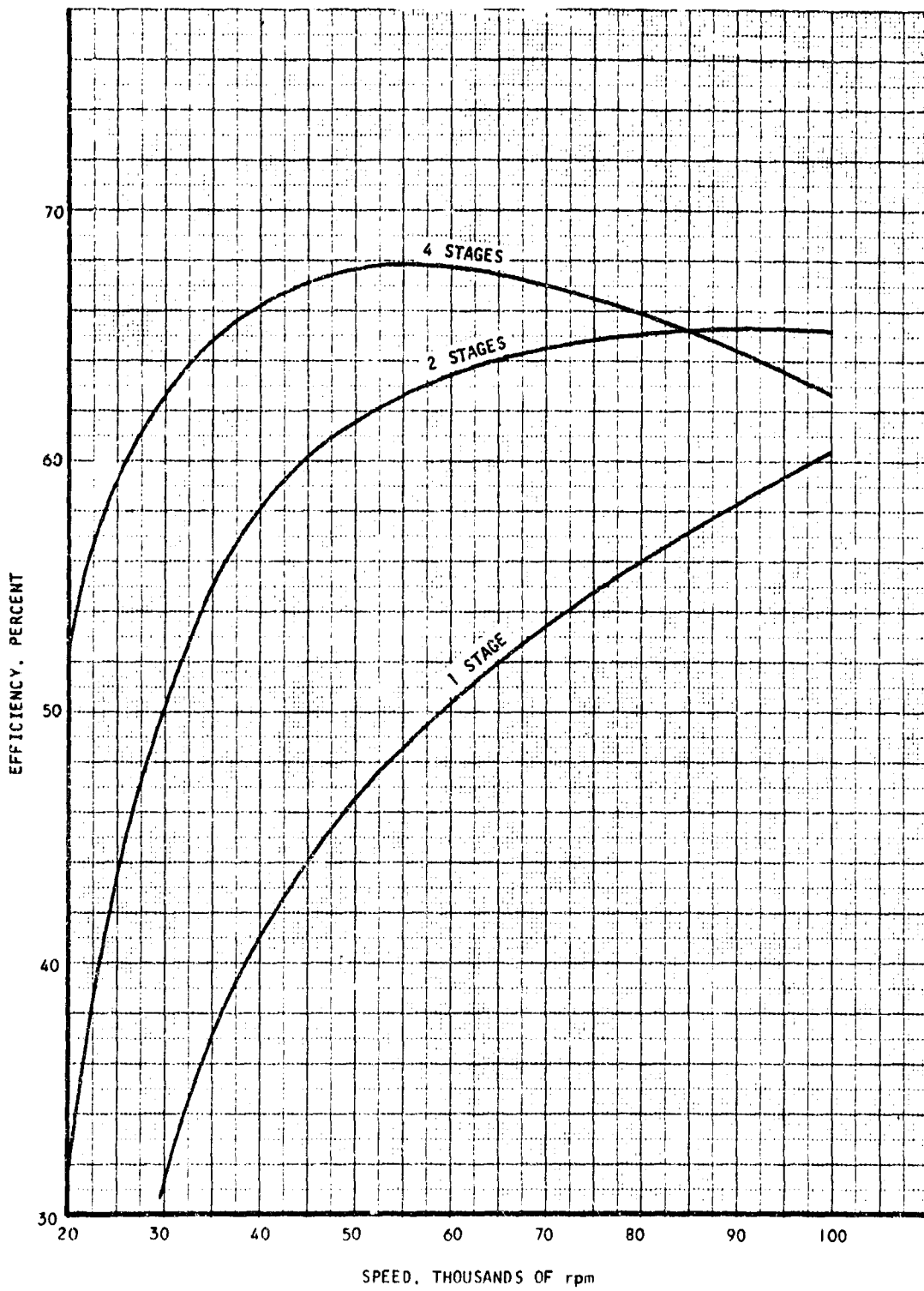
B-10274

Figure 7.   Efficiency Versus Speed
and Number of Stages

13
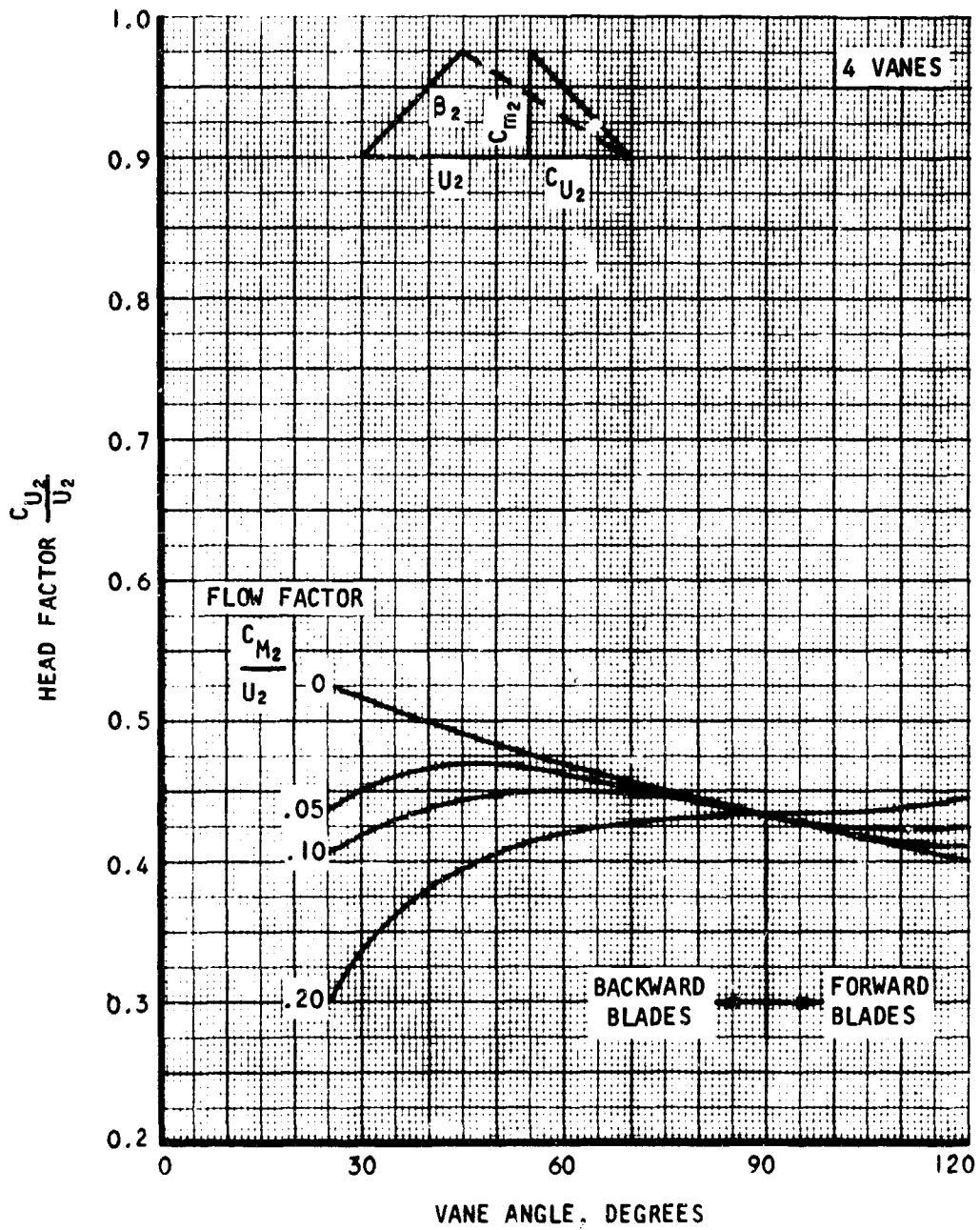
Figure 8 . Head Factor Versus Vane
Angle - 4 Vanes

A-17754

14
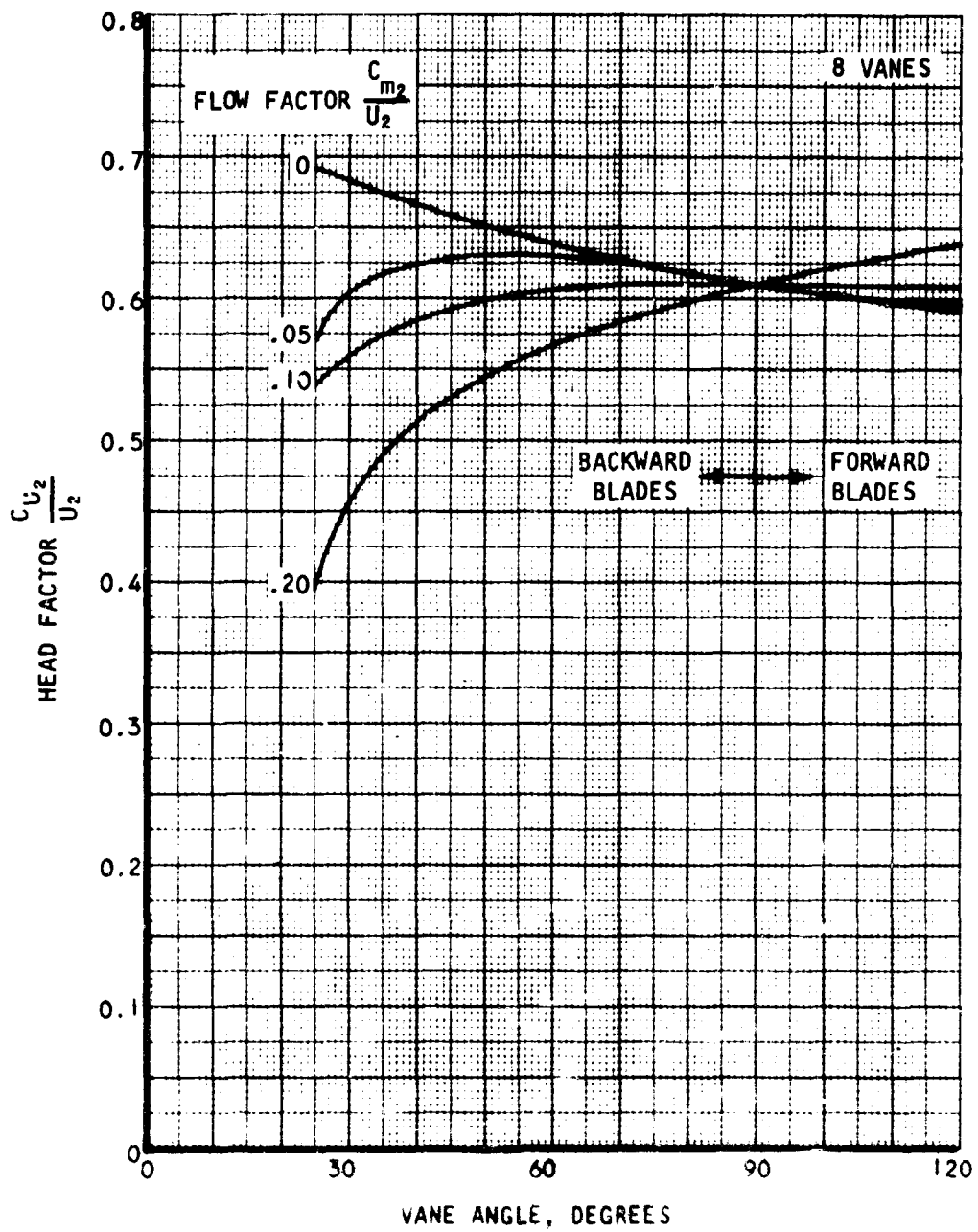
Figure 9. Head Factor Versus Vane
Angle - 8 Vanes
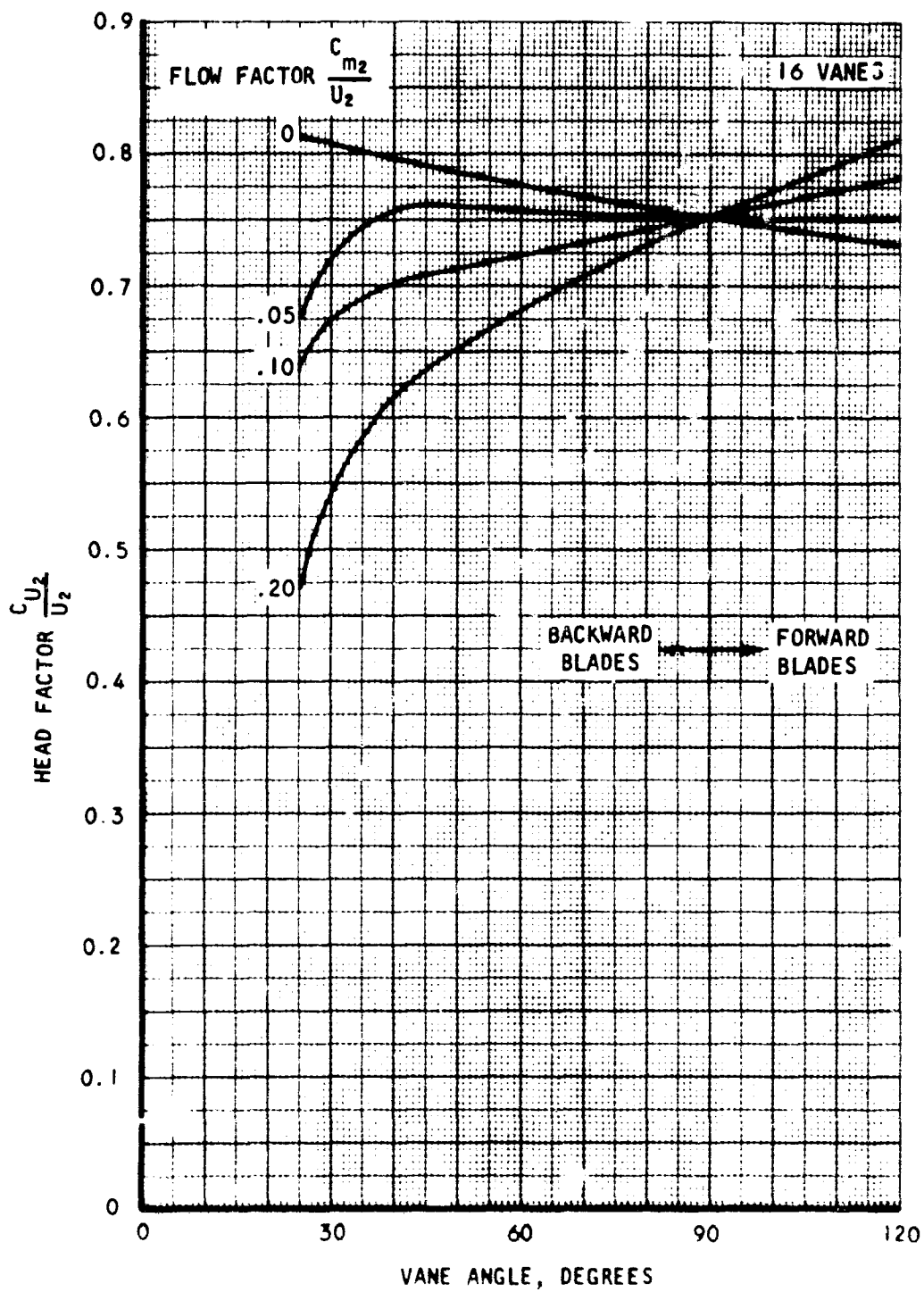
Figure 10. Head Factor Versus Vane
Angle - 16 Vanes

A-17756

16
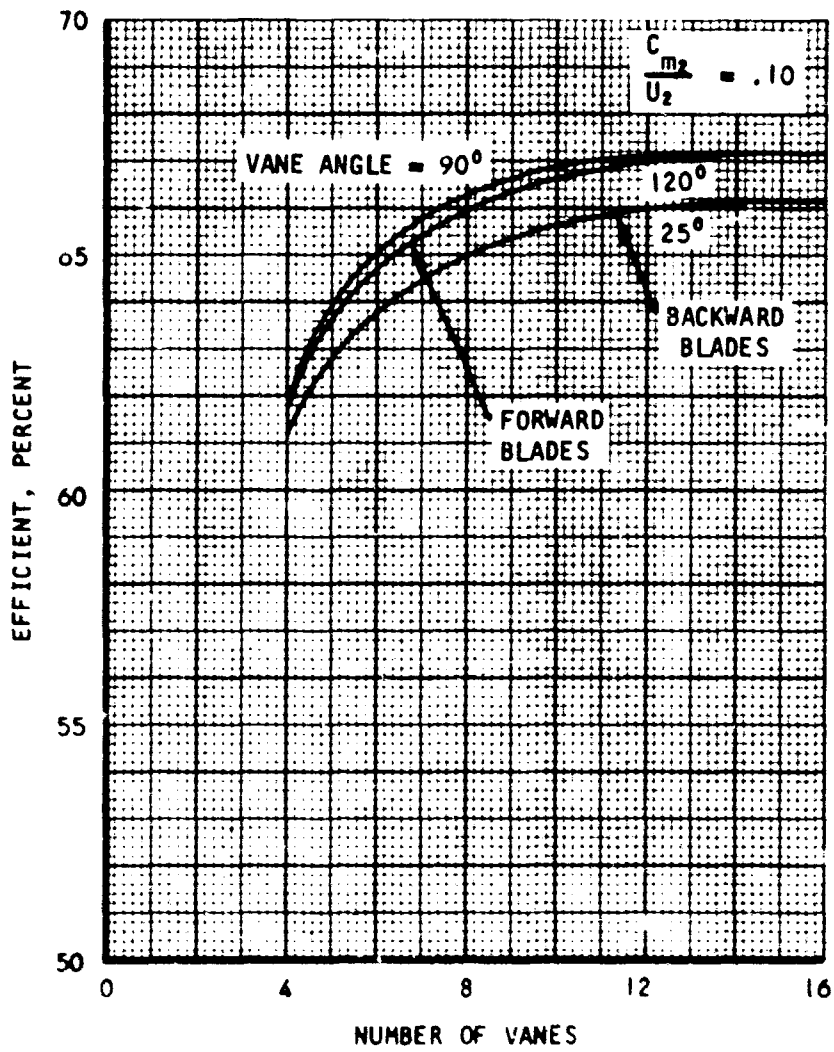
Figure 11. Efficiency Versus Number of Vanes
At Different Vane Angles
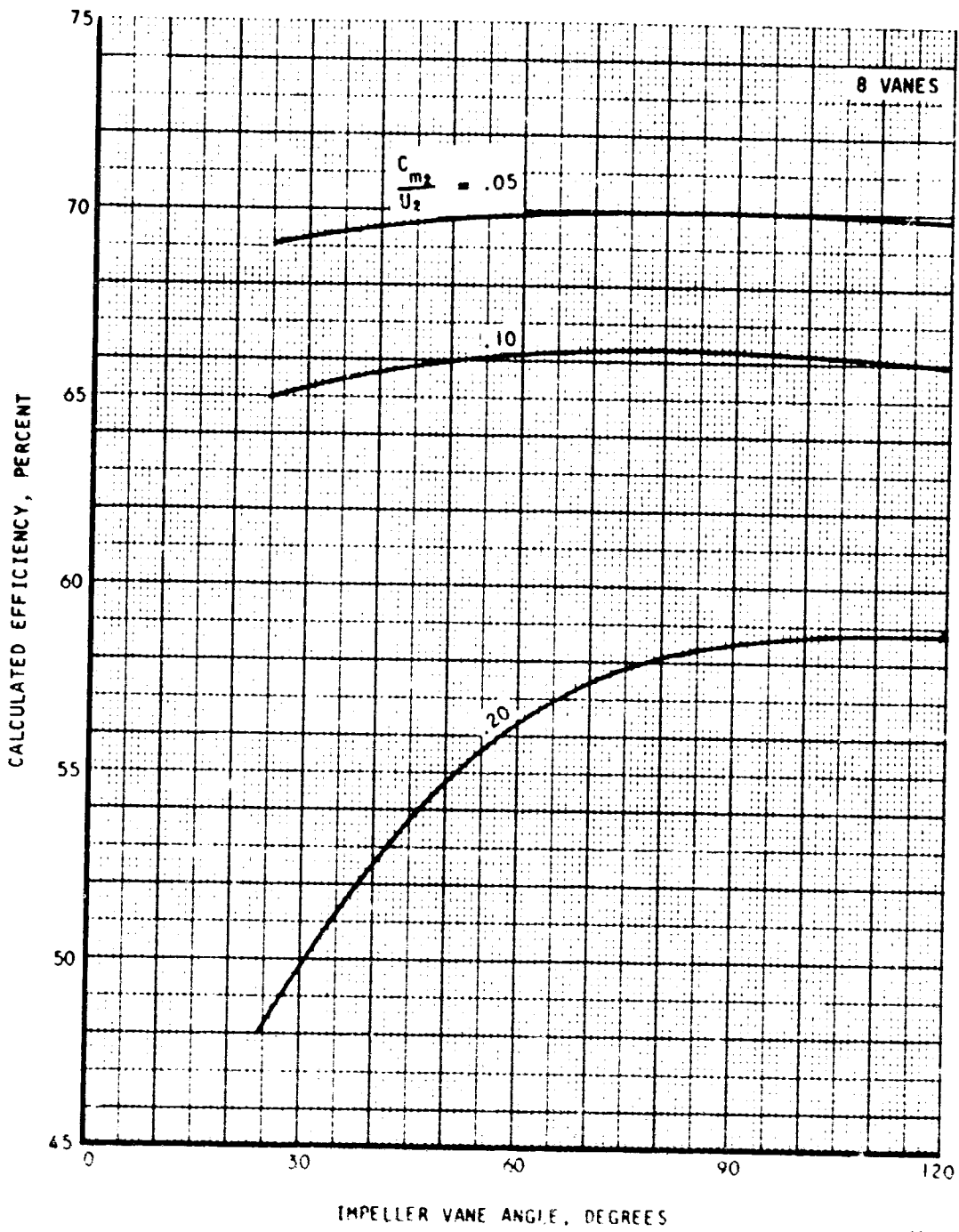
Figure 12. Efficiency Versus Vane Angle
At Different Flow Factors

18
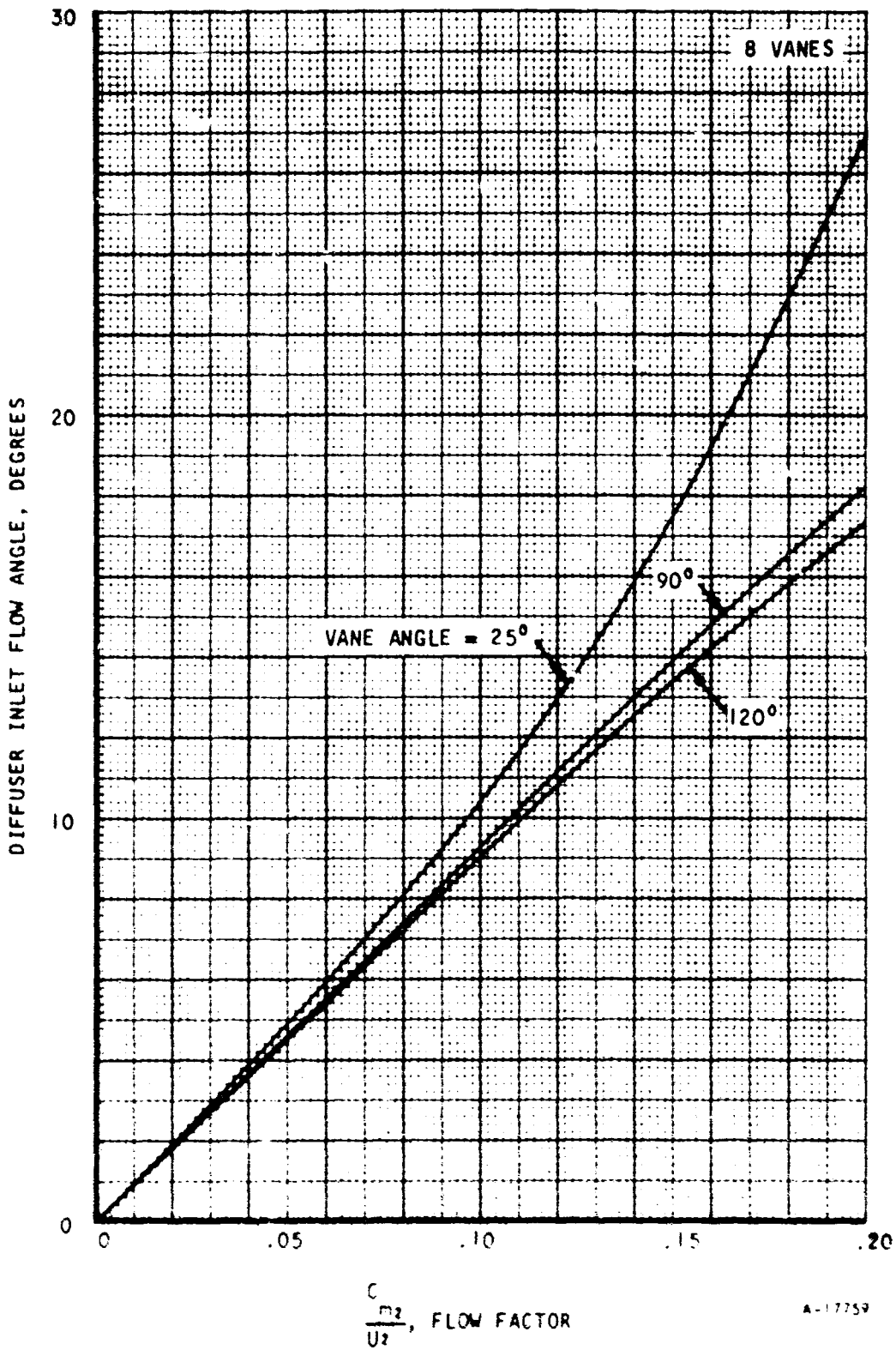
Figure 13. Diffuser Flow Angle Versus Flow
Factor and Vane Angle - 8 Vanes

19

Diffusing System

The success of the program depended upon achieving a high performance diffusing system. From this feasibility study, it was found that the problem was to design a diffuser of small height (0.050-0.100 in.) capable of handling a low Reynolds number of the order of 4,000-16,000 (based on the height of the vaneless space). In addition, this diffuser had to readily allow the transfer of the flow from one stage to the other.

From the results of various diffuser investigations, the following conceptual designs appeared promising:

1. Diffusing System

This system included a very short section of vaneless space (0.030-0.040 in.) between the impeller tips and the guide vanes to avoid mixing losses due to the wake of the blade. A set of 4 to 8 discrete diffusers is shown in Figure 14. These diffusing passages are designed with the proper rate of diffusion to handle the thick secondary layer as found at the inlet. In addition, three-dimensional diffusion, i.e., diffusion in the axial direction, must be considered to obtain a favorable cross section, in order to accommodate secondary flow development. Every diffusing channel is followed by a crossover tube designed to avoid secondary losses. This crossover tube leads to the inlet of the next stage.

2. Transition via a Mushroom Diffuser and Plenum

As an alternate to the concept of the crossover ducts, the flow at the exit of the diffusing channel, already at the initial stage of separation in a well-designed channel, is allowed to diffuse in a mushroom type of diffuser, Figure 15, and then dumped into the plenum with very small velocity. As a result, there exist no swirls in the plenum that would be accelerated at the inlet to the next stage, an effect that introduces considerable development in matching a multi-stage pump.

3. Guide Vanes - Annulus Space and Returning Vanes

The diffusing system includes these elements (Figure 16) in a standard approach to a multi-stage pump design. It does not hold too much promise for a low Reynolds number or small height application since the opportunities for mismatching these elements are considerable.

4. Guide Vanes with Boundary Layer Control

To handle the low Reynolds number and distorted flow of the diffuser, boundary layer control can be applied. Promising methods are:

a. Vortex Generator - The generation of vortices has been found to be helpful in the diffusion process. Conceptually, a small vane could be inserted in the middle of the blade channel for this purpose Figure 17.

CHANNEL CROSS-SECTIONS

CROSSOVER DUCT

CROSSOVER DUCT

IMPELLER
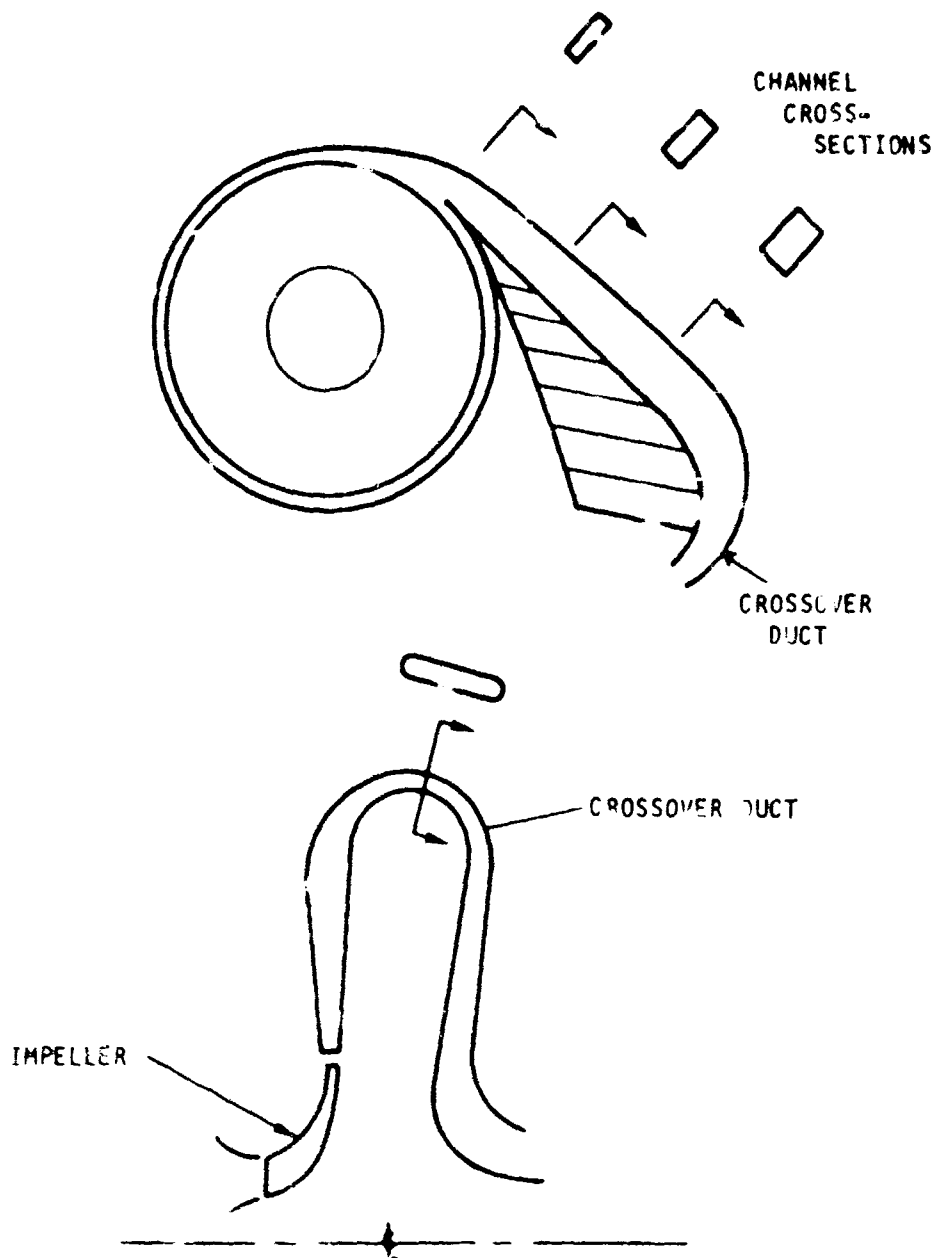
A-17760

Figure 14. Diffusing Channels
an Crossover Ducts

DIFFUSING CHANNEL

PLENUM
CHAMBER

MUSHROOM
DIFFUSER

PLENUM
CHAMBER

DIFFUSING
CHANNEL

IMPELLER
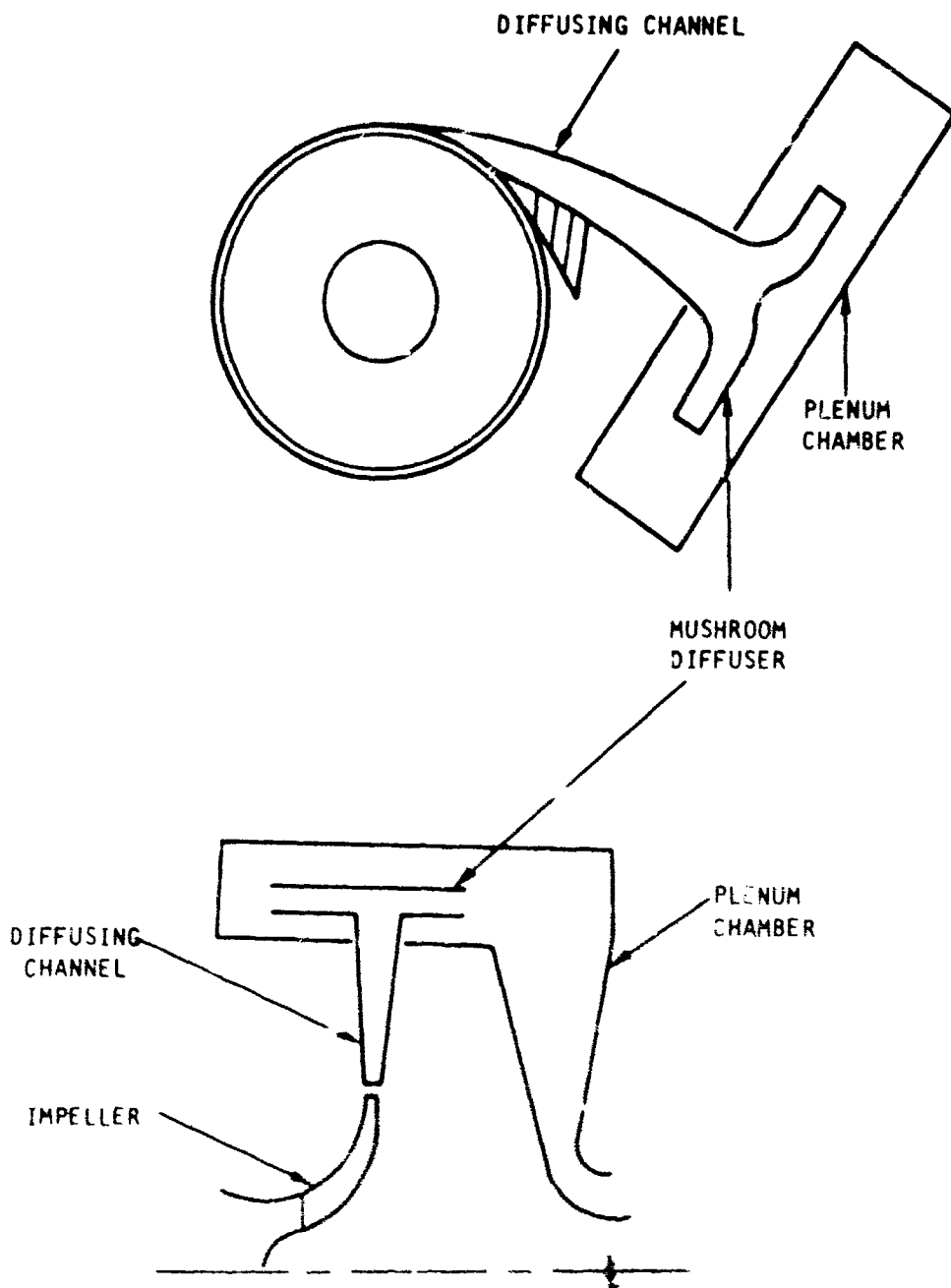
A-17261

Figure 15. Diffusing Channels and
Mushroom Diffuser

22

GUIDE
VANES

ANNULAR
BEND

IMPELLER
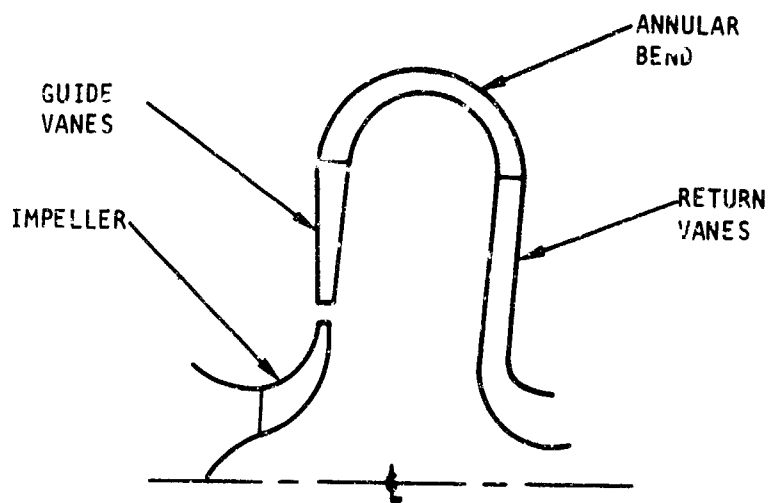
RETURN
VANES

A-17762

Figure 16 . Guide Vane Diffuser
and Returning Vane

23

DIFFUSING
CHANNEL
WITH CUSP
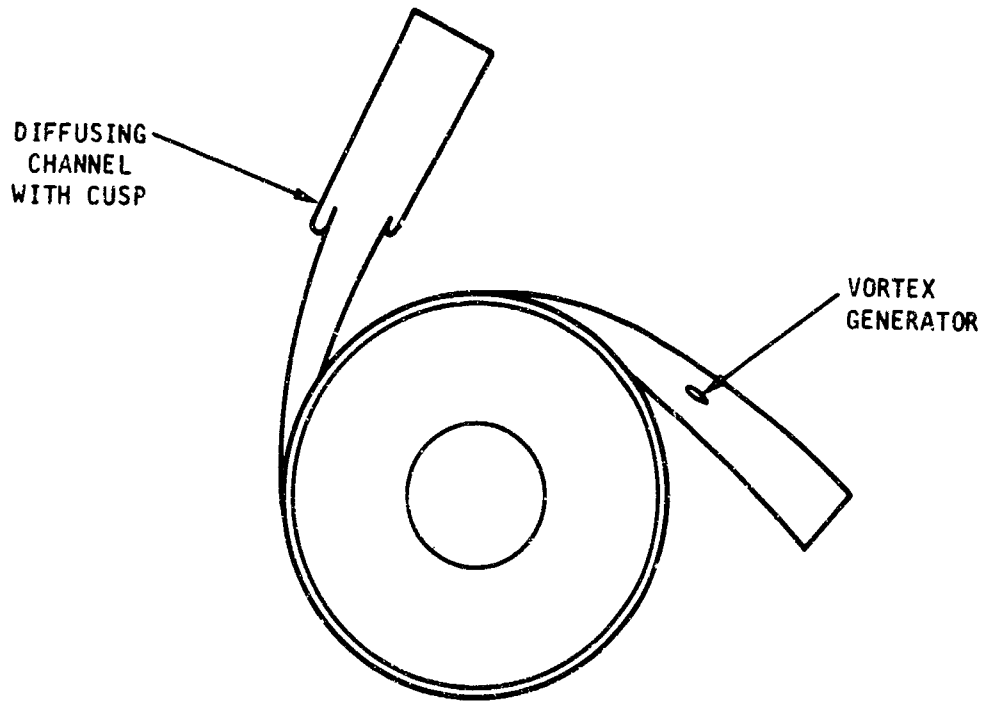
VORTEX
GENERATOR

A-17763

Figure 17. Vortex Generator
and Cusped Diffuser

24

b.   The Cusped Diffuser - Preliminary investigation by Reference 23 shows that use of a cusped design is most helpful in handling the diffusion of distorted flow. Physically, such a diffuser is also shown in Figure 17.

Results of the Feasibility Study

As a conclusion of this one-dimensional investigation, it appeared that a 60° vaned impeller (backward blading) with 8 blades, and a 120° vaned impeller (forward blading) with 8 blades and 8 splitter vanes are the two most promising solutions. The backward curved concept offered a more stable head-capacity curve. The forward curved impeller has a smaller disc, and probably better impeller performance. It has a lower degree of reaction and, therefore, emphasizes the achievement of a high performance diffuser.

Upon completion of the preliminary feasibility study, a generalized computer program, relating to all centrifugal pumps, was established. The conceptual theory and required input data for this program is reviewed below in the section that follows.

COMPUTER PERFORMANCE CALCULATION FOR CENTRIFUGAL PUMPS

This section presents the basis for calculating the performance of centrifugal pumps. The calculation is carried out with a computer program that handles the problem of performance at design point as well as that of off-design operation.

DESIGN POINT PERFORMANCE

Calculation of Design Geometry and Performance at Design Point

The first part of the calculation investigated the performance of different design combinations capable of meeting a given problem statement as expressed by the flow and pressure rise required by the fluid. The geometric dimensions, as well as the losses and efficiencies of these combinations, are presented to the designer, who can then choose the one most suitable for his purposes.

The program is based on one-dimensional calculation of the flow along the mean streamline, including friction, diffusion, loading, and boundary-layer-buildup factors. The equations contain experimental factors, which can be adjusted whenever the state of the art requires it.

The basic geometric design form of the pump is that of the Francis type, consisting of a centrifugal impeller having an integral mixed flow inducer portion and a radially arranged diffuser followed by a collector torus or scroll. This design arrangement, the most efficient combination, is shown in Figure 18 .

Within this general layout, there are many possible detail designs. The present program calculates four different inducer variations and four different diffuser designs.

1. Input Constants

The general design point performance program requires the following input values, which will be kept invariant during the calculations:

Flow, V_o - ft^3/sec

Pressure rise, ΔP_o - psi

Density, Y_o - lb/cu ft

Kinematic viscosity, v_* - ft^2/sec

Inducer design case (Case 1 to 4)

Diffuser design case (Case 1 to 4)

Impeller loss factors (ζ_1, ζ_2, ζ_3, ζ_8, ζ_9)

COLLECTOR

b_2

D_2

D_i

INLET

D_H
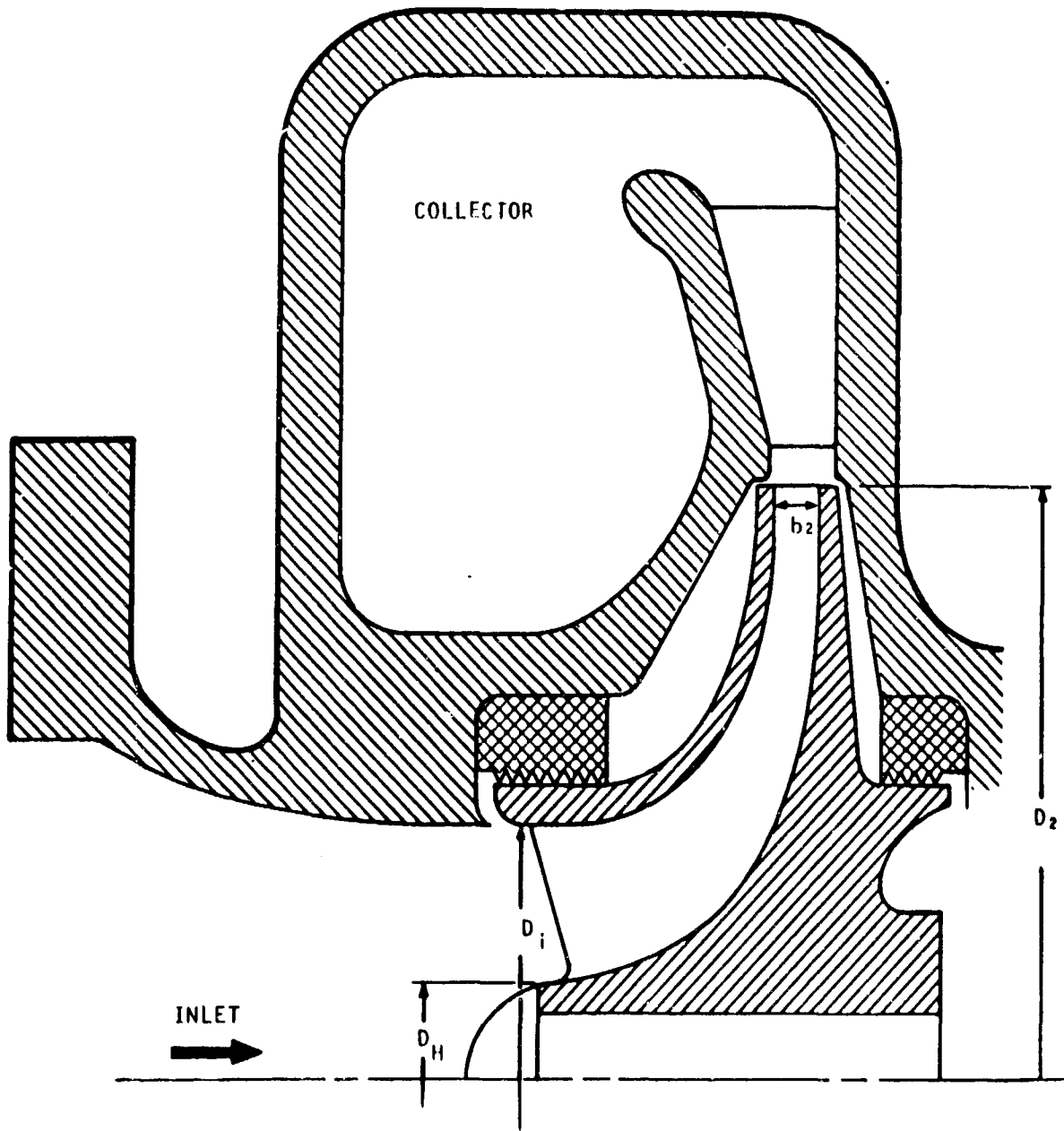
A-6976

Figure 18. Typical Centrifugal Pump

27

The necessary inputs for the inducer and diffuser design cases are different, depending on the case.

2. Input Variables

The performance of a pump impeller depends on (1) its geometric configuration, (2) the discharge vane angle, (3) the slip, which is primarily a function of the number of vanes, and (4) the discharge flow angle or flow factor. After these factors have been varied, the combination that performs best can be selected. In many cases, the optimum running speed is still to be established, so that the speed is also variable.

The variable inputs are then

Impeller tip vane angle, β_2, deg

Impeller slip factor, $\mu = \dfrac{C_{2_u}}{C_{2_u \infty}}$

Impeller flow factor, $\lambda = \dfrac{C_{2_M}}{u_2}$

Speed, N – rpm

3. Basic Relations

The basic relations used to establish the performance and geometrical characteristics of the pumps are derived in the following.

Pump Inducer

The size of the pump inducer is governed essentially by the availability of the suction head. A high suction head permits the flow to accelerate through the inducer without danger of cavitation. The inducer size is then reduced due to high-speed flow. With the condition of low NPSH (net positive suction head) the danger of cavitation is immediate, the flow speed must be kept low, and the inducer must be much larger. Thus, the following four alternates are considered for the sizing of the inducer:

1. The NPSH is given, and no cavitation at all is allowed.

2. Inlet vane angle is given, and no cavitation is allowed.

3. Inlet vane angle is given as 60 degrees; this case calculates low-pressure compressors, where compressibility effect is negligible.

4. There is cavitation at the inducer and inducer dimensions are precalculated.

Case 1 – NPSH Given and No Cavitation

The program calculates the inlet dimensions on the basis of the assumption that half of the NPSH can be used to produce the inlet velocity head, the other half of the head assuring a cavitation-free impact on the blades. This assumption, together with continuity requirements, yields the inlet diameter as

$$D_i^2 = \frac{576 \, V_o}{\pi \sqrt{32.175 \, NPSH}} + D_H^2 \quad (\text{inches})$$

Inlet flow angle is

$$\cot \beta_i = \frac{720 \sqrt{32.175 \, NPSH}}{\pi \, N \, D_i}$$

The velocities become

$$C_i = \sqrt{32.175 \, NPSH} \quad (\text{fps})$$

$$W_i = \sqrt{32.175 \, NPSH + \frac{N^2 \pi^2 D_i^2}{518,400}} \quad (\text{fps})$$

Case 2 – Inlet Vane Angle is Chosen – No Cavitation

The conventional pump inlet can be designed with this case, selecting 67.5° for blade angle; other values can be used just as well.

The inlet diameter is

$$D_i = \sqrt[3]{\frac{44,355 \, V_o}{N \, K_i \, \cot \beta_i}} \quad (\text{inches})$$

where K_i represents the restriction due to the hub

$$K_i = 1 - \left(\frac{D_H}{D_i}\right)^2$$

The velocities are given as:

$$U_i = \frac{\pi N D_i}{720} \quad (\text{fps})$$

$$C_i = U_i \cot \beta_i$$

$$W_i = \frac{U_i}{\sin \beta_i}$$

The velocity-head necessary to accelerate the fluid into the inlet is

$$NPSH_o : \frac{C_1^2}{64.35} \quad (ft)$$

The actual NPSH must be higher than this value.

Case 3 - 60-Degree Vane Angle Inducer

This case is the same as Case 2, except that the vane angle is fixed at 60 degrees, because this value gives the minimum inlet relative velocity for incompressible flow. It must be noted that the cavitation performance of such an inlet is not too good.

Case 4 - Cavitating Inducer

In a cavitating inducer, two-phase flow is encountered at the inlet. If the flow is assumed to be homogeneous, the density of the mixture can be approximated as

$$\frac{Y_o}{Y} = \left[1 + A \, \Delta h_o \right]^k$$

where Y_o density of the saturated liquid

Y = density of the mixture

Δh_o depression head, inlet, below the saturated state (TSH)

A and k are constant characteristics of the pumping fluid

For LH_2, the constants are

$$A \quad 0.02814 \qquad k \quad 0.4$$

This flow function, together with the diameters of the hub and tip of the inducer, is used to calculate the velocity and angle of the flow.

$$C_1 \left(\frac{D_1^2 \pi}{4} - \frac{D_H^2 \pi}{4} \right) \quad : \quad \frac{144 \, V_o}{\epsilon_1} \left[1 + A \left(\frac{C_1^2}{64.35} - NPSH \right) \right]^K$$

$$U_1 \quad \frac{D_1 N \pi}{720} \quad (fps)$$

$$W_1 \quad \frac{U_1}{\sin \beta_1} \quad (fps)$$

30

The flow angle is

$$\cot \beta_i \qquad \frac{C_i}{U_i}$$

The flow factor ϵ_i represents the resistance of the inlet. A value of 0.95 can be chosen if the inlet is an undisturbed coaxial design.

Losses at the Inlet

In the case of a shockless inlet, which is usual in normal pump design, the program does not separate the inlet loss from the general impeller losses. The cavitating inducer represents another case, because its incidence is designed to overcome, even at normal operating conditions, the effect of the very low angle and cavitation in the inducer throat. This operation results in additional losses, which will be calculated later in the part-load performance section.

Losses and Design Characteristics of the Impeller

The performance of a pump as measured by the pressure rise is often expressed in terms of energy in foot-pounds per pound of fluid flow or in head of fluid in feet. They are related together as

$$H_o \;=\; 144 \frac{\Delta P_o}{Y_o} \;\;(\mathrm{ft})$$

To deliver this energy, the pump impeller must develop a head, H_{th}, through a change in momentum imparted to the flow stream. The hydraulic efficiency of the pump, as related to the impeller and pump head, is

$$\eta_{HYD} \;=\; \frac{H_o}{H_{th}}$$

To start the calculation in the program, a first approximate value of η_{HYD} of 0.9 is assumed. Iteration is then carried out using the proper value for η_{HYD}.

1. Diameter

For convenience in performance calculation, dimensionless parameters are introduced by normalizing all values of head and losses with respect to $\dfrac{u_i^2}{g}$. Thus, the impeller head is associated with the head coefficient defined by

$$q \;-\; H_{th}\bigg/ \frac{u_i^2}{g}$$

The Euler momentum equation, then, relates q to other characteristic parameters of the impeller

$$q = \frac{C_{u_2}}{U_2} = \mu\,(1 - \lambda \tan \beta_2)$$

The diameter and tip speed of the wheel are derived from the three preceeding equations.

$$D_2 = \frac{720}{\pi N} \sqrt{\frac{32.175\ H_{TOT}}{q}} \quad (\text{inches})$$

$$U_2 = \sqrt{\frac{32.175\ H_{TOT}}{q}} \quad (\text{fps})$$

This gives the relative velocity at the impeller tip:

$$W_2 = U_2 \sqrt{\lambda^2 + (1 - q)^2} \quad (\text{fps})$$

2. Number of Blades

The other parameter of importance in the impeller design is the number of blades. The proper number depends upon the amount of flow "slip" at the impeller exit, upon the limit allowable for the blade loading, and upon other considerations such as the physical geometry and velocity triangles of the blades (Figure 19).

Following the investigation of Reference 11 which takes into account these various factors, the number of blades can be determined as

$$z_1 = \zeta_1 \frac{\pi\ \mu \cos \beta_2}{2\,(1 - \nu_2)\,(1 - \mu)}\ \left(1 + \frac{.08}{\zeta_1}\right)$$

where ζ_1 is an experimental factor which is normally close to 1.

$$\nu_2 = \frac{D_i}{D_2}, \text{ the impeller diameter ratio}$$

$$\zeta_1 = \frac{W_2}{W_i}, \text{ the ratio of velocity diffusion in the impeller}$$

The average length of the streamline in the flow passage is

$$\Delta l = \frac{0.8\ (D_2 - D_H)}{\cos \beta_i + \cos \beta_2} \quad (\text{inches})$$
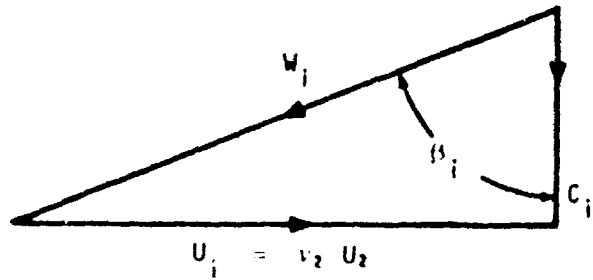
INLET - WITHOUT PREROTATION

$$U_i = \nu_2 U_2$$

$$C_2 = \sqrt{\lambda^2 + q^2}\ U_2$$

$$C_{2M} = \alpha U_2$$

$$C_{2u} = q U_2$$

$$C_{2u} = \lambda C_{2U}$$

$$C_{2u\infty} = (1 - \lambda\,TAN\beta_2)\,U_2$$
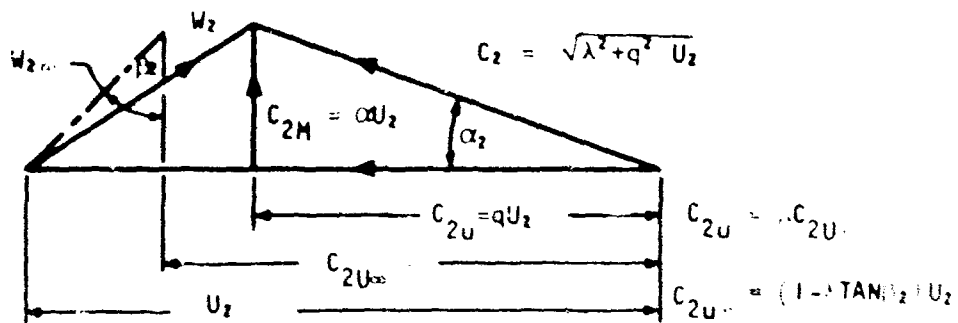
IMPELLER TIP

A-6979

Figure 19. Velocity Triangles at Mean Streamline

33

The average diameter of the impeller passage is calculated as

$$d_{HYD_i} = D_2 \left[\frac{1}{\frac{Z_1}{\pi \cos \beta_2} + \frac{1}{B_2}} + \frac{V_2}{\frac{2}{1 - v^2} + \frac{2Z_1}{\pi(1 + V_2)} \sqrt{1 + \tan^2\beta_i \left(\frac{1 + V_2}{2}\right)^2}} \right] \text{(inches)}$$

B_2, the dimensionless tip width of the wheel, is given by

$$B_2 = \frac{b_2}{D_2} = \frac{144 \, V_o}{\epsilon_2 \, \lambda u_2 \left(D_2^2 \pi - D_2 \frac{0.030 \, Z_1}{\cos \beta_2}\right)}$$

ϵ_2 is the restriction factor, generally assumed equal to 0.92.

The average relative velocity through the impeller is then needed

$$W_{AV} = \sqrt{\frac{W_i + W_2^2}{2}} \text{ (fps)}$$

The Reynolds number of the impeller passage is calculated with the values

$$Re_i = \frac{d_{HYD_i} \, W_{AV}}{12 \, v_*}$$

$$f_i = \frac{0.0462}{Re^{0.2}}$$

The skin friction loss coefficient through the impeller passage is

$$\Delta q_{SF} = \frac{\Delta H_{SF}}{q \frac{u_2^2}{g}} = \xi_2 \, \frac{f_i \, \Delta \ell_i}{d_{HYD_i}} \, \frac{W_{AV}^2}{u_2^2 \, q}$$

The experimental factor, ξ_2, is close to 1.

Another source of loss in the impeller arises from the diffusion of the flow in the blade passage. This is expressed by a blade loading factor, Δ, similar to the concept of the diffusion factor used in axial flow compressors. From Reference 11, Δ is given as

$$\Delta = 1 - \xi_1 + \frac{q \, (\cos \beta_i + \cos \beta_2)}{2 \frac{W_i}{u_2} \left[\frac{Z_1}{\pi} (1 - v_2) + 2 \, v_2\right]}$$

The loss coefficient associated with this diffusion is then

$$\Delta q_{DIFF} = \frac{\Delta H_{DIFF}}{q \frac{w_2^2}{g}} = \xi_3 \Delta^2 \left(\frac{w_i^2}{q u_2^2}\right)$$

ξ_3 is an experimental factor; for average calculations, 0.1 can be assumed.

In the experimental investigation of the interaction between the impeller and diffuser, it has been found that some of the flow that has passed the impeller does not enter the diffuser, but returns into the impeller, giving rise to a considerable energy loss. This phenomenon has not been fully investigated (References 11 and 15). At present, a recirculation loss parameter is used to account for this source of energy dissipation.

$$\Delta q_{RC} = \frac{\Delta H_{RC}}{q \frac{u_2^2}{g}} = \xi_4 \Delta \frac{q}{2}$$

The best value of ξ_4 factor has not yet been determined for all cases, but the calculations of shrouded impeller pumps show that it is close to zero. In the case of an unshrouded impeller, we arbitrarily assume the value 0.05. The foregoing are all of the internal losses of the impeller.

The internal static efficiency of the impeller is calculated as

$$\eta_{imp} = \frac{H_{TH} - \frac{C_2^2}{2g} - \Delta H_{DL}}{H_{TH} - \frac{C_2^2}{2g} + \Delta H_{SF} + \Delta H_{RC}}$$

or

$$\eta_{imp} = \frac{1 - \frac{\lambda^2 + q^2}{2q} - \Delta q_{DL}}{1 - \frac{\lambda^2 + q^2}{2q} + \Delta q_{SF} + \Delta q_{RC}}$$

Diffuser

An infinite variety of diffuser designs is possible. This program incorporates four different solutions, such as

1. Conical or parallel-sided straight-vaned diffuser

2. Multiscroll circular cross-section diffuser

35

3. Collector scroll (or torus)

4. Vaneless diffuser

The program calculates the transition portion from the impeller into the diffuser with an increased friction value. This increase of loss is due to the mixing of the uneven discharge from the impeller. The boundary-layer buildup is also estimated along this transition and the recovery of the following diffuser portion is estimated as a function of the calculated displacement thickness of the boundary layer (Reference 16).

Case I - Straight Wall Diffuser (Figure 20.)

The straight-wall diffuser of the geometry shown in Figure 20 is a design concept that lends itself readily to hardware fabrication.

For calculation purposes, it can be considered to be made up of a scroll element followed by a straight diffusing section. The boundaries between these elements appear as a throat. For high performance, diffusers are generally designed with a square throat section so that

$$\zeta_D = \frac{h_{THROAT}}{b_{THROAT}} = 1.5$$

The average velocity ratio in the scroll is

$$\left(\frac{c_{M2}}{c_u}\right) = \left(\frac{r}{r_2}\right) \frac{F(h)}{q} \sqrt{\lambda^2 + q^2}$$

where $\quad \dfrac{r}{r_2} = 1.04 + 0.69333\, \zeta_D\, B_2 \left(\dfrac{3 + 2\,\zeta_D \tan \gamma}{2 + \zeta_D \tan \gamma}\right)$

and $F(h)$ is a function characteristic of the geometry given by

$$F(h) = \frac{\lambda}{\sqrt{\lambda^2 + q^2}} + f_2 \left\{ \zeta_D(2 + \tan \gamma) + \frac{1}{2} \log_e \left(\frac{\zeta_D B_2 + 0.02}{0.02}\right) \right.$$
$$\left. - \left(\frac{2}{\tan \gamma} + \frac{1}{2}\right) \log_e \left[\frac{B_2(\zeta_D \tan \gamma + 2) + 0.02 \tan \gamma}{2B_2 + 0.02 \tan \gamma}\right] \right\}$$

Another parameter characterizing the flow in the diffuser is the Reynolds number

$$Re_{b_2} = 2B_2 \sqrt{\lambda^2 + q^2}\ Re_2$$

$$Re_2 = \frac{D_2 U_2}{12\ \nu*}$$

36
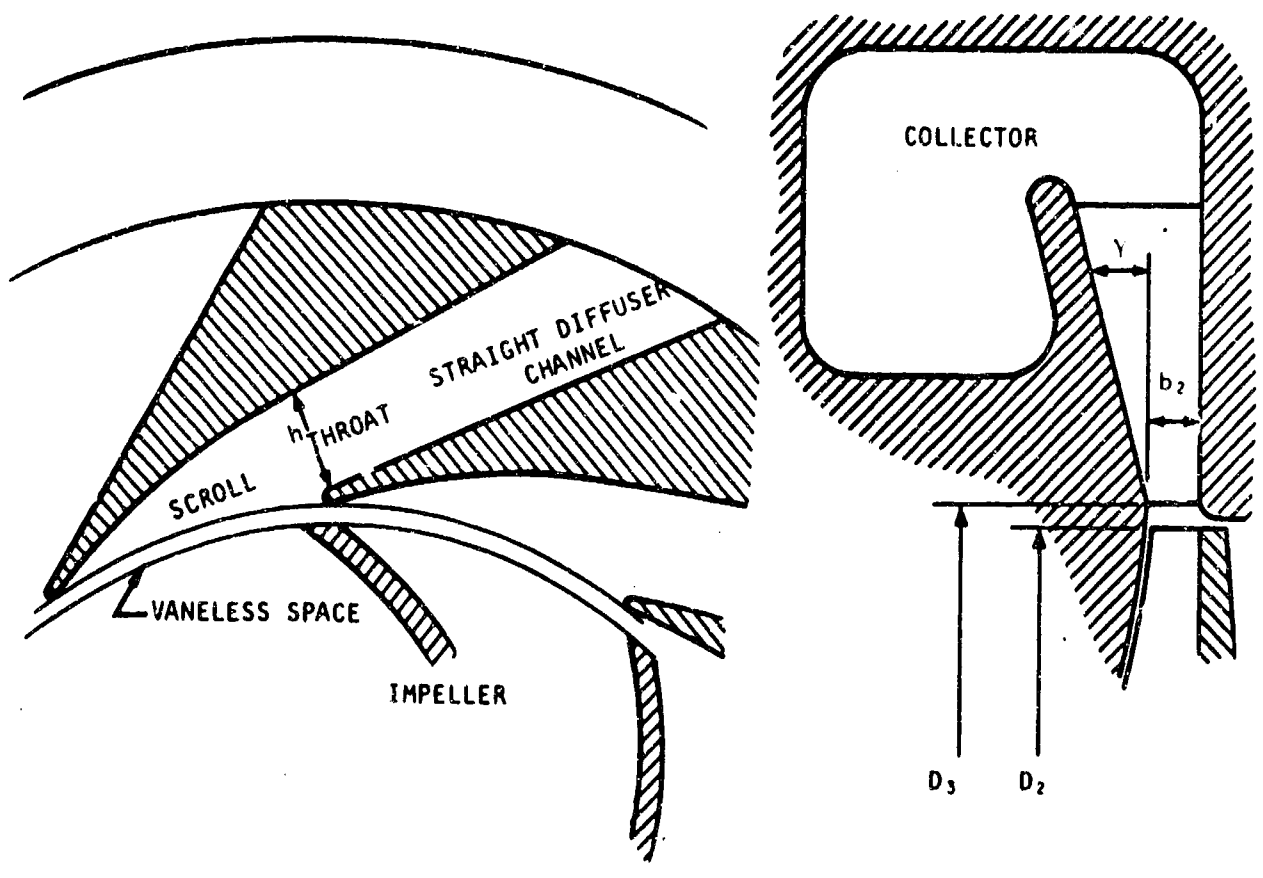
A-697'

Figure 2C.   Straight-Wall Diffuser

With D for turbulent flow, the local friction factor is

$$f_2 = \frac{0.0462}{Re_{b_2}^{0.2}}$$

This local friction factor can be used to a Reynolds number lower limit of 10^4.

For Re_{b_2} lower than 10^4, an adjustment has to be made, since the computer will extrapolate (11) for calculation purposes.

The actual vane number of the diffuser as given later is

$$Z_2 = \frac{2\pi}{\zeta_D B_2 (2 + \zeta_D \tan \gamma)} \left(\frac{C_{M_2}}{Cu} \right)$$

Practical reasons set the number of diffuser vanes between 6 and 16. Therefore, the program checks the value and, if it is different, adjusts the ζ_D value and recalculates.

This geometry represents the natural deceleration in the scroll. It gives the loss

$$\Delta q_{SC} = \frac{\lambda^2 + q^2}{2q} \frac{2f_2 \Delta \ell_2}{d_{H_2}} \left[1 + \left(\frac{Cu}{C_{M_2}} \right)^2 \frac{\lambda^2}{q^2} \right]$$

where   length of the flow path $\Delta \ell_2$ is

$$\Delta \ell_2 = D_2 \left[\frac{0.02 \sqrt{\lambda^2 + q^2}}{\lambda} + \sqrt{1.04 \frac{\pi^2}{Z_2^2} + \frac{B_2^2}{4}} \right] \text{ (inches)}$$

and the hydraulic diameter

$$d_{H_2} = D_2 \frac{4 B_2 \zeta_D (2 + \zeta_D \tan \gamma)}{2 + 2 \zeta_D + \zeta_D \tan \gamma} \text{ (inches)}$$

The loss in the following straight diffuser is then expressed as

$$\Delta q_{D_2} = \frac{\lambda^2 + q^2}{2q} \left(\frac{Cu}{C_{M_2}} \right)^2 \frac{\lambda^2}{q^2} \left[\zeta_5 + \zeta_6 f_2 \frac{\Delta \ell_2}{dH_2} \right]$$

The loss factors were chosen according to the test results presented in Figure 30. $\zeta_5 = 0.2$ and $\zeta_6 = 1.5$ give good approximations.

38
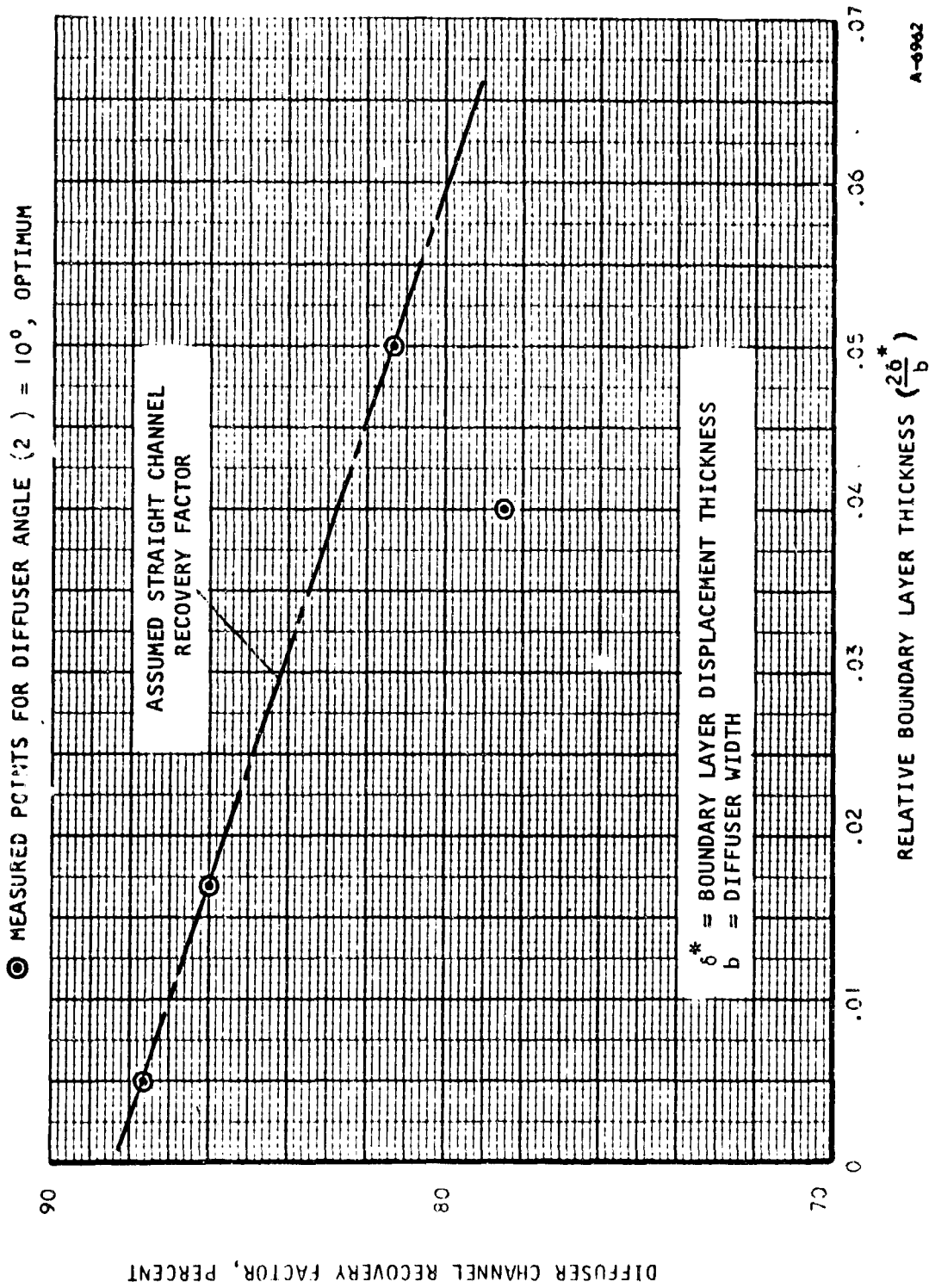
Figure 21. Influence of Boundary Layer Thickness on Diffuser Channel Pressure Recovery

A-6962

The overall diffuser loss is then

$$\Delta q_D = \frac{\Delta H_{DIFF}}{q\, u_2{}^2/g} = \Delta q_{SC} + \Delta q_{D2}$$

Case 2 - Multiscroll Diffuser with Circular Diffusers (Figure 22)

As the figure shows, the diffuser design consists of three portions – a vaneless space, a scroll and a straight circular diffuser.

As presented in Reference 15, the loss in the vaneless space is equal to

$$\Delta q_{2\text{-}3} = \frac{\delta}{2\cos\left(\frac{\alpha_2 + \alpha_3}{2}\right)}\left(1 + \frac{\cos^2\alpha_2}{1.0816\cos^2\alpha_3}\right)\frac{\lambda^2 + q^2}{2q}$$

where

$$\delta = \frac{0.32\, f_2}{B_2}$$

$$\cos\alpha_3 = \frac{(1 + \cos\alpha_2)^2\, e^\delta - \sin^2\alpha_2}{(1 + \cos\alpha_2)^2\, e^\delta + \sin^2\alpha_2}$$

$$\cot\alpha_2 = \frac{\lambda}{q}$$

The vaneless space is assumed to have a diameter

$$D_3 = 1.04\, D_2$$

The width ratio is given as

$$B_3 = \frac{b_2}{D_3}$$

In the scroll portion of the diffuser, the diameter ratio is given by

$$\frac{Z_2}{4\, B_3 \cot\alpha_3}\ \frac{D_3}{D_4}\left(\frac{D_4}{D_3} - 1\right)^2 = 1 + \frac{f_2\pi}{B_3 \cot\alpha_3}\left(\frac{D_4}{D_3} - 1\right)$$

The $\frac{D_3}{D_4}$ ratio is calculated from this equation.

The number of scrolls is an important design parameter. The single-volute collector design corresponds to $Z_2 = 1$. A higher number for Z_2 is considered. In the present program, Z_2 is set $Z_2 = 4$ for a typical calculation.

40
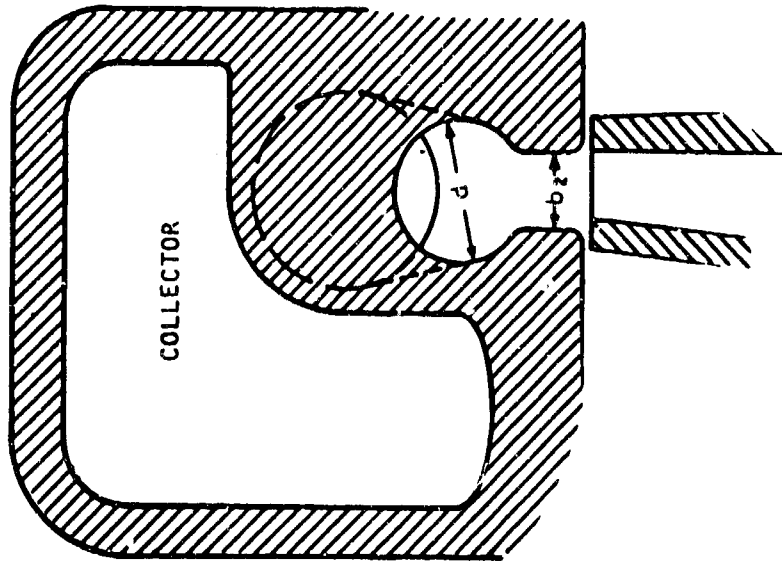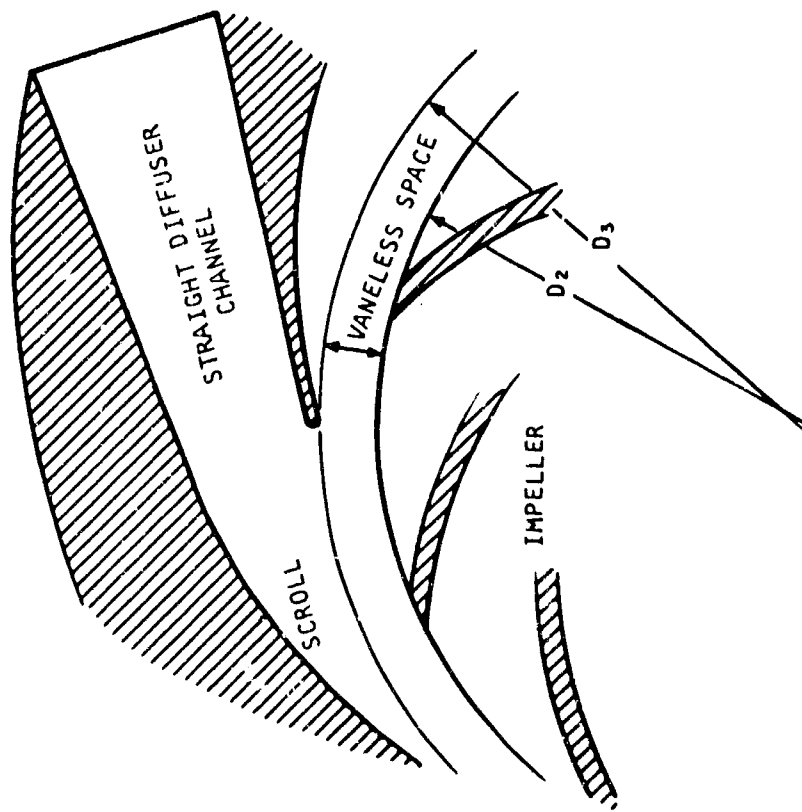
Figure 22.   Multiscroll Circular Cross-Section Diffuser

A-6978

41

The loss coefficient in the scroll is then

$$\Delta q_{3-4} = \frac{\pi f_2}{2} \left(\frac{\lambda^2 + q^2}{2q} \right) \left(\frac{D_2 \cos \alpha_2}{D_3 \cos \alpha_3} \right)^2 \left(\frac{1 + D_4/D_3}{D_4/D_3 + 2B_3 - 1} \right) \left[1 + \frac{B_3^2 \cos^2 \alpha_3}{(D_4/D_3 - 1)^2} \right]$$

For the straight circular diffusing element, the minimum possible loss achieved with the best recovery yields a loss coefficient of

$$\Delta q_{4-5} = \left(\frac{\lambda^2 + q^2}{2q} \right) \left(\frac{D_2 \cos \alpha_2}{D_3 \cos \alpha_3} \right)^2 \frac{B_3^2 \cos^2 \alpha_3}{\left(\frac{D_4}{D_3} - 1 \right)^4} \left[\zeta_6 + \frac{\zeta_7 (D_4/D_3 + 1)}{Re_{b_2}^{0.2}(D_4/D_3 - 1)} \right]$$

The boundary layer buildup factors are

$$\zeta_6 = 0.2 \text{ and } \zeta_7 = 0.0314$$

The total diffuser loss in the multiscore design is then

$$\Delta_{q_D} = \Delta q_{2-3} + \Delta q_{3-4} + \Delta q_{4-5}$$

Case 3 - Single Scroll and Diffuser

This case is similar to Case 2, except that $Z_2 = 1$.

Case 4 - Vaneless Diffuser

$$\Delta q_{2-3} = \frac{\delta}{2 \cos \left(\frac{\alpha_2 + \alpha_3}{2} \right)} \left(1 + \frac{\cos^2 \alpha_2 D_2^2}{\cos^2 \alpha_3 D_3^2} \right) \frac{\lambda^2 + q^2}{2q}$$

where $\delta = \frac{3 f_2 (D_3/D_2 - 1)}{B_2}$

$$\cos \alpha_3 = \frac{(1 + \cos \alpha_2)^2 e^{\delta} - \sin^2 \alpha_2}{(1 + \cos \alpha_2)^2 e^{\delta} + \sin^2 \alpha_2}$$

$$\cot \alpha_2 = \frac{\lambda}{q}$$

After the long vaneless space, a quite inefficient additional recovery is possible in the collector.

Here a fraction of the kinetic energy of the velocity leaving the impeller is assumed to be lost.

$$\Delta q_{3-4} = 0.66 \left(1 - \frac{\cos \alpha_2 \, D_2}{\cos \alpha_3 \, D_3} \right)^2 \frac{\lambda^2 + q^2}{2q}$$

The total diffuser loss in the vaneless diffuser is then

$$\Delta q_D = \Delta q_{2-3} + \Delta q_{3-4} + \Delta q_{4-5}$$

Hydraulic Performance of the Pump

The hydraulic performance measures directly the work which produces the pump pressure. This means that the head output of the pump must be equal to the required value after all the internal losses are deducted.

The hydraulic efficiency of the pump is then

$$\eta_{HYD} = \frac{H_o}{H_{TH}} \frac{1 - \Delta q_{DL} - \Delta q_D}{1 + \Delta q_{SF} + \Delta q_{RC}}$$

The hydraulic efficiency is now calculated from the above equation with various loss parameters which are obtained by starting the computation with an assumed value for η_{hyd}. The value from the above equation must be within 2 percent of the assumed value, or otherwise the computer will proceed to iterate.

Overall Efficiency and Power Input of the Pump

Besides the loss in energy in the impeller area diffuser passages, external losses must be considered. These are due to friction from the hub disc which supports the impeller blades and the leakage through the seal clearance.

The disk friction loss is often given as

$$\Delta q_{FR} = \frac{\xi_8}{10^5 \lambda q \, B_2} \left(\frac{10^6}{Re_2} \right)^2$$

The experimental factor $\xi_8 = 0.285$ is to be assumed for the case of a shrouded wheel and $\xi_8 = 0.366$ for an unshrouded wheel.

$$\Delta q_L = \frac{\xi_9 \cdot .006 \, v_1^2}{B_2} \sqrt{\frac{2q - \lambda^2 - q^2}{2q}}$$

The factors are $\xi_9 = 1.0$ for a shrouded impeller and $\xi_9 = 0.5$ or 0 for an unshrouded one.

The overall efficiency of the pump, from which the hydrodynamic power input is obtained, is then

$$\eta = \frac{H_{out}}{H_{in}} = \frac{\eta_{hyd}}{1 + \Delta q_{FR} + \Delta q_L}$$

43

PART-LOAD PERFORMANCE OF THE PUMP

The program calculates the estimated friction, diffusion and incidence losses of the design described by the design-point performance program for variable flow and speed values. Provision is also made for changing the fluid density and viscosity; the geometric design is fixed.

Input Variables

In addition to the design point input, additional data are necessary for the part-load program

ν - the viscosity of the fluid, which can be different from the design viscosity

γ_o = the density of the fluid, this can be also different

M_o = flow ratio in steps, defined as $M_o - \dfrac{\text{part load flow}}{\text{design flow}}$ at constant speed

N/N_o = speed ratio in steps

$$\frac{N}{N_o} = \frac{\text{part load speed}}{\text{design speed}}$$

NPSH   - net positive suction head; can be different from the design value

A a d K - cavitation expansion constants

a_1, a_2, a_3 - incidence loss constants of the inducer

Ψ_c cavitation loss constant

Ψ_3 diffuser incidence loss constant

Impeller Performance

1. Cavitation-Free Operation

The impeller inlet flow is equal to the nominal flow plus the increase due to leakage. Expressed by the flow factor, it is

$$M \quad M_o \cdot \Delta q_L$$

The leakage loss is taken from the original design point calculation as a first approximation

44

With the change in flow rate and speed, the flow factor at the impeller changes so that the head coefficient is now calculated

$$q = u (1 - \lambda_o M_o \tan \beta)$$

$$u = \frac{1}{1 + \zeta_1 \dfrac{\pi \cos \beta_2}{2Z} \dfrac{1}{(1 - \nu_2)} \left(1 + \dfrac{0.08}{\zeta_1}\right)}$$

with

$$\zeta_1 = \sqrt{\frac{M_o^2 \lambda_o^2 + (1 - q)^2}{\nu_2^2 + M_o^2 \phi_o^2}}$$

where $\quad \phi_o = \dfrac{C_o}{U_{2o}} = \nu_2 \cot \beta_{io}$

At off-design, an incidence is encountered at the inducer inlet so that the incidence loss is given as

$$\Delta q_{inc} = \psi_2 \left(\frac{W_i}{U_2}\right)^2 \frac{1}{2q}$$

where ψ_2 is an experimental constant. According to the test values on axial compressors, ψ_2 is a parabolic function of the incidence angle:

$$\psi_2 = a_1 + a_2 \Delta \beta_i + a_3 \Delta \beta_i^2$$

$$\Delta \beta_i = \left| \beta_i - \beta_{io} \right| \quad \text{(absolute value)}$$

$$\cot \beta_i = M \cot \beta_{io}$$

The average relative velocity in the impeller passages is

$$W_{AV} = \frac{U_2}{\sqrt{2}} \sqrt{(1 + \zeta_1)^2 (M^2 \cot^2 \beta_{io} + \nu_2^2)}$$

The Reynolds number calculated with this velocity inside the impeller passages is

$$Re_i = \frac{d_{HYD_i} W_{AV}}{12 \nu}$$

$$U_2 = \frac{D_2 \pi N_o}{720} \left(\frac{N}{N_o}\right)$$

d_{HYD_i} is given by the design point calculation. The new friction factor becomes

$$f_1 = \frac{0.0462}{Re_i^{0.2}}$$

45

With this factor, the friction is to be calculated

$$\Delta q_{SF} = \xi_2 \frac{f_1 \, \Delta \ell_1}{d_{HYD1}} \, \frac{W_{AV}^2}{U_2^2 \, q}$$

$\Delta \ell_1$ is to be taken from the design point calculation.

The diffusion factor through the impeller is

$$\Delta = 1 - \zeta_1 + \frac{q \, (\cos \beta_i + \cos \beta_2)}{2 \frac{W_i}{U_2} \left[\frac{Z_1}{\pi} (1 - \nu_2) + 2\nu_2 \right]}$$

where

$$\frac{W_i}{U_2} = \sqrt{\nu_2^2 + \nu_2^2 \cot^2 \beta_{io} \, M^2}$$

The diffusion loss is then

$$\Delta q_{DL} = \xi_3 \, \Delta^2 \left(\frac{W_i^2}{U_2^2 \, q} \right)$$

And the recirculation loss becomes

$$\Delta q_{RC} = \xi_4 \, \Delta \frac{q}{M_o \lambda_o}$$

The constants ξ_2, ξ_3, and ξ_4 are the same as in the design point program.

2. Cavitating Performance

The calculation of the cavitating impeller performance is similar to that for the previously described one, but since the density is not constant in the inlet, the inlet velocities are a function of the flow.

The head factor is

$$q = \mu \, (1 - \lambda_o \, M \tan \beta_2)$$

$$M = \frac{1}{1 + \xi_1 \frac{\pi \cos \beta_2}{2 Z_1 \, (1 - \nu_2)} \left(1 + \frac{0.08}{\zeta_1} \right)}$$

$$\zeta_1 = \sqrt{\frac{M^2 \lambda_o^2 + (1 - q)^2}{\nu_2^2 + S_1^2 M^2 \phi_o^2}}$$

$$\phi_o = \frac{C_{1o}}{U_2}$$

$$U_2 = \frac{D_2 \, \pi \, N_o}{720} \left(\frac{N}{N_o} \right)$$

$$C_{1o} = C_i \left(\frac{N}{N_o} \right)$$

The inducer entering velocity C_i results from the design point calculation. Following the correlation of the mixture density given previously, the density change at the inlet to the cavitating inducer changes with speed and flow rate as

$$\frac{\gamma\left(\text{at } M_o, \frac{N}{N_o}\right)}{\gamma(\text{at design})} = S_i = \left[\frac{1 + A\left(M_o^2 \frac{C_{io}^2}{2g} - NPSH\right)}{1 + A\left(\frac{C_i^2}{2g} - NPSH\right)}\right]^K$$

where the design point corresponds to the value of 1 for the parameters M_o and $\frac{N}{N_o}$. When the inlet velocity head $\left(M_o^2 \frac{C_{io}^2}{2g}\right)$ is smaller than the NPSH, no density changes take place. Then $S_i = 1$.

The inducer incidence loss is similar to the previous case:

$$\Delta q_{inc} = \psi_2 \frac{\left(\frac{W_i}{U_2}\right)^2}{2g}$$

where $\psi_2 = a_1 + a_2 \Delta\beta_1 + a_3 \Delta\beta_1^2$

$\Delta\beta_1 = \left|\beta_1 - \beta_{1o}\right|$ (absolute value)

$\cot \beta_1 = \dfrac{S_i M\phi_o}{v_2}$

$\left(\dfrac{W_i}{U_2}\right)^2 = v_2^2 + S_i^2 M^2 \phi_o^2$

The loss constants can be assumed to be

$a_1 = 0$

$a_2 = 0$

$a_3 = 0.025$

There is, however, an additional loss with cavitating operation--the cavitation loss:

$$\Delta q_{CAV} = \psi_C \left[\left[1 + A \left(M_0^2 \frac{C_{01}^2}{2g} - NPSH \right) \right]^K - 1 \right] (\nu_2^2 + S_1^2 M^2 \phi_0^2)$$

The value of ψ_C can be assumed to be between 0.5 and 1.0.

The impeller skin friction is

$$\Delta q_{SF} = \xi_2 \frac{f_1 \Delta \ell_1}{d_{HYD_1}} \frac{W_{AV}^2}{U_2^2 q}$$

where $f_1 = \dfrac{0.0462}{Re_1^{0.2}}$

$$Re_1 = \frac{d_{HYD_1} W_{AV}}{12 \nu}$$

$$W_{AV} = U_2 \sqrt{\frac{(1 + \zeta_1^2)(S_1^2 M^2 \phi_0^2 + \nu_2^2)}{2}}$$

The diffusion factor is

$$\Delta = 1 - \zeta_1 + \frac{q (\cos \beta_1 + \cos \beta_2)}{2 \frac{W_1}{U_2} \left[\frac{Z_1}{\pi} (1 - \nu_2) + 2\nu_2 \right]}$$

$$\frac{W_i}{U_2} = \sqrt{\nu_2^2 + S_1^2 M^2 \phi_0^2}$$

With these values, the diffusion loss is

$$\Delta q_{DL} = \xi_3 \Delta^2 \left(\frac{W_i^2}{U_2^2 q} \right)$$

and the recirculation loss will be

$$\Delta q_{RC} = \xi_4 \Delta \frac{q}{\lambda_0 M_0}$$

ξ_1, ξ_2, ξ_3, and ξ_4 factors are the same as in the design point program.

48

Diffuser Performance at Part Load

At off-design operation, the diffuser vanes or scrolls suffer incidence loss on their tip:

$$\Delta q_{DIN} = \psi_3 \frac{(q - q_o)^2 + (\lambda_o - M_o \lambda_o)^2}{2q}$$

ψ_3 factor is also a function of the incidence angle. As the angle of attack is normally very small with the low flow angles encountered in pump design practice, this value can be assumed constant and equal to unity.

The diffusion loss can be calculated by assuming the same relative loss percentage of the available energy as was assumed at the design point.

$$\Delta q_D = \Delta q_{Do} \frac{M_o q_o}{q} \sqrt{\frac{(\lambda_o^2 M_o^2 + q^2) q_o}{(\lambda_o^2 + q_o^2) q}}$$

where Δq_{Do} is the diffuser loss at design point.

Pressure Ratio

The head and pressure can be calculated from the hydraulic losses.

The total head output is

$$H_{TH} = \frac{q U_2^2}{32.175} \quad (ft)$$

The hydraulic efficiency is

$$\eta_H = \frac{1 - \Delta q_{INC} - \Delta q_{CAV} - \Delta q_{DL} - \Delta q_{RC} - \Delta q_{DIN} - \Delta q_D}{1 + \Delta q_{SF}}$$

The head of the pump becomes

$$H_o = \eta_H H_{TH} \quad (ft)$$

and the pressure rise is

$$\Delta P_o = \frac{\gamma_o H_o}{144} \quad (psi)$$

49

Outside Losses and Overall Efficiency

The wheel friction changes with the flow and the Reynolds number:

$$\Delta q_{FR} = \frac{\xi_8}{1000 \, \lambda_0 M_0 q B_2} \left(\frac{10^6}{Re_2}\right)^{0.2}$$

$$Re_2 = \frac{U_2 D_2}{12 \, v^{*}}$$

The leakage changes also

$$\Delta q_L = \frac{\xi_9 \, 0.006 \, v_2^2}{B_2} \sqrt{\frac{2q - \lambda_0^2 M_0^2 + q^2}{2q}}$$

ξ_8 and ξ_9 factors are similar to those of the design point.

The overall efficiency is calculated with these losses.

$$\eta = \frac{\eta_H}{1 + \Delta q_{FR} + \Delta q_L}$$

The power consumption of the wheel is then

$$HP = \frac{H_0 M_0 V_0 \gamma_0}{\eta \, 550} \left(\frac{N}{N_0}\right)$$

The program prints out the losses, the efficiencies, the head, the pressure and the horsepower values. In addition, it prints out a diagram of the pressure rise and the efficiency versus relative flow with relative speed as a parameter.

50

GEOMETRY AND PARAMETER CALCULATIONS, COMPARISON WITH TEST RESULTS, AND
NOMENCLATURE

Calculation of the Inlet Scroll of a Vaned Diffuser with Conical Sideplate

Figure 23 shows the general arrangement of the inlet scroll of a vaned
diffuser with conical sideplate. The numerical calculation of the inlet scroll
profile is based on the natural deceleration principle. This means that the
momentum of the fluid is decreased only by the friction on the walls. The
geometry of the diffuser scroll is shown in Figure 23 also.

The decelerating momentum is expressed by the friction on the walls:

$$dM = frc^2 (2h - 2h_o + b) \frac{\rho}{2} \cos\alpha \, dx$$

The mass element of the fluid is

$$dm = \rho(h - h_o) \frac{b_o + b}{2} \, dx$$

The width of the channel is a function of the sideplate angle:

$$b = b_o + (h - h_o) \tan \gamma$$

Combining these equations results in

$$\frac{dM}{dm} = \frac{f c^2 \cos\alpha \, r (2h - 2h_o + b)}{(h - h_o)(b_o + b)}$$

The momentum equation is given as

$$-\frac{dM}{dm} = \frac{d(c_u r)}{dt} = c \frac{d(c_u r)}{dx}$$

Finally, the first form of the differential equation is

$$\frac{d(c_u r)}{dx} = \frac{f c_u r (2h - 2h_o + b)}{(h - h_o)(b_o + b)}$$

The relation between x and h is given by the continuity. The volume
changes along a $d\varphi$ angle when the flow is incompressible:

$$dV = C_{Mo} b_o r_o d\varphi = \frac{c_u}{2} \left[(h - h_o) \tan \gamma + b + b_o \right] dh$$

The dx is expressed as a function of $d\varphi$

$$dx = rd\varphi = \frac{c_u r}{2b_o C_{Mo} r_o} \left[(h - h_o) \tan \gamma + b + b_o \right] dh$$
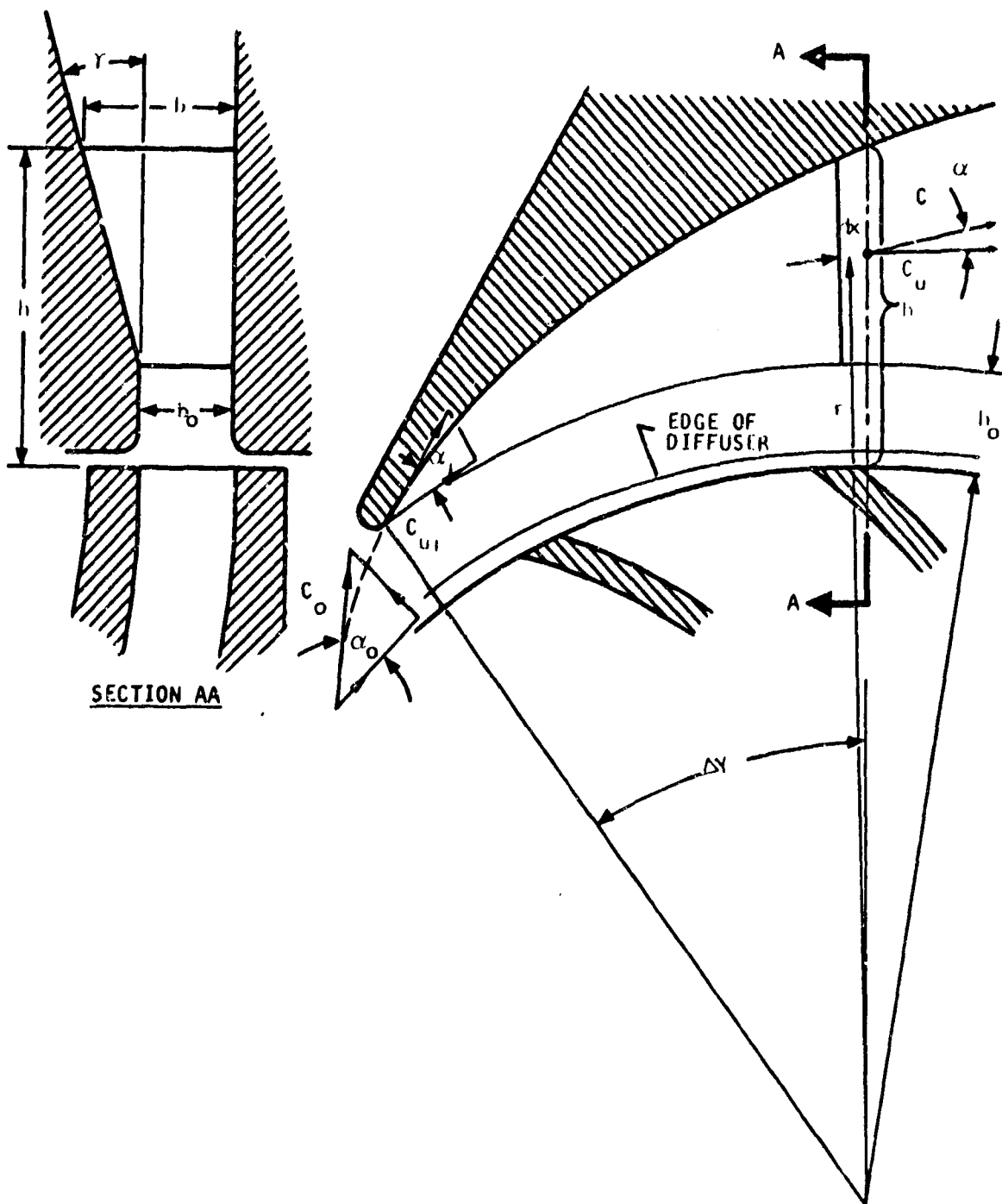
Figure 23. Diffuser Geometry and Velocities

A-6977

52

Since $dH = frc^2 (d\pi - b_o) \frac{b}{2} \cos\alpha\, dx$ and $dm = \rho \frac{d^2\pi}{4} dx$, combining these with Equations (14) and (15) results in

$$\frac{d(C_u r)}{(C_u r)^2} = -\frac{f\pi}{C_{Mo} b_o r_o} \left(1 - \frac{b_o}{\pi d}\right) d\,(d)$$

The integral is then

$$-\frac{1}{C_u r} = -A \left(d - \frac{b_o}{\pi} \log d\right) + \text{constant}$$

In this expression the logarithmic term represents the so called "tongue" effect--the increased friction due to the theoretically high losses connected with the very small diameter in the beginning of the scroll. This is only theoretically so; in practice, the channel always has a minimum width--the width of the vaneless diffuser portion where the flow can adjust itself and reduce the relative friction. Therefore, this logarithmic term of the equation can be replaced by a constant and an increased friction factor given by experimental comparison with existing diffuser results.

$$\frac{C_{uo} r_o}{C_u r} = 1 + \frac{f 2\pi (r - r_o)}{b_o \tan \alpha_o}$$

$$\frac{C_{uo}}{C_u} = \frac{r}{r_o} \left[1 + \frac{\pi f}{B_o \tan \alpha_o} \left(\frac{r}{r_o} - 1\right)\right]$$

$$\frac{C_{uo}}{C_u} = \left(1 + \frac{d}{D_o}\right) \left(1 + \frac{f\pi}{B_o \tan \alpha_o} \quad \frac{d}{D_o}\right)$$

The angular position of the cross section given in degrees of angle is

$$\Delta\varphi = \frac{90}{B_o \tan \alpha_o} \left(\frac{C_u}{C_{uo}}\right)\left(\frac{d}{D_o}\right)^2$$

This equation also can be expressed as the number of diffuser vanes

$$z = \frac{B_o \tan \alpha_o \left(\frac{C_{uo}}{C_u}\right)}{4\left(\frac{d}{D_o}\right)^2}$$

53

Estimating Straight Diffuser Recovery from Boundary Layer Thickness in the Throat

Reference 7 describes some tests conducted with straight and curved channels, measuring the maximum pressure recovery of different diffuser configurations having variable boundary-layer thicknesses in the diffuser inlet throat. In the report, the actual displacement thickness of the boundary layer is given.

The recovery factor of a diffuser is defined as the ratio of the pressure rise across the diffuser and the total inlet velocity energy entering the diffuser:

$$R_c = \frac{2g\Delta p}{\rho c_i^2}$$

The relative displacement thickness of the boundary layer at the inlet throat of the diffuser is given as the ratio of the integral average displacement thickness and the width of the throat, $\frac{2\delta^*}{b}$.

The measured test results were plotted in Figure 25 for straight channels and for curved-elliptic channels. The result shows the well known fact that the straight channel has better recovery than a curved one.

The measured performance points of the straight diffusion channels can be connected by a linear function. The general form of the loss vs relative boundary layer thickness will take the following form:

$$C_\ell = a_1 + a_2 \frac{2\delta^*}{b_2}$$

For general calculations, it seems to be better to replace the diffuser width by the hydraulic diameter of the diffuser throat

$$C_\ell = a_1 + a_3 \frac{\delta^*}{d_{HYD}}$$

The a_1 and a_3 constants are functions of the form of the throat. The circular cross section gives lower losses and higher recovery than a flat rectangular one.

With the help of this approximate equation of the pressure loss factor, it is possible to estimate the loss of the straight portion of the diffuser. The displacement thickness can be calculated from the average length of a streamline and the Reynolds number, while the hydraulic diameter is given by the geometry of the diffuser.
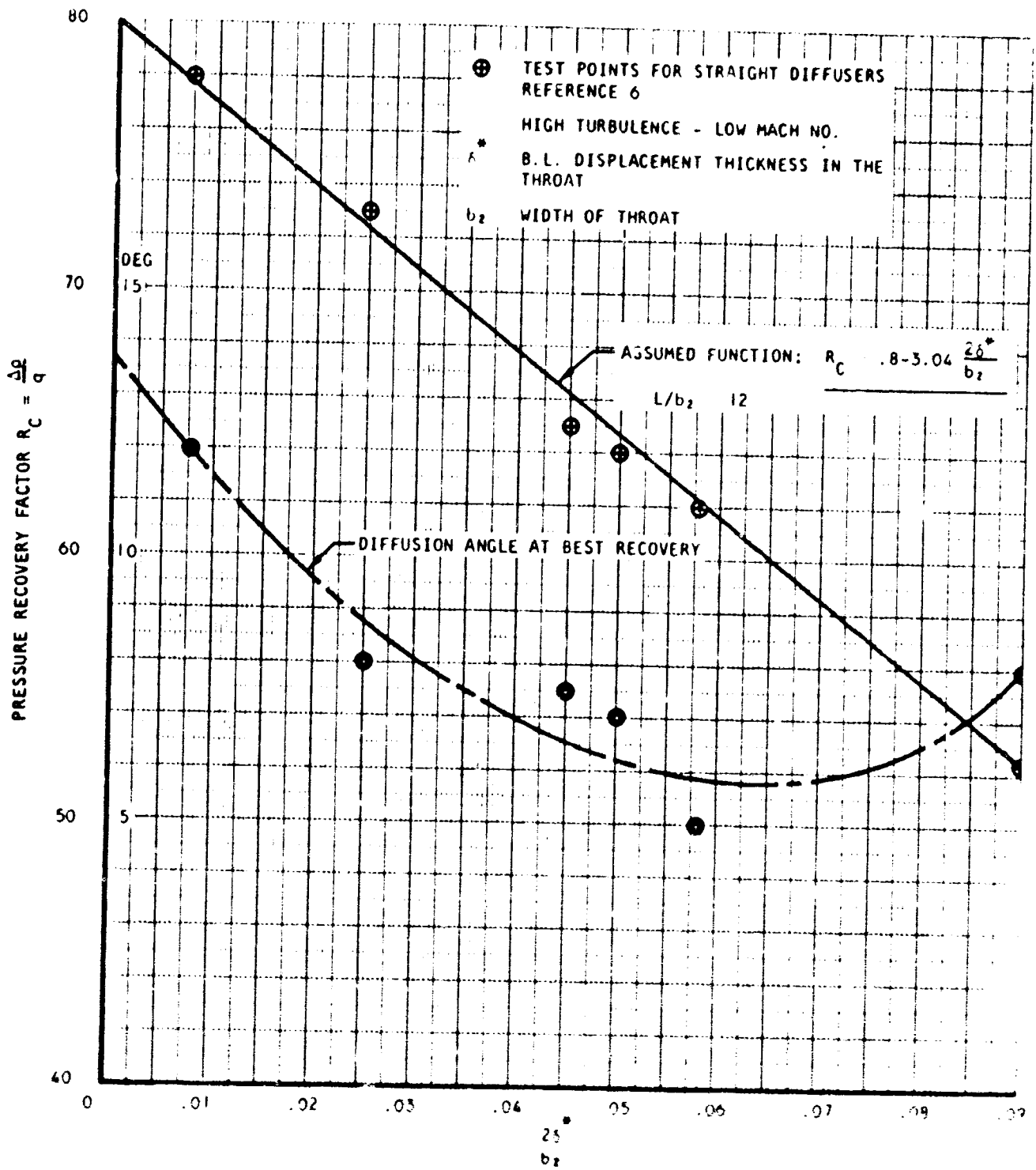
Figure 24. Diffusers - Maximum Recovery vs. Throat-Boundary-Layer Thickness

In the case of conical sidewalled vaned diffusers, the length of the streamline is Δl_2, the hydraulic diameter is d_{H2}. The displacement thickness with turbulent flow is a function of Reynolds number and length of the streamline:

$$\delta^* = \frac{a_4}{Re^{a_2}} \Delta l_2$$

The friction factor in the diffuser function is similarly a function of the Reynolds number, so the displacement thickness also can be expressed in the following form:

$$\delta^* = a_5 f_2 \Delta l_2$$

Combining the two previous equations gives

$$C_l = a_1 + a_3 a_5 f_2 \frac{\Delta l_2}{d_{H2}}$$

The total loss of diffusion after the throat is the product of the loss factor given above and the available velocity energy in the diffuser throat. The velocity ratio between the impeller tip and the diffuser throat can be calculated as shown in preceding paragraphs. The velocity energy ratio becomes

$$\frac{C_T^2}{2g\, H_{TH}} = \frac{q^2 + \lambda^2}{2q} \left(\frac{C_u}{C_{M_2}}\right)^2 \frac{\lambda^2}{q^2}$$

and the relative loss in the straight diffuser is

$$\Delta q_{DIFF\ 2} = \frac{\lambda^2 + q^2}{2q}\left(\frac{C_u}{C_{M_2}}\right)^2 \left(a_1 + a_3 a_5 f_2 \frac{\Delta l_2}{d_{H2}}\right)$$

or, with combined loss factors

$$\Delta q_{DIFF\ 2} = \frac{\lambda^2 + q^2}{2q} \left(\frac{C_u}{C_{u_2}}\right)^2 \left(\xi_5 + \zeta_6 f_2 \frac{\Delta l_2}{d_{H2}}\right)$$

Comparison with Test Results

As was emphasized earlier, this program calculates the performance of an assumed ideal pump configuration and does not compute efficiency of existing pump geometries. This fact must be kept in mind when calculations are compared with test results for existing machinery.

36

In order to compare the calculation results with statistical average and predicted optimum performances, a number of data were gathered on high-Reynolds-number pump performances and plotted in Figure 1. For comparative purposes, three points were calculated by the present computer program using water as fluid, assuming no cavitation and a Reynolds number close to 10^7. The specific speeds of the calculated samples were 500 to 1000 and 2000. The results of the calculations were also plotted in the diagram. The points fit the top efficiency curve quite well, the program therefore might be used to predict the performance of advanced pump designs with confidence.

Nomenclature

γ density (lb/cu ft)

    γ_o average liquid density

P   pressure (psia)

    ΔP_o pressure rise (psi)

H   head (ft/lb/lb)

    H_o actual head (ft)

    H_{TOT} total head developed by impeller (ft)

η efficiency

    η_o actual efficiency

    η_{HYD} hydraulic efficiency

β relative angle (degrees)

    β_i inlet flow angle

    β_1 inlet vane angle

    β_2 discharge flow angle

    β_{20} discharge vane angle

NPSH net positive suction head (ft)

D   diameter (inches)

    D_i inlet eye diameter

    D_H inlet hub diameter at D_i

    D_2 impeller tip diameter

V   flow (cfs)

    V_o liquid flow

N   speed (rpm)

C absolute velocity (fps)

$\quad C_i$ inlet velocity

$\quad C_2$ discharge velocity at impeller tip

$\quad C_{1_M}$ inlet meridional velocity

$\quad C_{2_M}$ discharge meridional velocity

$\quad C_{2_u}$ discharge tangential velocity

W relative velocity (fps)

$\quad W_i$ inlet relative velocity at impeller eye

$\quad W_{20}$ discharge relative velocity at impeller tip - theoretical

$\quad W_2$ discharge relative velocity at impeller tip - actual

U rotational velocity (fps)

$\quad U_i$ inlet rotational velocity at impeller eye

$\quad U_2$ discharge rotational velocity at impeller tip

K blockage factor

$\quad K_i$ inlet hub blockage factor

c flow contraction factor

K inlet density function exponent

A inlet density function constant (1/ft)

q total head factor (C_{2_u}/u_2)

μ slip factor $(C_{2_u}/C_{2_{u\infty}})$

λ flow factor (C_{2_M}/u_2)

v_2 impeller diameter ratio (D_i/D_2)

ζ_I impeller diffusion ratio (W_2/W_i)

ζ_D diffuser throat width ratio

Z number of vanes

$\quad Z_1$ of impeller

$\quad Z_2$ of diffuser

ξ loss constants

  ξ_1 heat

  ξ_2 impeller friction

  ξ_3 diffusion

  ξ_4 recirculation

  $\left.\begin{array}{l}\xi_5 \\ \xi_6 \\ \xi_7\end{array}\right\}$ diffuser boundary layer

  ξ_8 wheel friction

  ξ_9 leakage

$\Delta \ell_1$ mean streamline length (inches)

$\Delta \ell_2$ diffuser scroll streamline length (inches)

B_2 impeller width factor (b_2/D_2)

b_2 impeller tip width (inches)

d flow channel diameter (inches)

d_{HYD} hydraulic diameter (inches)

d_{Hi} diffuser scroll hydraulic diameter (inches)

Re Reynolds number

f friction factor

Δq loss (dimensionless)

  Δq_{SF} impeller skin friction loss

  Δq_{DL} impeller diffusion loss

  Δq_{RC} impeller recirculation loss

  Δq_{SC} diffuser scroll friction loss

  Δq_{D2} straight diffuser loss

  Δq_ℓ leakage loss

  Δq_{FR} disk friction loss

  Δq_D total diffuser loss

  Δq_{inc} inducer inlet incidence loss

ν_* kinematic viscosity (ft^2/sec)

Λ diffusion factor-impeller

γ diffuser wall angle (deg)

α absolute flow angle (deg)

  α_i inlet flow angle (prerotation)

  α_2 impeller discharge flow angle

  α_3 flow angle end of vaneless space

PERTINENT HYDRODYNAMIC DESIGN STUDIES

Selection of Design Points

A four-stage pump configuration has been chosen to deliver the 4000 psi required by the problem statement. Fluid incompressibility permits identical contouring of each stage. Thus, comparative investigation and test can be made for one stage only.

Two different designs reviewed in the feasibility study were chosen for fabrication and test for this program. The basis of selection was:

    a.   Performance at the design point

    b.   Performance at off-design conditions

    c.   Size and weight considerations

Two generalized calculations were established and put into the IBM computer program. The first program calculated the impeller and diffuser dimensions and velocities, pressures and losses associated therewith at the design point. The second program calculated off-design condition performance based on the above dimensions. The partial load performance calculation was repeated using different density and viscosity values representing a second fluid temperature.

The specified design conditions are:

Fluid	MLO 8200
Design Flow	30 gpm
Design pressure	975 psi per stage
NPSH (first stage)	100 psi
Temperature range	80 to 600°F
Density range	56.7 to 45.3 lb per cu ft
Kinematic viscosity range	3.49×10^{-4} to 0.198×10^{-4} ft^2 per sec
Design speed	45,000 rpm

Performance at Design Point

The fluid conditions at 600°F were conservatively selected as a basis for design point calculations. The lower density at this temperature requires a higher head pump output to attain the specified pressure.

The inlet geometry of the pump was maintained constant for each of the designs investigated, because cavitation-free operation can be achieved at the minimum inlet velocity point. The inlet dimensions are determined by the design flow, the NPSH of the first stage, and the minimum hub diameter, as dictated by structural considerations for the four-stage pump. The hub diameter used was 0.660 inch.

In addition to the fixed inlet geometry, the variables fed into the IBM program were:

Vane angle at impeller tip   60, 30, 0 and -30^0

Slip Factor $(C_{u2}/C_{u\infty})$ 0.6 to 0.9

Impeller tip flow factor (C_{M2}/U_2) 0.05 to 0.25

Program output was as follows:

Impeller and diffuser dimensions and velocities

Impeller and diffuser vane numbers

Reynolds numbers and friction factors

Boundary layer buildup in the channels (based on one-dimensional velocities)

Friction, diffusion and leakage losses

Hydraulic efficiency and pressure rise

Overall efficiency

The results were plotted and evaluated based on dimensions, performance and design simplicity.

Figures 25 and 26 , included herein, show the resultant performance curves of the 60^0 backward curved vaned pump impeller and the -30^0 forward curved configuration, respectively. The best performance was obtained using 12 and 30 impeller blades for the respective vane angle configurations. Therefore, these arrangements are shown in the figures.

The efficiency shown is computer calculated, and is necessarily based on an arbitrary diffuser design which is parallel walled and necessarily has higher friction and boundary layer buildup than a diffuser with conical side walls or increasing cross-sectional area. The reason for using the parallel-walled diffuser in the comparative computer program was that it permitted solution of the one-dimensional flow equations and loss functions in a closed loop form, as necessary for the general computer program.

61
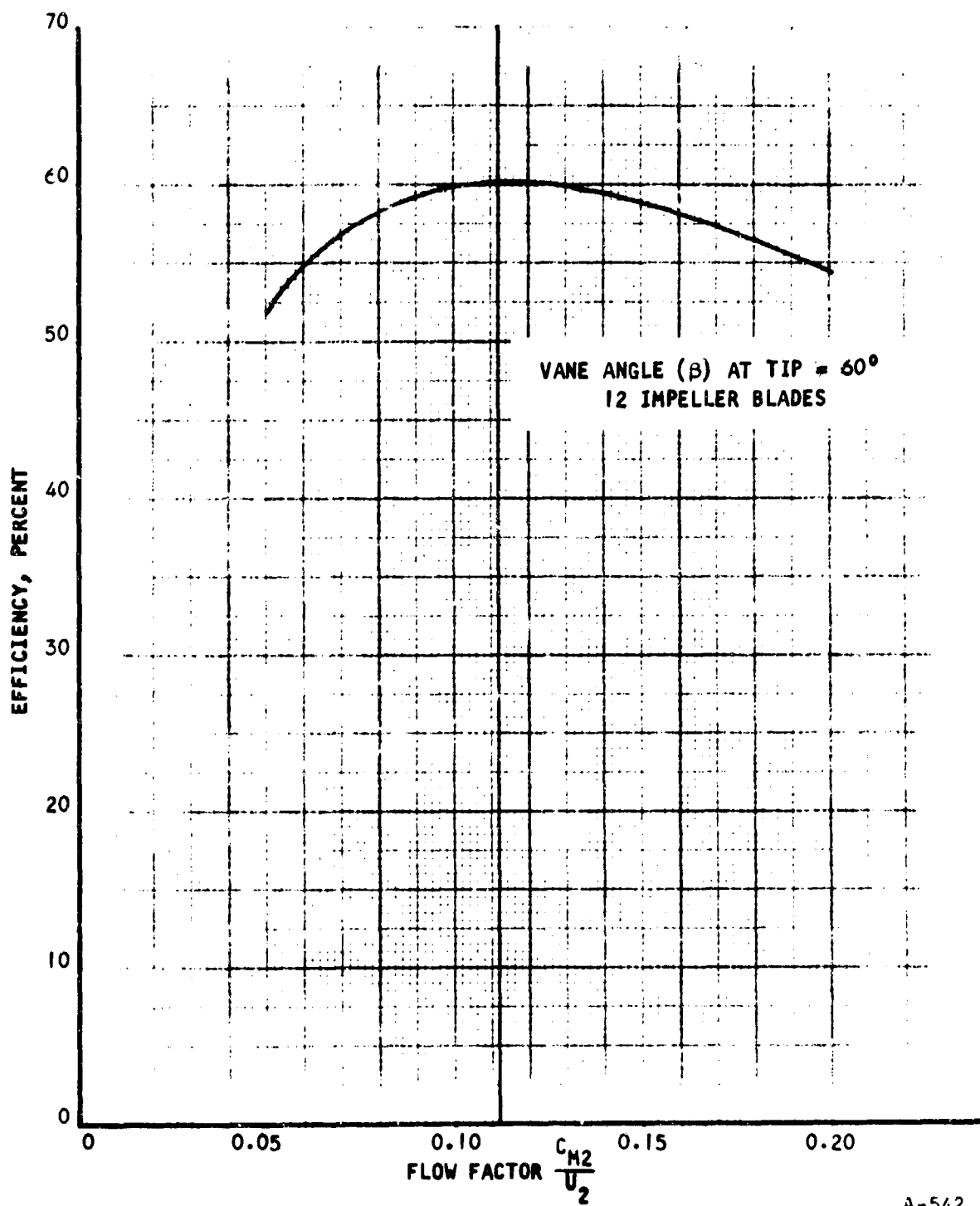
Figure 25. Pump Performance at Design Conditions
(IBM Calculated)

A-542

62

VANE ANGLE (β) AT TIP = -30°
30 IMPELLER BLADES

FLOW FACTOR $\dfrac{c_{M2}}{U_2}$
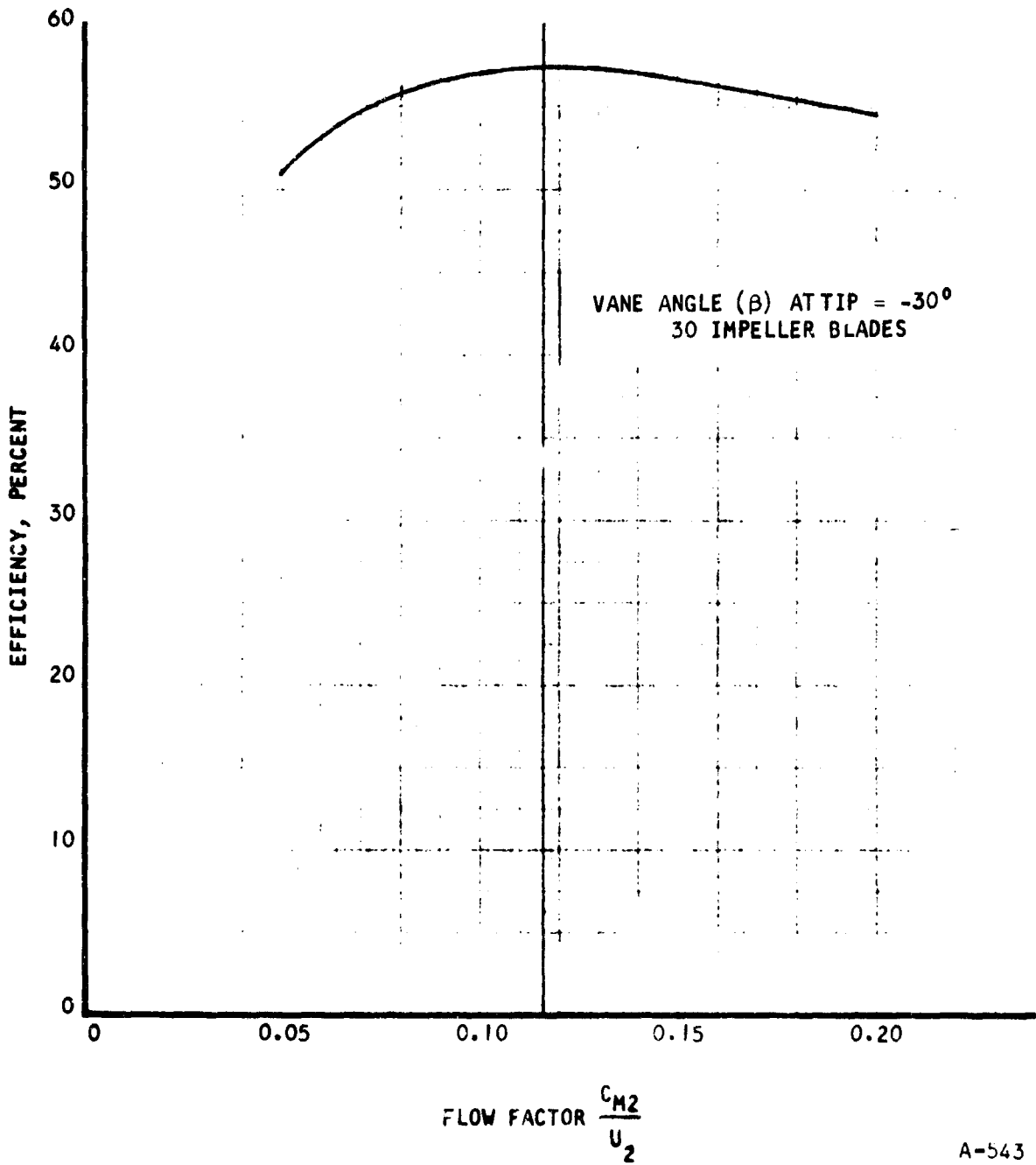
A-543

Figure 26. Pump Performance at Design Conditions
(IBM Calculated)

Off-Design Performance

To fully ascertain pump performance, an off-design performance analysis was also conducted, using 600^0F and 80^0F fluid temperatures.

The design condition pump geometry was reused for the off-design performance program, which determined pressures and losses at various fluid flow rates and viscosities.

Results are presented in Figures 27 and 28 , which show pump head and efficiency as functions of flow for the 60^0 backward curved and -30^0 forward curved impeller versions. The room-temperature performance run resulted in higher pressures but lower efficiencies than for hot operation due to increased density (and a lower Reynolds number) at the increased viscosity. This pressure increase can be reduced by decreasing pump speed to 41,000 rpm. This is easily accomplished if the pump were turbine driven. In the present case, the dynamometer driving the test unit can readily handle this speed change. On the other hand, the increased viscosity can produce higher system resistance, in which case the higher pressure may be desirable.

Relative Merits of Backward and Forward Bladed Designs

Comparison of the backward and forward curved impeller curves revealed that the former has a definite superiority in design point efficiency and better pressure curve stability. The **3.5**-percent calculated efficiency difference is due to the higher calculated losses in the diffuser. It is possible to minimize this loss with optimum diffuser design, and boost efficiency to the 64 to 65 percent level.

The main objection to the forward curved design is its unstable head-capacity curve. The curve presented in Figure 28 is the result of the computer calculations using average design parameters. It is certain that, with careful design of the components, the efficiency can be increased and the head-capacity curve can be stabilized. It should be added that the smaller and low friction producing forward curved pump design has greater performance improvement potential.

Detailed Design Consideration

1. Inlet Channel

To reduce diffusion in the impeller, the inlet must be contoured so that the relative inlet velocity at the impeller tip is at a minimum. A low specific speed pump impeller converts a very high percentage of the total energy into pressure, so that efficiency improvement is extremely important. Figure 29 shows the average relative velocity change for a shockless inlet at various inlet flow angles. The relative velocity becomes minimal at an inlet vane angle of approximately 68^0.

The inlet channel is contoured in the form of an elliptic toroid as shown in Figure 30. This form is well proven in various nozzle applications as one which produces smooth velocity distribution both across the channel and along
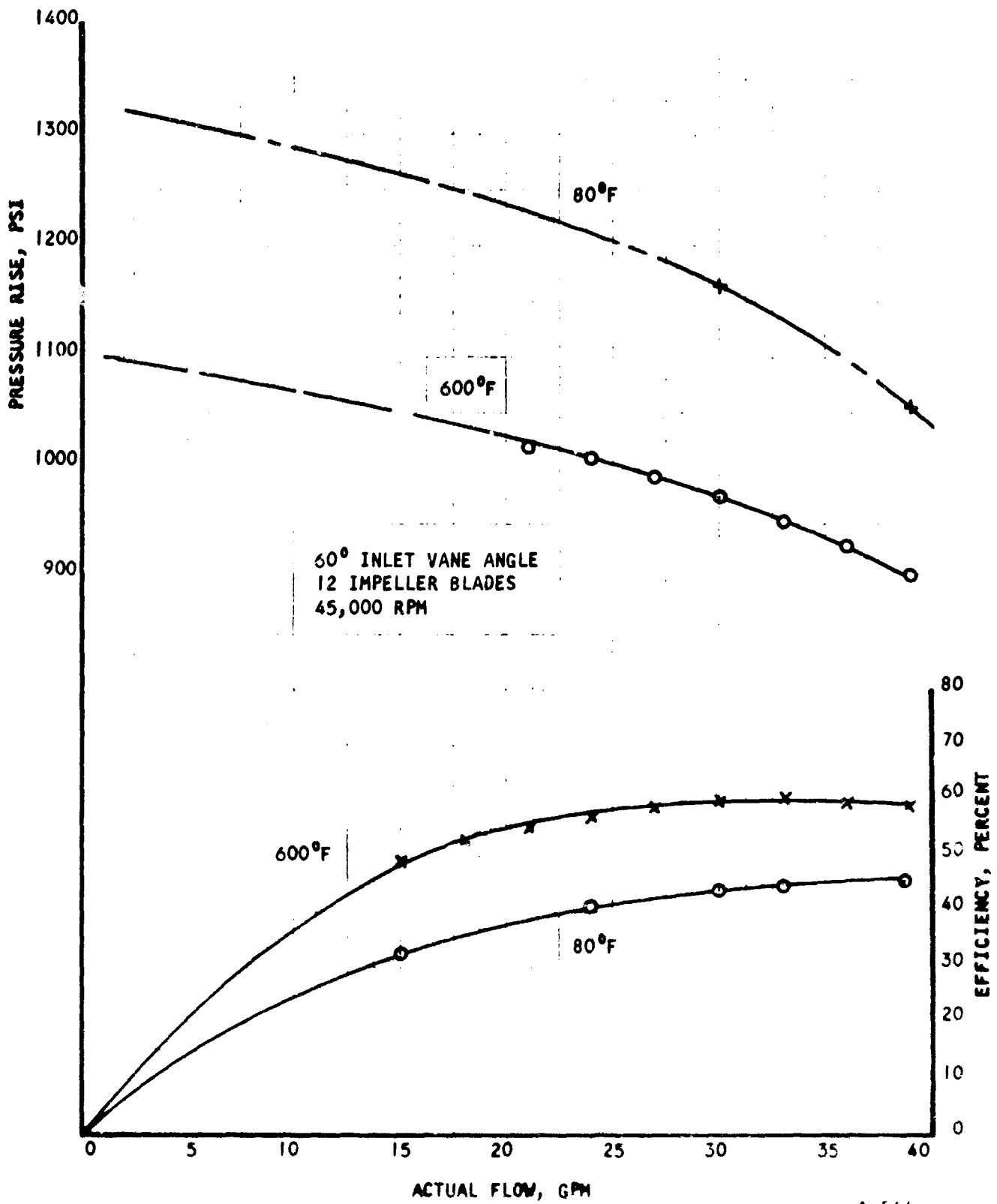
64

Figure 27. Head-Capacity Curve (IBM Calculated)
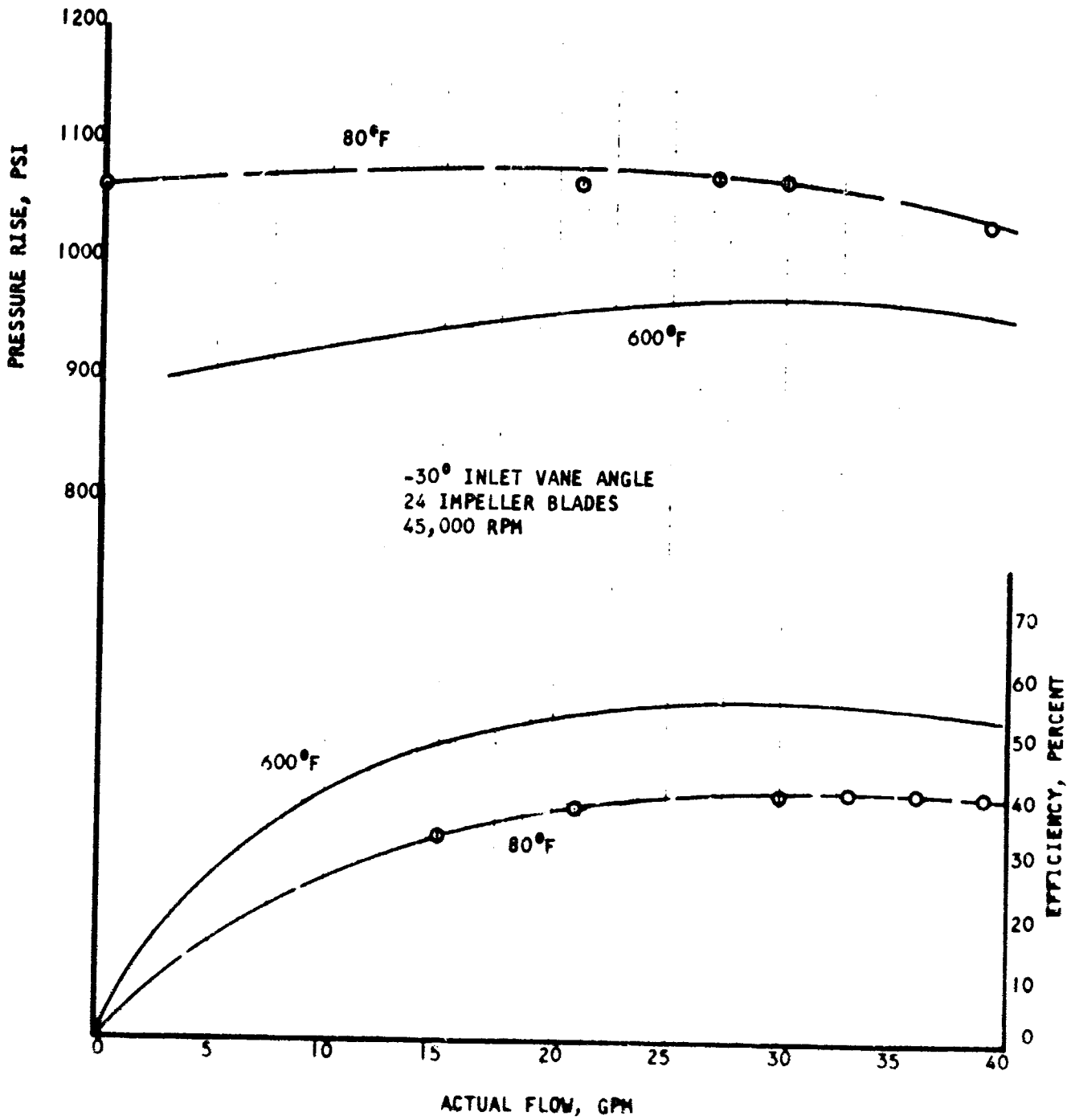
Figure 28. Head-Capacity Curve (IBM Calculated)

A-545
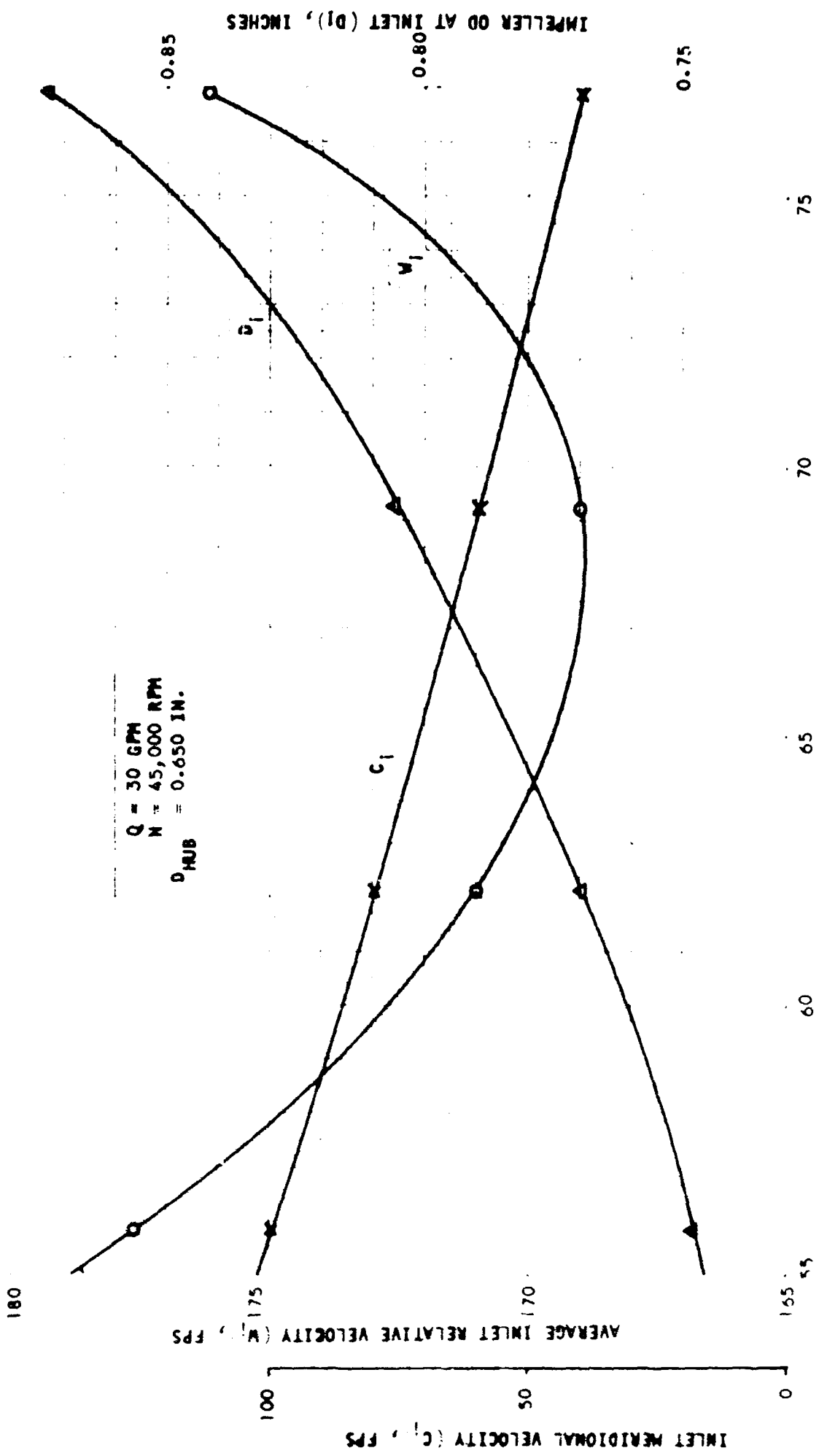
Figure 29. Impeller Inlet Conditions

A-546

67
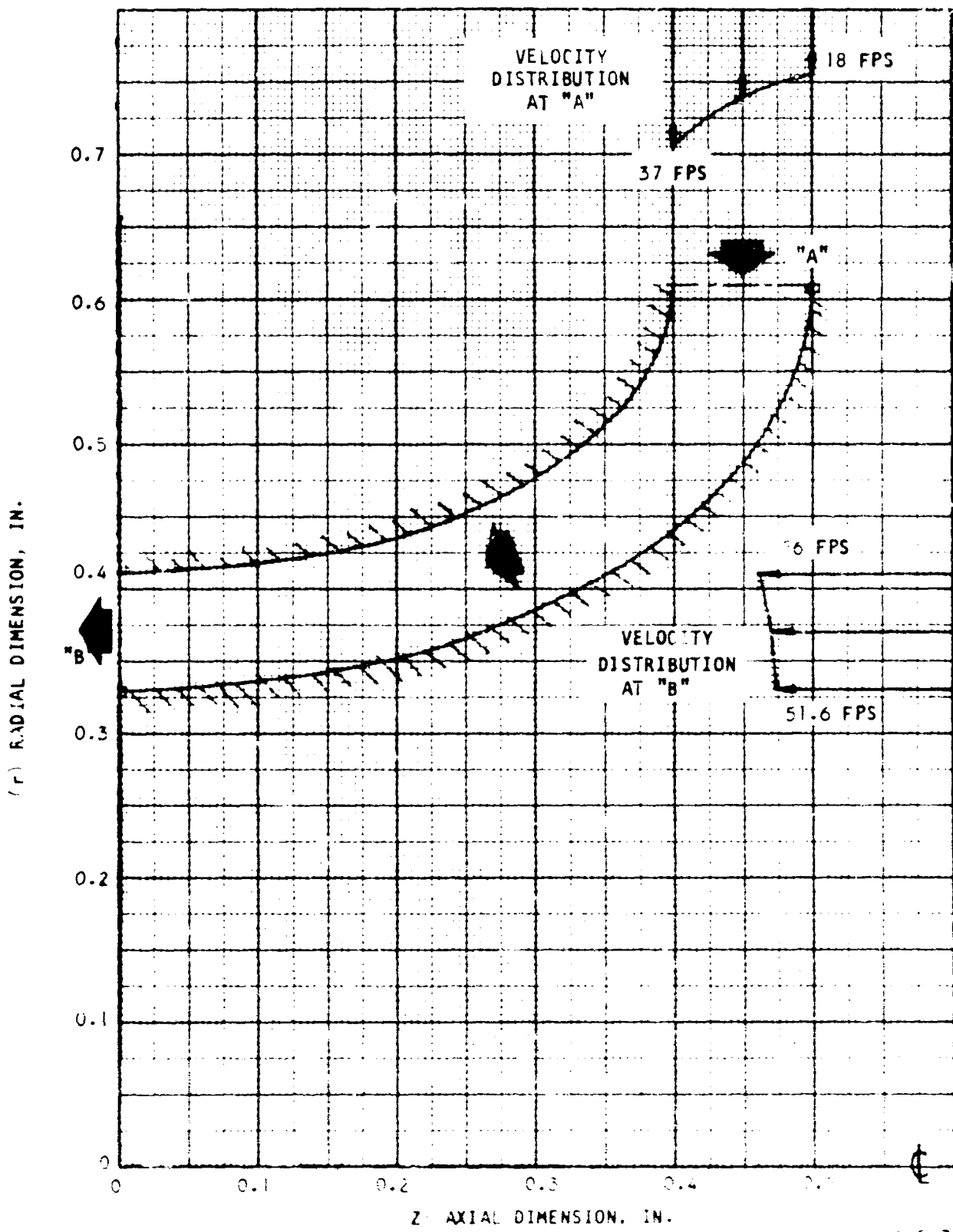
Figure 29. Inlet Channel Configuration

68

the shroud wall. The low pressure gradient associated with the high velocity at the impeller inlet face minimizes the possibility of flow separation and cavitation. The slightly elongated form of the channel was necessary to accommodate the inlet seal.

2. Impeller Design

a. 60° Backward Curved Impeller (Conventional Design) - The comparative IBM calculation, presented in Figure 25, shows an optimum design at the following conditions:

Flow factor $(\frac{c_{M2}}{U_2})$ = 0.11

Slip factor $(\frac{c_{U2}}{U_2})$ = 0.739

Number of blades (Z) = 12

Impeller diameter (D_2) = 2.308 inches

Impeller tip width (b_2) = 0.040 inch

These parameters provide the basis for the actual design. The inlet and the hub diameters were established as reviewed in the previous sections.

The design was established in five steps.

a. The shroud streamline was established between the eye diameter and the tip using a natural hyperbolic function to assure a smooth change in curvature and a big radius of curvature at the eye. This curve can be expressed by the equation:

$$r = \frac{a}{Z^{2n}} - \frac{b}{Z^n} + c$$

where r = the radius

Z = the axial coordinate

a, b, c, n = constants

b. The vane angle change along the shroud was established. This was done using the conformal transformation method. The vane is estab-lished as a parabolic arc in the transformed coordinate system, expressed as a function:

$$\tan \beta = \frac{d\xi}{d\eta} = a\xi + b$$

69

and

$$dm = rd\xi$$

$$dn = d\varphi$$

where β = vane angle

ξ and η = transformed coordinates

m = arc length along the shroud line

φ = angular position

r = radius

a and b = constants

c. The desirable relative velocity distribution along the shroud was assumed and the average flow areas and impeller widths were computed. This establishes the hub line.

d. An electric analog field plot was made to obtain two-dimensional, rotationless potential lines along the impeller passages.

e. The three-dimensional velocity distribution in the rotating passages was then calculated by the IBM computer.

Figure 31 shows the resultant velocity distribution along the shroud line for the 60° backward curved impeller. The number of vanes was increased from 12 to 16 because the three-dimensional calculation showed stagnation along the pressure side of the vanes.

The 16 vanes result in very good pressure and velocity distribution along the passage, but cause more than permissible blockage at the inlet. To avoid this, the number of vanes was reduced to 8 for the inlet portion and 16 (using splitter vanes) near the outlet, or large diameter, portion as shown in Figure 32.

The vane sections were radial elements from shroud to hub, thus assuring easy machinability. The thickness of the vanes is 0.020 in. at the inlet and a constant 0.030 in. thereafter. Slight tapering of the vanes toward the hub is also utilized due to structural considerations.
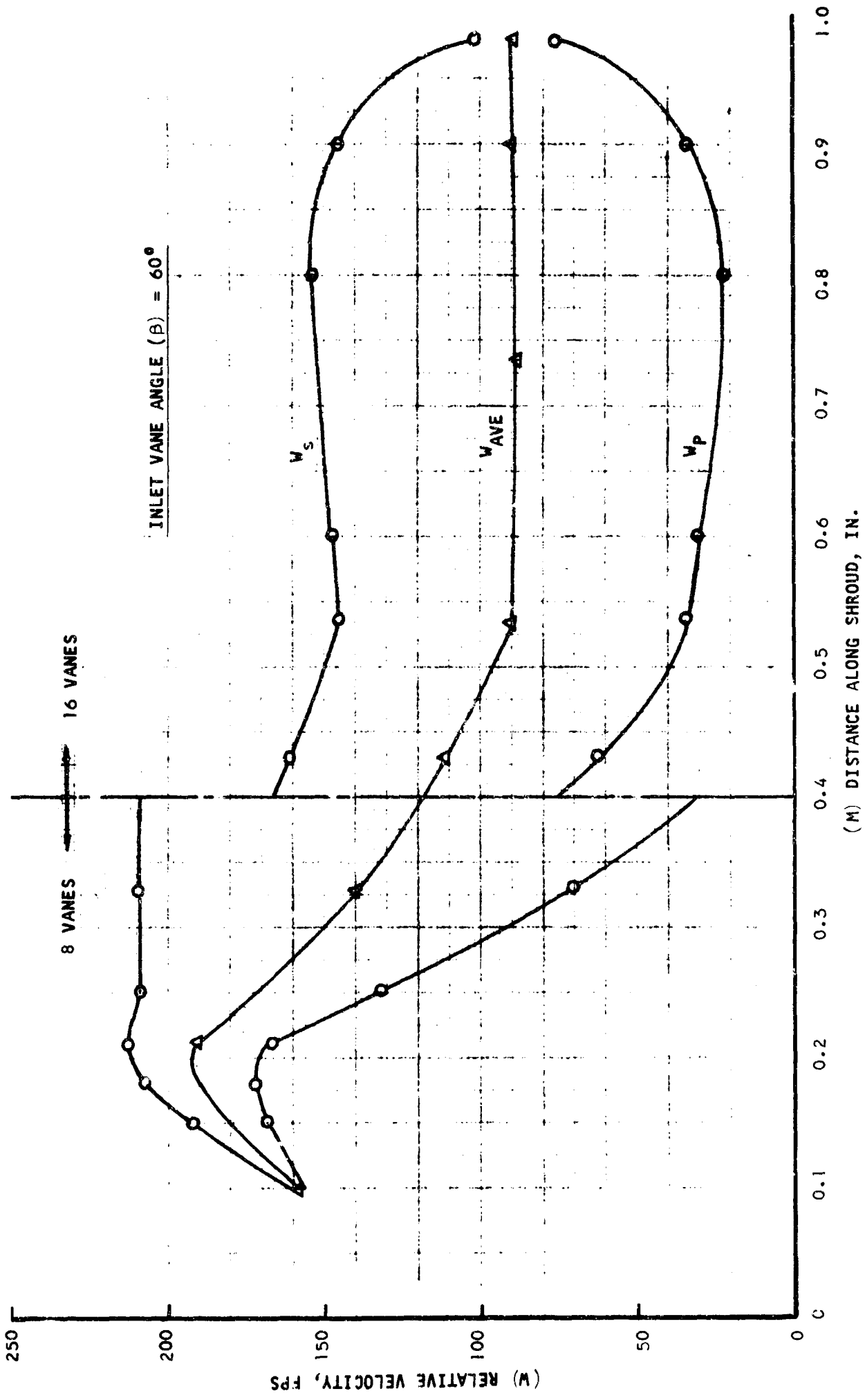
Figure 31. Impeller Velocity Distribution

A-548
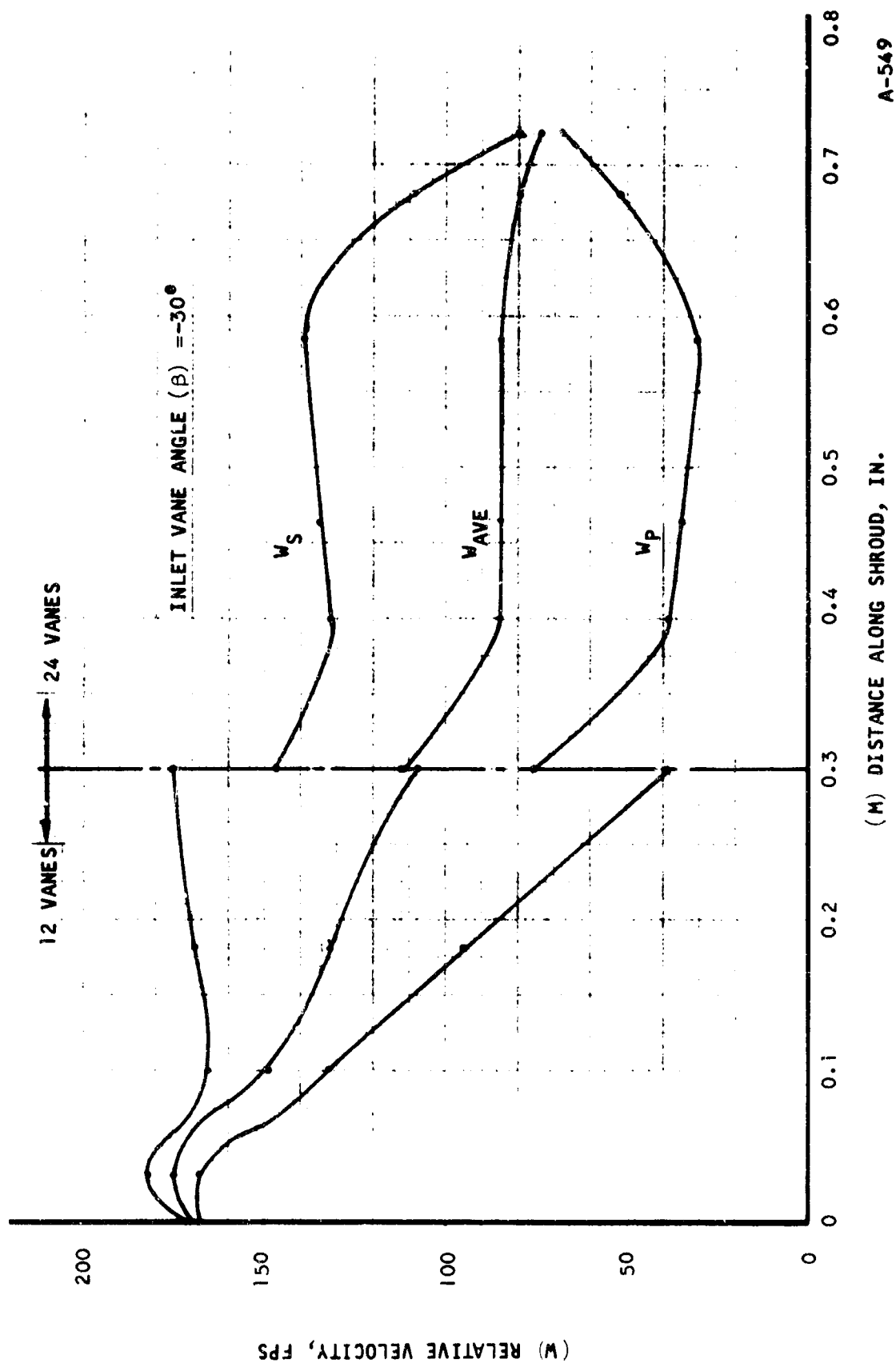
Figure 32. Impeller Velocity Distribution

72

b. <u>Minus 30° Forward Curved Impeller</u> - Figure 26 presents the optimum efficiency at the following conditions:

$$\frac{C_{M2}}{U_2} = 0.116$$

$$\frac{C_{U2}}{U_2} = 0.986$$

Number of blades (Z) = 30

Impeller diameter (D_2) = 1.986 inches

Impeller tip width (b_2) = 0.039 inch

The inlet tip and hub diameters are established as described previously.

The five design steps reviewed above were also utilized in this design.

A deviation from the established design point was necessary. The number of vanes was reduced from 30 to 24 because of inlet blockage considerations. The maximum number of vanes of 0.020 inch thickness is 12 at the inlet edge without creating a blockage problem. The resultant reduction in output pressure is calculated to be less than 0.5 percent. Incorporation of intermediate (or splitter) vanes in the large diameter portion results in the compromise value of 24 vanes.

Figure 32 presents the velocity distribution along the shroud for this case. The loading is higher than for the backward curved impeller case, but it is still acceptable and stagnation has been avoided.

The vane sections, as before, are radial elements from shroud to hub. The thickness of the blades is 0.020 in. at the inlet and is variable along the passage similar to impulse blades, thus attaining even channel cross-sectional area at increased curvature section. The blades are tapered toward the hub.

3. <u>Diffuser Design</u>

Designs of the two diffusers were completed which matched the impellers with the 60° backward curved and 30° forward curved vanes. A vaned diffuser was selected because of better efficiency and smaller overall diameter when compared to corresponding vaneless designs.

73

Peak diffuser performance is vital especially in connection with the forward curved impeller, because a higher kinetic energy must be converted into pressure in this lower reaction case. To assure a maximum performance, the following factors must be incorporated:

a. Minimum friction (short length and rapid deceleration).

b. Minimum boundary layer thickness (short length with slow deceleration).

c. Retarded separation (slow deceleration).

d. Maximum diffusion (rapid deceleration and long length).

These factors are somewhat contradictory. Therefore, determination of an optimum combination is necessary.

The design chosen is composed of three portions (refer to Figure 20):

a. Minimum vaneless annulus around the impeller.

b. Scroll design up to the throat area.

c. A straight diffusing channel.

The optimum recovery of a straight diffusing channel was investigated in Reference 7. Figure 24 shows the influence of the boundary layer thickness in the throat on the pressure recovery of the diffuser channel. This published curve was chosen to calculate the overall efficiency of the diffuser.

The diffuser inlet portion incorporating the vaneless annulus and scroll contours was calculated together. The basis of the calculation is to provide a natural deceleration of the flow induced by the radius increase and the friction on the walls. This theory is assumed to produce an effective deceleration rate and low friction without the danger of separation due to a pressure gradient that is too large.

The basic momentum equation that follows is in accordance with the above theory (designations are shown in Figure 23):

$$- \frac{dM}{dm} = \frac{d(C_u r)}{dx} \quad C = \frac{f\ C_u r(2h - 2h_o + b)}{(h - h_o)\ (b_o + b)}$$

and the continuity equation:

$$\frac{dx}{dh} = \frac{C_u r}{2b_o\ C_{M_1}\ r_1} \left[(h - h_o)\ \tan \gamma + b + b_o \right]$$

74

where M = momentum

      m = mass

      C_u = peripheral velocity

      r = radius

      x = distance in velocity direction

      C = velocity

      f = friction factor

      h = free channel height

      b = channel width

      C_M = radial velocity

      Y = angle of diffuser side wall

The two differential equations above were integrated and the resulting equations were programmed on the IBM computer. The computer output determined the geometry up to the throat, the velocity and pressure distributions and the losses up to the individual points.

Using these results, the boundary layer buildup was calculated up to the throat and, with this value, the optimum performance (recovery) of the straight diffuser portion was estimated in accordance with Reference 7 and Figure 24.
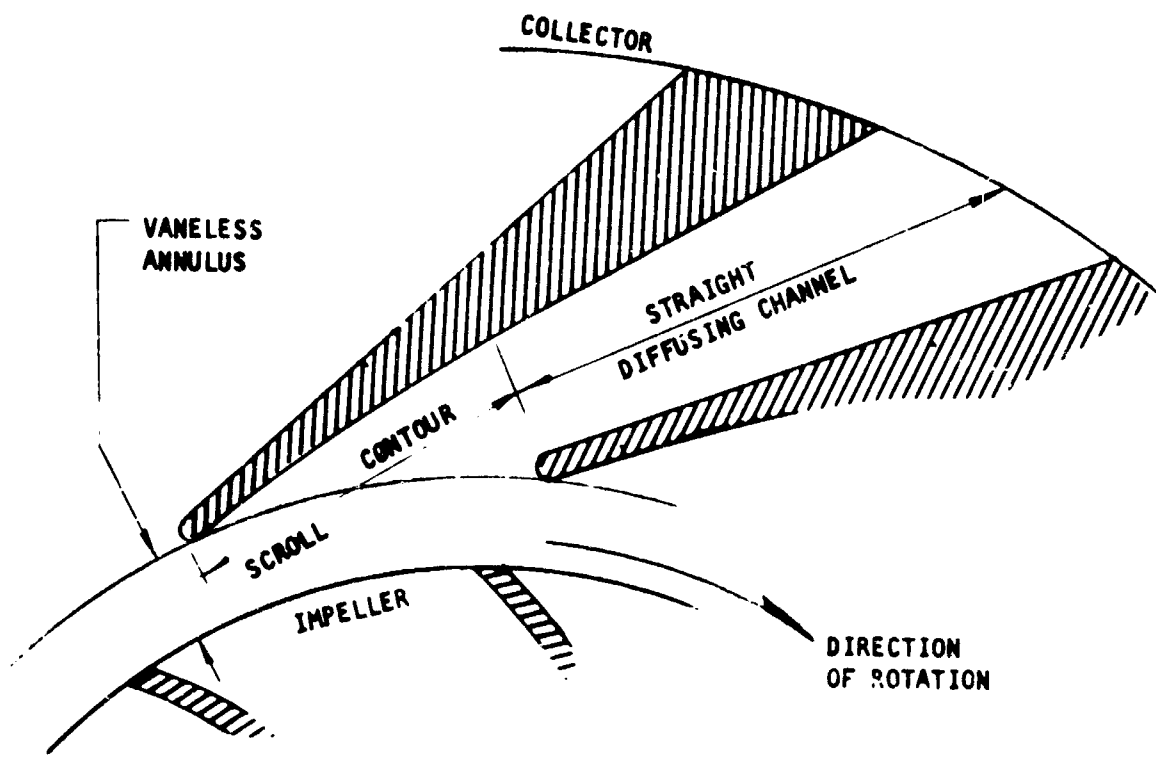
Figure 33. Vaned Diffuser Configuration

SECTION 4

MECHANICAL DESIGN

GENERAL

As was the case in the hydrodynamic design of the pump, mechanical design was strongly affected by the high fluid inlet temperature, and subsequent selection of the operating fluid. The final mechanical arrangement of the four-stage pump is shown in Figure 34. This design was based originally on use of $400^{\circ}F$ fluid temperature, and was later modified to accommodate the $600^{\circ}F$ inlet temperature.

Design problems were anticipated in the area of seals and bearings. A seal test rig was built, and a simple controlled gap floating carbon bushing was developed to provide interstage sealing. Metallic "0" rings were used for static seals, and bellows type carbon face seals were used for shaft seals.

Silverplated steel sleeve bearings were used to support the shaft, and after some problems with a hydrodynamic pocket bearing, a tilting pad bearing design was incorporated for the thrust bearing.

The unit was designed to be shaft driven by either a dynamometer (gear box input) or an air turbine motor (direct driven).

FLUID SELECTION

The specific requirements of the Problem Statement, Section 1, No. 1, outlines as a design goal that the pump shall handle MLO 8200 fluid or equivalent from room temperature to $600^{\circ}F$.

Since published data on MLO 8200 fluid (manufactured by Oronite Chemical Company) does not cover the temperature range above $500^{\circ}F$, and for some characteristics above $400^{\circ}F$, the Oronite Chemical Company was contacted, first to obtain any additional data on MLO 8200 fluid which might be available, and secondly, to obtain data on equivalent fluids.

The manufacturer could not recommend the use of MLO 8200 for temperatures above $520^{\circ}F$ and suggested the use of Oronite 70 to meet this problem. Data comparing the properties of Oronite 70 with MLO 8200 is appended at the end of this report.

One of the major disadvantages of the MLO 8200 fluid is the decay in viscosity, at elevated temperatures, the lower limit being the viscosity of the base stock. To show the range of viscosities expected, an extrapolated curve of viscosity as a function of temperature for both the base stock and MLO 8200 fluid is shown in Figure 35.

77

Figure 34. Redesigned Bearing Section of the Four-Stage Hydraulic Pump Shown in Layout Sketch L208403
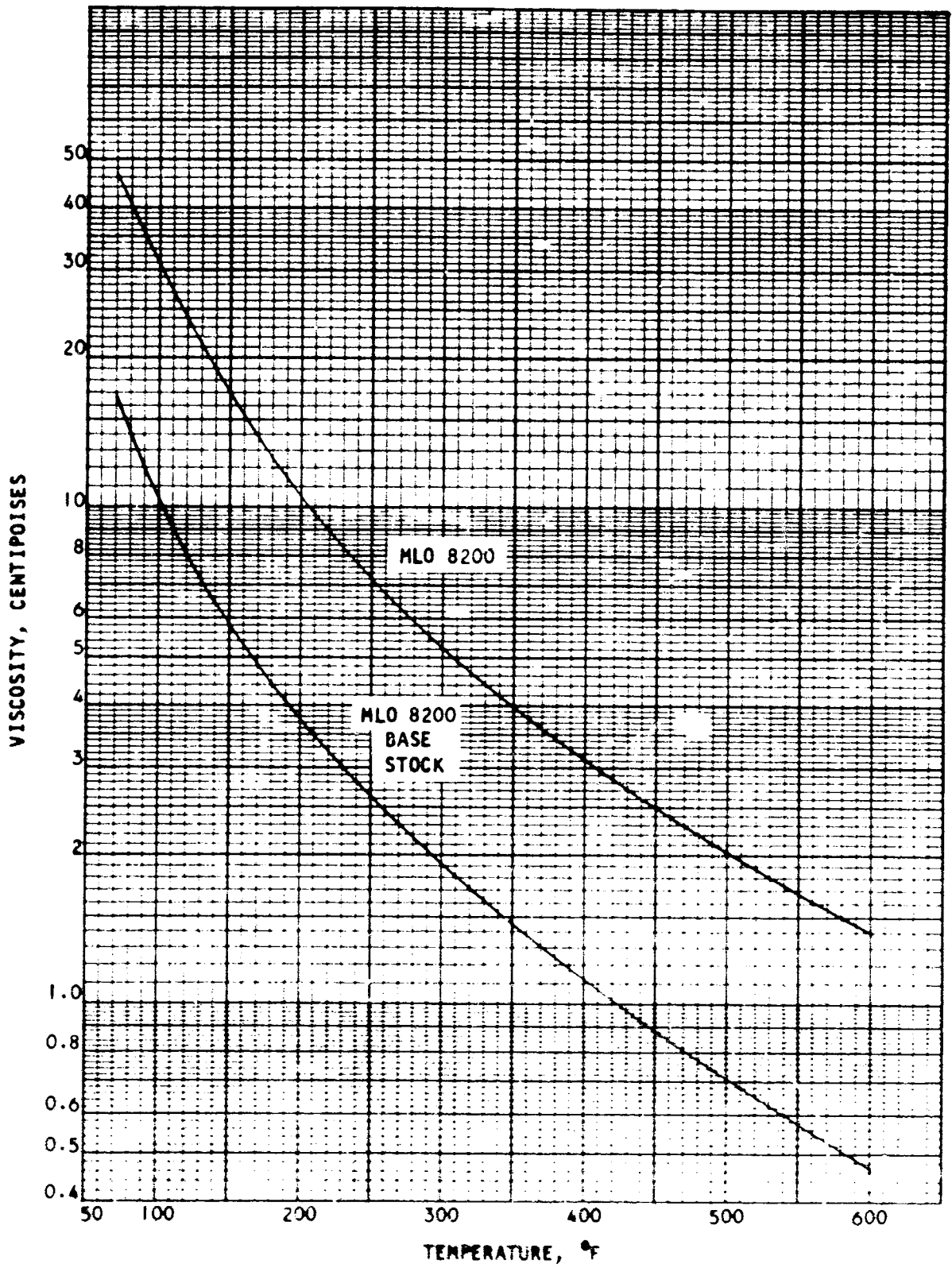
Figure 35. Viscosity of MLO 8200 Fluid

A-541

In spite of the reported disadvantages of using MLO 8200, the unit was designed for operation in this fluid. One major consideration was the opportunity to show the mechanical effects of pump operation in a fluid with obvious poor lubricity and lubrication characteristics.

BEARING SELECTION

Ball Bearings

For this application, major considerations favoring the use of ball bearings were their ability to take axial thrust loads and to maintain rotor alignment. Tests conducted at AiResearch indicated ball bearings of the required size could be operated successfully at 45,000 rpm while submerged in oil. These tests also showed, however, that the resultant bearing losses might be excessively high for this application.

Testing accomplished by both New Departure and Fafnir Bearing Company indicate a very poor life for 204 size bearings operating under moderate loads and at speeds of approximately one million DN (diameter x rpm).

The following is a summary of test results available from New Departure:

1. One group of M-50 bearing running at $350^\circ F$ under a load factor of 0.9 and flooded with Oronite 8200 ran 15 hours. On examination, they were found to be in excellent condition.

2. In another group running at $450^\circ F$ under similar conditions, all failed after 33 hours operation.

3. A viscosity study showed that, between $350^\circ F$ and $450^\circ F$ and over a time span of 150 hours, Oronite 8200 undergoes a severe viscosity reduction. This was found to be as high as 40 percent. Due to this reduction, the lubricant is capable of supporting only extremely light loads. Moderate loads (producing load factors of 1.0 and 3.0) result in metal to metal contact and eventual seizure. Heavy loads (producing load factors up to 0.9) result in bearing life in the range of 1 percent of calculated B-10 life.

Based on the above factors and the fact that there is further viscosity reduction in the $600^\circ F$ vicinity, it was recommended that, to obtain any degree of bearing life, the loads must be extremely light (load factors above 5.0). For the 204 size, the size contemplated for this application, operating at 50,000 rpm and at $600^\circ F$ to $650^\circ F$ under moderate loads, it would be impractical, if not impossible, to project any life forecast. New Departure engineers predicted it to be in the area of 10 hours or less.

Because of this evaluation and other similar information, it has
been decided to use journal bearing configurations exclusively.

Sleeve Bearings

Suitable materials for sleeve bearings such as graphite,
Meehanite AQ and silver or silver plated steel are available. Silver
plated steel journals were chosen. These bearings are compatible with
the fluid, have sufficient imbeddibility to accommodate some fluid
contamination, and are relatively simple to fabricate.

Because inlet pressure of 100 psi was available as a design cri-
terion, use of a simple hydrostatic bearing was selected. The inboard
journal was lubricated by moderately high pressure fluid bled from the
first stage discharge, and the outboard journal was lubricated by fourth
stage discharge fluid leakage.

Thrust Bearings

Because sleeve bearings were selected for the final design, a
thrust bearing was required to locate the rotor axially and absorb
any unbalanced hydraulic thrust load. Five thrust bearing designs
were investigated using a preliminary figure for unbalanced thrust
load. Of these, three appeared to be satisfactory. The first design
is a tilting pad thrust bearing manufactured by Industrial Tectonics,
Inc. This is a self-leveling unit and is unique in that the rotating
thrust collar is graphite and the pads are steel (the reverse of the
usual construction). Since graphite is compatible with MLO 8200 fluid
and is suitable for use at the temperatures involved, it was satisfactory
for the application.

The second design considered acceptable is the stepped pad con-
figuration which has the same normal load carrying capacity as a tilting
pad bearing and approximately the same losses. It is not self-aligning
and probably does not have quite as much reserve load carrying ability
for a given design load as the tilting pad bearing. However, it is
simpler mechanically and relatively easy to manufacture.

The third design considered applicable is the hydrodynamic pocket
thrust bearing. This unit is more difficult to manufacture than the
stepped pad bearing because of close tolerances even though it is simple
mechanically. Its losses, on the same design basis, are approximately
50 percent of the losses of either the tilting pad bearing or the
stepped pad bearing.

The initial four stage pump incorporated the hydrodynamic pocket
bearing design. This design was chosen on the basis of the extremely
low bearing losses. However, initial runs using MIL L-6081 fluid
indicated that extensive development would be required in order to fully
utilize the advantages of the pocket bearing. Therefore, the design was
modified to use the tilting pad design.

81

The Industrial Techtonics standard bearing was modified to use a thrust runner made from hardened 17-4 PH steel. The thrust surfaces were nitrided to provide an extremely hard wearing surface. The standard steel shoes (tilting pads) were silver plated in the same manner as the journal bearings.

The tilting pad thrust bearing develops its own hydrodynamic pressure, and requires lubrication only for cooling.

LUBRICATION

In order to provide a self-contained unit, bleeds were provided at each of the intermediate stages to provide bearing lubrication to both sides of the thrust bearing and to the inboard journal bearing. Throughout the testing, only first stage bleed was used. The bleed pressure was limited to approximately 200 psi maximum and bearing flows were kept at approximately 0.5 gallon per minute per bearing.

The outboard journal bearing was lubricated by leakage past the fourth stage seal. During preliminary room temperature runs, this leakage flow was measured, and results were in good agreement with values expected from seal leakage curves.

SEAL SELECTION

The following static seals were considered for this application: elastomer "O" rings, metallic "O" rings, crush gaskets, and proprietary metallic face seals.

Elastomer "O" Rings

A careful study of the various elastomer materials presently available has revealed that there are none now available which are both compatible with MLO 8200 fluid and, at the same time, suitable for operation at 600°F for periods in excess of a few hours. Consequently, this approach was abandoned.

Metallic "O" Rings

A review of literature and manufacturer catalogs indicated a vented silver-plated stainless steel "O" ring could be successfully utilized in this application. These seals depend on flange loading to deform the seal, however, in this development unit, heavy flange sections presented no problems.

Crush Gaskets

Asbestos-filled gaskets, such as "Flexitallic", manufactured by Flexitallic Gasket Company and "Guardian", manufactured by Garlock, Inc., are spirally wound gaskets which have been used successfully for years for high pressures at temperatures considerably higher than required by this

application. They do not require surfaces finished as highly as other seals, and are relatively inexpensive. However, they require high compression loading to be effective. There is no published data on loading requirements, nor any basis for design studies, since these gaskets are supplied for standard flanges. However, discussions with one supplier indicate the compressive loading should be taken as approximately 4.7 times the pressure to be sealed. Even with a very narrow gasket, this required a much higher loading than the published figures for vented metallic "O" rings for the same application. In view of this, investigation of this type of seal was abandoned.

Proprietary Metallic Face Seals

A number of proprietary metallic face seals were investigated for this application. From testing done for other applications, there was no question that several of these were satisfactory for use in the pump. They all require exceedingly well finished contact surfaces to be effective. These surfaces can be easily damaged during assembly and disassembly. Since this was a development unit, frequent assembly and disassembly was anticipated during the course of testing. Consequently, it was felt that these seals should not be used unless unexpected problems developed with metallic "O" rings.

Dynamic Shaft Seals

Since the four-stage pump configuration would have the first-stage inlet at the end where the shaft emerges, the highest pressure to be sealed against atmosphere on the rotating shaft was a 100 psig maximum inlet pressure. A face contact seal with a metallic bellows secondary seal was used. The pressures, temperatures, and rubbing speeds involved were well within the present state of the art. One question raised was the exact state of the seepage residue of 600°F, MLO 8200 fluid after exposure to the atmosphere. However, the problem was not considered to be severe enough to prevent the use of these seals.

Impeller and Interstage Shaft Seal

The high pressure rise per stage of this pump, the high rotative speed and the small space available all combine to render the impeller and inter-stage shaft seals a very difficult problem. Several approaches were considered. Among them were face contact seals, labyrinth seals, and controlled-gap floating bushing seals.

1. Face Contact Seals

This type of seal has desirable characteristics in that leakage and friction losses should be minimal; however, the problems of application to this pump are quite formidable. The lack of a suitable elastomer for 600°F service for use as a secondary seal limited the selection to metallic bellows type secondardy seals. Several manufacturers of face contact seals were contacted and two, Koppers Co. and Sealol, offered

83

a double bellows supported face contact seal. The space required for this arrangement was far in excess of that available. This factor, plus the problem of assembly and maintenance of the required normality and flatness of the mating rotating surface, caused abandonment of this approach.

2. Labyrinth Seals

Preliminary calculations indicate that a radial clearance substantially less than 0.001 inch must be maintained to reduce leakage losses of a labyrinth seal to an acceptable value. These close clearances might be maintained in service using a ball bearing supported rotor. However, since sleeve bearings were selected for the final design, labyrinth seals could not hold close radial clearances required.

3. Controlled-Gap Floating Bushing Seals

This type of seal limits the flow between the rotating and stationary elements by maintaining a very close radial clearance between the rotating element and a non-rotating floating bushing. The secondary seal is obtained by the pressure unbalance holding the bushing axially against a radial lapped surface on the housing.

Three different designs were considered. All three can be accommodated within the available space, and should have approximately equivalent leakage and friction losses. They differ only in materials and method of maintaining the desired clearance over the operating temperature range.

The first, proposed by Chicago Rawhide Manufacturing Co., consists of a graphite bushing shrunk in a bushing of the same material as the rotating element. The graphite is compatible with MLO 8200 fluid and is also a good bearing material at the highest anticipated temperature. The outer bushing serves to control the thermal expansion rate of the inner carbon bushing which is always under compression. Since the outer ring is of the same material as the rotating element, the thermal expansion rates would be the same and the clearance between rotating element and stationary floating bushing would remain constant over the range of temperatures expected.

The second arrangement, proposed by Koppers Company, consists of a stationary floating bushing of 440 C steel hardened to a 60-57 Rockwell "C" scale hardness mated against a hard chromeplated surface on a 17-4PH steel rotating element. This arrangement would show a slight decrease

84

in radial clearance with increasing temperature, a desirable feature when properly controlled.

The third arrangement consisted of a stationary floating bushing of Meehanite AQ which, in the temperature range under consideration, would have the same temperature coefficient of expansion as 17-4PH steel, the material used for the rotating element.

A seal test rig suitable for evaluating controlled-gap float.ng bushing seals was designed and fabricated. A sketch of this test rig is included in Figure 36. Figures 37 and 38 are photographs of the complete test setup including the air turbine drive motor. Figure 39 depicts the Meehanite AQ version of an impeller and interstage shaft seal. Alternate versions of this seal include: (1) A 17-4PH stainless steel floating bushing with a silver plated bore, (2) A carbon bushing shrunk in a 17-4PH ring (Chicago Rawhide Mfg. Co.), (3) A 440C stainless steel ring mated with a 17-4PH chrome plated shaft (Koppers Co., Inc.), and (4) A carbon bushing shrunk in an AM-355 stainless steel ring mated with a 17-4PH chrome plated shaft (Koppers Co., Inc.).

The seal test rig was arranged to measure rotational speed, the leakage rate past the seals and power input. The air turbine drive motor was selected for this application because of its availability and flexibility of speed and power control. The test setup had been arranged such that tests were conducted using a variety of fluids including low viscosity oil which is equivalent in viscosity at moderate temperatures to MLO 8200 Fluid at high temperatures.

Results of this test program are presented in Section 5. As a direct result of these tests, interstage seal, similar to item (2) above was successfully developed and incorporated into the design of the pump. One change in the seal design made as a result of the experience gained on the single-stage test rig was the addition of a wave spring to provide a posi- tive axial seating force at the seal. This design change eliminated the tendency of the seal to not seat as the pump was started.

BEARING CRITICAL SPEED CONSIDERATIONS

A dynamic analysis of the bearing system was made to investigate possible bearing critical speed problems. This analysis indicated the existence of the possibility that operation at 45,000 rpm might be close to a calculated critical speed. The analysis was dependent on assumptions made regarding relative shaft diameters and the spring stiffness of the bearings at dif- ferent speeds and under varying load conditions. Results of this analysis are presented in Figure .40, which shows bearing spring rate versus shaft speed at a 600°F fluid temperature. This figure also depicts critical speed modes at these spring rates.

It was felt that even if a critical speed coincides with operating speed, the hydraulic damping afforded by having the complete rotating assembly sub- merged in the hydraulic fluid would prevent excessive shaft excursion
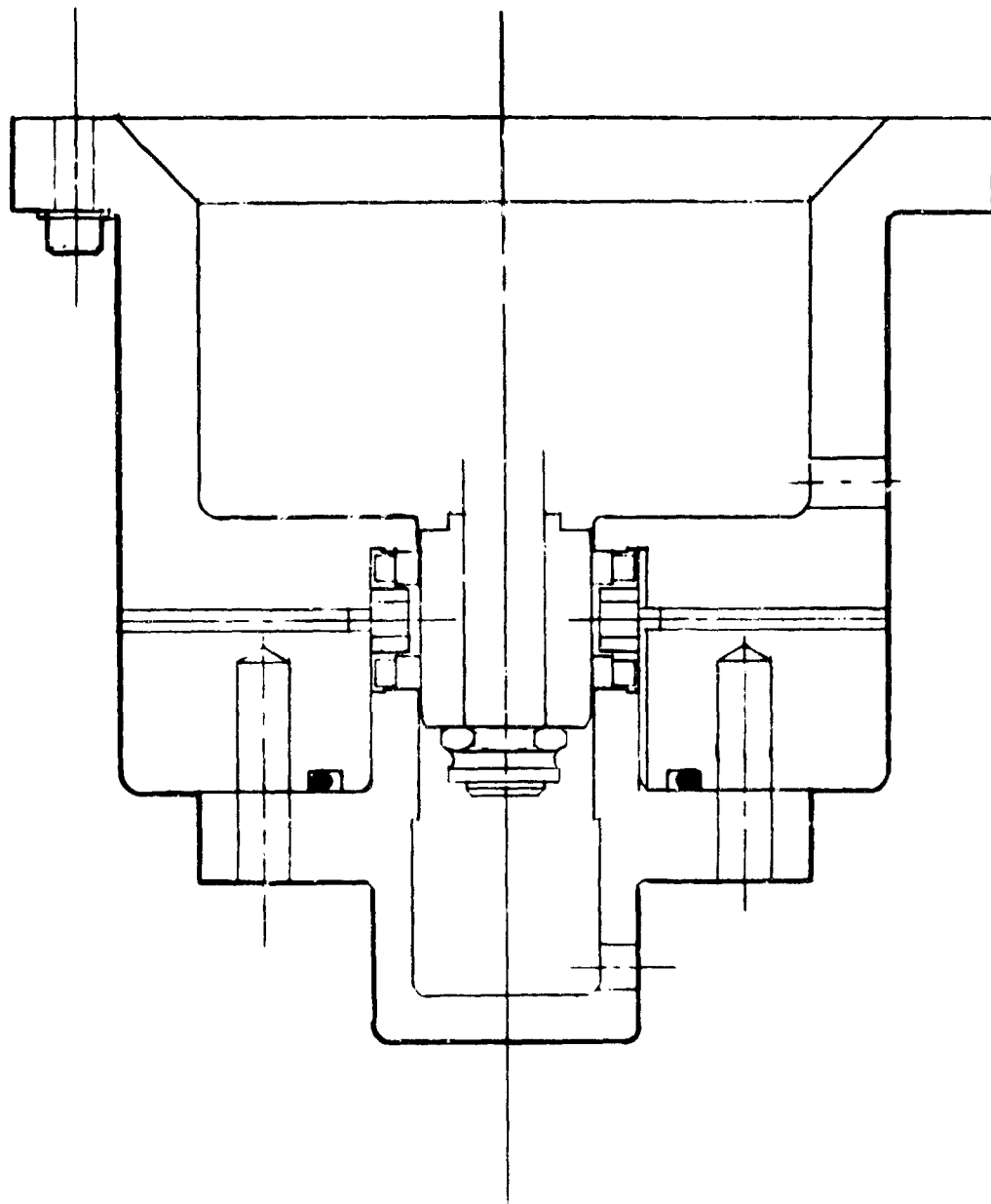
Figure 36. Dynamic Seal Test Rig (Cross Section)

48990-1
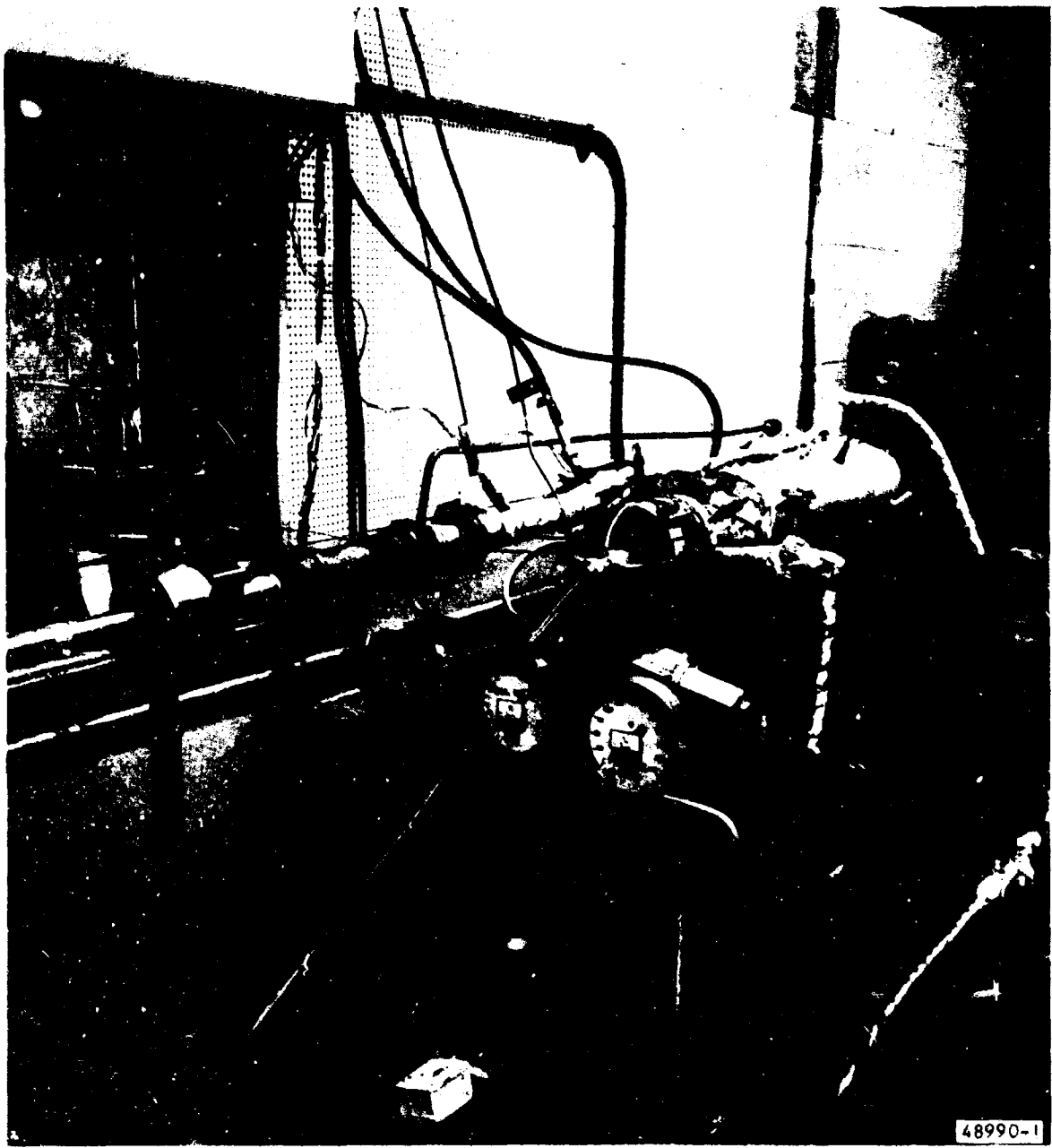
Figure 37.　Seal Test Setup

87

48990-3
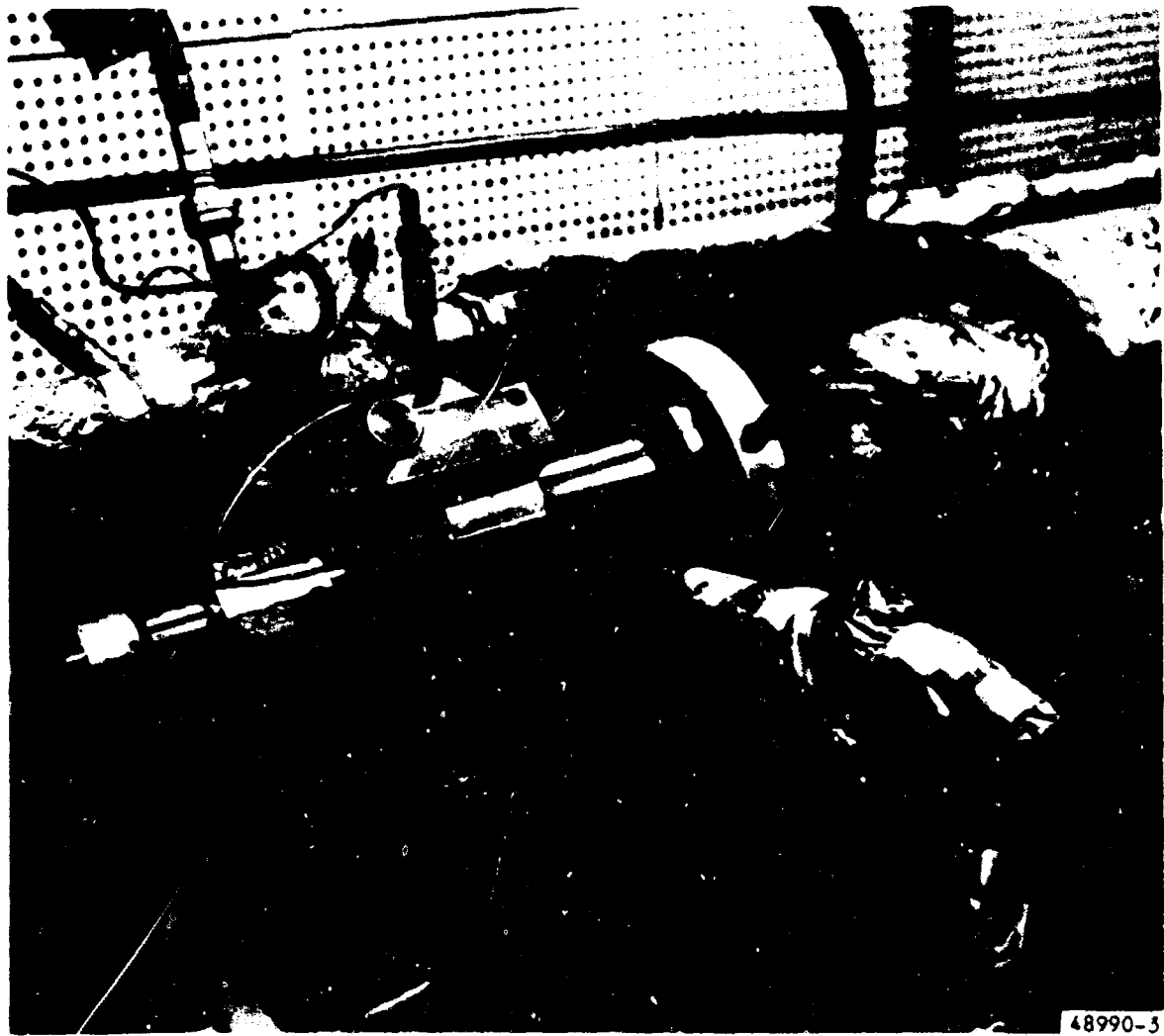
Figure 38. Seal Test Setup

48299-1

Figure 39.   Interstage Seal with Meehanite AQ Bushing
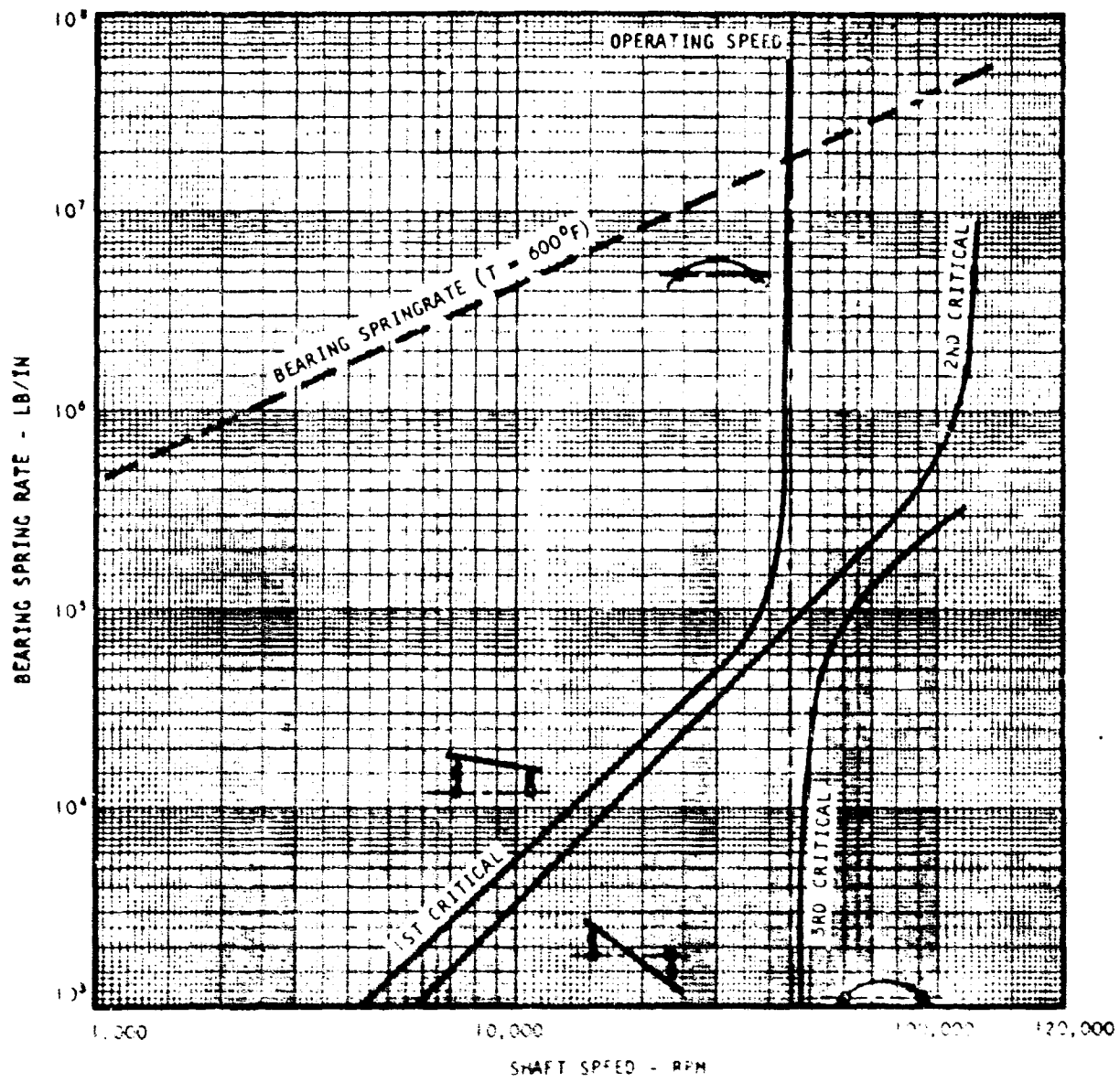
Figure 40. Critical Speed Analysis, ASD Hydraulic Pump

Actual testing of the four stage pump indicated that this damping did occur as no shaft criticals or excursions were noted at any operating speed-up to 47,000 rpm.

ASSEMBLY PROCEDURE

All four pump impellers were stacked on the drive shaft and locked axially against a shoulder by means of a locking nut. Positioning of the impellers with respect to their mating diffusers and maintenance of proper shoulder clearance was accomplished by a combination of shimming of the diffusers, and grinding the impeller hubs. As subsequent assemblies and disassemblies were made, it became increasingly difficult to maintain alignment. This fact became apparent during actual testing because of the low output flows attributed to this problem.

Figures 41 and 42 show the detail parts of the pump. Figure 43 shows a parts array of a disassembled pump and Figure 44 shows the complete assembled unit.

TURBINE DRIVE

In order to achieve the smoothest possible driving mechanism for the initial break-in, it was decided to adapt an existing air turbine drive to the pump. The compressor section of ?-707 cabin air compressor was discarded and a special adapter was made to match the turbine housing and pump inlet flange bolt circles. The spline was the same as that used on the pump so that no additional rework was needed.

Speed control was accomplished by varying turbine inlet air pressure, and by varying turbine nozzle area. standard pneumatic nozzle positioner was used for this latter purpose in conjunction with pressure regulated air supply.

Using a turbine to provide a direct driving means for the pump eliminates the need for a gear box and eliminates the shock of step speed changes.

54854-1

Figure 41. Hydrodynamic Elements, Four-Stage Pump
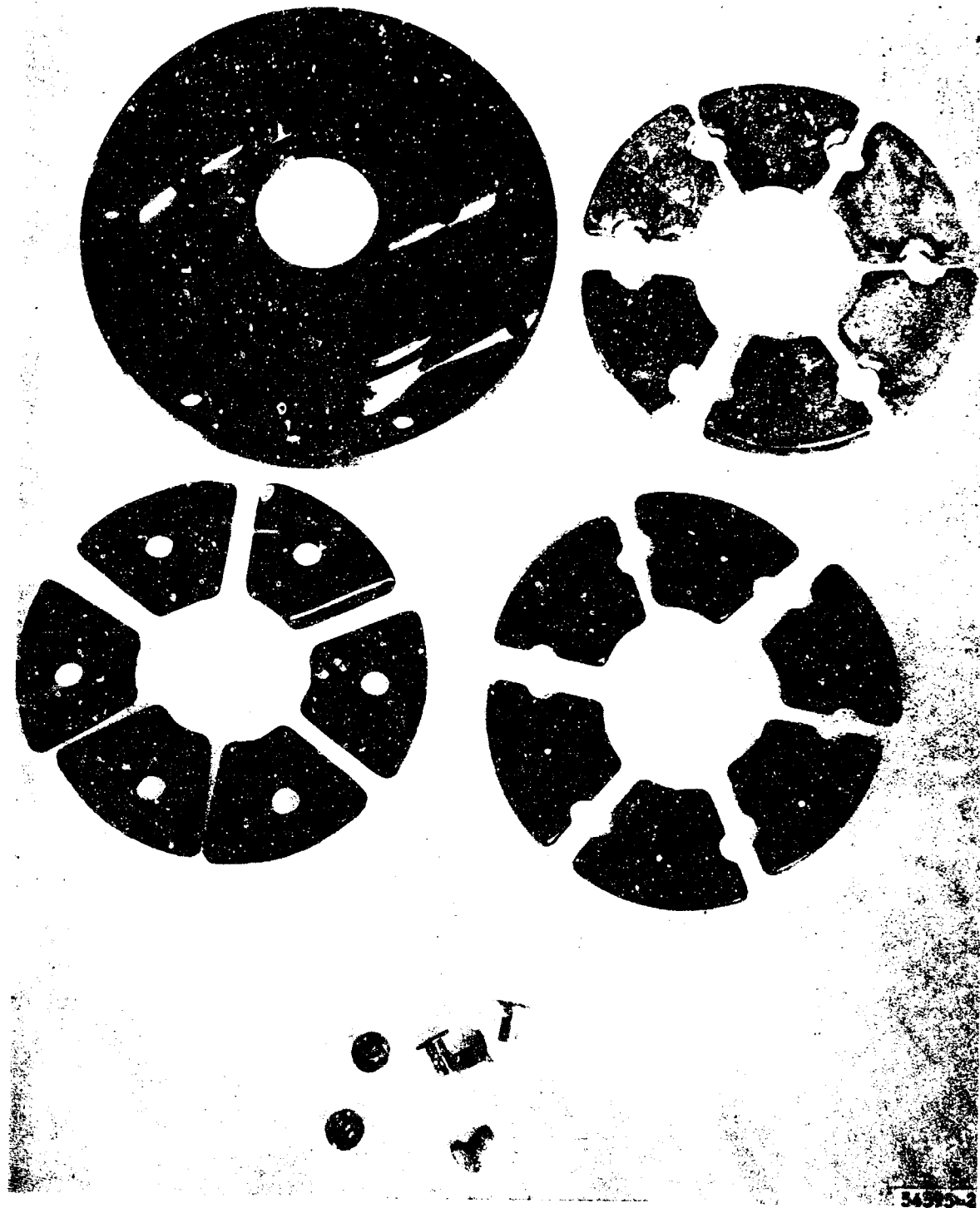
Figure   42.   Tilting Pad Thrust Bearing
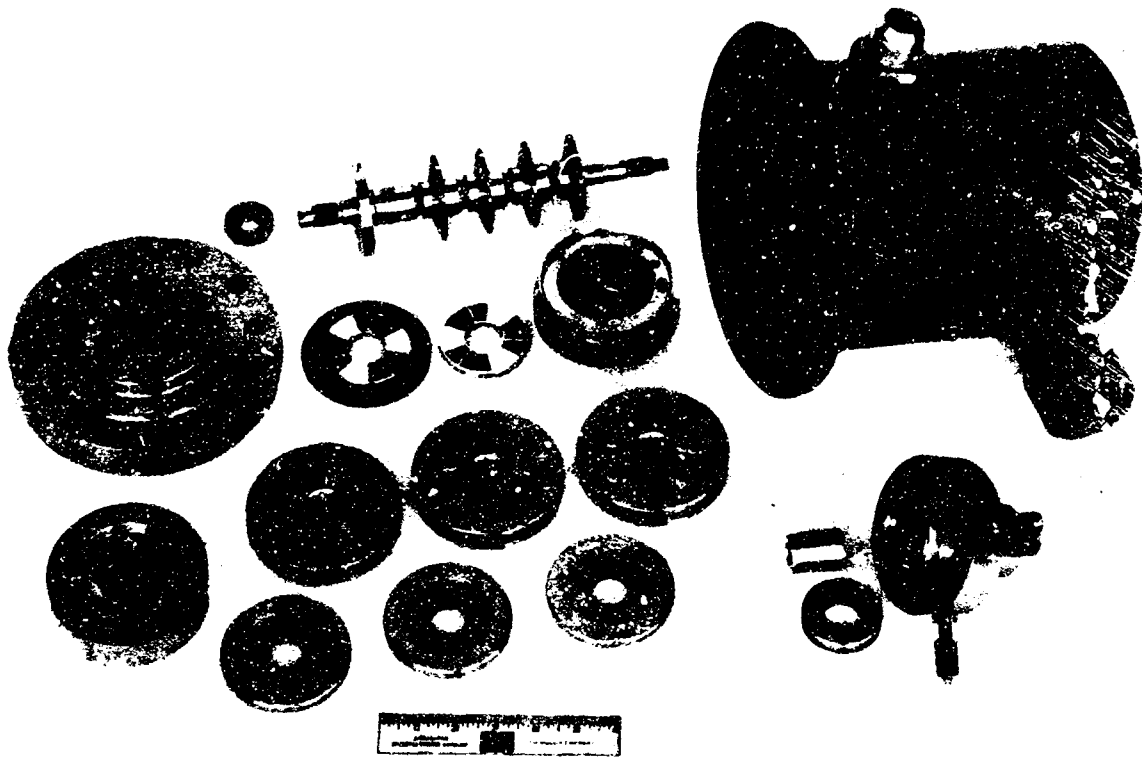
53315-2

Figure 43. Parts Array, Four-Stage Pump Assembly
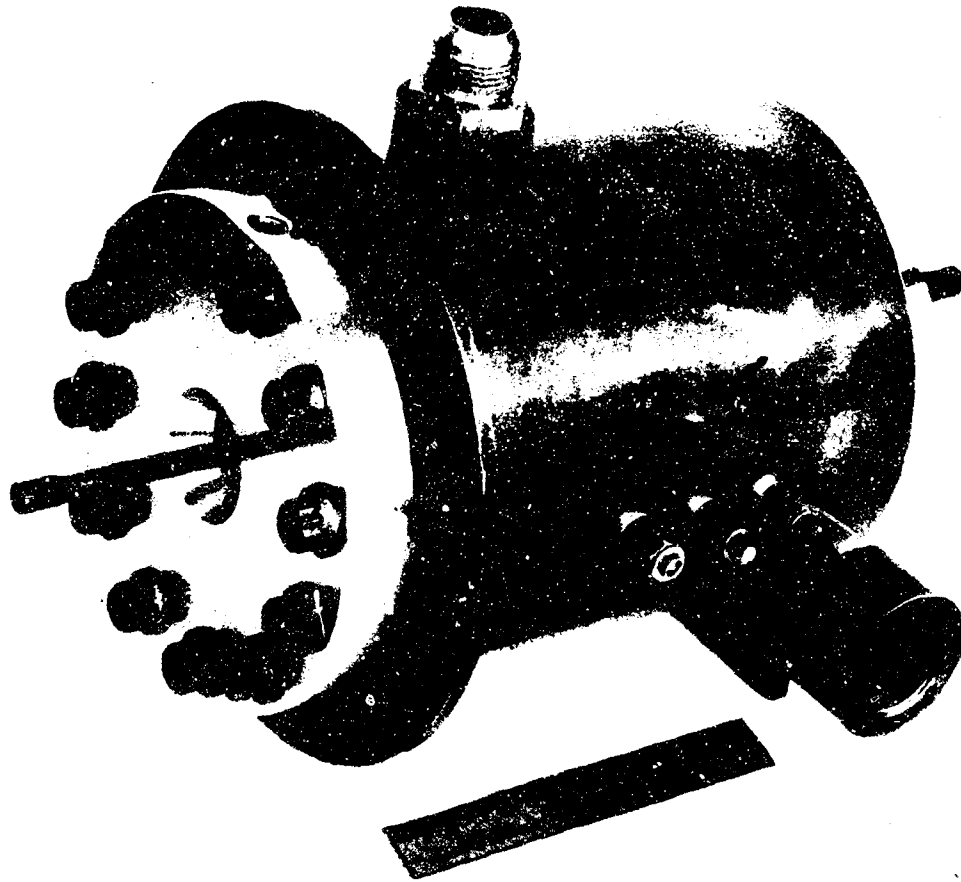
53315-1

Figure 44. Assembled Four-Stage Pump

SECTION 5

EXPERIMENTAL TESTING

GENERAL

This section is divided into three parts. The first is devoted to individual component testing of seals and a single stage pump, the second to the final pump design and the instrumentation provided and the third part to the discussion of pump testing and results obtained.

COMPONENT TESTING

Prior to the finalization of the design of the four stage pump, extensive development testing was accomplished, primarily of the inter-stage seal, and the hydrodynamic performance of the calculated impeller and diffuser design.

These component tests resulted in the development of an interstage seal suitable for this application and sufficient data was obtained to permit engineering application of this seal in other designs.

Design of the hydrodynamic components, as predicted by the computer program was confirmed by means of testing accompli hed on a single stage rig. In addition to design confirmation, these tests permitted further use of the computer program with an increased confidence factor.

Interstage Seal Tests

Testing of various seal configurations resulted in the selection and development of a controlled gap floating carbon bushing seal manufactured by Chicago Rawhide Company, Part Number 800561. This seal is shown in Figures 45 and 46. Testing was done on the air turbine seal test rig shown in Figures 47 and 48. Test runs were conducted at various speeds, fluid viscosities and pressure differentials.

Initial testing using the seal test rig resulted in two cases of shaft excursion which caused seal damage. This was investigated by the use of inductive-type proximity pick-ups and found to be caused by a shaft critical speed at about 41,000 rpm. The problem was solved by reducing the weight of the rotating parts on the seal end of the unit which increased the critical speed to above the 45,000 rpm operating speed.

A thorough investigation of the Chicato Rawhide Seal 800561 operating with a radial clearance of 0.0005 in. was conducted. Test results indicated the leakage at the viscosity corresponding to MLO 8200 at 600°F (1.98 centistokes) was 0.29 gpm at a seal pressure differential of 750 psi which is very close to the leakage assumed in the original pump design calculations.
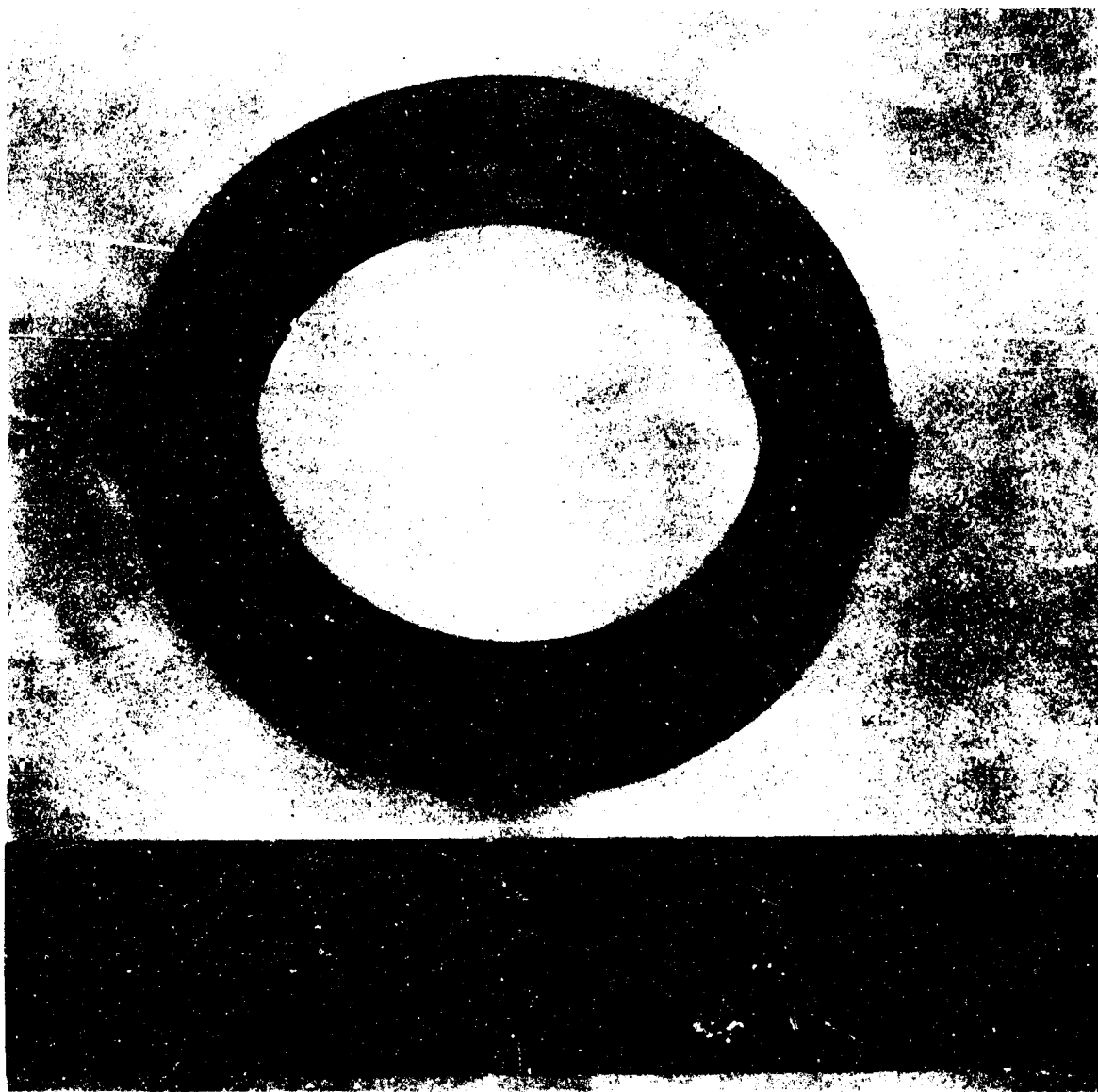
Figure   45.   Interstage Seal
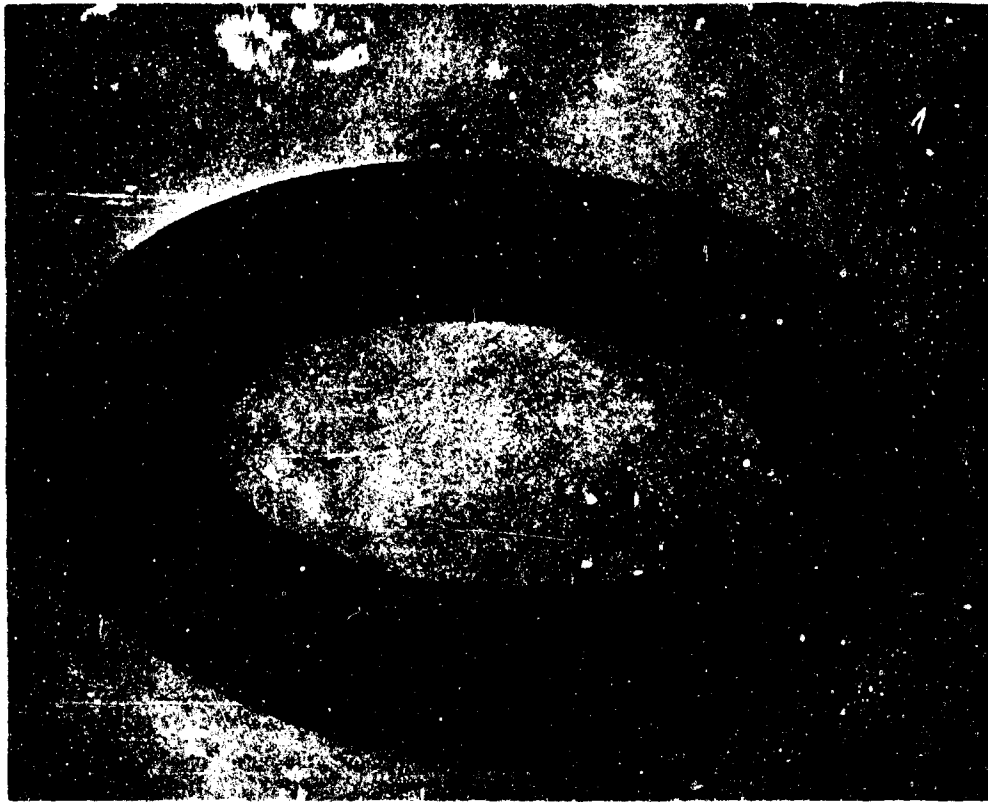
Figure 46. Interstage Seal
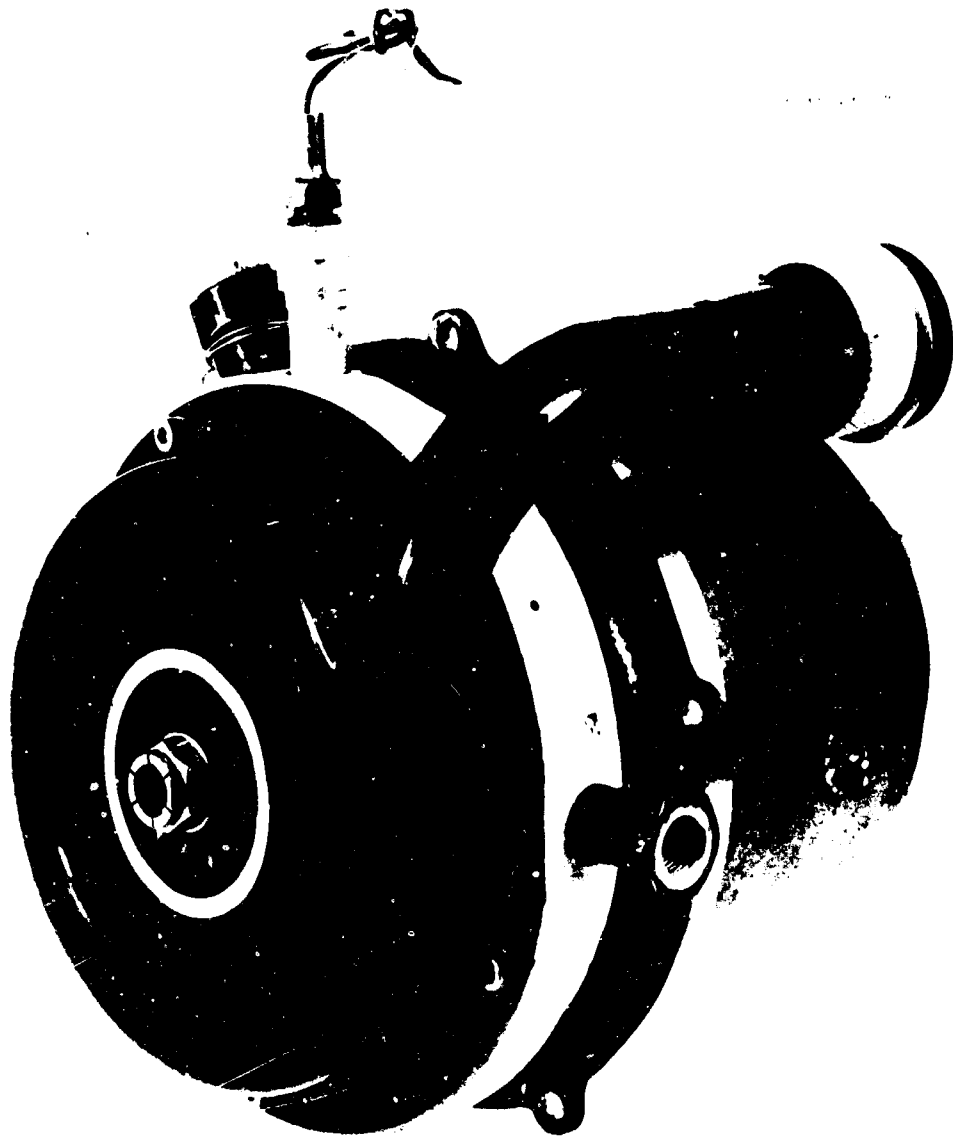
48299-5

Figure 47. Seal Test Rig
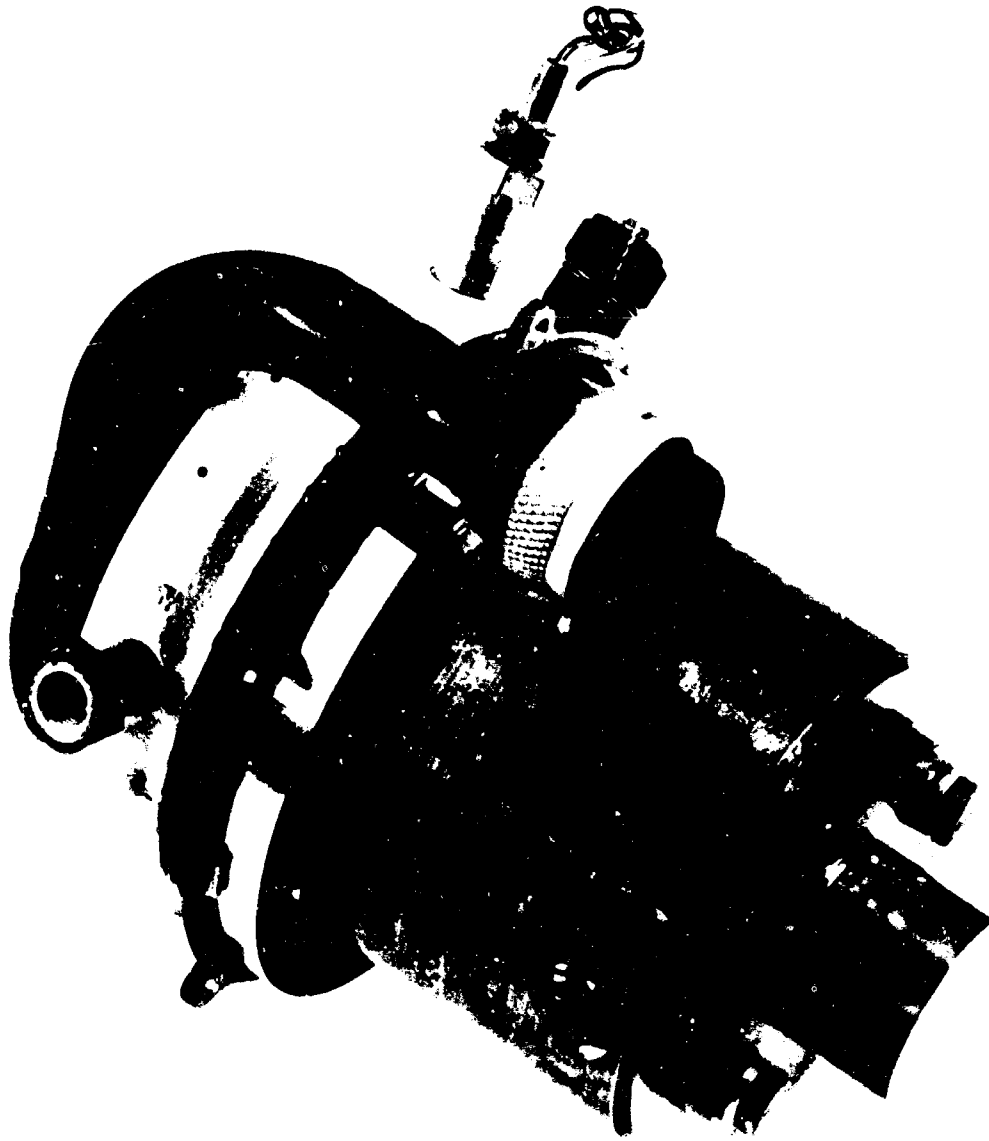
48299-2

Figure 48.   Seal Test Rig

This initial testing was conducted using jet engine lubricating oil (MIL-L-6081B, Grade 1005). Leakage values were measured at various constant speeds as shown on Figure 49 which indicate the effect of speed on the leakage was slight. Leakage at the 45,000 rpm speed was measured at three pressure differentials, 750 psi, 100 psi and 1250 psi as shown on Figure 50. The seals are expected to operate at 200 to 1000 psi differentials in the pump. In order to investigage the operation of the seals at higher fluid viscosities, a change to Sinclair L-1048 was made and data obtained at viscosities up to 29.5 centistokes as shown in Figure 51. Operation of the seals up to this point was normal, although the oil temperature rise became quite large (the temperature differential through seal at the 29.5 centistokes condition was 173°F). At the 36 centistokes condition after about three minutes run time, the leakage rate suddenly increased and the oil temperature rise decreased. On disassembly of the unit, it was found that the seal had rubbed on the downstream half of the bore only which resulted in increased clearance and consequently, the increased leakage.

It appears that this rubbing on one portion of the seal was caused by expansion of the rotating sleeve in this local area due to the considerable oil temperature rise as it passed through the seal. In the configuration tested in the seal test rig, there appears to be a viscosity limit of approximately 30 centistokes maximum with a radial clearance of 0.0005 inch at 45,000 rpm and 1000 psi pressure differential. However, it was felt that in the actual pump configuration, the viscosity limit would be considerably higher due to better heat transfer from the seal areas on the impeller to the large volume of fluid passing through the pump. For comparison, the viscosity MLO 8200 hydraulic fluid at 70°F is 49 centistokes and at 107°F is 30 centistokes.

Measurements were made of the power losses occurring in the seals, by measuring the power supplied by the air turbine (using turbine airflow and turbine air temperature drop data and deducting turbine bearing power). Also, power losses were determined by measurements of the leakage flow rate and temperature rise of the leakage oil as it passed through the seal. Plots of power losses based on the latter data are shown in Figures 52, 53 and 54. The power values measured by the two methods agreed quite well at viscosity values up to 8 centistokes. Above this point, the power measured by turbine air horsepower became higher than the oil horsepower values due to the increased drag losses of the rotating parts at locations other than the seals operating in high viscosity oil.

Throughout the calibration of the 60 degree backward curved impeller in the single-stage test rig, the floating bushing seals and carbon face type shaft seal performed very well. The leakage of the outboard bushing seal was measured throughout the test. The leakage rate agreed closely with the measurements made on the seal test rig, ranging from 0.143 gpm to 0.261 gpm at the 45,000 rpm speed. The internal pressure measuring ports, which were incorporated in the test rig, permitted monitoring of the impeller inlet eye seal pressure differential although the leakage
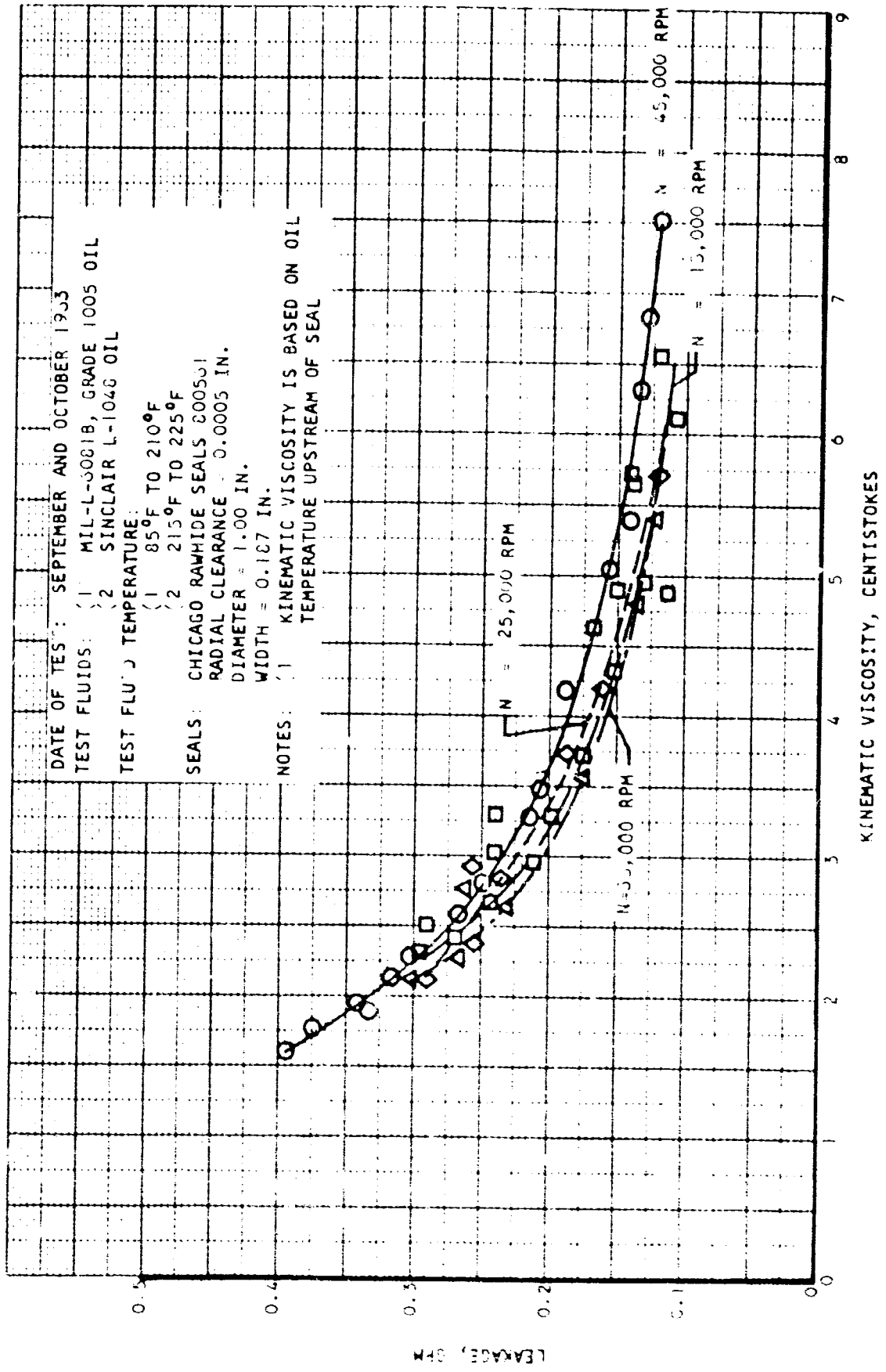
Figure 49. Leakage Data for Chicago Rawhide Seal Part 800561 at 300 psi Pressure Differential and Various Speeds
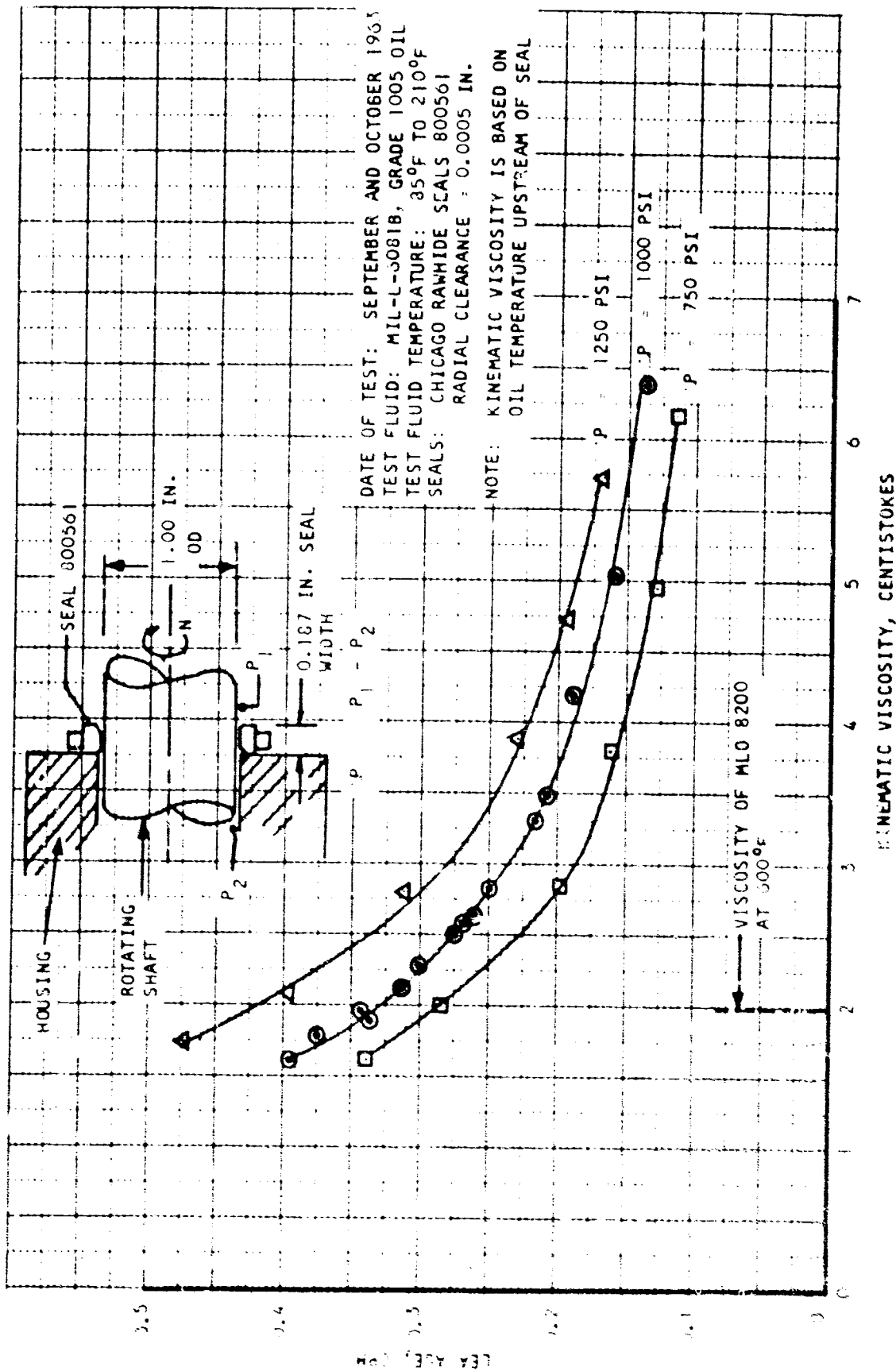
Figure 50. Leakage Data for Chicago Rawhide Seal Part 800561 at 45,000 RPM and Various Pressures
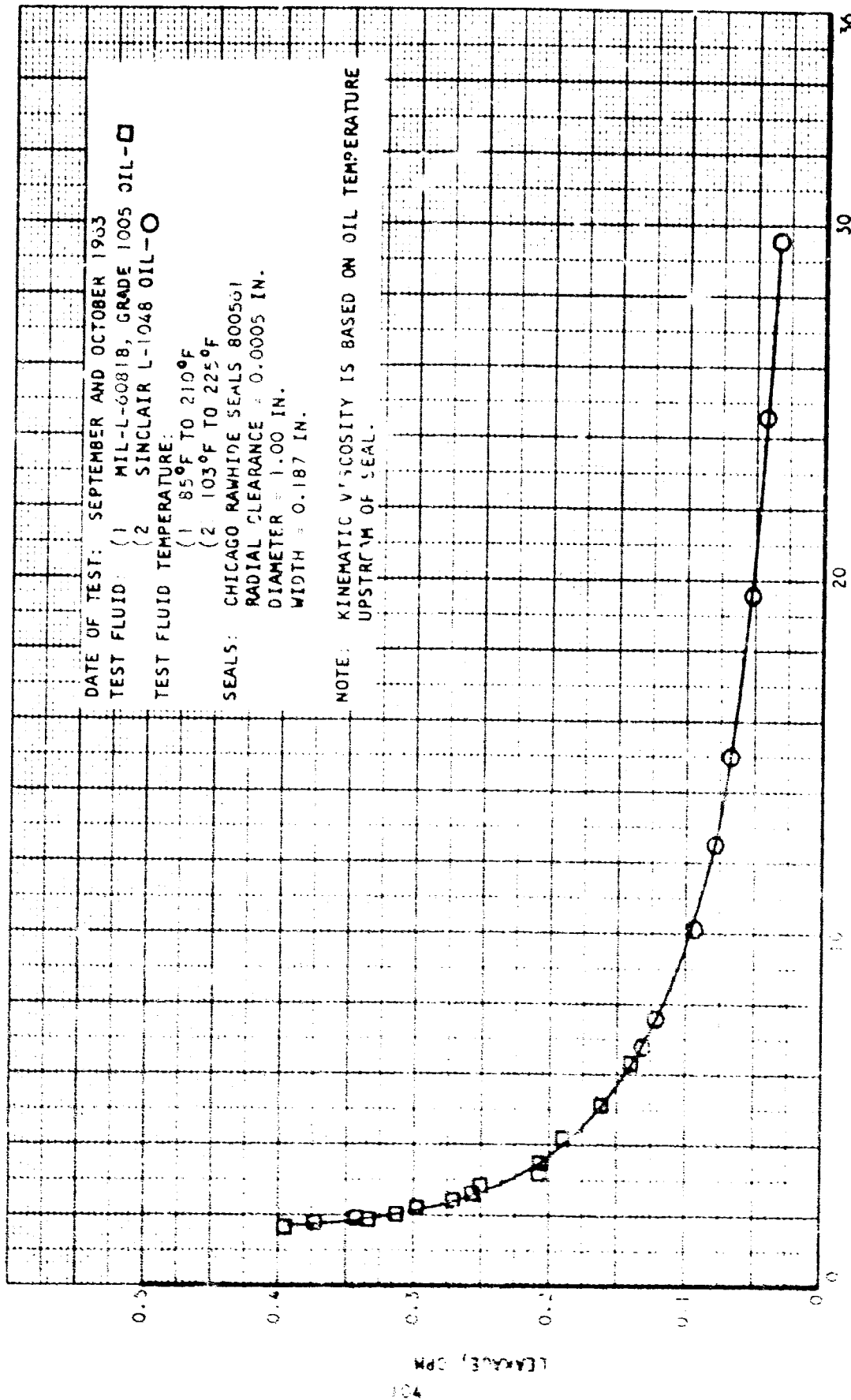
KINEMATIC VISCOSITY, CENTISTOKES

DATE OF TEST: SEPTEMBER AND OCTOBER 1963
TEST FLUID: (1) MIL-L-60818, GRADE 1005 OIL—□
             (2) SINCLAIR L-1048 OIL—○
TEST FLUID TEMPERATURE:
             (1) 85°F TO 210°F
             (2) 103°F TO 225°F
SEALS: CHICAGO RAWHIDE SEALS 800501
        RADIAL CLEARANCE = 0.0005 IN.
        DIAMETER = 1.00 IN.
        WIDTH = 0.187 IN.
NOTE: KINEMATIC VISCOSITY IS BASED ON OIL TEMPERATURE
      UPSTREAM OF SEAL.

LEAKAGE, GPM
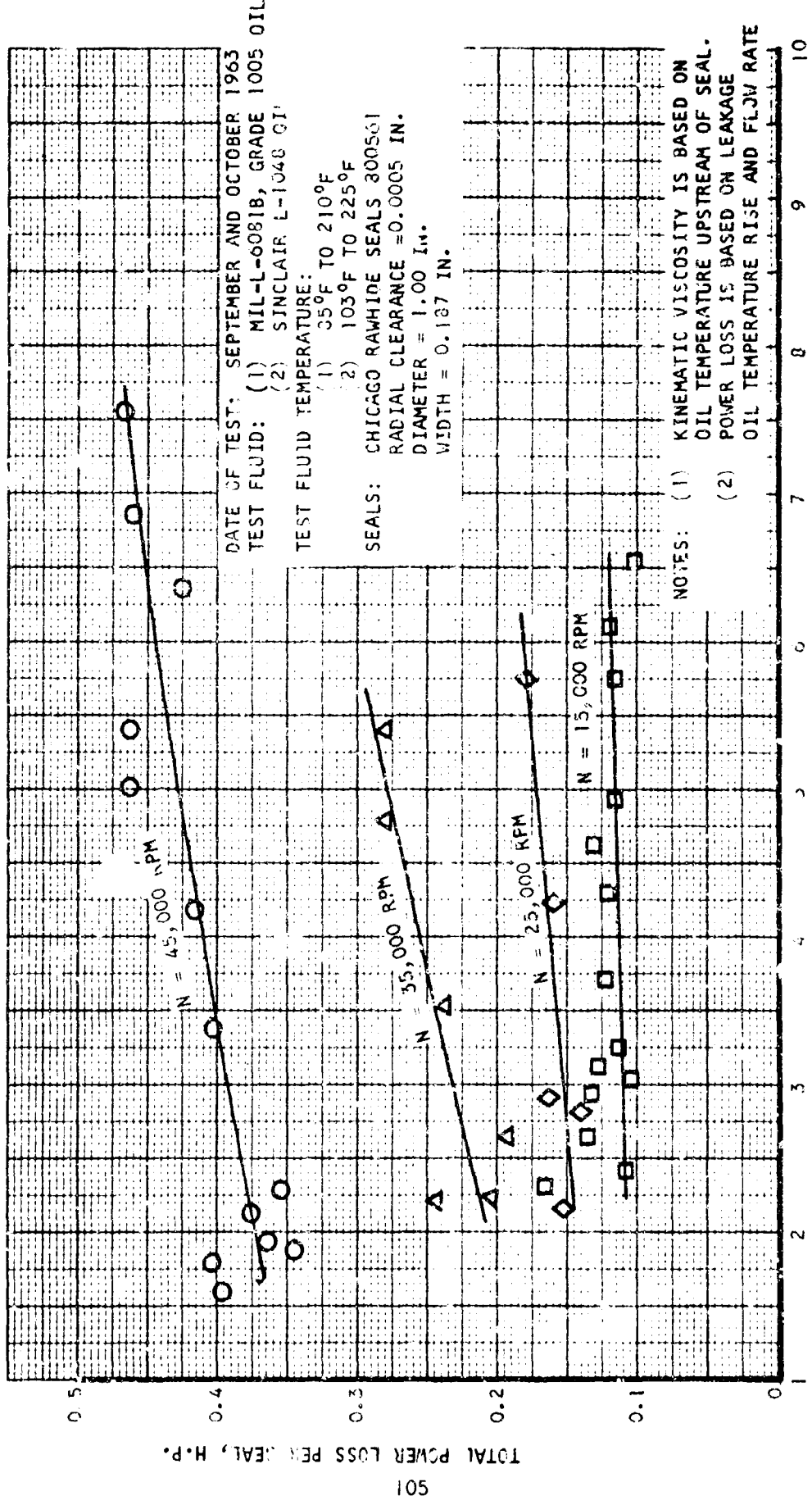
Figure 52. Power Losses for Chicago Rawhide Seal 800561 at 1000 PSI Differential Pressure and Various Speeds
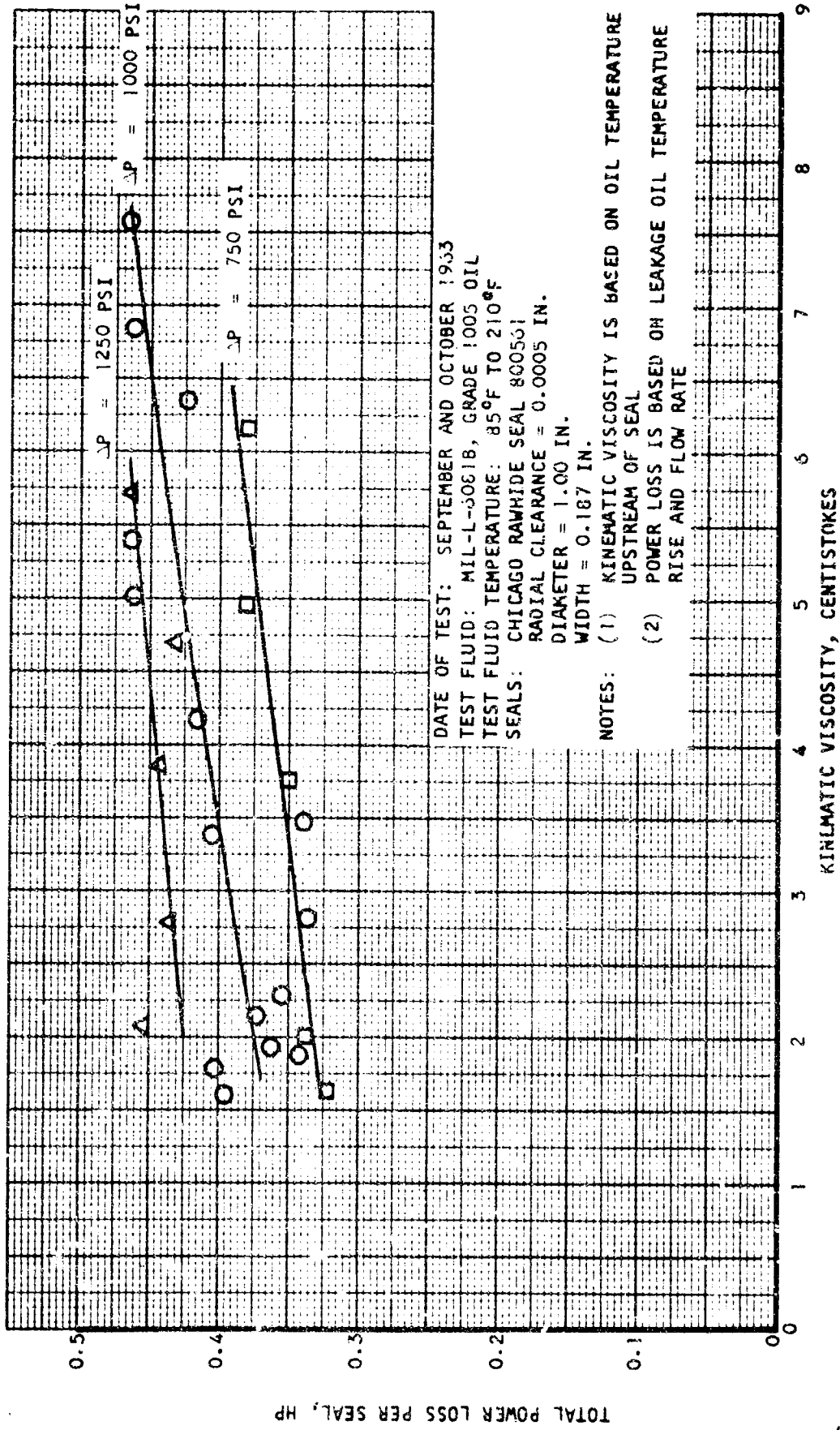
Figure 53. Power Losses for Chicago Rawhide Seal 800561
at 45,000 RPM and Various Pressures

DATE OF TEST: SEPTEMBER AND OCTOBER 1963

TEST FLUID: (1) MIL-L-6081B, GRADE 1005 OIL
(2) SINCLAIR L-1048 OIL

TEST FLUID TEMPERATURE:
(1) 85°F TO 210°F
(2) 103°F TO 225°F

SEALS: CHICAGO RAWHIDE SEALS 800561
RADIAL CLEARANCE = 0.0005 IN.
DIAMETER = 1.00 IN.
WIDTH = 0.187 IN.

NOTES: (1) KINEMATIC VISCOSITY IS BASED ON OIL TEMPERATURE UPSTREAM OF SEAL.
(2) POWER LOSS IS BASED ON LEAKAGE OIL TEMPERATURE RISE AND FLOW RATE

KINEMATIC VISCOSITY, CENTISTOKES

TOTAL POWER LOSS PER SEAL, H.P.

Figure 54. Power Losses for Chicago Rawhide Seal 800561 at 45,000 RPM and 1000 PSI Pressure Differential

107

rate could not actually be measured at this location. The pressures on each side of the impeller were nearly the same. This indicates similar leakages through both seals and also means that the axial thrust was close to being balanced. The leakage measurements and internal pressure measurements did not indicate any increase in seal clearances during the test run.

Single Stage Impeller Tests

To confirm the results of the analytical hydrodynamic design, a single stage impeller, incorporating 60 degree backward curved blades was fabricated and tested. Figures 55 and 56 show this impeller. Test rig details are shown in Figures 57 through 61, , and the test setup is shown in Figures 62 through 66 . The test rig was driven by means of a relatively low speed dynamometer and high speed gear box. This gear box is identical to that used on AiResearch Compressor Part 206420 (Lockheed L-188 Cabin Compressor).

All testing on the single stage rig was accomplished using MIL-L-6081B, Grade 1005 lubricating oil at 180°F to 190°F. This results in a kinematic viscosity of approximately 2 centistokes, the same as that of MLO 8200 fluid at 600°F.

Results of these tests are shown in Figures 67 and 68 . Figure 67 shows pressure rise versus flow at constant speed parameters from 15,000 to 45,000 rpm. Constant efficiency parameters are super-imposed showing a peak efficiency island of 65 percent of approximately 40,000 rpm and efficiency of 64.5 percent, maximum, at the maximum speed of 45,000 rpm. Shaft power input versus flow is presented in Figure 68 for the same constant speed parameters.

Data shown at a speed of 42,000 rpm is particularly significant because, when operating at this speed, the pump pressure rise is exactly equal to the pressure required in the four stage 4000 psi pump at the design point (using MLC 8200 fluid at 600°F). The efficiency shown on these curves is an overall efficiency based on hydraulic power output and pump shaft power input. Thus, it includes power losses in two ball bearings (running in an air-oil mist), one carbon face shaft seal and two floating bushing seals (one at the impeller inlet eye and one on the outboard side of the wheel). The shaft power input was measured by an electric motor dynamometer with deduction of power losses in the 12.26:1 ratio step-up gear box. These gear box losses were based on measurement of the gear box lubricating oil flow rate and oil temperature rise through the gear box.

An investigation was conducted to determine the effect of increased fluid viscosity on pump overall efficiency. Performance was measured at the 42,000 rpm speed at viscosities of 2, 3 and 4 centistokes. This was accomplished by cooling the oil to increase its viscosity. It was found that there was a reduction in peak efficiency of approximately 1.5 percent for each centistoke increase in viscosity. These results are shown in Figure 69 .

580012
Impeller Assembly
2.308 Diameter
60° Backward Curve Blade
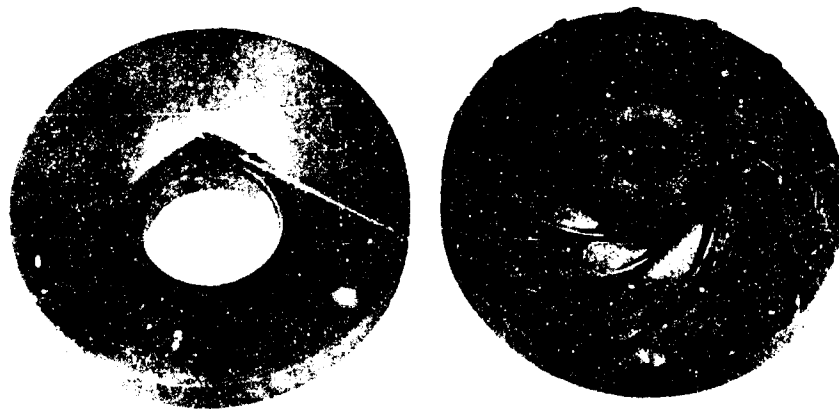
43685-2

Figure 55. Backward Curved Impeller

560011
Impeller Assembly
.308 Diameter
60° Backward Curved Blade
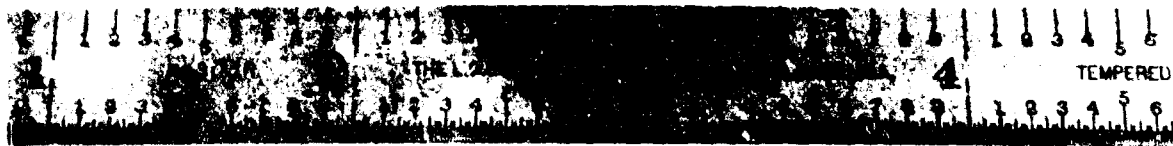
49129-3

Figure 56. 60° Backward Curved Impeller

110

Figure 57. Single Stage Impeller Test Rig

111
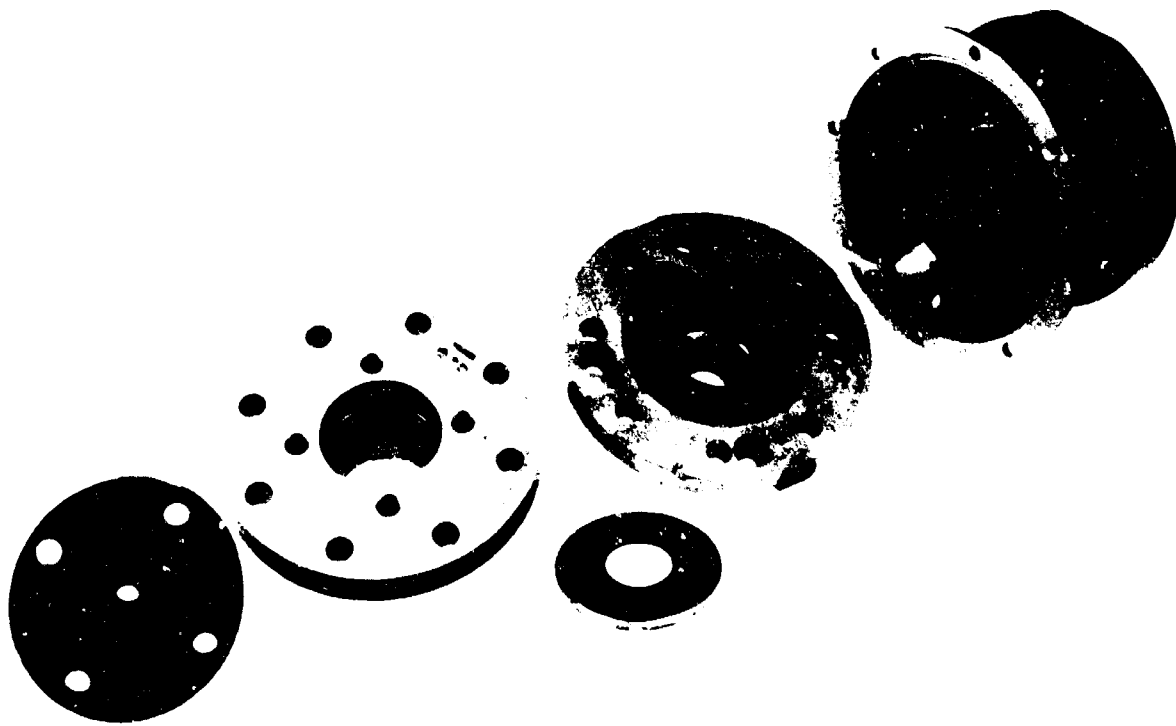
49135-1

Figure 58.   Details of Single-Stage Test Rig

49135-2

Figure 59.   Details of Single-Stage Test Rig

113
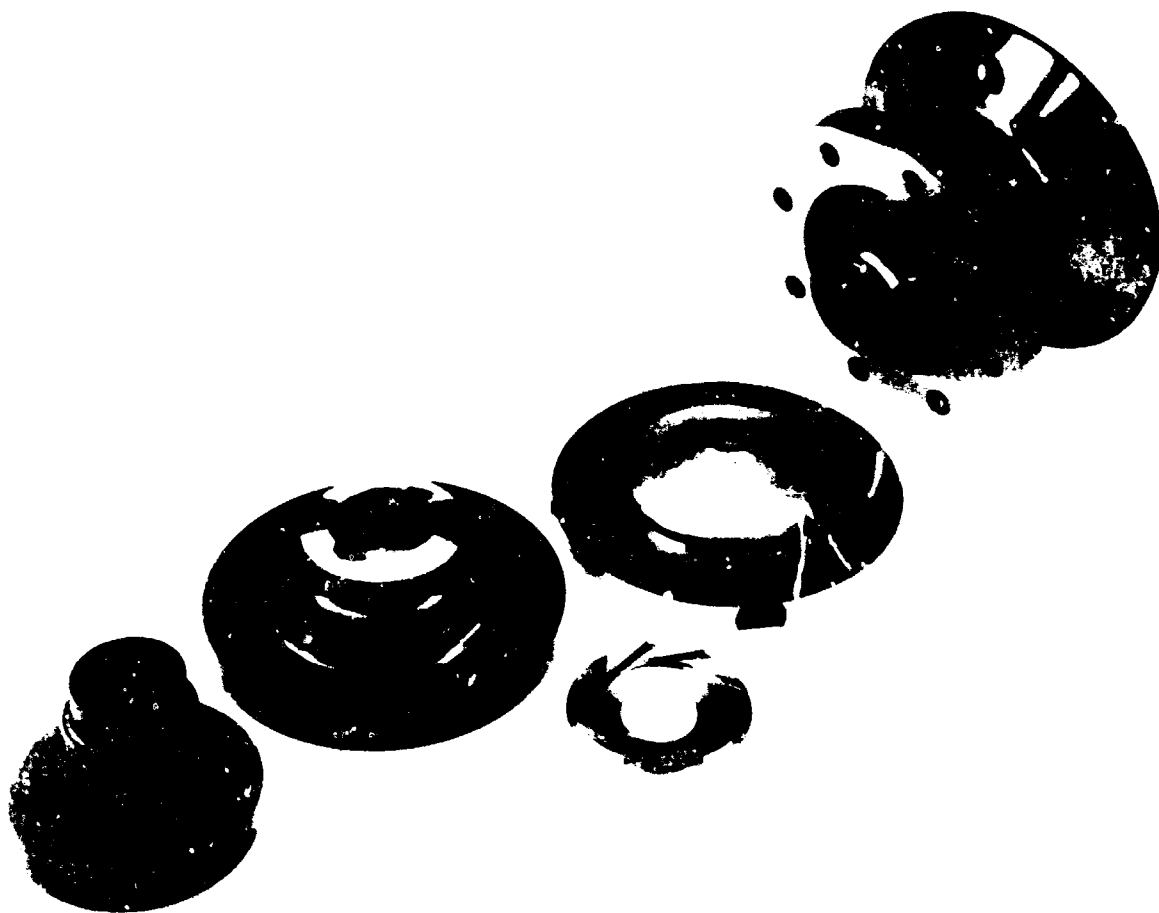
49135-3

Figure 60.   Details of Single-Stage Test Rig

114
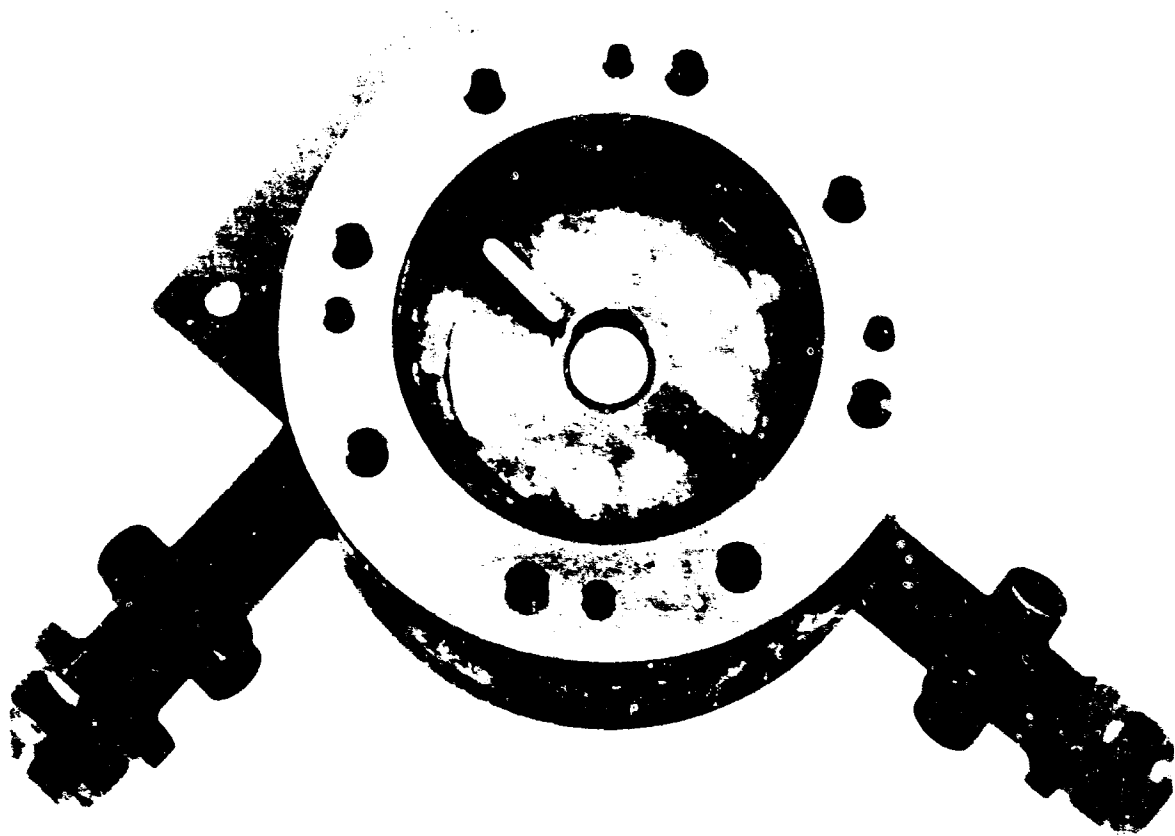
Figure 61. Detail of Single-Stage Test Rig

Figure ... construction ...
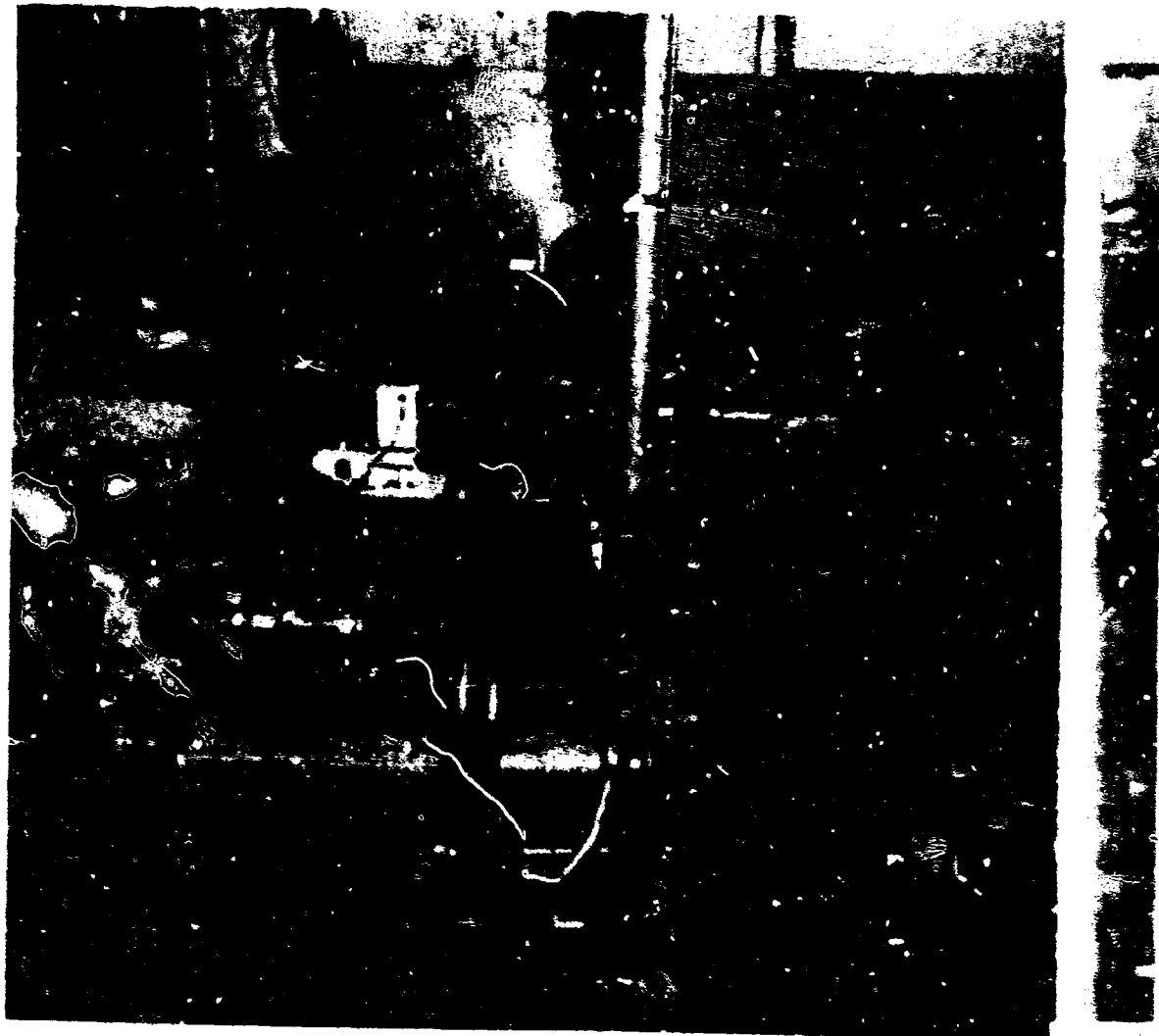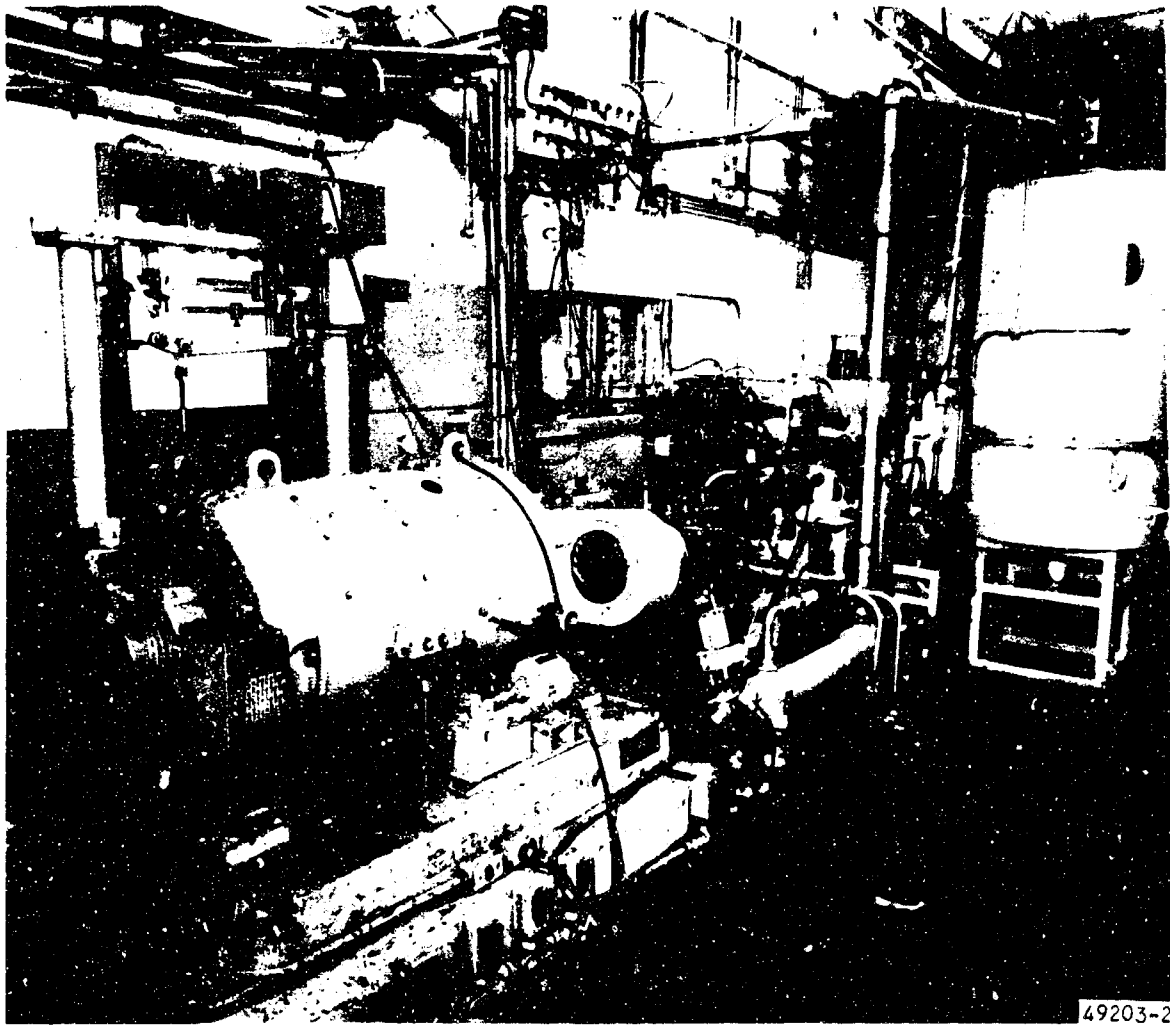
Figure 63. Single Stage Test Setup

49203-3
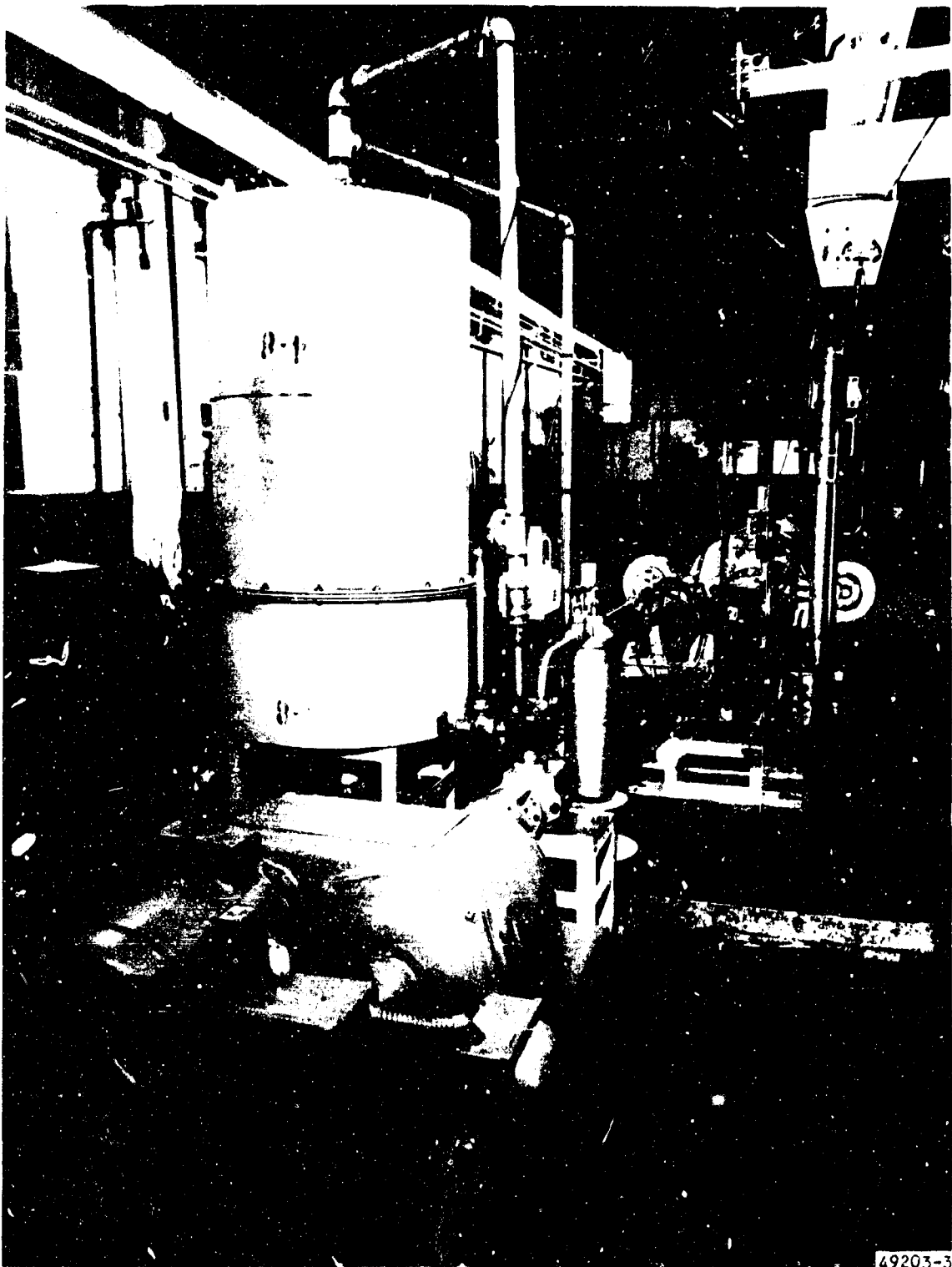
Figure 64.   Single Stage Test Setup
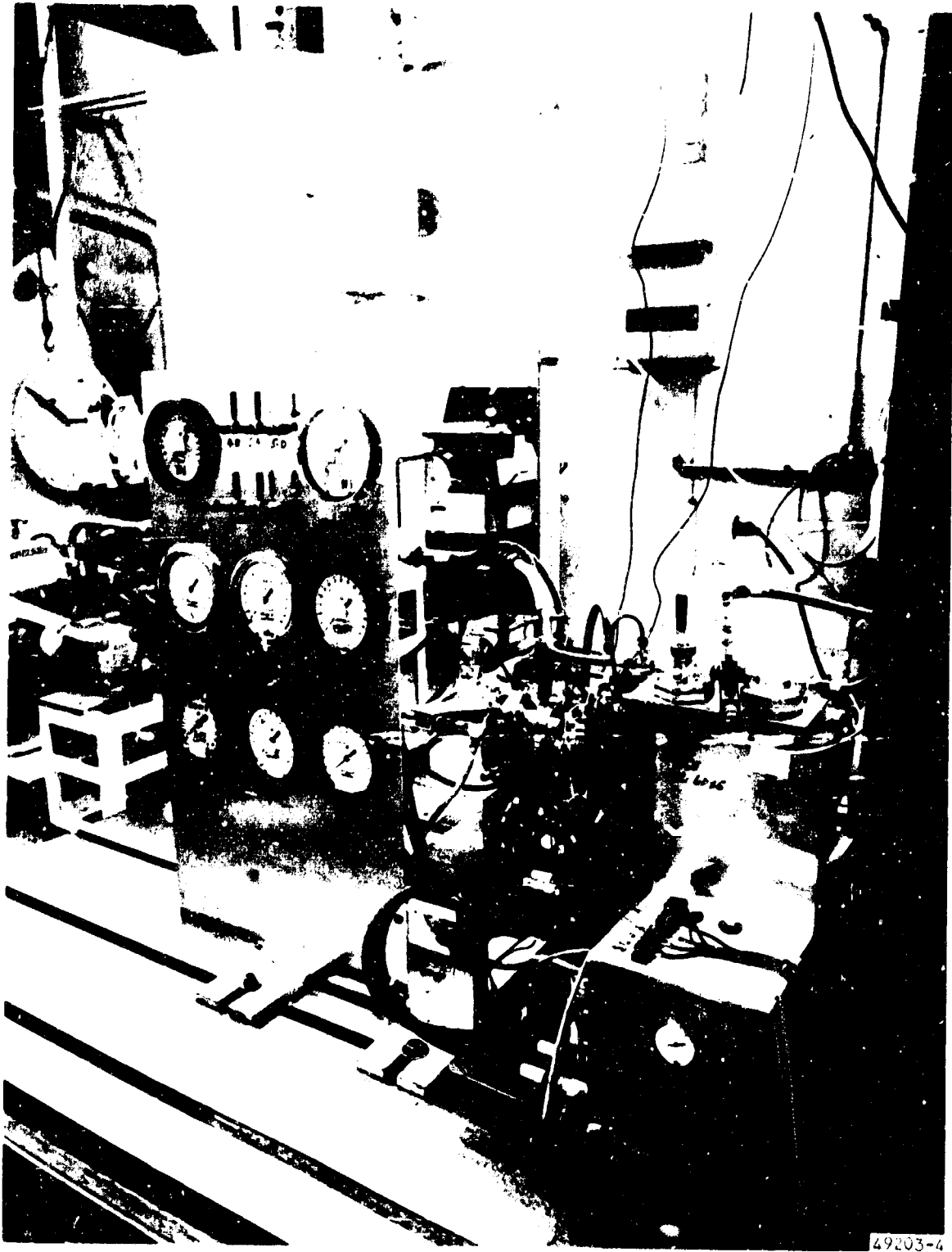
Figure 65.   Single Stage Test Setup

49203-5
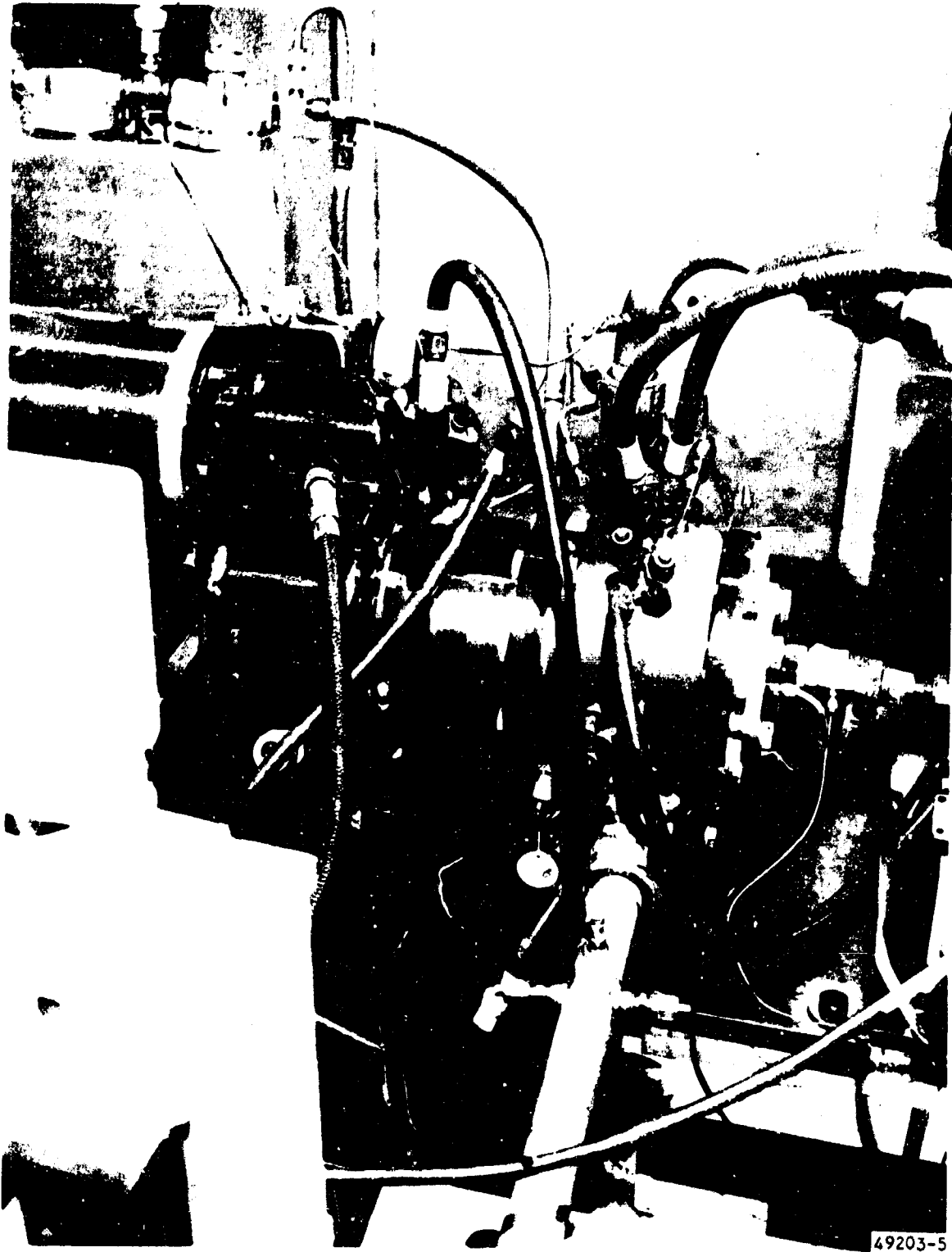
Figure 66. Single Stage Test Setup
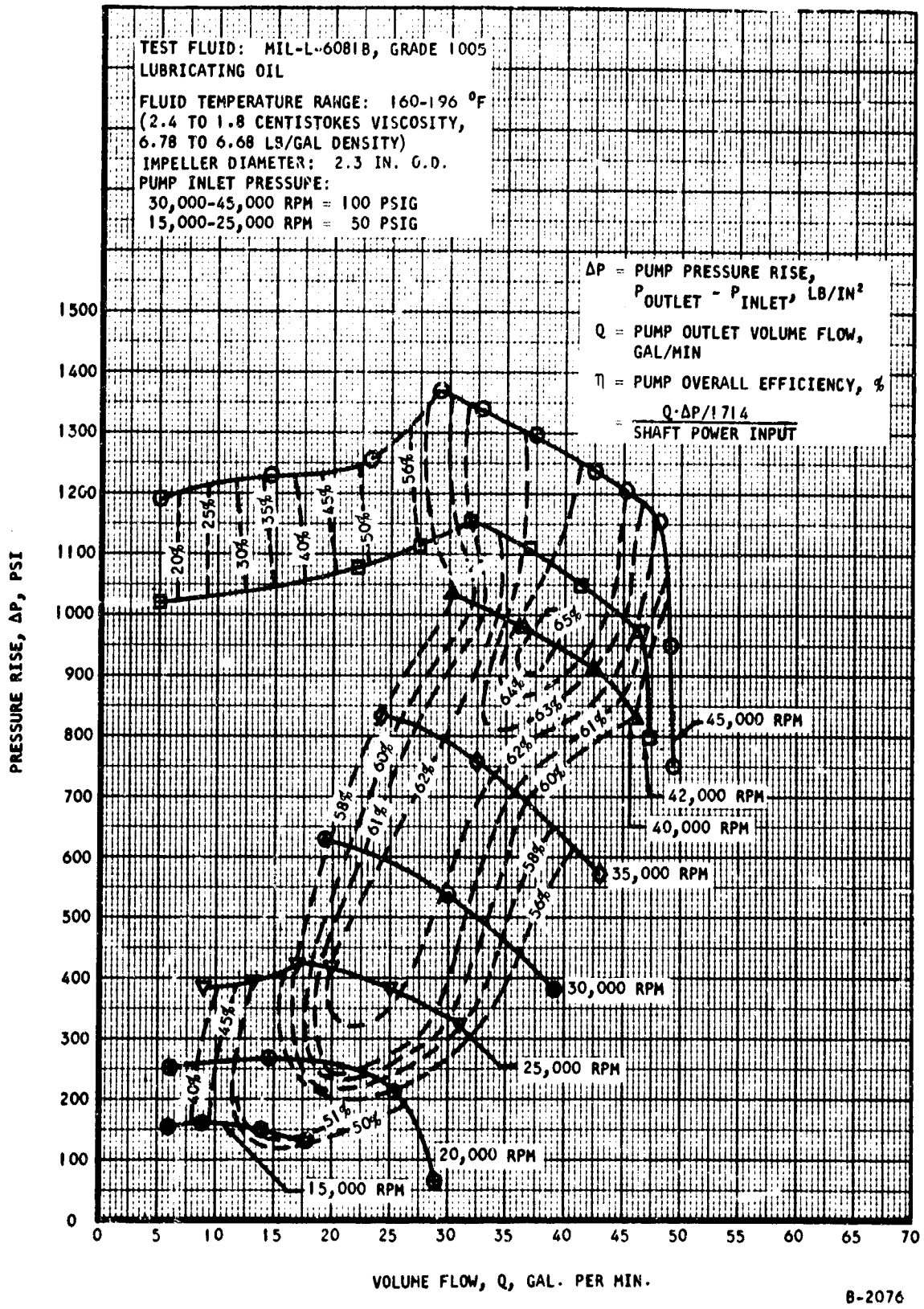
Figure 67. Calibration of Single-Stage Centrifugal Pump Assembly

121
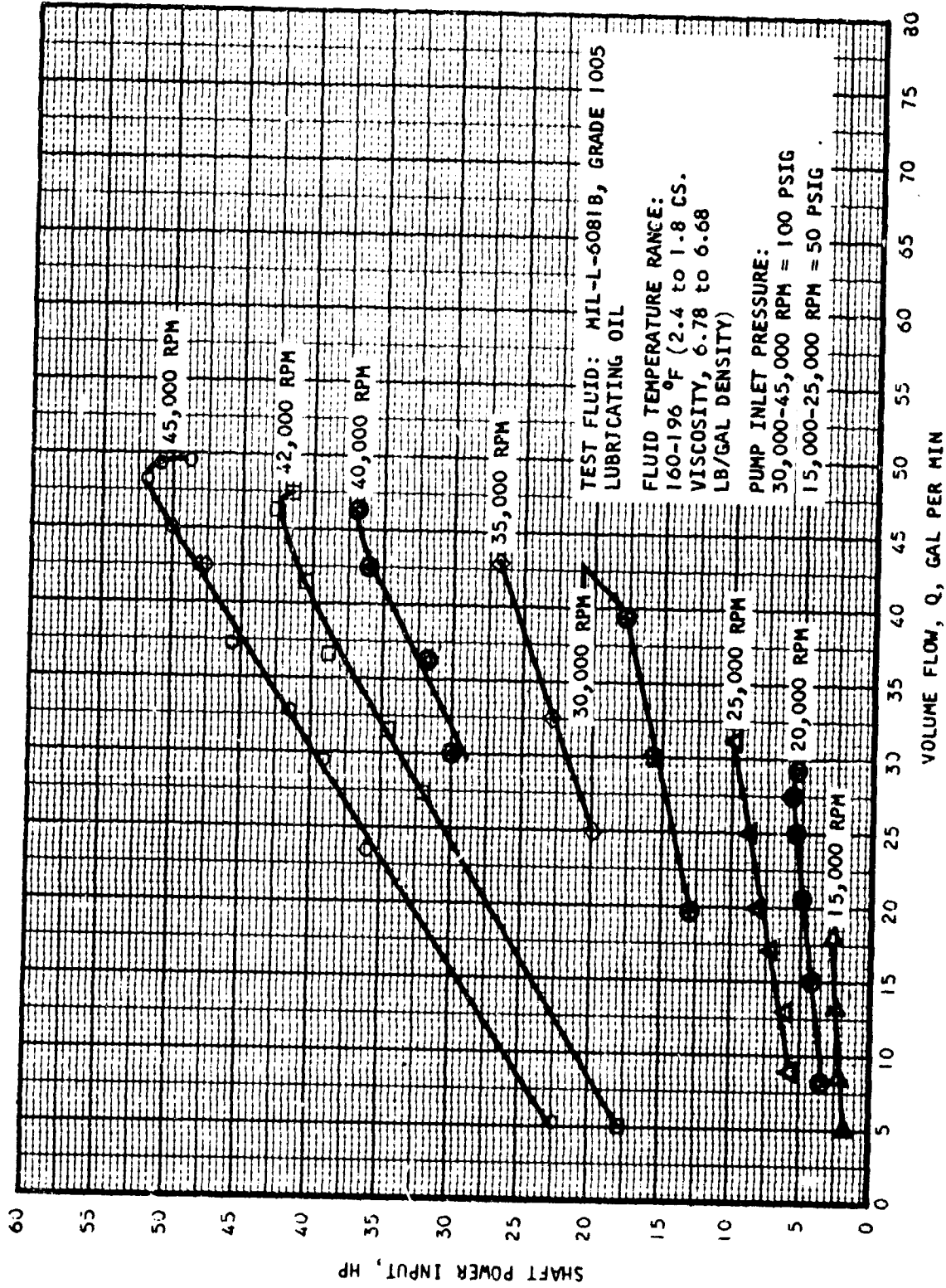
Figure 68. Input Power vs Flow, Single-Stage Centrifugal Pump Assembly

TEST FLUID: MIL-L-6081B, GRADE 1005
LUBRICATING OIL

FLUID TEMPERATURE RANGE:
160-196 °F (2.4 to 1.8 CS.
VISCOSITY, 6.78 to 6.68
LB/GAL DENSITY)

PUMP INLET PRESSURE:
30,000-45,000 RPM = 100 PSIG
15,000-25,000 RPM = 50 PSIG

A-8646
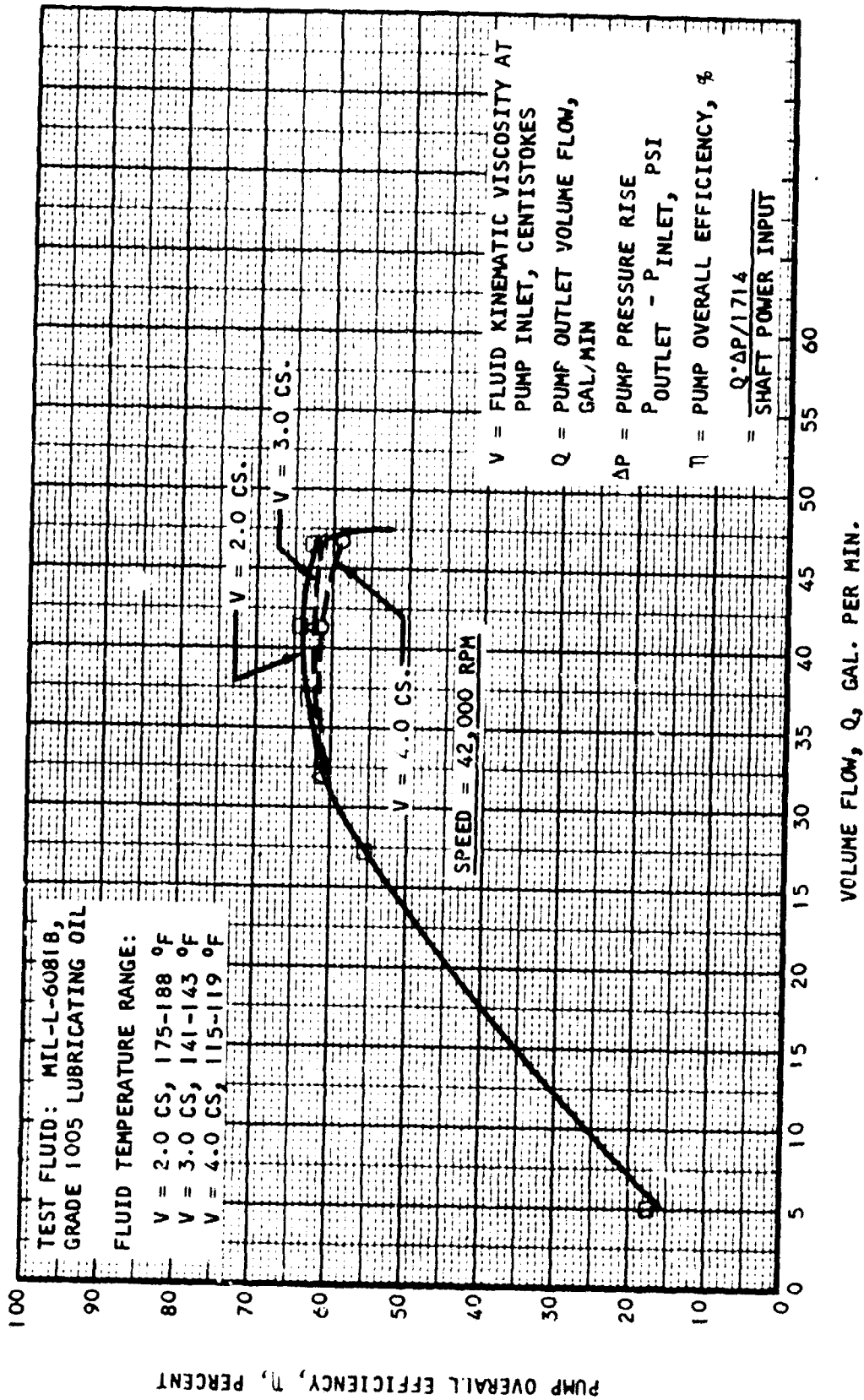
Figure 69. Effect of Fluid Viscosity on Pump Overall Efficiency,
Single-Stage Centrifugal Pump Assembly

123

The performance of the single-stage backward curved impeller was quite encouraging. Calculations made using this test data show an impeller hydraulic efficiency of 80 percent. This is an excellent efficiency for an impeller of this size and is 5 to 8 percent higher than the predicted impeller efficiency used in the original design work.

As can be seen from the pressure rise versus flow curves, the pump exceeds the required pressure rise. If the pressure rise of approximately 1300 psi, which occurs at 45,000 rpm, is corrected for the difference in densities of MLO 8200 fluid at 600°F and MIL-L-6081, Grade 1005 at 185°F (MIL-L-6081 is 14 percent more dense), it becomes 1148 psi pressure rise for MLO 8200 at 600°F. Since the required pressure rise per stage is 975 psi, the impeller diameter could be reduced slightly which might reduce internal disk friction losses thus increasing the overall efficiency to 66 to 70 percent.

The next test conducted, therefore, was a performance check at 45,000 rpm with 2.3 inches outside diameter backward curved impeller trimmed to 2.160 inches outside diameter. The 2.160 inch diameter was selected to provide the pressure rise required for the four-stage pump at 45,000 rpm. For this test, no changes were made in either the diffuser or in the shrouds in order to expedite performance of the test. It was found that the pump efficiency decreased about 2 percent. The decrease in pump pressure rise was more than would be predicted using an impeller diameter squared relationship. Pressure rise dropped from 1300 psi to 1100 psi and the stable flow range of the pump decreased by 4 gpm. However, it is probable that changing the diffuser and shroud designs to match the reduced impeller diameter would improve performance. The final four-stage pump will incorporate the 2.3-inch diameter impeller.

In addition to the 60 degree backward curved blade impeller, it was originally intended to conduct a series of similar tests incorporating a 30 degree forward curved impeller. The impeller, as shown in Figure 69 was fabricated and initial test runs started. It became apparent that use of this impeller caused static pressure variations between the impeller shroud and housing which lead to high axial thrust loads on the seals and bearings. Rather than develop a test rig to overcome this problem, it was decided to concentrate efforts on the complete four stage pump which was ready at the same time.

FOUR-STAGE PUMP

Test Setup

Initial test break in runs were made using lubricating fluid per MIL-L-6081B, Grade 1005. These tests were conducted at ambient room temperatures with a fluid inlet temperature of approximately 190°F. Figures 71 and 72 show the pump test setup for this run.

124

580014
IMPELLER ASSEMBLY
2.000 DIA.
30° FORWARD CURVE BLADE
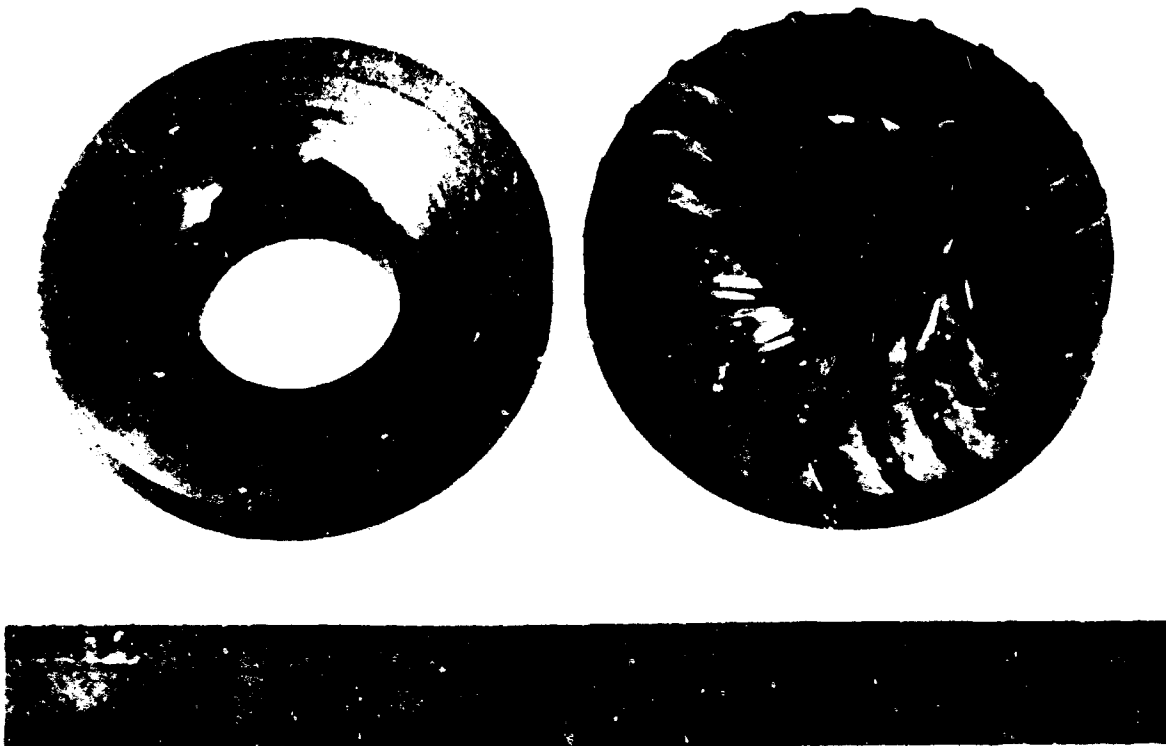
A9129-1

Figure 70.   30° Forward Curve Impeller
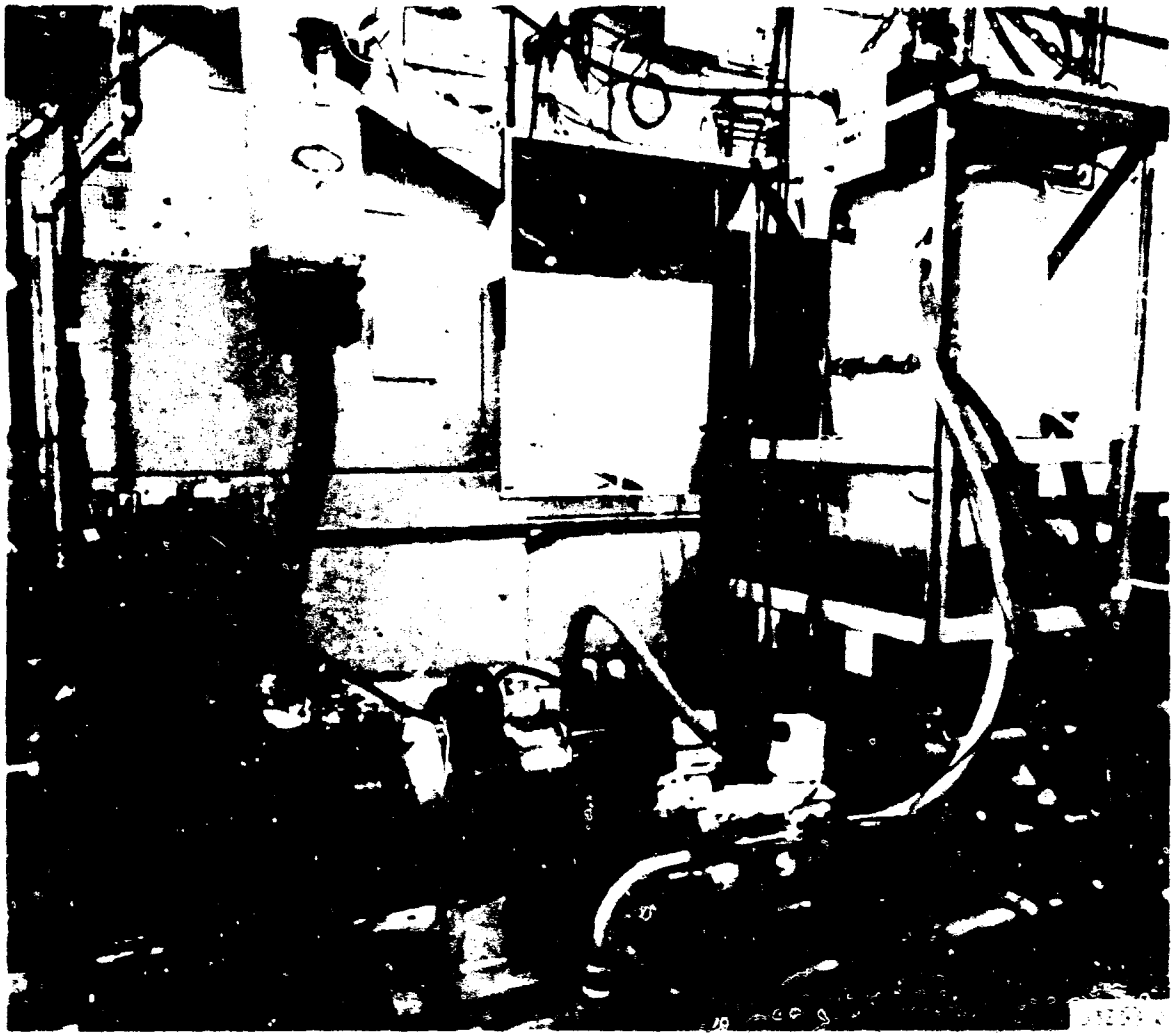
Figure 71. View of Pump and Turbine Drive Test Setup for Run 1

53258-1
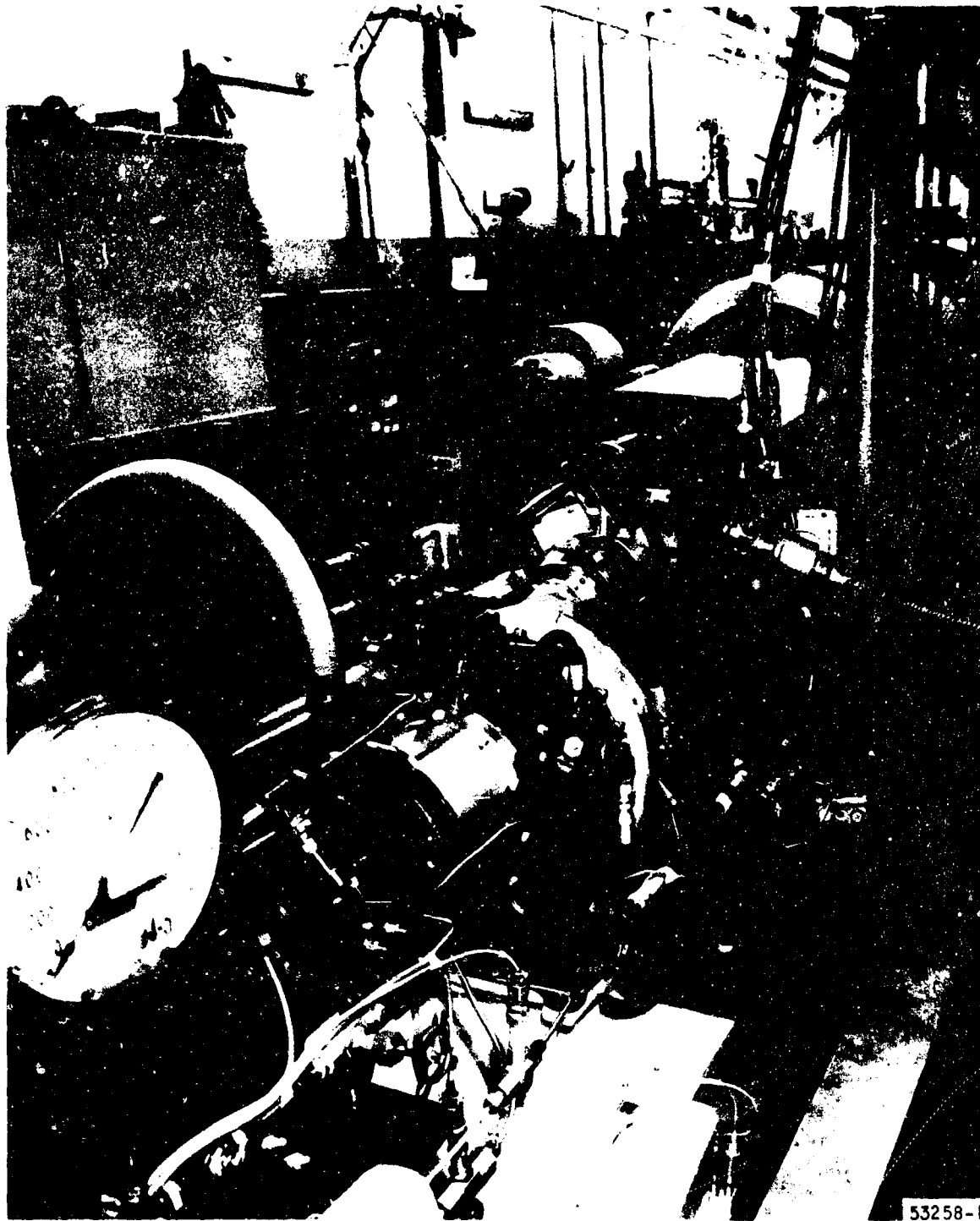
Figure 72. Pump and Turbine Drive Test Setup for Run 1
(Viewed from Pump End)

127

In order to achieve the smoothest possible driving mechanism for the initial break in, it was decided to adapt an existing air turbine drive to the pump. The compressor section of an AiResearch Part 206170 (Boeing 707) Cabin Air Compressor was removed and a special adapter was made to match the turbine housing and pump inlet flange bolt circles. Speed control was accomplished by varying turbine inlet air pressure, and by varying turbine nozzle area. The standard pneumatic nozzle positioner was used for this purpose and a pressure regulated air supply. Figures 73 and 74 show the pump, adapter, and turbine drive.

Use of an air turbine to provide a direct driving means for the pump eliminates the need for a gear box, and also eliminates the shock of step speed changes. Measurement of pump inlet power, however, depends on an accurate measure of turbine air weight flow and temperature drop. Bearing losses for the turbine drive have been well established by many previous tests.

Figure 75 presents a schematic of the setup for the high temperature tests of the four stage hydraulic pump using MLO 8200 fluid. Figures 76 and 77 show the actual test installation.

The pump generated heat raised the fluid temperature to the desired level, and this temperature was maintained by bypassing a portion of the discharge flow through a heat exchanger. Bearing leakage flow was returned to the inlet reservoir through another heat exchanger. The fluid reservoir was remotely placed in order to maintain the bulk temperature of the fluid at a reasonably low value (approximately 400^0F). Lubricating fluid for the thrust bearing and the inboard journal bearing was bled from the first stage discharge.

Because of safety considerations, the pump and heat exchanger were blanketed in a CO_2 atmosphere.

Instrumentation

During break in runs at low fluid temperatures (approximately 190^0F) and initial high temperature runs, shaft deflection instrumentation was included. Although this type instrumentation will not provide valid results at elevated temperatures, sufficient information was gathered to confirm that no excessive shaft excursions had occurred during the runs.

Total lubricating flow to the thrust bearing and inboard journal bearing was measured by means of a high temperature flow sensing element. This was used in conjunction with a remotely operated needle valve to regulate and monitor the fluid quantity bled from the first stage.

Outboard journal bearing flow was measured during the room temperature runs. This flow was in close agreement with the leakage rates as measured on the seal test rig, indicating a bearing flow of approximately 1.28 gallons per minute at 4000 psi discharge pressure. During high temperature runs, this flow was returned directly to the inlet reservoir in a closed loop and was not measured.

128
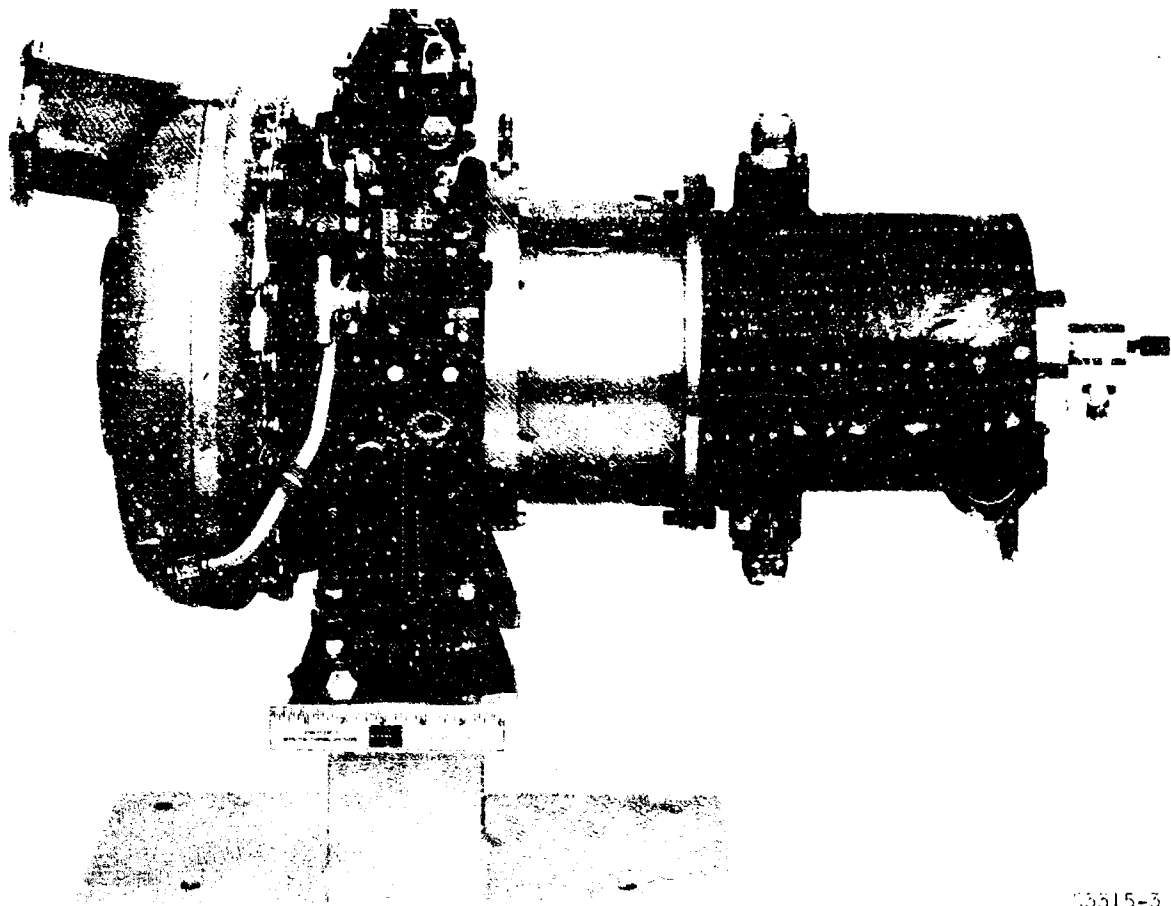
03515-3

Figure 73.   Four-Stage Pump Assembly and Turbine Drive

129
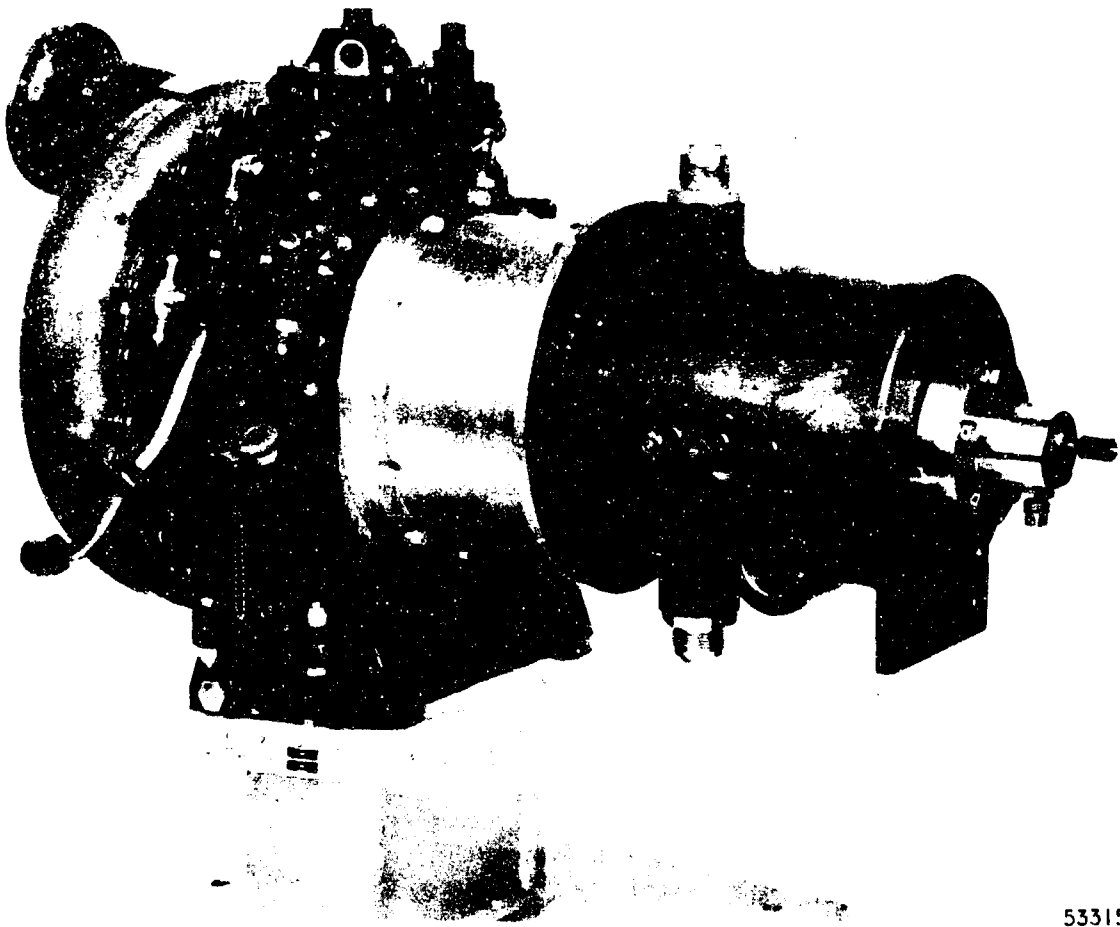
53315-4

Figure 74. Four-Stage Pump Assembly and Turbine Drive
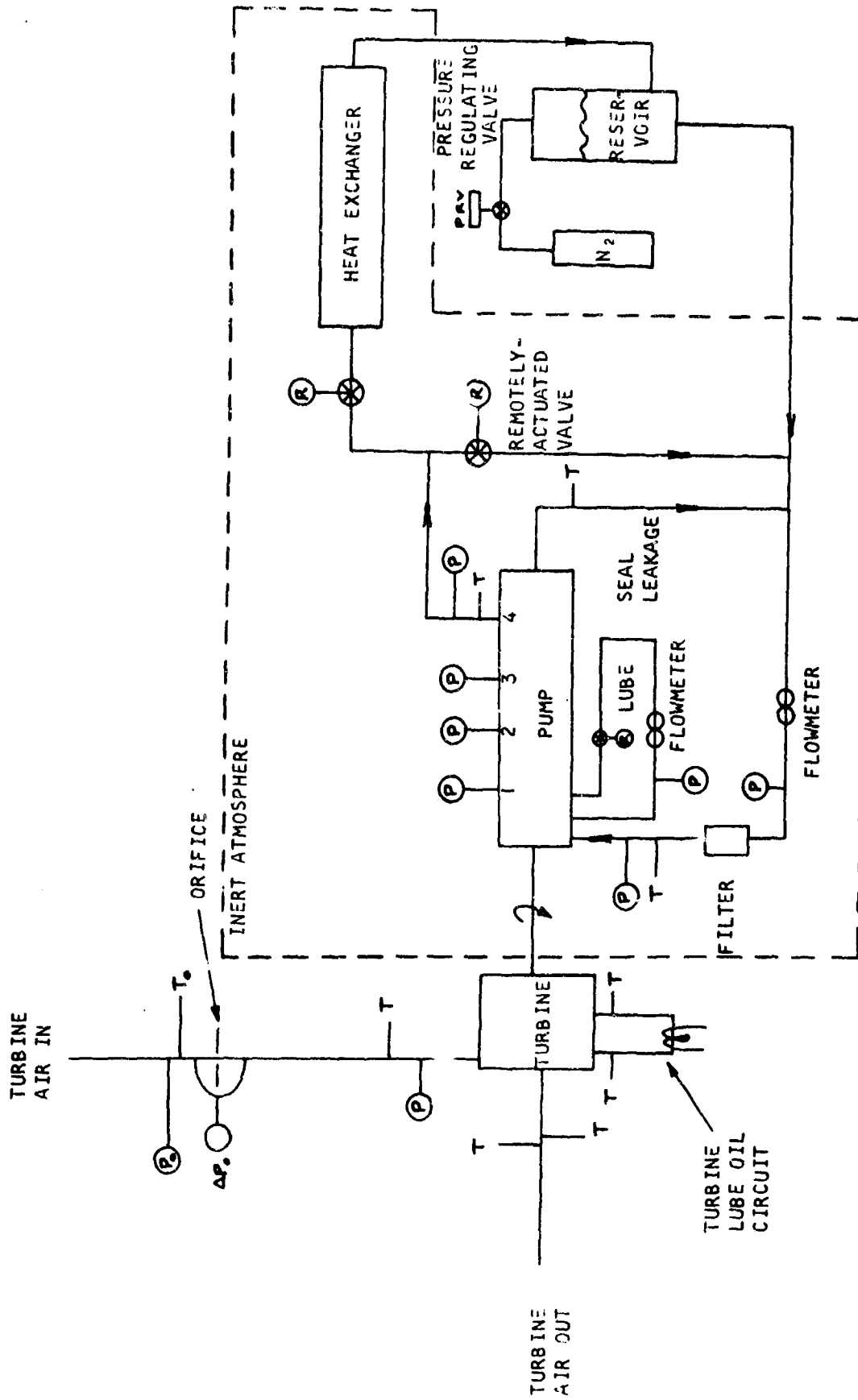
Figure 75. Schematic Diagram of Setup For Final High Temperature Test Run
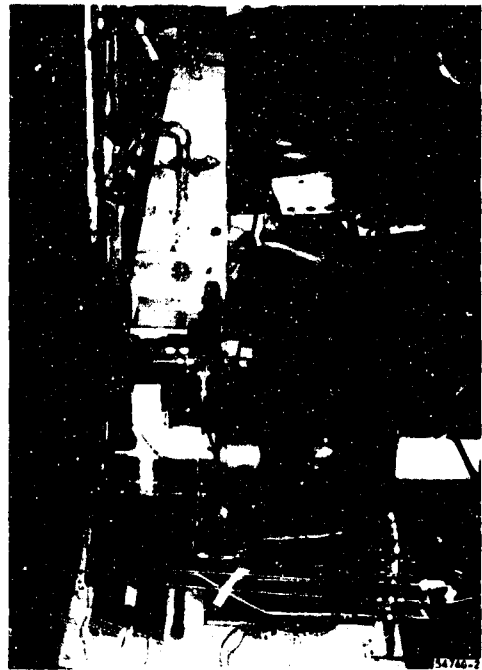
Figure 76. Test Installation for the High Temperature Tests of the Four-Stage Hydraulic Pump (L208043) Using MIL-O-8200 Hydraulic Fluid
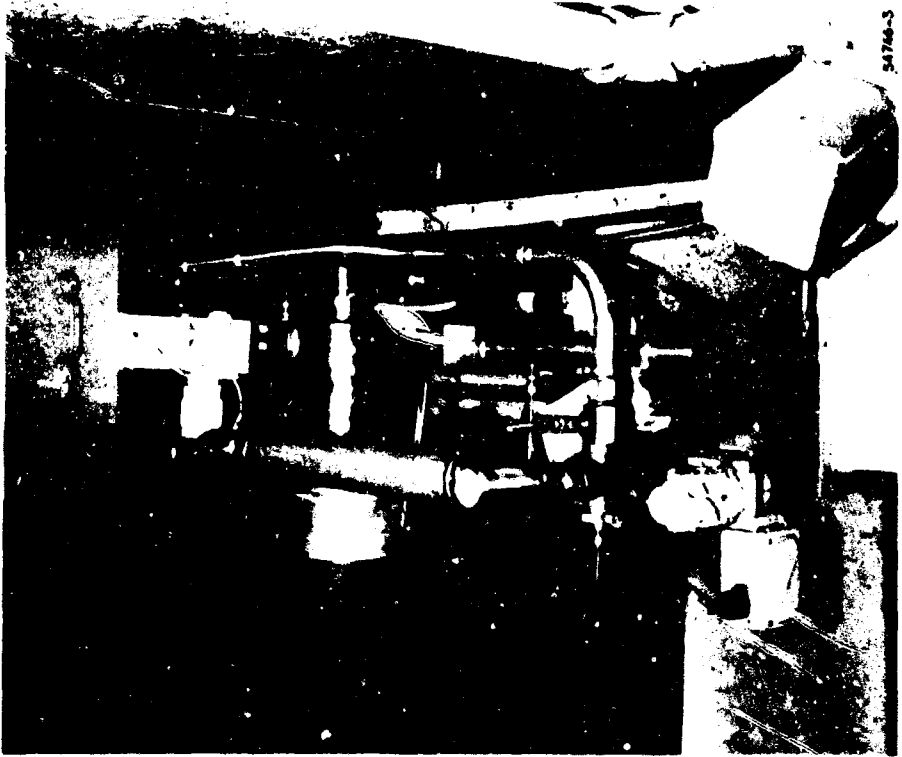
Figure 77. Test Installation for the High Temperature Tests of the Four-Stage Hydraulic Pump (L208043) Using MIL-O-8200 Hydraulic Fluid

133

Pump oil flow was measured by a high temperature flow sensing element in the pump inlet. Oil inlet and discharge temperature was measured as well as bearing drainage fluid temperatures were also measured at the outboard journal and thrust bearings.

Pump inlet pressures were measured before and after the inlet filter. Other gages were installed to measure pump discharge pressure, interstage pressure for each stage and bearing lubrication inlet pressure.

PUMP TESTING AND RESULTS

Four Stage Pump Tests

Testing of the four stage hydraulic pump had a two-fold purpose. First to prove the hydrodynamic design, and secondly to demonstrate an endurance life of 25 hours with a pump fluid inlet temperature of 600°F.

During testing, the pump achieved a peak efficiency of 62 percent. This includes all mechanical and parasitic losses associated with the pump unit but does not include mechanical or thermodynamic losses of the air turbine drive.

After the final thrust bearing configuration was established, the unit was operated for a total twenty hours and fifty minutes. Of this time, fluid inlet temperature was 400°F or greater for fourteen hours and twenty minutes, and 600°F for six hours and thirty minutes.

A total of ten short test runs were made, and were terminated for a variety of reasons associated with either the pump test or the pump test set up. Table 1 lists each of the runs, the major results, and reasons for shutdown. Test data for each of the runs is listed in Table 2 through 8. Data is included from the initial break-in runs made using MIL-L-6081B, Grade 1005 lubricating fluid and a hydrodynamic pocket thrust bearing.

The pump was completely disassembled following Run No. 3 and Run No. 7 low output flows were observed for all runs subsequent to Run No. 4, and during that run, flow could not be recorded accurately because of a flowmeter malfunction. During Run No. 3, when full output flow was measured, an overall pump efficiency of 62 percent was achieved. This efficiency was measured as follows:

Turbine shaft power

$$HP = \frac{W_T \Delta T}{177} = \frac{(104.0)(195)}{177} = 115 \text{ horsepower}$$

TABLE I

SUMMARY OF TEST RUNS

Test Run	Date	Remarks
1	9-3-65	Maximum temperature 350°F, flow low
2	9-7-65	Heat Exchanger Bypass Valve leak
3	9-8-65	Rear Seal failed
4	10-19-65	Discharge Valve failed
5	10-21-65	External leak
6	10-25-65	Low output
7	10-27-65	Shaft seal leak
8	12-1-65	Seal leak
9	12-2-65	Test stand leak
10	12-3-65	Fluid breakdown

TABLE 2

BREAK-IN TEST RUN, OUTLINE 580020(L 2C8043)

		AA	BB	CC	DD	EE	FF	GG	HH	Observed	Observed
Speed	rpm	10,000	15,120	19,980	25,020	30,240	30,120	30,180	35,200	35,000	40,000
Filter in pressure	psig	49.0	57.0	52.0	49.5	100.0	98.5	104.0	105.0	--	--
Pump in pressure	psig	48.2	55.5	51.0	48.2	98.5	96.5	99.0	77.5	100	100
First stage out pressure	psig	72	70	73	74	175	240	640	400	--	--
Second stage out pressure	psig	90	90	120	160	460	750	1200	1150	--	--
Third stage out pressure	psig	95	95	235	495	975	1260	1700	1960	3200	4000
Pump out pressure	psig	135	205	495	900	1560	1840	2300	2660		
Pump in temperature	°F	83	121	118	117	149	134	136	158	--	--
Pump out temperature	°F	85	127	130	136	171	161	173	202	--	--
Bearing lube oil temperature	°F	84	123	122	124	158	146	154	180	--	--
Inboard thrust bearing temperature	°F	86	125	129	128	156	157	157	185	--	--
Outboard thrust bearing temperature	°F	91	129	150	164	200	178	164	214	--	--
Outboard journal drain oil temperature	°F	87	131	139	146	180	171	183	236	--	--
Pump in flow	gpm	9.0	11.5	12.9	13.1	18.6	15.4	10.5	13.2	--	--
Pump out flow	gpm	9.2	11.6	12.6	12.6	18.5	15.3	10.4	13.0	--	18.0
Inboard thrust bearing flow	gpm	--	.20	.40	.20	.30	.57	1.37	.44	--	--
Outboard thrust bearing flow	gpm	.48	.41	.62	.60	1.00	1.13	.30	.12	--	--
Inboard journal bearing flow	gpm	.20	.20	.40	.40	1.26	1.35	1.50	1.26	--	--
Outboard journal bearing flow	gpm	.008	.015	.069	.146	.276	.318	.414	.557	--	--

136

TABLE 3

TEST RUN 1, OUTLINE 580020 (L 208043)

Data Point	A	B	C	D	E	F	G	H	I
Speed, rpm	25.000	30.000	30.500	30.000	30.000	35.000	40.000	40.000	40.000
Pump Inlet Pressure, psig	80.5	91.5	96.0	95.0	96.0	94.5	91.0	95.0	96.0
First-Stage Pressure, psig	125	135	250	455	605	405	360	1000	1000
Second-Stage Pressure, psig	285	480	740	965	1145	1125	1275	1930	2025
Third-Stage Pressure, psig	660	1010	1360	1525	1700	1980	2250	2900	3010
Pump Discharge Pressure, psig	1000	1525	1900	2040	2240	2600	3200	3860	4020
Bearing Inlet Pressure, psig	80.0	100.0	125.0	117.0	115.0	112.0	106.0	122.0	112.0
Oil Flow, gpm	14.6	17.3	14.7	15.2	14.2	15.9	17.8	15.0	14.2
Oil Inlet Temperature, °F	194	240	256	262	268	294	320	357	346
Oil Discharge Temperature, °F	212	267	288	291	296	333	368	392	407
Bearing Discharge Temperature, °F	232	278	290	296	303	335	368	387	401
Ambient Temperature, °F *	80	78	86	87	82	80	80	82	78
Reservoir Temperature, °F	143	241	258	270	276	301	324	342	353
Turbine Inlet Temperature, °F	152	189	204	207	221	218	205	204	202
Turbine Discharge Temperature, °F	45	57	70	72	70	62	38	33	30
Turbine Air Flow, lb/min	-	53.0	52.5	52.0	52.5	59.0	76.0	77.0	80.0

* Ambient Box Open

137

TABLE 4

TEST RUN 2 AND 3, OUTLINE 580020(L 208043)

Data Point	A	B	C	D	E
Speed, rpm	29.500	35.000	40,000	40.000	40.800
Pump Inlet Pressure, psig	104.0	102.0	96.0	98.0	117
First-Stage Pressure, psig	520	485	795	1055	1080
Second-Stage Pressure, psig	975	1130	1705	1990	2050
Third-Stage Pressure, psig	1500	1850	2650	2980	3060
Pump Discharge Pressure, psig	2000	2560	3590	3940	4060
Bearing Inlet Pressure, psig	110	105	100	104	120
Oil Flow, gpm	21.0	24.4	26.0	14.8**	23.6
Bearing Lube Flow, gpm	1.1	1.15	0.95	0.96	1.1
Oil Inlet Temperature, °F	385	461	414	397	497
Oil Discharge Temperature, °F	406	491	460	457	552
Bearing Lube Oil Discharge Temperature, °F	411	496	484	477	569
Seal Leakage Temperature, °F	374	452	467	468	541
Ambient Temperature, °F	160	187	202	232	228
Reservoir Temperature, °F	172	165	245	291	291
Turbine Inlet Temperature, °F	237	246	241	239	259
Turbine Discharge Temperature, °F	91	74	46	49	64
Turbine Air Flow, lb/min	68.3	80.0	105.0	100.0	104.0
Hydraulic Power, HP	23.2	35.0	53.6	**	65.9
Turbine Shaft Power, HP	56.2	77.7	115.5	107.0	115
Turbine Mechanical Losses, HP*	2.9	4.8	6.0	6.0	6.0
Pump Efficiency, %	43.5	48.0	49.5	**	62

** Pump discharge valve leak.
* Estimated from previous turbine qualification test.

Best Available Copy

138

TABLE 5

TEST RUN 4, 5 AND 6, OUTLINE 580020(L 208043)

Data Point	A	B	C	D	E	A	A	B	C
Speed, rpm	20.000	25.000	30.000	35.000	35.000	27.000	35.000	40.000	42.700
Pump inlet pressure, psig	82	73	98	99	56	85	115	119	102
First stage Pressure, psig	320	230	210	240	760	175	700	980	1060
Second stage pressure, psig	530	560	655	500	1490	340	1365	1905	1980
Third stage pressure, psig	740	930	1140	1150	2240	725	2050	2725	3000
Pump discharge pressure, psig	1000	1325	1660	1875	3000	1100	2750	3620	4000
Bearing inlet pressure, psig	90	75	100	98	64	85	120	112	100
Oil flow, gpm	14.7	22.0	27.0	32.0	15.9	17.0	18.0	13.0	11.5
Bearing lube flow, gpm	-	-	-	-	-	-	-	-	-
Oil inlet temperature, °F	351	360	363	400	405	422	612	602	594
Oil discharge temperature, °F	360	373	382	427	442	437	638	657	675
Turbine inlet temperature, °F	81	246	173	230	256	302	214	211	208
Turbine discharge temperature, °F	19	128	25	55	78	166	51	41	35
Turbine airflow, lb/min	49.5	57.0	72.0	84.0	83.0	52.0	70.0	96.0	104.0
Hydraulic power, HP	7.85	16.4	26.2	33.4	27.2	10.0	27.8	27.4	26.2
Turbine shaft power, HP	17.3	38.0	60.4	63.0	74.0	40.0	64.5	92.1	103.0
Turbine mechanical losses, HP*	1.6	2.3	3.2	4.5	4.5	2.7	4.8	6.0	7.0
Pump efficiency, percent	50.0	46.0	46.0	42.6	39.2	26.8	54.7	31.9	27.4

*Estimated from previous turbine qualification test

TABLE 6

TEST RUN 7, OUTLINE 580020 (L 205043)

Data Point	A	B	C	D	E	F
Speed, rpm	40,500	42,000	44,500	45,000	45,000	45,000
Pump inlet pressure, psig	128	129	128	127	186	175
First stage pressure, psig	1020	1070	790	680	720	720
Second stage pressure, psig	1935	2012	1845	1740	1775	1760
Third stage pressure, psig	2850	2980	2900	2800	2830	2840
Pump discharge pressure, psig	3850	4000	4100	4025	4000	4040
Bearing inlet pressure, psig	125	125	125	125	180	170
Oil flow, gpm	19.8	18.4	23.2	23.2	25.6	25.6
Bearing lube flow, gpm	1.10	.92	.78	1.04	1.03	1.02
Oil inlet temperature, °F	520	612	607	606	610	604
Oil discharge temperature,	562	655	650	650	650	647
Turbine inlet temperature, °F	242	255	253	256	260	264
Turbine discharge temperature, °F	45	57	40	42	45	45
Turbine airflow, lb/min	84.0	91.0	99.0	99.0	102.5	102.5
Hydraulic power, HP	43.6	41.6	53.9	53.0	57.2	58.0
Turbine shaft power, HP	96.0	105.5	124.0	124.0	129.5	129.0
Turbine mechanical losses, HP*	6.1	6.7	8.0	8.1	8.1	8.1
Pump efficiency, percent	48.5	42.2	46.4	45.9	46.2	47.9

*Estimated from previous turbine qualification test

140

TABLE 7

TEST RUN 8 AND 9, OUTLINE 580020 (L 208043)

Data Point	A	B	C	D	A	B
Speed, rpm	42,000	42,000	42,000	42,600	47,200	40,800
Pump inlet pressure, psig	103	103	103	102	90	93
First stage pressure, psig	1070	1070	1060	1060	260	960
Second stage pressure, psig	2050	2000	2000	2015	1400	1890
Third stage pressure, psig	3000	3000	3000	3050	2600	2800
Pump discharge pressure, psig	3950	3950	3950	4000	3800	3670
Bearing inlet pressure, psig	105	100	102	100	100	100
Oil flow, gpm	15.8	15.6	15.8	20.4	24.9	15.0
Bearing lube flow, gpm	1.05	1.00	1.05	.90	-	-
Oil inlet temperature, °F	544	550	554	601	601	553
Oil discharge temperature, °F	600	606	610	650	651	610
Turbine inlet temperature, °F	218	220	221	224	261	270
Turbine discharge temperature, °F	44	44	46	42	54	84
Turbine airflow, lb/min	94.5	94.2	93.5	101.5	113.0	81.5
Hydraulic power, HP	35.5	35.4	35.5	46.5	55.0	31.3
Turbine shaft power, HP	93.0	92.5	91.6	104.2	142.0	85.6
Turbine mechanical losses, HP*	6.7	6.7	6.7	7.0	9.1	6.3
Pump efficiency, percent	40.7	41.4	41.9	47.9	42.0	39.7

*Estimated from previous turbine qualification test

141

TABLE 8

TEST RUN 10, OUTLINE 580020(L 208043)

Data Point	A	B	C	D	E	F	G	H
Speed, rpm	42,000	42,000	42,000	42,000	42,000	42,000	42,000	42,000
Pump inlet pressure, psig	117	117	115	113	113	113	112	112
First stage pressure, psig	1050	1060	1060	1050	1030	1030	1030	1030
Second stage pressure, psig	2010	2000	2040	2035	2045	2045	2050	2050
Third stage pressure, psig	2900	2950	2940	2950	2950	2950	2950	2950
Pump discharge pressure, psig	3900	3900	3930	3940	3940	3940	3950	3940
Bearing inlet pressure, psig	120	117	117	115	113	113	112	112
Oil flow, gpm	14.5	13.0	14.0	14.0	14.0	14.0	13.0	13.0
Bearing lube flow, gpm	1.08	.82	.93	.80	1.04	1.04	1.04	1.04
Oil inlet temperature, °F	602	594	600	601	605	604	606	596
Oil discharge temperature, °F	653	648	653	654	658	600	662	654
Turbine inlet temperature, °F	249	255	260	263	265	268	268	254
Turbine discharge temperature, °F	66	73	76	78	80	82	82	74
Turbine airflow, lb/min	98	98	98	98	98	98	98	98
Hydraulic power, HP	32.2	32.2	32.2	32.2	32.2	32.2	32.2	32.2
Turbine shaft power, HP	101	101	101	101	101	101	101	101
Turbine mechanical losses, HP*	6.7	6.7	6.7	6.7	6.7	6.7	6.7	6.7
Pump efficiency, percent	34.6	34.6	34.6	34.6	34.6	34.6	34.6	34.6

*Estimated from previous turbine qualification test

142

Pump Hydraulic Power

$$HP = \frac{(Q)\ \Delta P}{1714} = \frac{(28.6)(3943)}{1714} = 65.9 \text{ horsepower}$$

*Mechanical Losses = 6.0 horsepower

This efficiency includes mechanical losses at the pump thrust and journal bearings, the nine controlled-gap floating-carbon bushings and the two mechanical face seals. It also includes hydraulic losses attributable to the effect of the bleeding of the pump's first stage to provide bearing lubrication.

Since no attempt was made to determine the minimum bearing lubrication flow, it seems reasonable to assume that efficiency could be raised even higher. An effort was made to get some feel for the effect of bearing flow. It was observed that a slight change in bearing oil flow (first-stage bleed) had a major effect on first-stage discharge pressure and pump total discharge pressure.

Discussion of Test Results

In discussions of test results and the problems encountered during testing, mechanical design of the equipment must be considered upper most since one of the test objectives was to demonstrate a pump life of 25 hours at high temperature operation and secondly many of the problems and delays were directly related to the mechanical design. The following is recapitulation of the major design and test problems.

1.   Thrust Bearing

The initial break-in runs were halted because of problems with the hydrodynamic pocket thrust bearing design. Following the break-in runs partial disassembly was made, and it was found that both sides of the thrust runner were badly worn. The mating thrust bearings were also scored, but the silver plated surface, was not badly worn. The inboard journal bearing plating was smeared and the journal showed many small surface cracks. The journal apparently lost radial clearance at the time the thrust bearing overheated. The outboard bearing and journal was in excellent condition. This would indicate that the bearing failure was not caused by an incompatibility of materials. Figure 78 shows both thrust runner surfaces, the thrust bearings, and both journals.

---

*From past data recorded during many development and qualification tests of AiResearch Cabin Turbocompressor 205900 which is the cabin turbocompressor used on all versions of the Boeing 707 series airplanes. The pump drive turbine is the turbine section of this well tested unit.
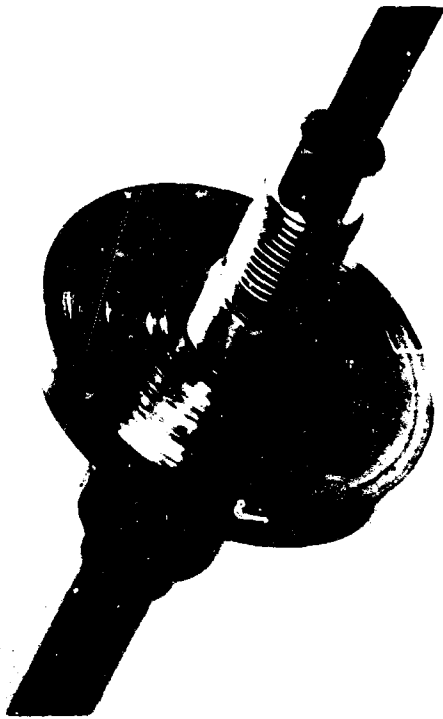
F-2481

Figure 78. Photographs of Pump Bearings After
Operating at 40,000 rpm and 4000 psi

The design of the hydrodynamic pocket thrust bearing incorporated a spherical surface mating with a spherical seat to accommodate slight misalignments and surfaces that were out of normal. The bearing was prevented from rotating by a single loose-fit dowel pin. From the almost identical wear patterns on both sides of the thrust runner, it appeared that high-speed operation of the thrust runner caused both thrust bearings to rotate about the retaining dowel pin. This resulted in loss of axial clearance (nominally 0.006 in.) as the bearings moved along the spherical seat and pinched against the runner. This is further indicated by the similar wear patterns on the thrust bearings at identical radial positions with respect to the retaining dowel pin.

This particular bearing design was originally selected because of the low losses compared to other thrust bearing designs. However, rather than expend additional effort to develop this rather costly bearing, a standard pivoted shoe type thrust bearing was installed and used successfully for all subsequent runs. Figure 79 shows this bearing following Run No. 3.

2. Carbon Face Shaft Seals

The unit disassembly following Run No. 3 was caused by failure of the outboard shaft seal. The seal was installed to duplicate thrust loads that occurred during break-in runs when the outboard bearing lubrication flow was measured at ambient pressure rather than pump inlet pressure. The seal apparently failed because of high temperatures encountered and the low lubricity of the MLO 8200 fluid.

Local heating, as a result of the seal failure, caused burning of the outboard journal and seal runner. Figure 80 shows the journal. As can be seen in Figure 80, there are additional score marks in the area of the floating carbon seals. This was apparently the result of journal thermal expansion caused by the mechanical seal failure. Wear at the outermost bushing was measured as 0.001 inch.

During the test runs, the need of a outboard mechanical face seal was checked by venting the chamber behind the seal to the fluid reservoir. Normally this chamber was vented to ambient pressure; no change in thrust bearing loading was noted between these modes of operation. Therefore, it was concluded that this seal is not required with the present bearing design, and it was eliminated for all subsequent runs.

A second problem with carbon face shaft seals was noted following Run No. 7 and again following Run No. 8. The answer to the question regarding the effect of the high temperature MLO 8200 fluid interacting with ambient air at the input shaft (see Section 4, Page 103) was noted. During Run No. 7, the unit was operated with a fluid inlet temperature of $600^{\circ}F$ for approximately two hours. A shut down was made to refill the CO_2 tanks used to provide the inert atmosphere. At the restart, a major leak was noted at the input shaft. Fluid seepage residue had built up to the level of the carbon nose, lifting the nose from the seal runner and permitting free flow of the fluid past the seal. Figure 81 shows this buildup.
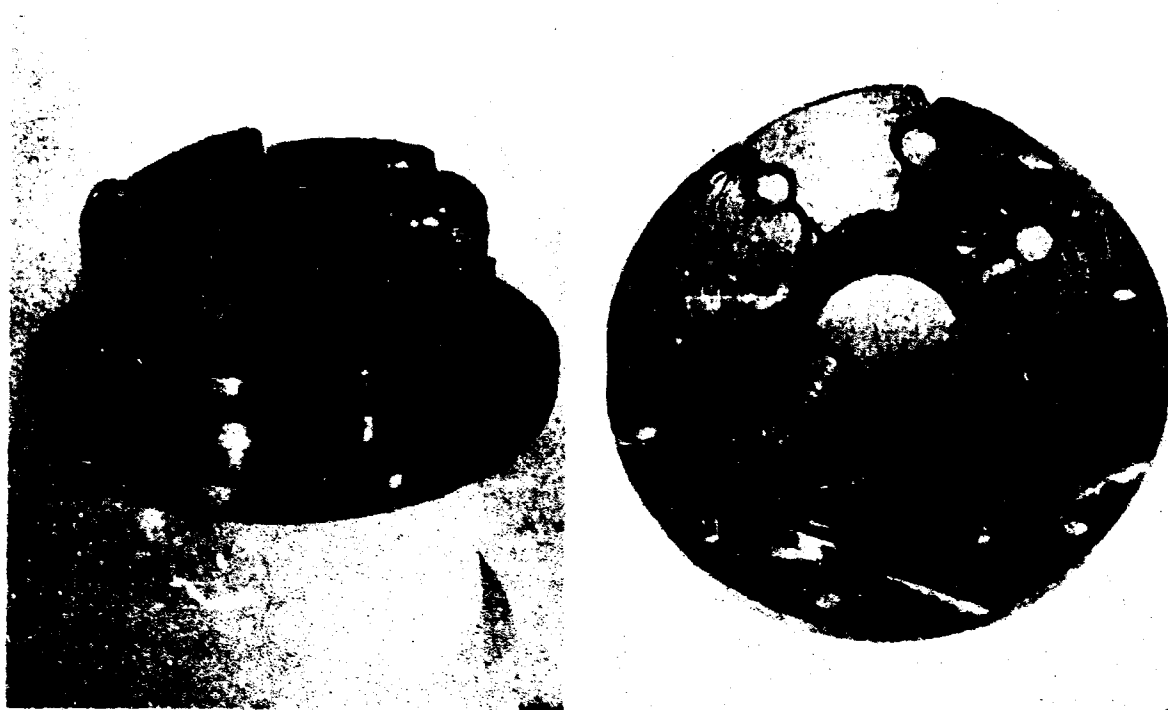
Figure 79.   Thrust Bearing Assembly Before and After
Test Showing Excellent Condition

F-2902
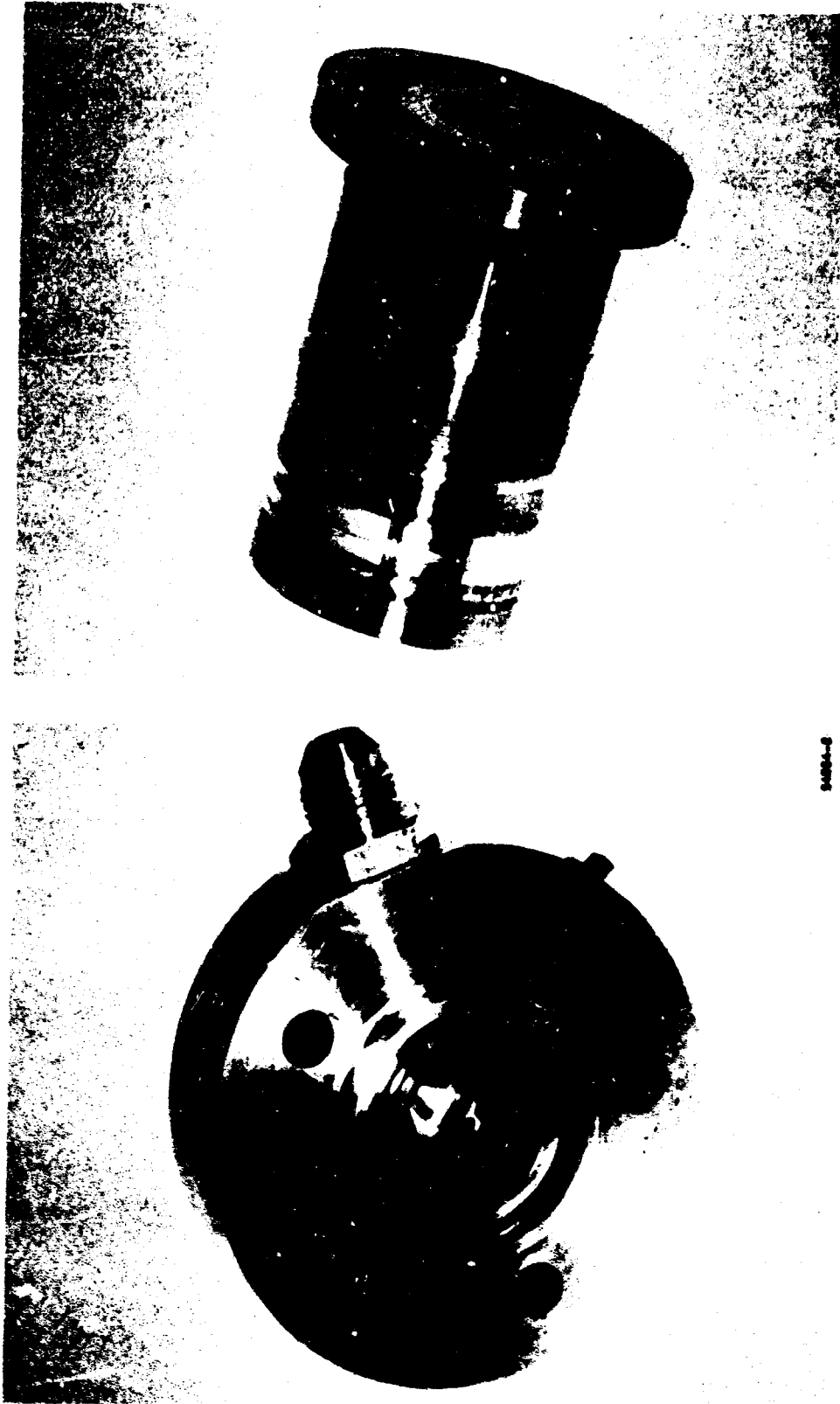
Figure 80. End Cap, Carbon Seals and Sleeve of Outboard Journal Revealing Burning as a Result of Face Seal Failure

55177-3

Figure   81.   Carbon-Face Shaft Seal After Test No. 7

A probe was installed to direct inerting gas directly into this area for Run No. 8, however, the sludge still developed. An additional high pressure probe was then installed and Runs No. 9 and No. 10 completed.

3. Low Pump Flow

As mentioned previously, for most of the test runs, pump flow was lower than design flow rate. This has been mainly attributed to the inability of properly matching impellers and diffusers. Pump tip width is only 0.040 inch. The unit was shimmed during assembly to match each of the four impeller stages with the mating diffuser and to provide a shroud clearance of 0.019 to 0.021 inch on each side of the impeller. However, because of the method of shimming (grinding the impeller hub to suit) and because of the cumulative effect of the tolerance stack up, it was extremely difficult to maintain the proper clearances, and impossible to check for tip matching and shroud clearances after the final assembly was made. In this respect. it is suggested that future designs incorporate a modular principal in order to prevent the excessive tolerance stack up.

4. Fluids

The final run was halted because of a complete breakdown of the MLO 8200 fluid. In addition to the known poor lubricating qualities of this fluid, which is a mixture of alkyl silicate ester compounds has several well known potential problems. These are thermal degradation, oxidation. and susceptibility to hydrolysis. The effects of this breakdown are an in-crease in acidity, a reduction of the flashpoint and the precipitation of the products of decomposition.

The mode of failure either during or following the final test run was hydrolysis, noted by an extremely high water content of the fluid after the test.

As a result of the fluid breakdown, both journals failed, and some damage was noted at the thrust bearing runner. Figures 82 and 83 show the bearings following this run.

5. Test Setup

Many delays and stoppages were caused by leaks and failures of test stand components. Although these problems are not within the scope of this contract, the area is mentioned in order to emphasize the need for extreme care in design and selection of test stand components.

149
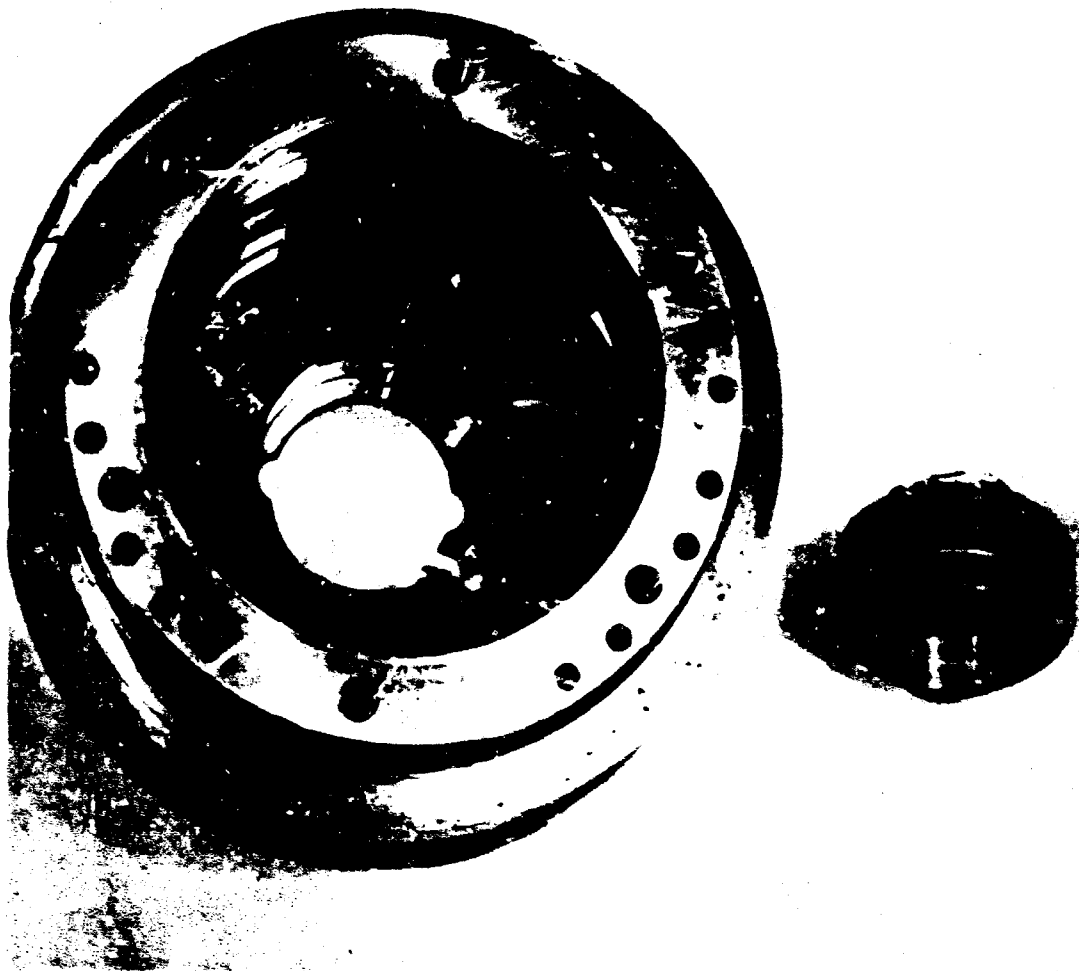
55701-1

Figure 82. Inboard Journal After Test No. 10

Figure 83.   Outboard Journal After Test No. 11

151

REFERENCES

1. Bosch, H. B. et al. <u>Advanced inducer study</u>. Thompson Ramo Woolridge Inc., Cleveland. Report ER-5288, NASA-CR-50993 (N63-21124), 1963.

2. Wilcox, W. W. et al. "Performance of an inducer-impeller combination at or near boiling conditions for liquid hydrogen." <u>Advances in cryogenic engineering. Volume 8: proceedings of the 1962 cryogenic engineering conference.</u> New York, Plenum Press, 1963. p.446-55.

3. Jakobsen, J. K. "On the mechanism of thread breakdown in cavitating inducers." <u>ASME Trans. Jl. of Basic Engineering</u>, 86D:291-305(1964).

4. Jekat, W. K. <u>The Worthington inducer</u>. Worthington Corp., Harrison, N. J. NASA report NASA-CR-56315 (N64-27880), 1964.

5. Eck, B. <u>Ventilatoren</u>. Berlin, Springer, 1953.

6. Coppage, J. E. et al. <u>Study of supersonic radial compressors for refrigeration and pressurization systems</u>. AiResearch Mfg. Co., Los Angeles. WADC-TR-55-257 (AD 110467), Dec. 1956.

7. Waitman, B. A., L. R. Reneau, and S. J. Kline. "Effect of inlet conditions on performance of two-dimensional subsonic diffusers." <u>ASME Trans. Jl. of Basic Engineering</u>, 83D:349-60(1961).

8. Bragg, S. L., and W. R. Hawthorne. "Some exact solutions of the flow through annular cascade actuator discs." <u>Jl. of the Aeronautical Sciences</u>, 17:243-249 (1950).

9. Horlock, J. H. <u>Some actuator-disc theories for the flow of air through an axial turbo-machine</u>. Gt. Brit. Aeronautical Research Council, 1958. Report ARC-R&M-3030 (ARC 15,491). Report was written in Dec. 1952.

10. Jahnke, E. and F. Emde. <u>Tables of functions with formulae and curves</u>. New York, Dover Publications, 1943.

11. Coppage, J. E. et al. <u>Study of supersonic radial compressors for refrigeration and pressurization systems</u>. AiResearch Mfg. Co., Los Angeles. WADC-TR-55-257 (AD 110467), Dec. 1956.

12. Wislicenus, G. F. <u>Fluid mechanics of turbomachinery</u>. New York, McGraw-Hill, 1947.

13. Balje, O. E. "A contribution to the problem of designing radial turbo-machines." <u>ASME Trans.</u> 74:451-72(1952).

REFERENCES (continued)

14. Eckert, B. Axial- and radialkompressoren. 2. verb und erweiterte aufl., Berlin, Springer, 1961.

15. Dean, R. C. and Y. Senoo. "Rotating wakes in vaneless diffusers." ASME Trans. Jl. of Basic Engineering, 82D:563-74(1960).

16. Sunstrand Turbo Division, Sunstrand Machine Tool Co., Rockford, Ill. Study of turbine and turbopump design parameters. Volume IV: low specific speed turbopump study. Report S/TD 1735. 1959 (AD 232638).

17. Energy conversion systems reference handbook. Volume VIII: other devices, by R. Wall et al. Electro-Optical Systems, Inc., Pasadena, Calif. WADD-TR-60-699. 1960.

18. Stepanoff, A. J. Centrifugal and axial flow pumps. 2nd ed. New York, Wiley, 1957.

19. Florant, L. F. and H. F. Snider. Centrifugal pumping of liquid hydrogen. Ohio State University Research Foundation. Technical report 333-4. 1950.

20. Zabriskie, W. and B. Sternlicht. "Labyrinth seal leakage analysis." ASME Trans. Jl. of Basic Engineering, 81D:332-40(1959).

21. Rotzoll, R. "Untersuchungen an einer langsamlaufigen kreiselpumpe bei verschiedenen Reynolds-zahlen." Konstruktion im Maschinen-, Apparate und Gerätebau, 10:121-30(1958).

22. Ringleb, F. O. "Two-dimensional flow with standing vortexes in ducts and diffusers." ASME Trans. Jl. of Basic Engineering, 82D:921-28(1960).

APPENDIX

ORONITE HIGH TEMPERATURE HYDRAULIC FLUID 70

Oronite High Temperature Hydraulic Fluid 70 is a new silicate ester fluid developed for the Oronite Division, California Chemical Company, by the California Research Corporation. The fluid was designed as a replacement for Oronite 8200 Fluid in the B-70 Bomber Program. The improvements sought in the development program were a higher operating temperature and better shear stability. Because of the stage of development of the B-70 hydraulic system, it was necessary that the new fluid be suitable as a direct replacement for Oronite 8200 Fluid in the system. This meant the new fluid must be compatible with 8200 Fluid and with all the parts in the system and that there be no major differences in the physical properties of the two fluids. All of these goals were achieved in Oronite 70 Fluid, and additional improvements were found in other 70 Fluid properties. The operating range for Oronite 70 Fluid is -65°F to +630°F versus a range of -65°F to +520°F for Oronite 8200 Fluid.

The attached table gives comparative test data for Oronite 70 Fluid, Oronite 8200 Fluid and MIL-H-5606 Fluid, and the requirements of MIL-H-8446B specification. In the following discussion, the properties of Oronite 70 Fluid, Oronite 8200 Fluid and 5606 Fluid are compared. It is recognized that 5606 Fluid is not a high temperature hydraulic fluid and it is not designed to operate in the high temperature ranges where Oronite 70 Fluid and Oronite 8200 Fluid can be used. The comparison has been included only because 5606 Fluid is such a well known reference in the industry.

1. **Shear Stability**

    Oronite 70 Fluid possesses excellent shear stability as measured by the sonic oscillator test. Comparative 2-hour sonic oscillator tests run on 70 Fluid, 8200 Fluid and 5606 Fluid, 70 Fluid retained 98% of its original viscosity as measured at 210°F versus 67% and 56% retention for 8200 Fluid and 5606 Fluid, respectively.

2. **Thermal Stability**

    Oronite 70 Fluid has much better thermal stability than 8200 Fluid. 70 Fluid loses only 13% of its 210°F viscosity when held at 600°F for 20 hours versus a viscosity loss of 64% for 8200 Fluid under the same conditions. Comparative tests were not run on 5606 Fluid because its maximum operating temperature is only 275°F.

3. **Viscosity Temperature Properties**

As shown in the attached table, Oronite 70 Fluid has lower initial over-all viscosity than 8200 Fluid. However, because of its superior thermal and shear stability, the viscosity of 70 Fluid holds up much better than the viscosity of 8200 Fluid and 5606 Fluid after a relatively short period of operation. After a short period of operation, the viscosity of Oronite 70 Fluid will be higher than that of 8200 Fluid or 5606 Fluid. Oronite 70 Fluid does not contain the conventional polymeric viscosity index improver, and for this reason, the fluid has better thermal and shear stability and hence, better over-all viscosity properties.

4. **Density**

The density of 70 Fluid (0.953 gm per cc) is slightly higher than that of Oronite 8200 Fluid (0.932 gm per cc) or 5606 Fluid (0.860 gm per cc). Weight, of course, is an extremely critical factor in aircraft design. However, the above increase of 2.3% in the density of 70 Fluid is with-in acceptable limits for the B-70 Program.

5. **Flash Point and Autogenous Ignition Temperature**

The flash point of 70 Fluid is 430°F versus 395°F for 8200 Fluid and 225°F for 5606 Fluid. The autogenous ignition temperature of 70 Fluid is 735°F versus 760°F for 8200 Fluid and 475°F for 5606 Fluid.

6. **Hydrolytic Stability**

Oronite 70 Fluid and 8200 Fluid both meet the requirements of MIL-H-8446B hydrolytic stability tests. The appearance and weight change of the copper is essentially the same for both fluids. However, the vis-cosity increase and acid number of the fluid is slightly higher for 70 Fluid than for 8200 Fluid. No comparison is made here with 5606 Fluid since the hydrolytic stability tests of a petroleum oil is meaningless.

7. **Oxidation and Corrosion Stability**

Oronite 70 Fluid gives better results than 8200 Fluid on the MIL-H-8446B oxidation and corrosion stability test. The weight change and appear-ance of the metal specimens is essentially the same for both fluids. However, the viscosity change and final acid number of the fluids is better for 70 Fluid than for 8200 Fluid. The viscosity change of 70 Fluid is only +10% versus -19% for 8200 Fluid and the final acid number of 70 Fluid is 0.1 versus 0.6 for 8200 Fluid. Direct comparisons with the oxidation corrosion stability of 5606 Fluid cannot be made since this fluid is normally tested under less severe conditions. In the MIL-H-8446B oxidation and corrosion test used on 70 Fluid and 8200 Fluid, the sample is held at 400°F for 72 hours. 5606 Fluid is normally tested at 250°F for 168 hours. Under these latter conditions, 5606 Fluid shows a viscosity change of +3.4% and a final acid number of 0.1%.

8. Vapor Pressure

The vapor pressure of 70 Fluid is markedly better than 8200 Fluid or 5606 Fluid. At 400°F, the vapor pressure in millimeters of mercury for 70 Fluid is 0.8, for 8200 Fluid - 3.0, and for 5606 Fluid - 220.

9. Lubricity

Oronite 70 Fluid gives essentially the same results on the four ball wear test as Oronite 8200 Fluid indicating similar lubricity properties of these two fluids. Four ball wear test conducted at 167°F showed that 5606 has slightly better lubricity than 70 Fluid. However, four ball wear test cannot be conducted on 5606 Fluid at 400°F since this fluid will decompose at that temperature.

10. Foaming Tendency

One of the outstanding characteristics of Oronite 70 Fluid is that it does not form any foam. In all of the foam tests which have been run on this fluid, the volume of foam formed is too samll to be measured. The foam breaks immediately. In comparative foam tests, Oronite 70 Fluid gave no foam, 8200 Fluid gave 350 millimeters of foam and 5606 gave 45 millimeters of foam.

In summary, Oronite High Temperature Hydraulic Fluid 70 has several advantages over Oronite High Temperature Hydraulic Fluid 8200. It has a wider operating temperature, better thermal oxidative and shear stability than 8200.Fluid, and is a nonfoaming fluid. Oronite 70 Fluid has better over-all viscosity properties than 8200 Fluid and has a lower vapor pressure and higher flash point than 8200 Fluid. The minor disadvantages of slightly poorer hydrolytic stability and higher density are greatly offset by this new fluid's many advantages.

Oronite 70 Fluid is a new concept in high temperature hydraulic fluid design. The absence of a conventional polymeric viscosity index improver greatly enchances the fluid's properties. The conventional polymeric viscosity index improver is the weakest link in a hydraulic fluid from a thermal and shear standpoint. Because of the absence of the viscosity index improver in 70 Fluid, this fluid's viscosity properties are not degraded over a period of time by thermal or shear action.

TABLE 9

PROPERTIES OF TYPICAL ORONITE HIGH TEMPERATURE HYDRAULIC FLUIDS 70 AND 8200

Property	Oronite Fluid 70[1]	Oronite Fluid 8200[2]	Military Specification Requirement
Viscosity at 400°F, cs	2.24	3.8	2.5 Minimum
Viscosity at 210°F, cs	7.56	11.27	To Be Measured
Viscosity at 100°F, cs	24.40	32.52	To Be Measured
Viscosity at -20°F, cs	346	350	No Requirement
Viscosity at -65°F, cs	2593	2296	2500 Maximum
Density at 100°F, g/cc	0.936	0.915	To Be Measured
Flash Point, COC, °F	450	395	395 Minimum
Acid Number, FH 510	Nil	<0.10	No Requirement
Acid Number, ASTM D 664[3]	0.1[4]	<0.10	0.2 Maximum
pH, ASTM D 664[3]	8.7	6 to 8	No Requirement
Autogenous Ignition Temperature, °F	735	760	700 Minimum
Hydrolytic Stability, 200°F for 48 Hours			
Appearance of Copper	Pass[4]	Slight Discoloration	No Pitting or Corrosion
Weight Change of Copper, mg/cm²	+0.01	+0.01	0.5 Maximum
Viscosity Change at 210°F, %	-8.7	-1.0	
Acid Number Increase of Fluid	0.0	0.0	0.5 Maximum
Acid Number of Water	0.02	0.0	0.5 Maximum
Insolubles, %	0.09	0.05	0.5 Maximum
Hydrolytic Stability, 400°F for 8 Hours[5]			
With 1% Water, Viscosity Change at 210°F, %	-35	-40[6]	No Requirement
With 2% Water, Viscosity Change at 210°F, %	-47	-50[6]	No Requirement
Oxidation and Corrosion Stability, 400°F for 72 Hours			
Weight Change of Metals, mg/cm²			
Silver	+0.01	0.00	±0.2
Aluminum	0.00	+0.02	0.00	±0.2
Steel	-0.01	+0.03	0.00	±0.2
Copper	-0.18	+0.01	±0.4
Appearance of Metals	No Corrosion	No Corrosion	No Corrosion, Slight Discoloration Permitted
Viscosity Change at 210°F, %	+11 / +9	-19 / -20	
Acid Number, Final, ASTM D 664[3]	0.1	0.6 / 0.7	1.0 Maximum
Appearance of Fluid	Bright, No Insolubles	Bright, No Insolubles	No Insolubles or Sludge
Pour-Ball Wear Test (2 Hours, 1200 rpm, 52100)			
At 167°F 10 kg, mm	0.98, 0.72	0.71	No Requirement
At 167°F 40 kg, mm	0.93, 0.99	1.32	No Requirement
At 400°F 10 kg, mm	0.93, 1.02	1.03	No Requirement
At 400°F 40 kg, mm	1.91, 2.01, 1.56, 1.98	1.38 / 1.41, 1.61	No Requirement
Shear Stability,[7] Retention of 210°F Viscosity, %	98	67	No Requirement
Evaporation at 350°F			
Qualitative (1 Hour)	Not Tacky	Not Tacky	No Requirement
Quantitative (6-1/2 Hours), %	4.2	6 to 8	No Requirement
Foaming Tendency at 200°F, ml	Nil	About 500	600 Maximum
Foam Stability, Volume at 10 Min., ml	Nil[9]	Nil	10 Maximum
Thermal Stability			No Requirement
600°F for 6 Hours	Viscosities of Fluid as Removed from Capsule	Viscosities of Fluid After Heating[10]	Viscosities of Fluid as Removed from Capsule	Viscosities of Fluid After Heating[10]	
Viscosity at 400°F, cs (Change; %)	7.02 (-7.1)	2.33 (+4.0)	5.27 (-5)	3.94 (-49)	No Requirement
Viscosity at 210°F, cs (Change; %)	22.32 (-8.5)	8.05 (+6.5)	25.34 (-5)	9.65 (-30)	No Requirement
Viscosity at 100°F, cs (Change; %)		25.92 (+6.2)		18.08 (-45)	No Requirement

1. Batch 7600-49. Prepared from DO 1655, DO 1658, and DO 1661.
2. Data taken from Technical Data Book on Oronite Hydraulic Fluids. Data not taken from this source are indicated by Footnote 6.
3. Determined by Precision-Dow Recordomatic Titrometer.
4. Comparable to that of Oronite 8200 Fluid.
5. With copper specimen in sealed Pyrex ampoule.
6. This test was run on Oronite 8200 fluid simultaneously with Oronite 70 fluid. Any test run on 8200 fluid and indicated by this footnote (6) is a "back-to-back" comparison with the Oronite 70 fluid.
7. Determined in sonic oscillator, 10,000 cps, room temperature.
8. By ASTM D 972-56.
9. The few bubbles which were formed were completely gone in a few seconds.
10. Placed in beaker and stored in oven at 275°F for 60 minutes and then in oven at 400°F for 20 minutes.
11. Not determined because of small amounts of volatile compounds in fluid.

158

TABLE 10

COMPARISON OF PROPERTY REQUIREMENTS

	Oronite 70 Fluid	Oronite 8200 Fluid	MIL-H-5606 Fluid	MIL-H-8446n Specification
Flash Point, COC, °F	430	395	225	395 Minimum
Viscosity, cs				
At -65°F.	2593	2235	2187	2500 Maximum
At -20°F.	346	363	-	-
At +100°F.	24.4	32.5	14.2	To be measured
At +210°F.	7.6	11.3	5.1	To be measured
At +400°F.	2.35	3.82	1.92	2.5 Minimum
Density at 60°F., gm/cc	0.953	0.932	0.860	To be measured
Autogenous Ignition Temperature, °F.	735	760	475	700 Minimum
Oxidation & Corrosion Stability				
At °F./Hours	400/72	400/72	250/168	-
Weight change of metals mg/cm²				
Silver	+ 0.01	0.00	OK	+ 0.2
Aluminum	0.00	0.00	OK	+ 0.2
Steel	- 0.01	+ 0.02	OK	+ 0.2
Copper	- 0.18	+ 0.03	OK	+ 0.4
Appearance of Metals	No Corrosion	No Corrosion	No Corrosion	No Corrosion
Viscosity Change of Fluid At 210°F., %	+ 10	- 19	3.4 at 130°F.	± 3%
Final Acid No. of Fluid	0.1	0.8	0.1	1.0 Maximum
Insolubles, Weight %	None	None	None	-
Shear Stability, % Retention of 210°F. Viscosity	98	67	56	-
Vapor Pressure, at 400°F. mm	0.8	3.0	220	5.0 Maximum
Foam Tendency at 200°F. By Federal Method 3212, ml of Foam	Nil	350	45	600 Maximum

159

TABLE 10 (Continued)

	70	8200	5606	MIL-H 8446B
Thermal Stability				
Viscosity at 210°F. (% Change)				
At 500°F.				
6 Hours	7.38 (-2.4)	8.2 (-27)	--	--
20 Hours	7.38 (-2.4)	6.1 (-46)	--	--
40 Hours	7.26 (-4.0)	5.2 (-54)	--	--
At 600°F.				
6 Hours	7.1 (-5.6)	5.2 (-54)	--	--
20 Hours	6.6 (-13)	4.0 (-64)	--	--
40 Hours	5.2 (-32)	3.2 (-72)	--	--
Hydrolytic Stability				
Appearance of Copper	OK	OK		No Pitting or Corrosion
Weight Change of Copper				
Mg/Cm²	+ 0.01	+ 0.01		0.5 Maximum
Vis. Change at 210°F., %	- 8.7	- 1.0		+ 20
Acid No. increase of Fluid	0.1	0.0		0.5 Maximum
Acid No. of Water	0.02	0.0		0.5 Maximum
Insolubles, %	0.09	0.05		0.5 Maximum

160

THERMAL STABILITY COMPARISON
ORONITE HIGH TEMPERATURE HYDRAULIC FLUIDS 70 AND 8200

Percent Viscosity Change as Measured at 210°F

| Temperature and Time | 70 Fluid | | 8200 Fluid | |
	Fluid as Removed from Capsule	Fluid After Removing Volatiles	Fluid as Removed from Capsule	Fluid After Removing Volatiles
600°F				
6 hours	-7.1	+6.5	-54	-50
20 hours	-13	+2.6	-64	-59
40 hours	-32	-10	-72	62
630°F				
6 hours	-13	+4.6	-63	-54
20 hours	-38	-5.6	-73	-57
40 hours	-49	+26	---	---

In the above test 10 ml samples of the hydraulic fluid were sealed in stainless steel capsules under an atmosphere of helium. The fluids were heated to 600°F and 630°F for the time periods indicated above. The samples were removed from the capsules and the viscosities measured at 210°F. The volatiles formed during the high temperature period in the capsules were removed by evaporation and the viscosities were remeasured. The results reported above are the per cent changes in the viscosities from the original viscosities as measured at 210°F. The original 210°F viscosities were for 70 Fluid 7.56 centistokes and for 8200 Fluid 11.27 centistokes.

FIGURE 84

PROPERTIES OF ORONITE
HIGH TEMPERATURE HYDRAULIC
(AND REFERENCE FLUIOS
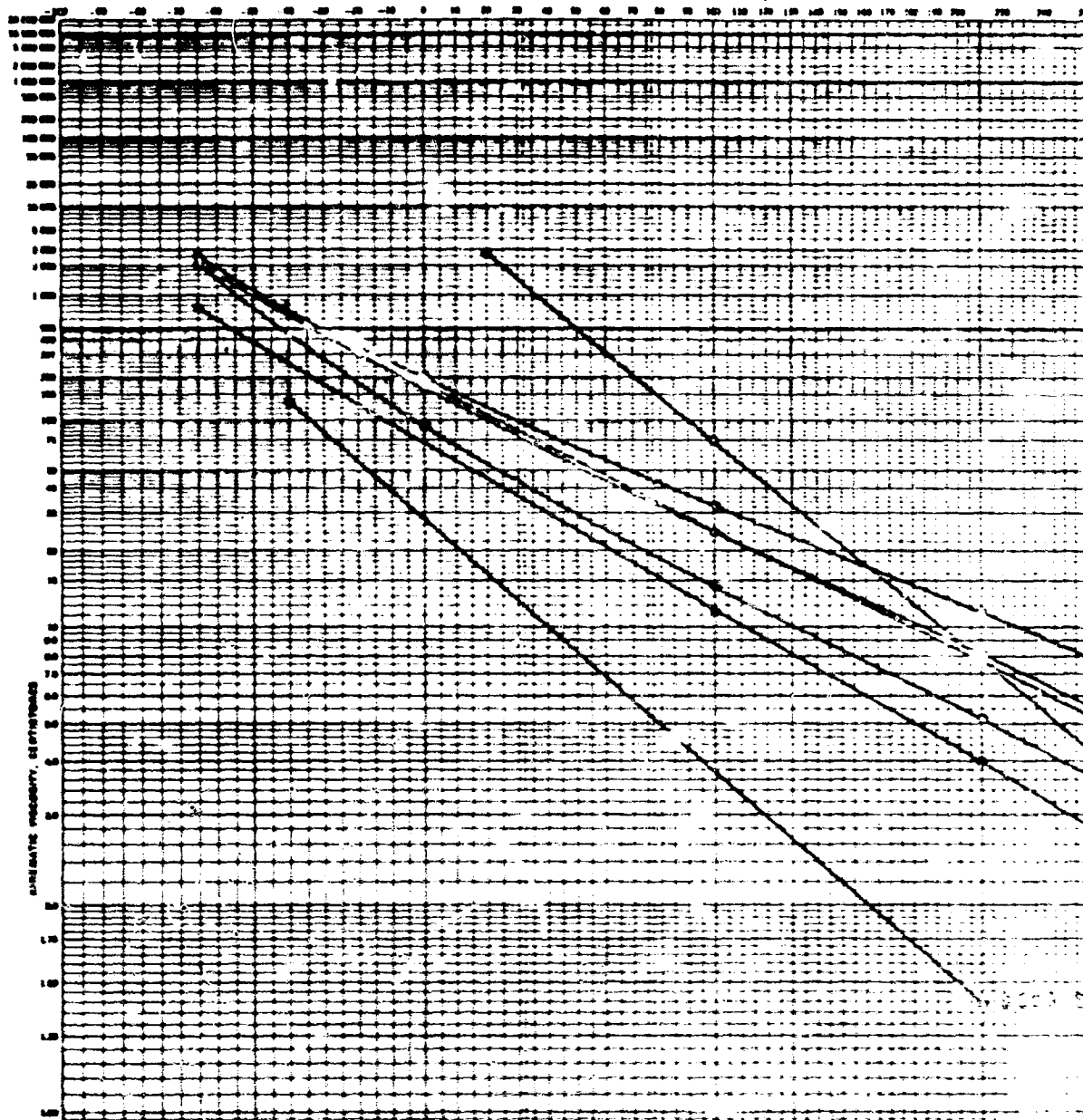
FLUID	FLASH POINT, COC, °F	VAPOR PRESSURE, AT 275°F, MM
5606*	225	18
5606 BASE STOCK*	225	~18
8515	395	0.05
8200	395	0.05
DISILOXANE BASE STOCK	395	0.05
70	430	<0.05
72778	420	0.05

3-20-42

* FOR REFERENCE PURPOSES ONLY.
NOT MARKETED BY ORONITE.

FIGURE 84 (continued)

ITE
IC FLUIDS
IOS)

VISCOSITY-TEMPERATURE CHART
MODIFIED FROM A.S.T.M. (D 341-39)

SAK   RD 622358

163

COMPUTER PROGRAMS FOR PERFORMANCE CALCULATION (PROGRAMS A-0545 AND A-0546)

The following paragraphs present the computer program written for the method of performance calculation developed previously.

Program A-0545 calculates pump designs for all combinations of input values for N, β_ℓ, μ, and λ. If desired, it will then calculate off-design points for different values of M_o and N/N_o. Automatic plotting of ΔP and η curves for pump off-design is also possible. Programs A-0546 and D-0100 are chained to A-0545 for this purpose.

Input for A-0545

If only the pump design point program is used, 11 cards of input are needed for each case. If the pump off-design program is used, 14 cards of input are needed for each case. Input for pump design point program:

1. Card No. 1   FORMAT 72H

   Alphanumeric heading card
   "1" in column 1

2. Card No. 2   FORMAT 5F10.5

γ_o, lb/cu ft,	Density	
V_o, cu ft/sec,	Flow	
ΔP_o, psi,	Pressure rise	
ν_*, ft^2/sec,	Kinematic viscosity	
Test	- 0 if pump design point program	
	- 1 if pump off-design point program	

3. Card No. 3, Inlet   FORMAT I10, 7F10.5

Case No.	1 NPSH Given - noncavitating	
	2 β_i given	
	3 Best performance	
	4 Diameters and NPSH given - cavitating operation	
D_H, in.	Hub diameter	
NPSH, ft	Net positive suction head	
β_i, deg	Inlet flow angle	

164

K_i Hub-blockage $K_i = 1 - \left(\dfrac{D_H}{D_i}\right)^2$

D_i, in.   Inlet tip diameter

$\left.\begin{array}{l} A,\ 1/ft \\ \\ K \end{array}\right\}$ Density function constants

4.   Card No. 4   FORMAT F10.5

     ε_i Blockage factor

5.   Card No. 5, N values   FORMAT I10, 7F10.5/
                                                8F10.5

     No. of N values   (max 10 values)

       N_1 RPM

       N_2

       N_3

       etc.

6.   Card No. 6, Impeller   FORMAT 4F10.5

       ξ_1

       ξ_2

       ξ_3 Loss constants

       ξ_4

7.   Card No. 7, β_2 values   FORMAT I10, 7F10.5/
                                                  8F10.5

     No. of β_2 values

       $\beta_2(1)$

       $\beta_2(2)$ Impeller tip vane angle

       $\beta_2(3)$

       etc.

8. Card No. 8, μ values

    No. of μ values

        μ_1

        μ_2 Slip factor $\quad \dfrac{C_{u_2}}{C_{u_2\infty}}$

        μ_3

        etc.

FORMAT I10, 7F10.5/
        8F10.5

9. Card No. 9, λ values

    No. of λ values

        λ_1

        λ_2 Flow factor $= \dfrac{C_{m_2}}{U_2}$

        λ_3

        etc.

FORMAT I10, 7F10.5/
        8F10.5

10. Card No. 10, Diffuser

    Case No.   1 = Vaned diffuser

                 2 = Scroll diffuser

                 3 = Collector ring

                 4 = Vaneless diffuser

    ζ_D Throat side-to-width ratio

    γ, deg   Wall angle

    ζ_5 Boundary layer factor

    ζ_6 Boundary layer factor

    ζ_7 Loss coefficient

    $\dfrac{D_3}{D_2}$ Vaneless space diameter ratio

FORMAT I10, 6F10.5

11. Card No. 11, Outside Losses   **FORMAT 2F10.5**

                       Wheel friction loss factor

                       Leakage loss factor

Input for Pump off-design program:

     Cards 1 thru 11 of previous section are needed in addition to the following

12. Card No. 12   **FORMAT 8F10.5**

        F_1

        a_1

        a_2, 1/Deg   Incidence loss coefficients

        a_3, 1/Deg^2

        ψ_C Cavitation loss coefficient

        ξ_2

        ξ_3

        ξ_4

13. Card No. 13   **FORMAT 5F10.5**

        ψ_3 Diffuser incidence loss coefficient

        ξ_8

        ξ_9

        ν_* -ft^2/sec   Kinematic viscosity for part load

        γ -lb/cu ft   Density for part load

           NPSH, ft   Net positive suction head for part load

167

14. Card No. 14   **FORMAT 6F10.5**

M_o Mass flow ratio

M_o

$(M_o)_N$

$(N/N_o)_o$ Speed ratio

$\Delta(N/N_o)$

$(N/N_o)_n$

Input for A-0546

If plotting of pump off-design points is desired, two blank cards plus the following cards should be inserted behind the data deck.

1. Card No. 1   **FORMAT 3I10**

No. of problems to plot

No. of N/N_o values for 1st problem

No. of M_o values for 1st problem

2. Card No. 2   **FORMAT 2I10**

No. of N/N_o values for 2nd problem

No. of M_o values for 2nd problem

3. Repeat Card No. 2 for as many problems as are to be plotted.

Output

The output consists of three parts (a copy of a sample output is attached).

1. The input is printed out

2. For a particular N, β_2, μ and λ the following quantities are printed out:

a. Inlet Case

N, RPM   Speed

D_i, inches   Inlet diameter

β_i, deg   Inlet flow angle

NPSH, ft   Net positive suction head

168

W_i, FPS   Inlet relative velocity inducer

ζ_o/ζ Suction density ratio

b.   Impeller Input

β_2, Deg   Impeller tip vane angle

                        Slip factor ($Cu_2/Cu_{2\infty}$)

                        Flow factor (C_{m2}/u_2)

c.   Impeller Answers

    1   q Head factor

       D_2, inch   Impeller tip diameter

       U_2, FPS   Impeller tip velocity

       ξ_i Impeller relative velocity ratio

       Z_i Number of vanes

    2   B_2 Impeller width ratio ($= b_2/D_2$)

       R_{ei} Impeller channel ave. Reynolds No.

       Δq_{SF} Impeller friction loss

       Δq_{DL} Diffusion loss

       Δq_{RC} Recirculation loss

       η_{imp} Impeller efficiency (Internal)

d.   Diffuser Answers

    If Case No. 1 - the following line is printed:

    1.   Case No.

       Re_{b_2} Diffuser inlet Reynolds No.

       Re_2 Impeller tip Reynolds No.

       ξ_2 Number of diffuser vanes

       Δq_{sc} Scroll friction

       $\Delta q_{diff\ 2}$ Straight diffuser loss

       Δq_D Total diffuser loss

169

If Case No. 2 - the following line is printed:

1. Case No.

Δq_{2-3} first   ⎫

Δq_{3-4} second   ⎬   diffuser loss

Δq_{4-5} third   ⎭

Δq_d Total diffuser loss

For both Cases 1 and 2, the following 2nd line is printed:

2. η_{hyd} Hydraulic efficiency

    $H_{TOT,}$ ft   Total head

    Δq_{FR} Wheel friction

    Δq_L Leakage

    η Overall efficiency

3. If pump off-design program is calculated for a constant N/No, the following is printed for each value of Mo:

a.   Mo   Mass flow ratio

    q   Head factor

    $\Delta \beta_i$, deg   Incidence angle

    η_H Hydraulic efficiency

    ΔP, psi   Pressure rise

    η Overall efficiency

b. N/No is then varied and line A is repeated for all values of Mo. This is continued until N/No equals final value of N/No.

4. Items 2 and 3 are repeated for all values of N, ∂_2, μ and λ.

170

Application of the IBM Programs to Performance Calculation

1.   Generalized Performance of Centrifugal Pumps

In order to compare the calculation results with statistical average and predicted optimum performances, a number of data were gathered on high-Reynolds-number pump performances and plotted in Figure 42. For comparative purpose, three points were calculated by the present computer program using water as fluid, assuming no cavitation and a Reynolds number close to 10^7. The specific speeds of the calculated samples were 500 to 1000 and 2000. The results of the calculations were also plotted in the diagram. The points fit the top efficiency curve quite well; the program therefore might be used to predict the performance of advanced pump designs with confidence.

2.   Performance Characteristics of the LH_2 Pump

The performance calculation procedure developed previously has been applied to establish the characteristic curves of the pump designed and built in this program. Figures 38 and 39 present the characteristics over a wide range of speed and flow.

Execution Instructions

Program A-0545 consists of three chains. Chains 2 and 3 are Programs A-0546 and D-0100 and are used only for plotting.

Tape 22 is always required by Program A-0545. If plotting is called for, tape 22 will be the plotter tape. When plotting is done, tapes 21 and 11 are used as work tapes.

Each of the programs just mentioned takes approximately 1-1/2 min per case with 150 solutions.

Following this page are given:

1.   Flow chart of program

2.   Fortran listing of program

3.   Sample input data listing

4.   Sample output listing

5.   Sample plots

Figure 85. Flow Chart of Program
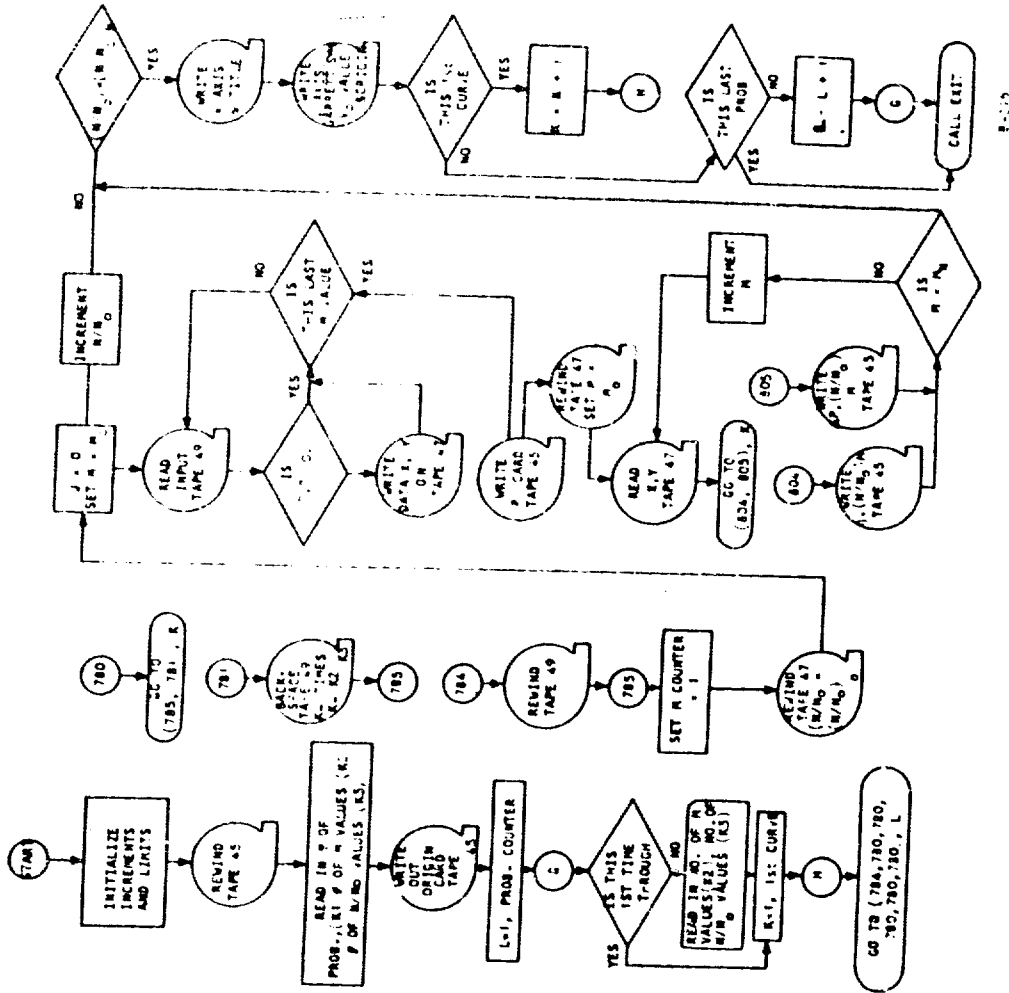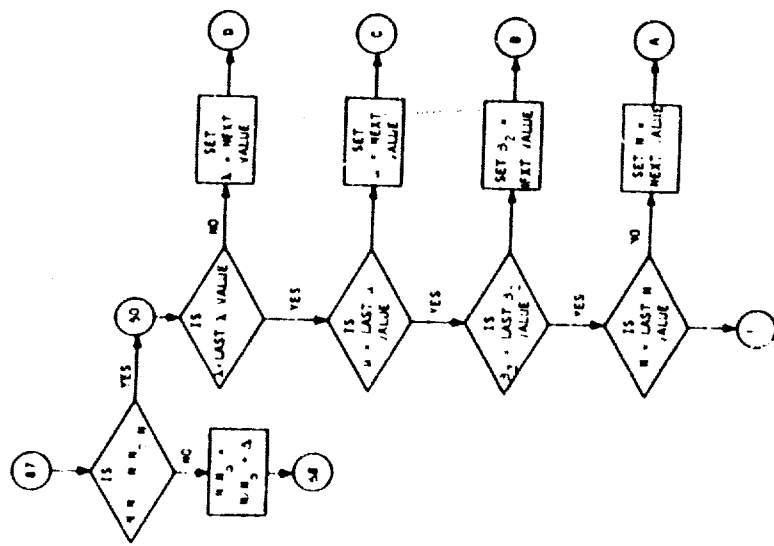
Figure 85 (Continued)

173

```
           JOB       A0546        PUMP DESIGN PLOT PROGRAM WITH GARLIC CHAIN
    125 FORMAT(5F14.7)
    126 FORMAT(18HP2I0.0     10.0       ,I2,I4+,4X,1H1,4X,F4.2,6X,4F10.1)
    127 FORMAT(10X,2F10.7)
    128 FORMAT(2H0 ,2F7.1)
    129 FORMAT(13HX 0.0      .0,20X,18H          MO(N/NO))
    130 FORMAT(5CHAC5.     9.0  .12  PUMP - PART LOAD PERFORMANCE/)
    131 FORMAT(13HY 0.0   0.0,23X,18HOVERALL EFFICIENCY)
    132 FORMAT(13HY 0.0   0.0,20X,13HPRESSURE RISE, PSI)
    133 FORMAT(12HG 2.0     9.5)
    134 FORMAT(19HA01.5     8.6  .12  FLOW, CUFT/SEC = F7.3/)
    136 FORMAT(1HE)
    137 FORMAT(10X,F10.7,F10.4)
    138 FORMAT(3I10)
        DIMENSION ANS1(2),YOR(2),DELTY(2)
        XOR=0.0
        DELTX=2.0
        YOR(1)=0.0
        YOR(2)=0.0
        DELTY(1)=1.0
        DELTY(2)=4000.
        XORIGN=0.0
        YORIGN=0.0
        REWIND 45
        READ INPUT TAPE 41,138,K1,K2,K3
        WRITE OUTPUT TAPE 45,128,XORIGN,YORIGN
        DO 816 L=1,K1
        IF(L-1)779,779,778
    778 READ INPUT TAPE 41,138,K2,K3
    779 DO 815 K=1,2
        GO TO (784,780,780,780,780,780),L
    780 GO TO (785,781),K
    781 K4=K2*K3
        DO 782 I=1,K4
    782 BACKSPACE 49
        GO TO 785
    784 REWIND 49
    785 DO 806 I=1,K2
        REWIND 47
        J=0
        DO 803 I=1,K3
        READ INPUT TAPE 48,125,VO,ANS1(2),ANS1(1),ANS,ANNO
        IF(ANS1(K))803,802,802
    802 J=J+1
        WRITE OUTPUT TAPE 47,125,ANS,ANS1(K)
    803 CONTINUE
        WRITE OUTPUT TAPE 45,126,J,ANNO,XOR,DELTX,YOR(K),DELTY(K)
        REWIND 47
        DO 806 I=1,J
        READ INPUT TAPE 47,125,ANS,ANS1(K)
        GO TO (804,805),K
    804 WRITE OUTPUT TAPE 45,127,ANS,ANS1(K)
        GO TO 806
    805 WRITE OUTPUT TAPE 45,137,ANS,ANS1(K)
    806 CONTINUE
        WRITE OUTPUT TAPE 45,129
        WRITE OUTPUT TAPE 45,130
        GO TO (808,809),K
```

174

```
808 WRITE OUTPUT TAPE 45,131
    GO TO 810
809 WRITE OUTPUT TAPE 45,132,
810 WRITE OUTPUT TAPE 45,133,
    WRITE OUTPUT TAPE 45,134,V0
    XORIGN-18.
815 WRITE OUTPUT TAPE 45,128,XORIGN,YORIGN
316 CONTINUE
    WRITE OUTPUT TAPE 45,136
    ENDFILE 45                                          A0546
    REWIND 45                                           A0546
    REWIND 46
    CALL CHAIN(03,46)                                   A0546
    END
```

```
*     JOB       A0545      KLEPF/MX 032564 PUMP PART LOAD PERFORMANCE
*E    COMP      A0545
C     GENERAL PUMP EFFICIENCY
      DIMENSION ALAMDA(10),AMUI(10),BETA2I(10),ANI(10)
  100 FORMAT (I10,7F10.5/(8F10.5))
  101 FORMAT (8F10.5)
  102 FORMAT(I9,6F10.3,10X,35HINLET CASE NO.,N,DI,BI,NPSH,WI,ZETA)
  103 FORMAT (57H0   4 SCROLL OERLIKON, D4/D3, DOES NOT CONVERGE, D4/D3-1
     1 =F8.1,11H, D4/D3-2 =F8.1,12H, ALPHA-3 = F8.5)
  104 FORMAT (36H0   CASE 4 CI DOES NOT CONVERGE CI1=F10.5,6H, CI2=F10.5
     1)
  105 FORMAT (22H0   INPUT-  DENSITY =F7.3,8H, FLOW =F7.3,15H, PRESS. R
     1ISE =F6.1,15H, KINEM.VISC. =F9.6)
  107 FORMAT(40H0   IMPELLER Z1 IS GREATER THAN 100, Z1 =F10.5,6H, Q = F1
     10.5,7H, D2 = F10.5,9H, ZETA1 =F10.5)
  108 FORMAT (F8.1,2F10.3,40X,27HIMPELLER- BETA-2, MU, LAMDA/F8.2,F10.2,
     1F10.1,F10.4,F10.1,20X,29H0, D2, U2, ZETA1, Z1/F8.5,F10.1,4F10.5,10
     2X34HB2, REI, DQSE, DQDL, DQRC, ETA-IMP)
  109 FORMAT (47H0   DIFFUSER Z2 NOT BETWEEN 6 AND 16, ZETA D1 = F8.3,12H
     1, ZETA D2 = F8.3,7H, Z2 = F8.2)
  110 FORMAT(2F10.5,13H   D403, D4D3N)
  114 FORMAT(34H0   HTOT DOES NOT CONVERGE, HTOT = F10.5, 11H,   HTOT2 = F
     110.5)
  115 FORMAT(I8,2F10.0,F10.2,3F10.5, 7X45HDIFFUSER CASE NO.,RED2,RE2,Z2,
     1DQSC,DQDIF2,DQD)
  116 FORMAT(I8,4F10.5,30X,40HDIFFUSER CASE NO., D023, D034, D045, DQD)
  117 FORMAT (8X,F10.5,F10.3,3F10.5,20X,29HETA-HYD, HTO', DQRE, DQL, ETA
     1)
  118 FORMAT (72H
     1                         )
  119 FORMAT(29H0   Q DOES NOT CONVERGE, Q1 = F10.5,7H, Q2 = F10.5,7H, MU
     1 = F10.5)
  120 FORMAT(5F14.7)
  121 FORMAT(F8.2,2F10.4,F10.5,F10.2,10X26H   MO, U, DELTA-B, ETAH, HO/8X
     1,F10.3,F10.5,F10.1,30X,16HDELTA-P, ETA, HP)
  122 FORMAT (6X,7HN/NO = F8.3)
  123 FORMAT(24H1   PART LOAD PERFORMANCE/)
  124 FORMAT (36H0PART LOAD CIP DOES NOT CONVERG CI1=F10.5,6H, CI2=F10.5
     1)
C     INLET
      REWIND 48
    1 READ INPUT TAPE 41,118
      WRITE OUTPUT TAPE 42,118
C     TEST = 0 IF PUMP DESIGN POINT PERF,  = 1 . IF PUMP OFF DESIGN PERF
      READ INPUT TAPE 41,101,       GAMO,VO,DPO,VSTAR,TEST
      IF(GAMO+VO+DPO)201,200,201                                        A0545
  200 ENDFILE 48
      REWIND 48
      CALL CHAIN(02,46)                                                 A0545
  201 READ INPUT TAPE 41,100,ICASE,DH,   ANPSH,BI,AKI,DI,A,AK,CI
      READ INPUT TAPE 41,100,N1,(ANI(I),I=1,N1)
      READ INPUT TAPE 41,101,           X1,X2,X3,X4
      READ INPUT TAPE 41,100,N2,(BETA2I(I),I=1,N2)
      READ INPUT TAPE 41,100,N3,(AMUI(I),I=1,N3)
      READ INPUT TAPE 41,100,N,(ALAMDA(I),I=1,N)
      READ INPUT TAPE 41,100,ICASE2,ZETAD,GAMMA,X5,X6,X7,D3D2
      READ INPUT TAPE 41,101,X8,X9
      IF (TEST)3,3,2
```

```
   2 READ INPUT TAPE 41,101,X1PL,A1,A2,A3,PSIC,X2PL,X3PL,X4PL,PSI3,X8PL
     1,X9PL,VSTAPL,GAMP,ANPSP
     READ INPUT TAPE 41,101,AMOO,DELTM,AMN,ANSOO,DELTAN,ANNON
   3 GAMR=GAMMA*.01745329
     TGAM=SINF(GAMR)/COSF(GAMR)
     CONS4=2./TGAM+.5
   4 WRITE OUTPUT TAPE 42,105,GAMO,VO,DPO,VSTAR
     DO 50 K1=1,N1
     AN=ANI(K1)
     GO TO (5,6,8,9),ICASE
   5 CONS1=(32.175*ANPSH)**.5
     DI=(576.*VO/(3.1415927*CONS1)+DH*DH)**.5
     BI=ATANF(3.1415327*DI*AN/(720.*CONS1))
     WI=(32.175*ANPSH+(AN*3.1415927*DI/720.)**2)**.5
     BI =BI*57.29578
     GO TO 15
   6 BIR=BI*.01745329
     CBI=COSF(BIR)
     CTBI=CBI/SINF(BIR)
   7 DI=(44354.36*VO/(CTBI*AN*AKI))**.33333
     UI=3.1415927*AN*DI/720.
     CI=UI*CTBI
     WI=UI/SINF(BIR)
     ANPSH =CI*CI/64.35
     GO TO 15
   8 BI=60.
     GO TO 6
   9 AKI=1.-(DH/DI)*DH/DI
     JI=DI*AN*3.1415927/720.
     CONS1=144.*VO/(FI*DI*DI*AKI*.7853982)
     J=1
     CI1 = CONS1
     IF(CONS1*CONS1/64.35-ANPSH)14,14,10
  10 CI2=CONS1*(1.+A*(CI1*CI1/64.35-ANPSH))**AK
     IF(ABSF(CI1/CI2-1.)-.0001)14,14,11
  11 J=J+1
     IF(J-50)12,12,13
  12 CI1=CI2
     GO TO 10
  13 WRITE OUTPUT TAPE 42,104,CI1,CI2
     CI1=(CI1+CI2)/2.
  14 BI=4.ANF(UI/CI1)
     WI=UI/SINF(BI)
     ZETA=(1.+A*(CI1*CI1/64.35-ANPSH))**AK
     BI =BI*57.29578
  15 WRITE OUTPUT TAPE 42,102,ICASE,AN,DI,BI,ANPSH,WI,ZETA
   C  IMPELLER CALCULATIONS
     BIR=BI*.01745329
     CBI=COSF(BIR)
     TBI=SINF(BIR)/CBI
     DO 50 K2=1,N2
     BETA2=BETA21(K2)
     BT2=BETA2*.01745329
     SB2=SINF(BT2)
     CB2=COSF(BT2)
     TB2=SB2/CB2
     DO 50 K3=1,N3
```

177

```
      AMU=AMUI(KJ)
      CONS16=X1*1.5707963*AMU*CB2/(1.-AMU)
      DO 50 I=1,N
      CONS8=ALAMDA(I)*ALAMDA(I)
      Q=AMU*(1.-ALAMDA(I)*TB2)
      CONS3=(CONS9+Q*Q)/(2.*Q)
      CONS5=(CONS8+Q*Q)**.5
      CONS6=ALAMDA(I)/CONS5
      CONS17=(CONSP+(1.-Q)**2)**.5
      CONS18=1.-CONS3
      J2=1
      HO=144.*DPO/GAMO
      ETAHYD=.9
      HTOT=HO/ETAHYD
   16 U2=(32.175*HTOT/Q)**.5
      D2=720.*U2/(3.1415927*AN)
      W2=U2*CONS17
      V2=DI/D2
      ZETA1=W2/WI
      Z1=CONS16*(1.+.08/ZETA1)/(1.-V2)
      IF(Z1-100.)21,21,20
   20 WRITE OUTPUT TAPE 42,107,Z1,Q,D2    ,ZETA1
      GO TO 50
   21 DEL1=.8*(D2-DH)/(CB1+CB2)
      B2 =144.*VO/(.9*ALAMDA(I)*U2*(D2*D2*3.14159-D2*.03*Z1/CB2))
      DHYD1=D2*(1./(71/(3.1415927*B2)+1./CB2)+V2/(2./(1.-V2)+(2.*Z1/(3.1
     1415927*(1.+V2)))*(1.+TB1*TB1*(1.+V2*V2)/2.)**.5))
      WAVE=((WI*WI+W2*W2)*.5)**.5
      REI=DHYD1*WAVE/(12.*VSTAR)
      F1=.0462/REI**.2
      DQSF=X2*DEL1*WAVE*WAVE*F1/(DHYD1*U2*U2*Q)
      DELTA=1.-ZETA1+Q*(CB1+CB2)/(2.*WI*(Z1*(1.-V2)/3.1415927 +2.*V2)/U2
     1)
      DQDL=X3*(DELTA*WI/U2)**2/Q
      DQRC=X4*DELTA*Q/ALAMDA(I)
      ETAIMP=(CONS18-DQDL)/(CONS18+DQSF+DQRC)
C     DIFFUSER
      GO TO(22,37),ICASE2
C     VANED DIFFUSER W/CONICAL SIDEWALLS
   22 RE2=D2*U2/(12.*VSTAR)
      REB2=2.*B2*RE2*CONS5
      F2=.0462/REB2**.2
      DEL=.1
      J1=0
      J=1
      ZETAD1=ZETAD
   23 CONS7=ZETAD1*TGAM
      RRO=1.04+.69333*ZETAD1*B2*(3.+2.*CONS7)/(2.+CONS7)
      FH=CONS6          +F2*(ZETAD1*(2.+TGAM)+.5*LOGF((ZETAD1*CB2+.02)/
     1.02)-CONS4*LOGF((B2*(ZETAD1*TGAM+2.)+.02*TGAM)/(2.* B2+.02*TGAM)))
      CM2CU=RRO*FH*CONS5/Q
      Z2=6.283185*CM2CU/(ZETAD1* B2*(2.+CONS7))
      J1=J1+1
      IF(J1-50)24,24,34
   24 IF(Z2-6.0)26,36,25
   25 IF(Z2-16.0)36,36,29
   26 GO TO (28,28,27),J
```

```
   27 DEL = DEL*0.1
   28 J = 2
      ZETAD1 = ZETAD1 - DEL
      GO TO 23
   29 GO TO (31,39,31),J
   30 DEL = DEL*0.1
   31 J = 3
      ZETAD1 = ZETAD1 + DEL
      GO TO 23
   34 WRITE OUTPUT TAPE 42,109,ZETAD,ZETAD1,22
      GO TO 50
   36 DEL2=D2*(.02/CONS6             +(1.04*(3.1415927/22)**2+ B2* B2/4.)**
     11.5)
      DH2=D2* 4.* B2*ZETAD1*(2.*CONS7)         /(2.+2.*ZETAD1*CONS7)
      DQSC=CONS3+12*DEL2*(1.+(ALAMDA(1)/(Q*CM2CU))**2)/(1.5*DH2)
      DQDIF2=CONS3*(ALAMDA(1)/(Q*CM2CU))**2*(X5+X6*F2*DEL2/DH2)
      DQD=DQSC+DQDIF2
      GO TO 43
   37 DELTAC=F2*.32/ B2
      REB2=2.*B2*CONS5*RE2
      RE2=D2*U2/(12.*VSTAR)
      ALPHA2=ATANF(ALAMDA(1)/Q)
      CALP2=COSF(ALPHA2)
      SALP2=SINF(ALPHA2)
      CONS9=(1.+CALP2)**2*EXPF(DELTAC)
      CALP3=(CONS9-SALP2*SALP2)/(CONS9+SALP2*SALP2)
      ALPHA3=ASINF((1.-CALP3*CALP3)**.5)
      DQ23=DELTAC*(1.+CALP2*CALP2/(1.0816*CALP3*CALP3))*CONS3/(2.*COSF((
     1ALPHA2+ALPHA3)/2.))
      F2=.0462/REB2**.2
      D3=1.04*D2
      SB2= B2*D2
      CONS11=-1.+2.*SB2/D3
      CONS12=(SB2*CALP3/D3)**2
      CONS13=3.1415927*F2/8.
      CONS14=SINF(ALPHA3)*SINF(ALPHA3)
      D4D3=1.3
      J3=1
   38 CONS15=CONS13*(1.+D4D3)/(D4D3+CONS11)
      D4D3N=(CONS12/((CONS14/(D4D3*D4D3)-CONS15)/(1.+CONS15)))**.25+1.
      IF (ABSF(D4D3/D4D3N-1.)-.001)42,42,39
   39 J3=J3+1
      IF(J3-50)40,40,41
   40 D4D3=D4D3N
  401 IF(D4D3-1.)400,38,38
  400 D4D3=D4D3+.1
      GO TO 401
   41 WRITE OUTPUT TAPE 42,104,D4D3,D4D3N,ALPHA3
      GO TO 50
   42 DQ34=1.5707963*CONS3*F2*(D2*CALP2/(D3*CALP3))**2*((1.+D4D3)/(D4D3+
     1CONS11))*(1.+(B2*CALP3/(D3*(D4D3-1.)*(D4D3-1.)))**2)
      DQ45=CONS3*(D2*CALP2*SB2*CALP3/(D3*CALP3*D3*(D4D3-1.)*(D4D3-1.)))*
     1*2*(X6+X7*(D4D3+1.)/(RE2**.2*(D4D3-1.)))
      DQD=DQ23+DQ34+DQ45
      GO TO 43
   43 ETHYD2=(1.-DQDL-DQD)/(1.+DQSE+DQRC)
      HTOT2=HO/ETHYD2
```

179

```
      IF(ABSF(HTOT2/HTOT-1.)-.02)47,47,44
   44 J2=J2+1
      IF(J2-50)45,45,46
   45 HTOT=HTOT2
      GO TO 16
   46 WRITE OUTPUT TAPE 42,114,HTOT,HTOT2
      GO TO 50
   47 DQFR=X8*(1.0E6/RE2)**.2/(1.E3*ALAMDA(I)*Q* B2)
      DQL=X9*.006*V2*V2*(1.-CONS3)**.5/ B2
      ETA=ETHYD2/(1.+DQFR+DQL)
      WRITE OUTPUT TAPE 42,108,BETA2,AMU,ALAMDA(I),
     1                                 Q,D2,U2,ZETA1,Z1,B2,REI,DQSF,DQ
     1DL,DQRC,ETAIMP
      GO TO (48,49),ICASE2
   48 WRITE OUTPUT TAPE 42,115,ICASE2,REB2,RE2,Z2,DQSC,DQDIF2,DQD
      GO TO 491
   49 WRITE OUTPUT TAPE 42,116,ICASE2,DQ23,DQ34,DQ45,DQD
  491 WRITE OUTPUT TAPE 42,117,ETHYD2,HTOT2,DQFR,DQL,ETA
      IF(TEST)50,50,492
  492 WRITE OUTPUT TAPE 42,123
      ANNO=ANNOO
   68 WRITE OUTPUT TAPE 42,122,ANNO
      AMO=AMOO
   69 ANPL=ANNO*AN
      AM=AMC+DQL
      VUP=VC*AMC*ANNO
      UIP=UI*ANNO
      CONS1=144.*V(P/(EI*DI*DI*AK1*.7853982)
      J=1
      CI1P = CONS1
      IF(CONS1*CONS1/64.35-ANPSP)/10,710,700
  700 CI2P=CONS1*(1.+A*(CI1P*CI1P/64.35-ANPSP))**AK
      IF(ABSF(CI1P/CI2P-1.)-.0001)710,710,701
  701 J=J+1
      IF(J-50)702,702,703
  702 CI1P=CI2P
      GO TO 700
  703 WRITE OUTPUT TAPE 42,124,CI1P,CI2P
      CI1P=(CI1P+CI2P)/2.
  710 BIPL=ATANF(UIP/CI1P)
      DELTBI = ABSF(BIPL*57.29578-BI)
      WIP=UIP/SINF(BIPL)
      CONS1=CI1*CI1/64.35-ANPSP
      CONS2=CI1P*CI1P/64.35-ANPSP
      IF(CONS1)704,704,705
  704 RI=1.0
      GO TO 706
  705 RI=(1.+A*CONS1)**AK
  706 IF(CONS2)707,707,708
  707 RIP=1.0
      GO TO 709
  708 RIP=(1.+A*CONS2)**AK
  709 U2P=U2*ANNO
   73 CONS1=(WIP/U2P)**2
      CONS2=AMO*AMO*ALAMDA*ALAMDA
      CONS3=X1PL*3.141592 7*CB2/(2.*71*(1.-V2))
      CONS4=1.-ALAMDA*AMO*TB2
```

A0545
A0545
A0545
A0545

180

```
      AMUPL=AMU
      J=1
      QPL1=AMUPL*CONS4
   74 ZETA1=((CONS2+(1.-QPL1)**2)/CONS1)**.5
      AMU2=1./(1.+CONS3*(1.+.09/ZETA1))
      QPL2=AMU2*CONS4
      IF(ABSF(QPL1/QPL2-1.)-.05)78,78,75
   75 J=J+1
      IF(J-50)76,76,77
   76 QPL1=QPL2
      GO TO 74
   77 WRITE OUTPUT TAPE 42,119,QPL1,QPL2,AMU2
   78 PSI2=A1+A2*DELTBI+A3*DELTBI*DELTBI
      DQINC=PSI2*CONS1/(2.*QPL2)
      WAVEU2=.5*(CONS1+CONS2+(1.-QPL2)**2)
      IF(ICASE-4)80,81,80
   80 PSIC=0.0
      DQCAV=0.0
      GO TO 84
   81 DQCAV = PSIC*(RIP-1.)*CONS1/QPL2
   84 WAVE=WAVEU2**.5*U2P
      REI=DHYD1*WAVE/(12.*VSTAPL)
      F1=.0462/REI**.2
      DQSF=X2PL*F1*DFL1*WAVEU2     /(DHYD1*QPL2)
      WIU2=CONS1**.5
      CL=COSF(BIPL)
      DELT=1.-ZETA1+QPL2*(CL+CH2)/(2.*WIU2*(Z1*(1.-V2)/3.1415927+2.*V2))
      DQDL=X3PL*DFLT*DELT*CONS1/QPL2
      AM=AMO
      DQRC=X4PL*DELT      /(ALAMDA*AM)
      DQDIN=PSI3*((QPL2-Q)**2+(ALAMDA-AM*ALAMDA)**2)/(2.*QPL2)
      DQDPL=DQD*AM*Q*((CONS2+QPL2*QPL2)*Q/((ALAMDA*ALAMDA+Q*Q)*QPL2))**.
     15/QPL2
      HTOT=QPL2*U2P*U2P/32.175
      ETAH=(1.-DQINC-DQCAV-DQDL       -DQDIN-DQDPL)/(1.+DQSF +DQRC)
      HO=ETAH*HTOT
      DELTP=GAMP*HO/144.
      RE2=U2P*D2/(12.*VSTAPL)
      DQFR=X8PL*(1.E6/RE2)**.2/(1.E3*ALAMDA*AMO*QPL2*B2)
      DQLPL=X9PL*.006*V2*V2*((2.*QPL2-CONS2+QPL2*QPL2)/(2.*QPL2))**.5/B2
      ETA=ETAH/(1.+DQFR+DQLPL)
      HP=HO*AMO*VO*GAMP*ANNO/(ETA*550.)
      ANS=AMO*ANNO
      WRITE OUTPUT TAPE 48,120,VO,DELTP,ETA,ANS,ANNO
      WRITE OUTPUT TAPE 42,121,AMO ,QPL2,DELTBI,ETAH,HO,DELTP,ETA,HP
      IF(AMO-AMN )86,87,87
   86 AMO=AMO+DELTM
      GO TO 69
   87 IF(ANNO-ANNON)88,89,89
   88 ANNO=ANNO+DELTAN
      GO TO 68
   89 CONTINUE
   50 CONTINUE
      GO TO 1
      END
```